Nanobodies targeting complement

Detecting and blocking complement activation

Eva M. Struijf

Nanobodies targeting complement

Detecting and blocking complement activation

Eva Madelon Struijf

Nanobodies targeting complement
PhD thesis, Utrecht University, the Netherlands

ISBN: 978-94-6483-435-2

Author: Eva Struijf
Cover design: Eva Struijf & Lenie Struijf
Provided by thesis specialist Ridderprint, ridderprint.nl
Printing: Ridderprint
Layout and design: Jildou Hengst, persoonlijkproefschrift.nl

About the cover: The cover shows a drawing of a llama, created by my mother Lenie Struijf, to honor the two llamas Lotte and Ines that were used during my studies. The pattern is an artistic impression of the shape of a nanobody and depicts the large amount of nanobodies that were developed, screened, and characterized during these studies.

Printing of this thesis was kindly financially supported by QVQ Holding BV; Hycult; and Infection & Immunity Utrecht.

Nanobodies targeting complement

Detecting and blocking complement activation

Nanobodies tegen complement

Detectie en remming van complement activatie

(met een samenvatting in het Nederlands)

Proefschrift

ter verkrijging van de graad van doctor aan de
Universiteit Utrecht
op gezag van de
rector magnificus, prof.dr. H.R.B.M. Kummeling,
ingevolge het besluit van het college voor promoties
in het openbaar te verdedigen op

woensdag 29 november 2023 des ochtends te 10.15 uur

door

Eva Madelon Struijf

geboren op 24 februari 1995
te Akersloot

Promotor:
Prof. dr. S.H.M. Rooijakkers

Copromotoren:
Dr. B.W. Bardoel
Dr. D.A.C. Heesterbeek

Beoordelingscommissie:
Prof. dr. F. van Wijk
Prof. dr. P. Gros (voorzitter)
Prof. dr. N. Van De Kar
Prof. dr. R.M. Schiffelers
Dr. B.A. Heesters

Paranimfen:
Dr. L. Aguinagalde Salazar
J. Egido Egido, MSc

Dit proefschrift werd (mede) mogelijk gemaakt met financiële steun van de Nederlandse Organisatie voor Wetenschappelijk Onderzoek (NWO) met een “TTW Industrial Doctorate” beurs (nummer NWA.ID.17.036, toegekend aan E.M. Struijf) en QVQ Holding BV, Utrecht, Nederland.

Ter nagedachtenis aan Gerard en Gré

Table of content

1

General introduction

1. The human immune system

In the fight against pathogens, the human body is armed with several lines of defense (1). The first line of defense consists of several physical barriers, including the skin, tears, mucus layers and epithelial cells and prevents pathogens from entering the human body. When a physical barrier is breached, the innate immune system is activated within minutes to hours. Activation of the innate immune system initiates and helps the development of a pathogen specific response by the adaptive immune system, also known as the second line of defense. The adaptive immune response is at full strength after several days to weeks, tries to eliminate the infection if still present and develops memory to be able to respond more rapidly when the same pathogen is encountered in the future. In both the innate and adaptive immune system, a division in the cellular and humoral response can be made. The cellular response contains myeloid innate immune cells such as neutrophils, macrophages, and dendritic cells and lymphoid adaptive immune cells such as T-cells, B-cells, and NK-cells. The humoral response consists of circulating antimicrobial peptides, antibodies, and the complement system.

2. The complement system

The complement system, discovered by Jules Bordet in 1896, is an important part of the humoral innate immune system that offers rapid protection against invading pathogens (2). This system consists of more than 30 different proteins that circulate in plasma and other body fluids (2–6). Complement proteins are mainly synthesized in the liver but can also be produced locally by several types of immune cells, including immature dendritic cells, monocytes, and macrophages (7, 8). The three major effector functions of the complement system are [1] opsonization of (foreign) particles for phagocytosis, [2] attraction of immune cells to the site of activation and [3] direct lysis of (foreign) particles (2, 5, 9–11). In addition, the complement system bridges the innate and adaptive immune system by formation of opsonins and chemo attractive molecules. Although the elimination of pathogens is often described as the most important function of the complement system, it has become evident that complement also plays vital roles in maintaining homeostasis. It does so by recognizing and removing immune complexes, apoptotic, and tumorous cells. This homeostatic role of complement starts already during early embryogenesis, for example during the development of the neural crest (12, 13). Later in life complement is involved in many processes, including synapse maturation, lipid metabolism, angiogenesis, and tissue regeneration (14).

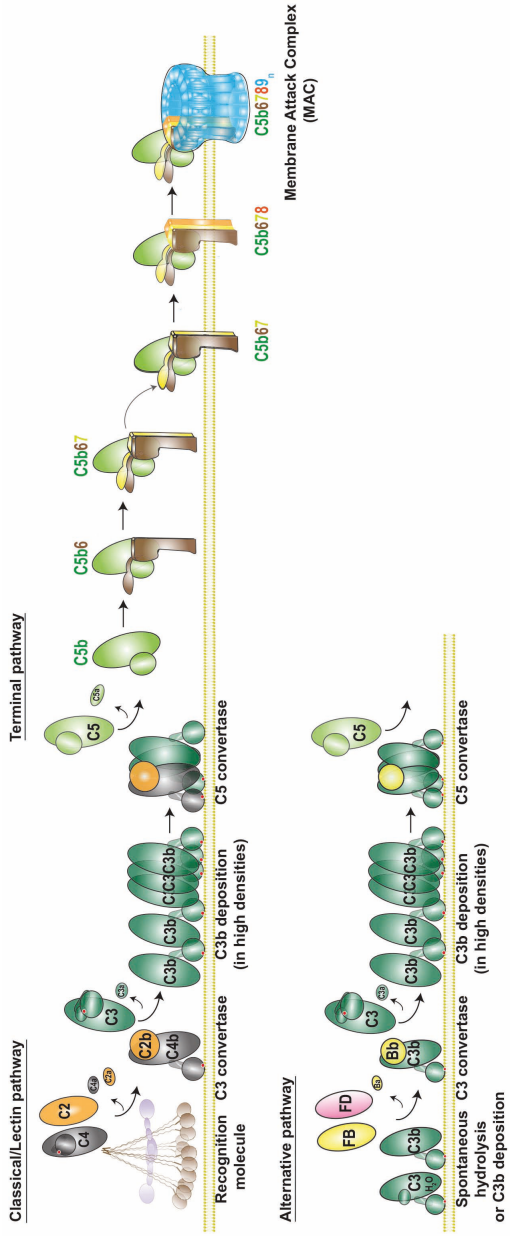

Figure 1: Schematic representation of complement activation on the target cell surface in a stepwise manner.

2.1. Activation of the complement system

The complement system can be activated via three different pathways: the classical pathway (CP), the lectin pathway (LP) and the alternative pathway (AP) (8). **Figure 1** depicts a schematic overview of the three pathways. The CP is initiated when complement component C1q recognizes the Fc-tails of surface-bound antibodies. It is most efficient when antibodies are arranged in hexamers, as this provides a docking place for the globular heads of C1q (15). When C1q is associated with proteases C1r, and C1s, it is referred to as the C1-complex. Upon binding of the C1-complex to surface-bound antibodies, C1r activates protease C1s, which then cleaves complement component C4 in C4a and C4b (8). Components C4a is released in the supernatant and C4b covalently binds the target surface. There complement component C2 can interact with C4b, which is then also cleaved in C2a and C2b by the C1-complex. C2a is released into the supernatant, while C2b stays bound to C4b, forming the C4b2b complex, also known as the C3 convertase. The LP recognizes carbohydrates specifically present on pathogens and dying cells, using proteins such as mannose binding lectin (MBL). MBL resembles the structure and function of C1q but interacts with mannose associated serine proteases (MASP-1 & MASP-2) instead of C1r and C1s. Similar as in the CP, MBL associated with MASP molecules cleave complement components C2 and C4, resulting in the formation of surface bound enzymatic complexes, called C3 convertases or C4b2b. Next, C3 convertases formed by the CP or LP cleave complement component C3 in C3a and C3b. C3a is an anaphylatoxin which is released in the supernatant and attracts immune cells to the site of complement activation. C3b is the activation product that is deposited on the target cell, where it functions as an opsonin for phagocytic cells. The AP gets activated when C3 is cleaved by the CP and LP C3 convertases and C3b is deposited on the target surface. This allows Factor B (FB) to bind C3b, forming the AP proconvertase C3bB. Next, complement component Factor D (FD) can interact, which cleaves FB in Ba and Bb. Ba is released in the supernatant, and Bb remains bound to C3b, resulting in the formation of the AP C3 convertase, C3bBb. Next, AP C3 convertases cleave native C3 molecules in C3a and C3b, which subsequently form the building blocks of more C3 convertases. Consequently, the AP is responsible for the largest amount of C3b deposition and is often referred to as the amplification loop of the complement system. Studies estimated that ~80% of the effector functions of the complement system are a result of AP complement activation (16, 17). Next to CP- and LP-mediated initiation of the AP, it is shown that *in vitro* the AP can be initiated by spontaneous hydrolysis of the C3 molecule (C3(H_2O)). This initiates a huge conformational change in C3, which resembles the formation of C3b, without the release of C3a. Consequently, C3(H_2O) either in solution or on a surface can interact with FB and form AP C3 (pro) convertases (18). Although *in vitro* studies estimated that the spontaneous hydrolysis of C3 occurs at a constant rate of 0.2-0.4% per hour, it stays under debate whether this

tick-over mechanism of C3 really contributes to initiation of the alternative pathway *in vivo* (19, 20).

2.2. The terminal pathway

Upon formation of C3 convertases, the density of deposited C3b molecules rapidly increases on a target cell surface. When a critical density of C3b molecules is reached, C3 convertases switch substrate from C3 to C5, and are then called C5 convertases. C5 convertases cleave native C5 molecules in anaphylatoxin C5a and the activation product C5b. Even though the exact composition and conformational changes required to form these C5 cleaving enzymatic complexes are still poorly understood, the C5 convertases are referred to as C4b2bC3b (CP & LP) and C3bBbC3b (AP). Complement's terminal pathway (TP) is initiated when the different C5 convertases cleave native C5 molecules into C5a and C5b. The chemoattractant C5a is released in solution and recruits immune cells bearing a C5a receptor (C5aR) to the site of infection(9, 10). The highly instable C5b quickly interacts with complement component C6 to form the stable C5b6 complex (21). Next, C5b6 interacts with complement component C7, forming the C5b-7 complex. This exposes a hydrophobic domain in C7 which allows C5b-7 to stably bind to the cell surface. There it will interact with component C8, which allows the C5b-8 complex to insert itself (partially) in the membrane. Finally, the C5b-8 complex will interact with ~18 C9 molecules, which results in the assembly of a porin-like structure, now called the Membrane Attack Complex (MAC). This pore-forming complex has an inner diameter of 10nm, disrupts membranes and thereby induces particle lysis (22, 23). **Figure 1** schematically represents the different steps involved in complement activation and propagation of the terminal pathway.

2.3. Cleavage of central complement proteins C3 and C5

Complement activity is driven by a series of proteolytic events that induce large conformational changes in the different proteins. The cleavage of complement components C3 and C5 (by C3 and C5 convertases) are central steps because it triggers the three major effector functions of the complement system (**Figure 2**). Here we describe what is currently known about the molecular steps underlying C3 and C5 activation.

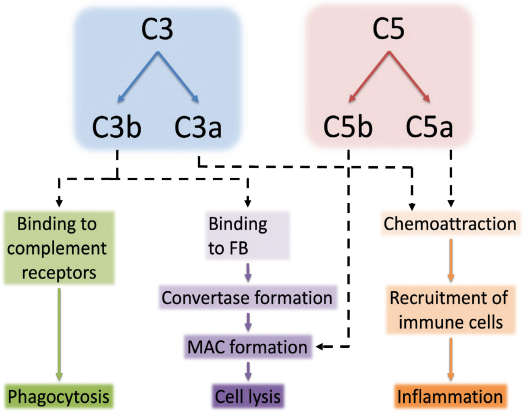

Figure 2: Schematic representation of the different effector functions of complement activation that occur upon cleavage of C3 and C5.

2.3.1. Conversion of C3 to C3b

Complement component C3 belongs to the C3/C4/C5 protein family (24–26). It is comprised of an alfa and beta chain. With a core of 8 macroglobulin (MG) domains, a C345c domain (also known as netrin module (NTR)), a linking (LNK) domain, a C1r/C1s UEGF BMP1 (CUB) domain, an anaphylatoxin (ANA, or C3a) domain and a thioester domain (TED), C3 consists of 13 domains and has a total size of 186 kDa (**Figure 3**) (18, 27). During C3 conversion, the ANA/C3a domain (9 kDa) is cleaved off and released in the supernatant. There it functions as a chemoattractant by recruiting immune cells expressing a C3a receptor (C3aR) to the site of complement activation (**Figure 2**). In C3, the ANA/C3a domain is located near the center of the C3 molecule and upon its release, the remaining C3b molecule (177 kDa) undergoes a major conformational rearrangement. The biggest rearrangements occur in the CUB and TED domains, which move down towards the bottom of the MG-ring (**Figure 3**). These movements reveal a thioester moiety in the TED domain that C3b uses to covalently attach to a surface. This exposes previously hidden interfaces that allow C3b to interact with various complement receptors, proteins, and regulators. First, deposited C3b can bind to phagocytic cells that express complement receptors, such as CR1 and CRIg, and thereby C3b induces phagocytosis of the target cell (28). Second, C3b can interact with FB (in a magnesium dependent manner) to form C3 (pro) convertases and subsequently C5 convertases. This further activates the complement cascade which eventually can lead to formation of the MAC and cell lysis (**Figure 2**). Last, C3b can interact with positive and negative regulators that either amplify or dampen the effector functions of C3b, which will be discussed in more detail below (regulation of the complement system).

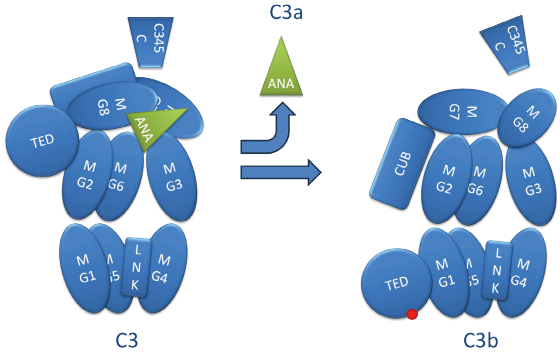

Figure 3: Schematic representation of the different domains present in complement components C3 and C3b and structural rearrangements that happen upon C3 cleavage. Figure adapted from Janssen et al. in Nature (18).

C3 activation explained by a metaphor

Janssen et al. described the conversion of C3 into C3b by a metaphor of a puppeteer (18). In its uncleaved form (C3), the body of the puppeteer stands up straight, with its puppet near its shoulder, while in the cleaved form (C3b), the puppeteer bends over with its right shoulder and brings the puppet down with its right arm. In this metaphor the head of the puppet is domain C345c, the body are domains MG1-6 and the LNK domain, the shoulders are domains MG7 & MG8, the neck is the anchor region, the arm is the CUB domain, and the puppet the TED (**Figure 4**).

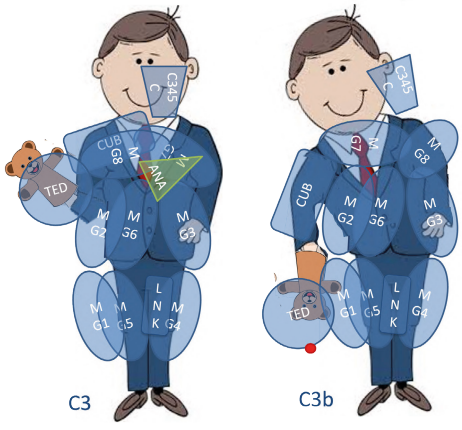

Figure 4: Schematic representation of the "puppeteer-metaphor", inspired by Janssen et al. (18) to understand the C3 structure and its rearrangements upon formation of C3b.

2.3.2. Conversion of C5 to C5b and formation of the C5b6 complex

Complement component C5 (190 kDa) also belongs to the C3/C4/C5 protein family and structurally resembles complement component C3 (24–26). Like C3, it consists of two disulfide chains (alpha 115 kDa and beta 75 kDa) and has 13 different domains (**Figure 5**) (29). The CUB-, LNK-, C345C- and 8 MG domains are all annotated the same as in C3, while C5d (equivalent of TED) and ANA or C5a (equivalent of C3a) are annotated differently. The most prominent difference between C3 and C5 is that the reactive thioester (which C3(b) uses to covalently attach to target surfaces) is not present in C5. When C5 is cleaved by convertases, the C5a (8 kDa) domain is released and functions as a potent chemoattractant recruiting immune cells to the site of complement activation (**Figure 2**). C5b (181 kDa) undergoes a large conformational rearrangement, which is similar to the rearrangement observed for C3 to C3b conversion and initiates the terminal pathway which eventually leads to MAC formation (**Figure 2**). Where the TED domain in C3 relocates completely to the bottom of the MG-ring, the C5d domain only moves halfway. This new conformation of C5b is metastable and reveals (neo-)epitopes that are recognized by the next complement component C6. C6 (103 kDa) is a protein that belongs to the MAC-perforin/cholesterol-dependent cytolysin (MACPF/CDC) protein superfamily (30–33). In its circulating form its shape is tall and flat, and the protein consists of a central MACPF domain and multiple factor I-MAC (FIM), complement control protein (CCP) and thrombospondin-like (TS) domains (**Figure 5**). Upon C5b formation, C6 folds in a hairpin shape around the C5d domain using an extensive interface. This interaction stabilizes C5b and forms the bimolecular C5b6 complex (282 kDa) (34, 35). The C5b6 complex has high structural homology with precursor proteins C5 and C6, but also contains many neo-epitopes which allow subsequent interaction with the next complement component, C7 (36).

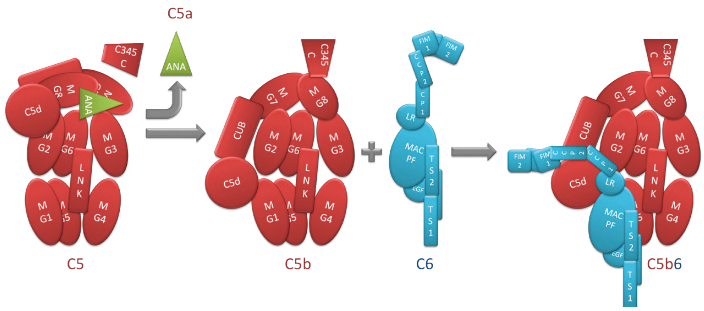

Figure 5: Schematic representation of the structural orientation of the different domains present in complement components C5, C5b, and C6 and structural rearrangements that happen upon C5 cleavage and C5b6 formation. Figure adapted from Fredslund et al. in Nature Immunology and Hadders et al. in Cell reports (29, 35)

2.3.3. C3 and C5 convertase structures

With the help of many structural studies on C3, C3b, FB, and C3bBb the structure and function of the AP C3 convertase is very well understood (18, 21, 37–45). In contrast to the C3 convertases, the structure and molecular mechanism of C5 convertases have not yet been unraveled completely and it remains poorly understood what conformational changes and interactions are required for a C3 convertase to become a C5 convertase. Interestingly, the substrate molecules C3 and C5 are highly homologous, but they interact with the C3/C5 convertase in a slightly different manner (29). Both molecules most likely use domains MG4, MG5 and MG7 to interact with C3b molecules but the domain-to-domain orientation of MG4 and MG5 is slightly different in C5 compared to C3 (45). The monomeric C3bBb complex can interact with both C3 and C5 molecules but has a high preference for C3 molecules and is therefore called the C3 convertase (37, 38, 45). It was estimated that for every C5 molecule that is cleaved by C3bBb, 9.000 C3 molecules are cleaved (37). The high preference for C3 molecules changes when C3b molecules cluster around the C3 convertase. It was estimated that C3b clustering increases the affinity for C5 with a 100-1000-fold (45). This suggests an important role for C3b in increasing the substrate affinity for C5 and therefore in the transformation from a C3 to a C5 convertase. SPR data confirmed this, by showing that the interaction of C5 with the convertase is independent of the catalytic domain (Bb) (46). Initially it was believed that a higher density of C3b molecules results in convertases with C3b-C3b dimers that are covalently attached, which increases the affinity for C5 (38). Later it was found that C3b-C3b dimers do not have to be covalently linked, but that a high surface density of C3b molecules in a correct orientation is enough to increase the affinity for C5 (21). The requirement of at least two C3b molecules for binding of C5 was supported by a study that revealed two C3b binding sites on one C5 molecule (37). Despite the huge effort that was taken in the last decades to understand how C3 convertases change substrate specificity, the exact molecular details concerning the orientation and molecular interactions of one or multiple ‘extra’ C3b molecules with the C3bBb complex is a burning question in the field.

2.4. Regulation of the complement system

In the complement system, regulation and balance are crucial to maintain homeostasis. Examples of these regulatory mechanisms are that complement proteins and complexes are activated in a unidirectional manner and that some protein complexes have a short half-life (8). For example, convertases are only stable for 1-2 minutes on eukaryotic cell membranes without binding of regulators (47). Upon FB cleavage, the affinity of Bb for C3b drastically decreases, and is too low to bind C3b back when detached, resulting in irreversible dissociation. The half-life of convertases can be increased by a 6 to 10-fold when positive regulatory protein properdin (Factor P, FP) associates with C3b

and stabilizes its interaction with Bb (48, 49). Most negative regulators act by binding to C3b molecules, to either prevent convertase formation or accelerate the decay of convertase activity. High levels of homology are observed between regulators, and they all map to the newly exposed binding interfaces that appear in C3b after C3 conversion (50). This common binding interface might make the regulators look redundant to each other. However, the subtle differences in where, how, and how much they are expressed, indicate that all regulators are important in this delicate system. Examples of negative regulators are factor H (FH), factor I (FI), decay accelerating factor (DAF, CD55), membrane cofactor protein (MCP), complement receptor 1 (CR1), and CD59 (8). FH (either soluble or surface-bound) is a regulator that prevents convertase formation, accelerates decay of already formed convertases and recruits other regulatory proteins, such as FI to inactivate C3b molecules by sequential cleavage steps. FI cleaves C3b twice in the CUB domain, releasing C3f and forming the inactive iC3b (6, 18, 51, 52). iC3b can no longer form (pro-)convertases since it cannot interact with FB, but it still has pro-inflammatory effects as an opsonin that can interact with CRIg, CR1, CR2, complement receptor 3 (CR3) and complement receptor 4 (CR4) on neutrophils. To further regulate iC3b molecules, FI interacts with cofactor CR1 and cleaves iC3b a third time in the CUB domain, resulting in soluble C3c and surface bound C3dg. These fragments are no longer recognized by receptors on cells, and therefore mark the end of complement activation.

2.5. Complement in disease

The importance of complement regulation is proven by existence of many complement-mediated diseases in which aberrant activation of complement is an underlying cause or a contributor to disease progression. The list of complement-mediated diseases is still growing and covers a wide variety of diseases, affecting almost all organs (53). In multiple blood-related diseases, such as paroxysmal nocturnal hemoglobinuria (PNH), atypical hemolytic uremic syndrome (aHUS), and C3 glomerulopathy (C3G), genetic mutations in complement components or regulators and autoantibodies directed to complement components or cellular targets induce overactivation of the complement system and are the root cause of the disease. PNH is caused by genetic mutations in surface-bound complement regulators CD55 and CD59, which normally inhibit convertase and MAC formation. aHUS and C3G are also caused by genetic mutations in AP complement proteins but can also be caused by autoantibodies directed to these proteins. Furthermore, uncontrolled complement activation can be a consequence of infection, for example in the case of sepsis or acute respiratory distress syndrome (ARDS). Because complement plays a role in a long list of diseases, a lot of research has been done in the last decades to identify and develop novel complement inhibitors.

2.6. Complement inhibitors

2.6.1. Man-made inhibitors

In the 1950s the first study on complement intervention elucidated that antibody inhibition in rabbits suffering from intracapillary glomerulonephritis reduced complement activation and that these rabbits had less disease symptoms (54). In the 1990s multiple recombinant complement regulating proteins and small molecule complement inhibitors were investigated, but almost all showed either off-target effects and toxicity or failed to proceed into clinical development (55). Since the role of complement in health and disease became clearer in the last decade, the search for novel compounds that could either enhance or block the complement system has drastically increased (53, 55). Complement-targeting molecules that have been identified and are under investigation mostly include monoclonal antibodies, nanobodies, and peptides. Nonetheless, the general success rate for therapeutic use is rather low. It is believed that this is due to the lack of in-depth knowledge about disease mechanisms, incomplete understanding of the molecular interactions of the complement system and the absence of appropriate tools to study complement *in vitro* and *in vivo* (55).

Fortunately, a few very potent complement inhibitors have been successfully developed, were introduced in the clinic, and now improve the lives of many patients (53, 55, 56). In 2007, a humanized monoclonal antibody (mAb) that inhibits C5 cleavage, Eculizumab (Soliris®), has entered the clinic as the first complement inhibiting drug. It was first approved for the treatment of PNH and later also for aHUS, general myasthenia gravis (gMG) and neuromyelitis optica spectrum disorder (NMOSD) (57, 58). In 2019, Ravulizumab, a next-generation antibody of Eculizumab with a longer half-life was approved for the treatment of PNH and aHUS (59, 60). Although treatment with Eculizumab or Ravulizumab is highly beneficial for many patients, anaphylactic side effects and variations in response profiles are still problematic. Furthermore, a genetic polymorphism in C5 (C5 R885H) was identified in a group of poor responders, and it was found that Eculiuzmab and Ravulizumab can no longer bind and inhibit this genetic variant of C5 (61–63). In 2021, the first C3-targeting complement inhibitor, called Empaveli (or pegcetacoplan), has received FDA approval for the treatment of PNH (64). This drug is an analog of the cyclic peptide compstatin, which inhibits C3 cleavage by preventing convertase formation. The use of Empaveli in other complement-mediated diseases, such as C3G and AMD is currently under clinical investigation. With only three molecules available, the amount of treatment options is rather limited and due to excessive developmental costs, unfortunately also rather expensive (53, 55). Therefore, there is still a demand for novel, well characterized complement targeting molecules.

2.6.2. Microbial complement inhibitors

To withstand complement attack, human pathogens have evolved mechanisms to evade the complement system at different levels. Several bacteria have evolved specific complement-inhibitory molecules that block the complement reaction at several stages. Examples include, the convertase targeting proteins SCIN, Efb, and Ecb, expressed by *Staphylococcus aureus* (*S. aureus*) and PaE and PaAP, expressed by *Pseudomonas aeruginosa* (65–67). *S. aureus* also expresses SSL7, a protein that binds C5 and prevents its cleavage (68). Furthermore, VCP, SPICE and IMP are proteins expressed by vaccina virus, variola virus, and cowpox virus, respectively, that all mimic C3b-binding regulators and thereby prevent convertase formation (69). Moreover, ticks (*Ornithodoros moubata, Rhipeciphalus pulchellus* and *Rhipicephalus appendiculatus*) contain OmCI, CirpT, and RaCI3 in their saliva, which are all C5 inhibiting proteins (44, 70, 71).

3. Llama-derived nanobodies

In 1986, 21 years before the FDA approval of Eculizumab, the first monoclonal antibody therapy was approved by the FDA. This antibody was targeted against CD3 and was given to prevent kidney transplant rejection (72). The high potential of antibody therapy was directly recognized and the search for novel therapeutic antibodies rapidly increased for all kind of fields and purposes in life sciences. It was seven years later when a new type of functional antibodies was discovered in serum derived from llamas (llama glama, family of camilidae) (73). Next to conventional antibodies (cAb), camelids produce antibodies that lack the CH1 domains and light chains (**Figure 6**). The antibodies exist in isotypes IgG2 and IgG3 and are called heavy chain-only antibodies (HCAb). Where cAbs recognize their antigen with a combination of the VH and VL domains, HCAbs recognize their antigen with a single variable domain, located on the N-terminus. This domain is designated as the variable heavy chain of heavy chain antibodies (VHH), and are also known as Nanobodies®, and single domain antibodies (sdAb) (**Figure 6**). Nanobodies recognize their antigens with three distinct complementarity-determining regions (CDR), which are prone to somatic mutations, can vary in length and flexibility, and bind a repertoire of antigens that is as diverse as the repertoire of cAbs (74, 75).

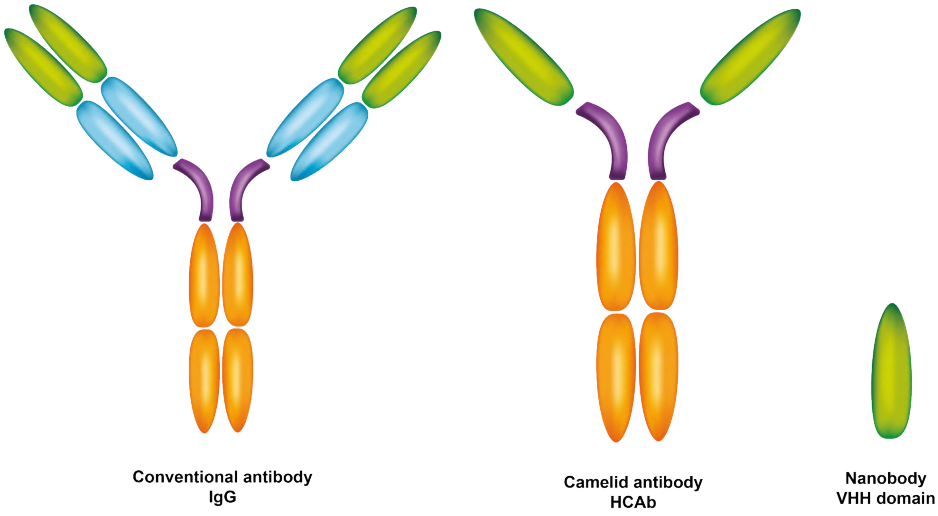

Figure 6: Schematic representation of the different domains present in conventional IgG antibodies, heavy-chain-only antibodies (HCAb) derived from camelids and nanobodies (or VHH domains).

3.1. Why nanobodies?

As described above, complement activation is driven by conformational changes. In order to discriminate between complement activation products and precursor proteins, molecules that can recognize conformational epitopes are required. Multiple nanobodies, including the anti-von Willebrand factor (VWF) nanobody caplacizumab (or Cablivi®) and nanobodies binding G-protein coupled receptors have shown that nanobodies are specifically well equipped to recognize conformational epitopes and outperform cAbs in this aspect (76–79)). One of the reasons for this is that the nanobody paratope is shaped convex, while the cAb paratope is shaped concave (**Figure 7**) (80). Furthermore, the length of the CDR3 is longer in nanobodies than in cAbs, which allows it to adopt a larger variety of shapes and thereby increases the binding diversity and target specificity of nanobodies. Next to their unique shape, nanobodies possess many more properties that make them interesting molecules to use. For example, they often bind their target with high affinity, are easy to produce in bacterial or yeast expression systems and are easily labeled with (fluorescent) tags. Finally, since nanobodies are single domain molecules, they can be used in phage display systems, which enables screening and selection of nanobodies with different properties in a high-throughput way.

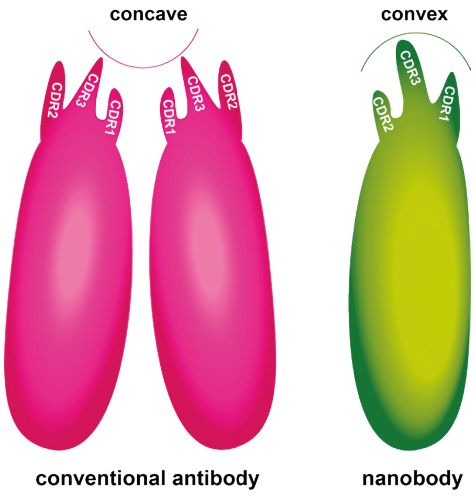

Figure 7: Schematic representation of antigen-binding domains of a conventional antibody and a nanobody.

4. Aim of the thesis

The role of the complement system in health and disease is extensively being studied. Although huge progress is made in the last decades, there are still major fundamental and clinical questions that yet remained unanswered. Novel tools and therapeutics that can activate, inhibit, and/or discriminate complement precursor proteins from activation products are therefore still needed. In this thesis we aim to develop llama-derived nanobodies directed towards different complement components. We focused on central complement component C5 and activation products C3b and C5b6. While the C5-targeting nanobodies identified in this study can interfere with complement activity, the C3b- and C5b6-targeting nanobodies uniquely discriminate complement activation products from their precursors. The here identified nanobodies can serve as tools to gain a better understanding of the molecular mechanisms of complement activation and hold promise for further development as diagnostic tools and therapeutics.

References

1. Parkin, J., and Cohen, B. (2001) An overview of the immune system. *Lancet*. **357**, 1777–1789
2. Dunkelberger, J. R., and Song, W. (2009) Complement and its role in innate and adaptive immune responses. *Cell Res.* **20**, 34–50
3. Freeley, S., Kemper, C., and Le Friec, G. (2016) The " ins and outs " of complement- driven immune responses. *Immunol Rev.* **274**, 16–32
4. Krishnan, V., Xu, Y., Macon, K., Volanakis, J. E., and Narayana, S. V. L. (2007) The Crystal Structure of C2a, the Catalytic Fragment of Classical Pathway C3 and C5 Convertase of Human Complement. *J Mol Biol*. **367**, 224–233
5. Walport, M. J. (2001) Complement - First of Two Parts. *N Engl J Med*. **344**, 1058–1066
6. Gros, P., Milder, F. J., and Janssen, B. J. C. (2008) Complement driven by conformational changes. *Nat Rev Immunol*. **8**, 48–58
7. Volanakis, J. E. (1995) Transcriptional Regulation Of Complement Genes. *Annu Rev Immunol*. **13**, 277–305
8. Merle, N. S., Church, S. E., Fremeaux-Bacchi, V., and Roumenia, L. T. (2015) Complement system part I – molecular mechanisms of activation and regulation. *Front Immunol.* **6**, 1–30
9. Strainic, M. G., Liu, J., Huang, D., An, F., Lalli, P. N., Shapiro, V. S., Dubyak, G. R., Heeger, P. S., and Edward, M. (2008) Locally Produced Complement Fragments C5a and C3a Provide Both Costimulatory and Survival Signals to Naive CD4+ T Cells. *Immunity.* **28**, 425–435
10. Lalli, P. N., Strainic, M. G., Yang, M., Lin, F., Medof, M. E., and Heeger, P. S. (2008) Locally produced C5a binds to T cell – expressed C5aR to enhance effector T-cell expansion by limiting antigen-induced apoptosis. *Blood*. **112**, 1759–1767
11. Kolb, W. P., and Müller-Eberhard, H. J. (1969) The membrane attack mechanism of complement. *J Exp Med*. **140**, 167–184
12. Reichhardt, M. P., Lundin, K., Lokki, A. I., Recher, G., Vuoristo, S., Katayama, S., Tapanainen, J. S., Kere, J., Meri, S., and Tuuri, T. (2019) Complement in Human Pre-implantation Embryos: Attack and Defense. *Front Immunol*. **10**, 1–12
13. Carpanini, S. M., Torvell, M., and Morgan, B. P. (2019) Therapeutic Inhibition of the Complement System in Diseases of the Central Nervous System. *Front Immunol*. **10**, 1–17
14. Ricklin, D., Hajishengallis, G., Yang, K., and Lambris, J. (2010) Complement: a key system for immune surveillance and homeostasis. *Nat. Immunol*. **11**, 785–797
15. Diebolder, C. A., Beurskens, F. J., De Jong, R. N., Koning, R. I., Strumane, K., Lindorfer, M. A., Voorhorst, M., Ugurlar, D., Rosati, S., Heck, A. J. R., Van De Winkel, J. G. J., Wilson, I. A., Koster, A. J., Taylor, R. P., Saphire, E. O., Burton, D. R., Schuurman, J., Gros, P., and Parren, P. W. H. I. (2014) Complement Is Activated by IgG Hexamers Assembled at the Cell Surface. *Science (1979)*. **343**, 1260–1263
16. Harboe, M., Ulvund, G., Vien, L., Fung, M., and Mollnes, T. E. (2004) The quantitative role of alternative pathway amplification in classical pathway induced terminal complement activation. *Clin Exp Immunol*. **138**, 439–446
17. Harboe, M., Garred, P., Karlstrøm, E., Lindstad, J. K., Stahl, G. L., and Mollnes, T. E. (2009) The down-stream effects of mannan-induced lectin complement pathway activation depend quantitatively on alternative pathway amplification. *Mol Immunol*. **47**, 373–380
18. Janssen, B. J. C., Christodoulidou, A., McCarthy, A., Lambris, J. D., and Gros, P. (2006) Structure of C3b reveals conformational changes that underlie complement activity. *Nature*. **444**, 213–216
19. Fromell, K., Adler, A., Åman, A., Manivel, V. A., Huang, S., Dührkop, C., Sandholm, K., Ekdahl, K. N., and Nilsson, B. (2020) Assessment of the Role of C3(H2O) in the Alternative Pathway. *Front Immunol*. **11**, 1–13
20. Ekdahl, K. N., Mohlin, C., Adler, A., Åhman, A., Anan Manivel, V., Sandholm, K., Huber-Lang, M., Fromell, K., and Nilsson, B. (2019) Is generation of C3(H2O) necessary for activation of the alternative pathway in real life? *Mol Immunol*. **114**, 353–361

21. Berends, E. T. M., Gorham, R. D. J., Ruyken, M., Soppe, J. A., Orhan, H., Aerts, P. C., Haas, C. J. C. De, Gros, P., and Rooijakkers, S. H. M. (2015) Molecular insights into the surface-specific arrangement of complement C5 convertase enzymes. *BMC Biol*. **13**, 1–13
22. Sharp, T. H., Koster, A. J., and Tomography, C. (2016) Heterogeneous MAC Initiator and Pore Structures in a Lipid Bilayer by Phase-Plate Cryo-electron Report Heterogeneous MAC Initiator and Pore Structures in a Lipid Bilayer by Phase-Plate. *CellReports*. **15**, 1–8
23. Morgan, B. P., Boyd, C., and Bubeck, D. (2017) Molecular cell biology of complement membrane attack. *Semin Cell Dev Biol*. 10.1016/j.semcdb.2017.06.009
24. Schreiber, R. D., and Müller-Eberhard, H. J. (1978) Assembly of the cytolytic alternative pathway of complement from 11 isolated plasma proteins*. *Journal of Experimental Medicine*. **148**, 1722–1727
25. Muller-Eberhard, H. J. (1988) Molecular organization and function of the complement system. *Annual review Biochemistry*. **57**, 321–347
26. Bramham, J., Thai, C. T., Soares, D. C., Uhrín, D., Ogata, R. T., and Barlow, P. N. (2005) Functional insights from the structure of the multifunctional C345C domain of C5 of complement. *Journal of Biological Chemistry*. **280**, 10636–10645
27. Janssen, B. J. C., Huizinga, E. G., Raaijmakers, H. C. A., Roos, A., Daha, M. R., Nilsson-Ekdahl, K., Nilsson, B., and Gros, P. (2005) Structures of complement component C3 provide insights into the function and evolution of immunity. *Nature*. **437**, 505–511
28. Vandendriessche, S., Cambier, S., Proost, P., and Marques, P. E. (2021) Complement Receptors and Their Role in Leukocyte Recruitment and Phagocytosis. *Front Cell Dev Biol*. 10.3389/fcell.2021.624025
29. Fredslund, F., Laursen, N. S., Roversi, P., Jenner, L., Oliveira, C. L. P., Pedersen, J. S., Nunn, M. A., Lea, S. M., Discipio, R., Sottrup-Jensen, L., and Andersen, G. R. (2008) Structure of and influence of a tick complement inhibitor on human complement component 5. *Nat Immunol*. **9**, 753–760
30. Aleshin, A. E., Schraufstatter, I. U., Stec, B., Bankston, L. A., Liddington, R. C., and DiScipio, R. G. (2012) Structure of complement C6 suggests a mechanism for initiation and unidirectional, sequential assembly of Membrane Attack Complex (MAC). *Journal of Biological Chemistry*. **287**, 10210–10222
31. DiScipio, R. G., Linton, S. M., and Rushmere, N. K. (1999) Function of the factor I modules (FIMS) of human complement component C6. *Journal of Biological Chemistry*. **274**, 31811–31818
32. Chakravarti, D. N., Chakravarti, B., Parra, C. A., and Muller-Eberhard, H. J. (1989) Structural homology of complement protein C6 with other channel-forming proteins of complement. *Proc Natl Acad Sci U S A*. **86**, 2799–803
33. Lukassen, M. V, Franc, V., Hevler, J. F., and Heck, A. J. R. (2021) Similarities and differences in the structures and proteoform profiles of the complement proteins C6 and C7. *Proteomics*. 10.1002/pmic.202000310.This
34. Aleshin, A. E., DiScipio, R. G., Stec, B., and Liddington, R. C. (2012) Crystal structure of C5b-6 suggests structural basis for priming assembly of the membrane attack complex. *Journal of Biological Chemistry*. **287**, 19642–19652
35. Hadders, M. A., Bubeck, D., Roversi, P., Hakobyan, S., Forneris, F., Morgan, B. P., Pangburn, M. K., Llorca, O., Lea, S. M., and Gros, P. (2012) Assembly and Regulation of the Membrane Attack Complex Based on Structures of C5b6 and sC5b9. *Cell Rep*. **1**, 200–207
36. DiScipio, R. G. (1992) Formation and structure of the C5b-7 complex of the lytic pathway of complement. *Journal of Biological Chemistry*. **267**, 17087–17094
37. Rawal, N., and Pangburn, M. K. (2001) Structure/function of C5 convertases of complement. *Int Immunopharmacol*. **1**, 415–422
38. Pangburn, M. K., and Rawal, N. (2002) Structure and function of complement C5 convertase enzymes. *Biochem Soc Trans*. **30**, 1006–1010
39. Milder, F. J., Gomes, L., Schouten, A., Janssen, B. J. C., Huizinga, E. G., Romijn, R. A., Hemrika, W., Roos, A., Daha, M. R., and Gros, P. (2007) Factor B structure provides insights into activation of the central protease of the complement system. *Nat Struct Mol Biol*. **14**, 224–228

40. Rooijakkers, S. H. M., Wu, J., Ruyken, M., van Domselaar, R., Planken, K. L., Tzekou, A., Ricklin, D., Lambris, J. D., Janssen, B. J. C., van Strijp, J. A. G., and Gros, P. (2009) Structural and functional implications of the complement convertase stabilized by a staphylococcal inhibitor. *Nat Immunol*. **10**, 721–727
41. Torreira, E., Tortajada, A., Montes, T., Rodríguez de Córdoba, S., and Llorca, O. (2009) 3D structure of the C3bB complex provides insights into the activation and regulation of the complement alternative pathway convertase. *Proc Natl Acad Sci U S A*. **106**, 882–887
42. Forneris, F., Ricklin, D., Wu, J., Tzekou, A., Wallace, R. S., Lambris, J. D., and Gros, P. (2010) Structures of C3b in complex with factors B and D give insight into complement convertase formation. *Science (1979)*. **330**, 1816–1820
43. Alcorlo, M., Tortajada, A., Rodriguez de Cordoba, S., and Llorca, O. (2013) Structural basis for the stabilization of the complement alternative pathway C3 convertase by properdin. *Proceedings of the National Academy of Sciences*. **110**, 13504–13509
44. Jore, M. M., Johnson, S., Sheppard, D., Barber, N. M., Li, Y. I., Nunn, M. A., Elmlund, H., and Lea, S. M. (2016) Structural basis for therapeutic inhibition of complement C5. *Nat Struct Mol Biol*. **23**, 378–386
45. de Jorge, E. G., Yebenes, H., Serna, M., Tortajada, A., Llorca, O., and de Córdoba, S. R. (2018) How novel structures inform understanding of complement function. *Semin Immunopathol*. **40**, 3–14
46. Rawal, N., and Pangburn, M. K. (2000) Functional Role of the Noncatalytic Subunit of Complement C5 Convertase. *The Journal of Immunology*. **164**, 1379–1385
47. Pangburn, M. K., and Muller-Eberhardt, H. J. (1986) The C3 convertase of the alternative pathway of human complement Enzymic properties of the bimolecular proteinase The association of Factor B with C3b (the major fragment of complement component C3) in the presence of Mg2+ results in the formation of. *Biochem. J.* **235**, 723–730
48. van den Bos, R. M., Pearce, N. M., Granneman, J., Brondijk, T. H. C., and Gros, P. (2019) Insights Into Enhanced Complement Activation by Structures of Properdin and Its Complex With the C-Terminal Domain of C3b. *Front Immunol*. **10**, 1–19
49. Fearon, D. T., and Austen, K. F. (1975) Properdin: binding to C3b and stabilization of the C3b-dependent C3 convertase. *J Exp Med*. **142**, 856–863
50. Forneris, F., Bertram, P., Sfyroera, G., Xue, X., Ricklin, D., Wu, J., Liszewski, M. K., Gros, P., Atkinson, J. P., Lin, Z., Tzekou, A., Hauhart, R., Volokhina, E., Granneman, J. C., and Lambris, J. D. (2016) Regulators of complement activity mediate inhibitory mechanisms through a common C3b-binding mode. *EMBO J.* **35**, 1133–1149
51. Lachmann, P. J. (2019) The Story of Complement Factor I. *Immunobiology*. **224**, 511–517
52. Xue, X., Wu, J., Ricklin, D., Forneris, F., Crescenzio, P. Di, Schmidt, C. Q., Granneman, J., Sharp, T. H., Lambris, J. D., and Gros, P. (2018) Regulator-dependent mechanisms of C3b processing by factor I allow differentiation of immune responses. *Nat Struct Mol Biol*. **24**, 643–651
53. Zelek, W. M., Xie, L., Morgan, B. P., and Harris, C. L. (2019) Compendium of current complement therapeutics. *Mol Immunol*. **114**, 341–352
54. Schwab, L., Moll, F. C., Hall, T., Brean, H., Kirk, M., Van Zandt Hawn, C., and Janeway, C. (1950) Experimental hypersensitivity in the rabbit. *J. Exp. Med.* **91**, 505–26
55. Harris, C. L. (2018) Expanding horizons in complement drug discovery: challenges and emerging strategies. *Semin Immunopathol*. **40**, 125–140
56. Bortolotti, M., Barcellini, W., and Fattizzo, B. (2023) Molecular pharmacology in complement-mediated hemolytic disorders. *Eur J Haematol*. 10.1111/ejh.14026
57. Dmytrijuk, A., Robie-Suh, K., Cohen, M. H., Rieves, D., Weiss, K., and Pazdur, R. (2008) FDA Report: Eculizumab (Soliris(R)) for the Treatment of Patients with Paroxysmal Nocturnal Hemoglobinuria. *Oncologist*. **13**, 993–1000
58. Rother, R. P., Rollins, S. A., Mojcik, C. F., Brodsky, R. A., and Bell, L. (2007) Discovery and development of the complement inhibitor eculizumab for the treatment of paroxysmal nocturnal hemoglobinuria. *Nat Biotechnol*. **25**, 1256–1264
59. Lee, J. W., and Kulasekararaj, A. G. (2020) Ravulizumab for the treatment of paroxysmal nocturnal hemoglobinuria. *Expert Opin Biol Ther*. **20**, 227–237

60. Rondeau, E., Scully, M., Ariceta, G., Barbour, T., Cataland, S., Heyne, N., Miyakawa, Y., Ortiz, S., Swenson, E., Vallee, M., Yoon, S.-S., Kavanagh, D., and Haller, H. (2020) The long-acting C5 inhibitor, Ravulizumab, is effective and safe in adult patients with atypical hemolytic uremic syndrome naïve to complement inhibitor treatment. *Kidney Int*. 10.1016/j.kint.2020.01.035
61. Nishimura, J., Yamamoto, M., Hayashi, S., Ohyashiki, K., Ando, K., Brodsky, A. L., Noji, H., Kitamura, K., Eto, T., Takahashi, T., Masuko, M., Matsumoto, T., Wano, Y., Shichishima, T., Shibayama, H., Hase, M., Li, L., Johnson, K., Lazarowski, A., Tamburini, P., Inazawa, J., Kinoshita, T., and Kanakura, Y. (2014) Genetic Variants in C5 and Poor Response to Eculizumab. *New England Journal of Medicine*. **370**, 632–639
62. Schatz-Jakobsen, J. A., Zhang, Y., Johnson, K., Neill, A., Sheridan, D., and Andersen, G. R. (2016) Structural Basis for Eculizumab-Mediated Inhibition of the Complement Terminal Pathway. *The Journal of Immunology*. **197**, 337–344
63. Brachet, G., Bourquard, T., Gallay, N., Reiter, E., Gouilleux-Gruart, V., Poupon, A., and Watier, H. (2016) Eculizumab epitope on complement C5: Progress towards a better understanding of the mechanism of action. *Mol Immunol*. **77**, 126–131
64. Hoy, S. M. (2021) Pegcetacoplan: First Approval. *Drugs*. **81**, 1423–1430
65. Rooijakkers, S. H. M., Ruyken, M., Roos, A., Daha, M. R., Presanis, J. S., Sim, R. B., van Wamel, W. J. B., van Kessel, K. P. M., and van Strijp, J. A. G. (2005) Immune evasion by a staphylococcal complement inhibitor that acts on C3 convertases. *Nat Immunol*. **6**, 920–927
66. Jongerius, I., Köhl, J., Pandey, M. K., Ruyken, M., Van Kessel, K. P. M., Van Strijp, J. A. G., and Rooijakkers, S. H. M. (2007) Staphylococcal complement evasion by various convertase-blocking molecules. *Journal of Experimental Medicine*. **204**, 2461–2471
67. Hong, Y., and Ghebrehiwet, B. (1992) Effect of Pseudomonas aeruginosa elastase and alkaline protease on serum complement and isolated components C1q and C3. *Clin Immunol Immunopathol*. **62**, 133–138
68. Laursen, N. S., Gordon, N., Hermans, S., Lorenz, N., Jackson, N., Wines, B., Spillner, E., Christensen, J. B., Jensen, M., Fredslund, F., Bjerre, M., Sottrup-Jensen, L., Fraser, J. D., and Andersen, G. R. (2010) Structural basis for inhibition of complement C5 by the SSL7 protein from Staphylococcus aureus. *Proc Natl Acad Sci U S A*. **107**, 3681–3686
69. Agrawal, P., Nawadkar, R., Ojha, H., Kumar, J., and Sahu, A. (2017) Complement evasion strategies of viruses: An overview. *Front Microbiol*. 10.3389/fmicb.2017.01117
70. Nunn, M. A., Sharma, A., Paesen, G. C., Adamson, S., Lissina, O., Willis, A. C., and Nuttall, P. A. (2005) Complement Inhibitor of C5 Activation from the Soft Tick Ornithodoros moubata. *The Journal of Immunology*. **174**, 2084–2091
71. Reichhardt, M. P., Johnson, S., Tang, T., Morgan, T., Tebeka, N., Popitsch, N., Deme, J. C., Jore, M. M., and Lea, S. M. (2020) An inhibitor of complement C5 provides structural insights into activation. *Proc Natl Acad Sci U S A*. **117**, 362–370
72. Liu, J. K. H. (2014) The history of monoclonal antibody development - Progress, remaining challenges and future innovations. *Annals of Medicine and Surgery*. **3**, 113–116
73. Hamers-Casterman, C., Atarhouch, T., Muyldermans, S., Robinson, G., Hammers, C., Songa, E. B., Bendahman, N., and Hammers, R. (1993) Naturally occurring antibodies devoid of light chains. *Nature*. **363**, 446–448
74. Conrath, K. E., Wernery, U., Muyldermans, S., and Nguyen, V. K. (2003) Emergence and evolution of functional heavy-chain antibodies in Camelidae. *Dev Comp Immunol*. **27**, 87–103
75. Nguyen, V. K., Hamers, R., Wyns, L., and Muyldermans, S. (2000) Camel heavy-chain antibodies: diverse germline VHH and specific mechanisms enlarge the antigen-binding repertoire. *EMBO J*. **19**, 921–930
76. De Genst, E., Silence, K., Decanniere, K., Conrath, K., Loris, R., Rg Kinne, J., Muyldermans, S., and Wyns, L. (2006) Molecular basis for the preferential cleft recognition by dromedary heavy-chain antibodies. *PNAS*. **103**, 4586–4591
77. Lauwereys, M., Arbabi Ghahroudi, M., Desmyter, A., Kinne, J., Hölzer, W., De Genst, E., Wyns, L., and Muyldermans, S. (1998) Potent enzyme inhibitors derived from dromedary heavy-chain antibodies. *EMBO J*. **17**, 3512–3520

78. Lee, H. T., Park, U. B., Jeong, T. J., Gu, N., Lee, S. H., Kim, Y., and Heo, Y. S. (2021) High-resolution structure of the vWF A1 domain in complex with caplacizumab, the first nanobody-based medicine for treating acquired TTP. *Biochem Biophys Res Commun.* **567**, 49–55
79. De Groof, T. W. M., Bobkov, V., Heukers, R., and Smit, M. J. (2019) Nanobodies: New avenues for imaging, stabilizing and modulating GPCRs. *Mol Cell Endocrinol.* **484**, 15–24
80. Bathula, N. V., Bommadevara, H., and Hayes, J. M. (2021) Nanobodies: The Future of Antibody-Based Immune Therapeutics. *Cancer Biother Radiopharm.* **36**, 109–122

2

Identification of a C3b-specific nanobody that blocks alternative pathway convertases

Eva M. Struijf[1], Jamie S. Depelteau[2], Joanne E. van Keulen[1], Maartje Ruyken[1], Gillian Dekkers[3], Danique Y. Siere1, Edward Dolk[3], Bart W. Bardoel[1], Raimond Heukers[3], Dani A.C. Heesterbeek[1], Suzan H.M. Rooijakkers[1]

[1]Medical Microbiology, University Medical Center Utrecht, Utrecht University, Utrecht, the Netherlands
[2]Structural Biochemistry, Bijvoet Centre for Biomolecular Research, Department of Chemistry, Faculty of Science, Utrecht University, Utrecht, the Netherlands
[3]QVQ Holding BV, Utrecht, the Netherlands
 # Corresponding author: s.h.m.rooijakkers@umcutrecht.nl

ABSTRACT

The human complement system is a protein network in blood that fights invading pathogens and is involved in maintaining homeostasis. Overactivation of the complement system is associated with a wide variety of inflammatory and autoimmune diseases. A central step in the complement reaction is the cleavage of complement protein C3 by C3 convertases. Upon C3 conversion, the anaphylatoxin C3a is released and the remaining C3b molecule undergoes a conformational change after which it mediates several important effector functions, such as opsonization and convertase formation. In this study we developed nanobodies that specifically target activated C3b but not precursor C3. Phage libraries were generated from llamas immunized with purified C3b. After phage display panning and screening of crude periplasmic extracts, we identified eight unique clones that bound better to C3b than to C3 in ELISA. After purification and characterization, we prioritized one nanobody (UNbC3b-1) that binds C3b with a high apparent affinity, recognized surface-bound C3b, and efficiently inhibits complement activity in the alternative pathway. Using flow cytometry and size exclusion chromatography, we showed that UNbC3b-1 specifically recognizes C3b but not C3. AlphaFold2 predictions indicate that UNbC3b-1 interacts with C3b via the MG8 and CUB domains. Functional studies revealed that UNbC3b-1 inhibits C3b and C5b-9 deposition in the alternative pathway, but not the classical pathway. Further mechanistic studies revealed that UNbC3b-1 acts at the level of the AP C3/C5 convertase. While UNbC3b-1 prevents cleavage of C3 and C5 by purified convertases, it does not prevent formation of proconvertase C3bB or C3bBb. Altogether, we developed and characterized a novel nanobody that specifically binds to C3b and inhibits AP convertases.

INTRODUCTION

The complement system is a large protein network in blood that is part of the human innate immune system. It is involved in maintaining homeostasis, by removal of apoptotic cells and immune complexes, and plays a crucial role in the fight against invading pathogens (1, 2). Activation of the complement system (via the classical (CP), lectin (LP) or alternative pathway (AP)) results in the formation of enzymatic complexes (C3 convertases) that cleave central complement component C3 into C3a and C3b (1, 2). Cleavage of C3 initiates the formation of pro-inflammatory chemoattractants (C3a and C5a), opsonins (e.g. C3b and iC3b) and membrane attack complexes (MAC) that can directly lyse target cells. The complement system is tightly regulated to prevent uncontrolled activation, nevertheless unwanted overactivation is associated with a wide variety of inflammatory and autoimmune diseases, including paroxysmal nocturnal hemoglobinuria (PNH), C3 glomerulopathy (C3G), age-related macular degeneration (AMD), rheumatoid arthritis, and many other diseases (3–5).

Native C3 is a large protein (~186 kDa) comprised of an alpha chain (~120 kDa) and a beta chain (~75 kDa) that are covalently bound to each other (6, 7). The protein consists of eight macroglobulin (MG) domains, a linker domain (LNK), an anaphylatoxin domain (ANA), a complement C1r/C1s, Uegf, Bmp1 (CUB) domain, a thioester-containing domain (TED), and a C-terminal domain (C345c or CTC) (8, 9). The ANA domain (C3a), which is cleaved off during C3 conversion, is located near the center of the molecule and has a size of 9 kDa. The remaining C3b molecule has a size of 177 kDa and undergoes major conformational rearrangements in which the CUB and TED domains make the largest movements, exposing the reactive thioester with which C3b attaches to a surface (**Fig. 1A**).

Activation of the CP and LP, initiates a proteolytic cascade involving complement proteins C1, C2 and C4 on the target cell surface, which results in the formation of the CP/LP C3 convertase, C4b2b (1). The AP is initiated when C3b molecules are formed via the CP and LP, or when C3 is hydrolyzed into the conformationally C3b-like molecule, C3(H_2O). Together with C3b, or C3(H_2O), complement components Factor B (FB) and Factor D (FD) form the AP C3 convertase, C3bBb (1). Active AP C3 convertases interact with native C3 molecules via the MG4-5 domains in C3 and C3b (10). This interaction docks the scissile loop of C3 into the active site of the serine protease (SP) domain of Bb and allows C3 cleavage. The small anaphylatoxin domain, C3a is released in the fluid phase, where it functions as a chemoattractant and C3b deposits on the nearest surface by interacting with its newly exposed reactive thioester in the TED domain (11, 12). Deposited C3b functions as an opsonin, helping phagocytic cells to recognize

and engulf target cells (1, 2). Furthermore, newly deposited C3b molecules induce an amplification loop when they interact with FB and FD, forming new AP C3 convertases, that in turn convert many other C3 molecules. When the deposition of C3b molecules reaches a high density, C3 convertases switch substrate from C3 to C5, forming C5 convertases (CP/LP: C4b2bC3b, AP: C3bBbC3b) (13–16). Newly formed C5 convertases cleave circulating complement component C5, in anaphylatoxin C5a and activation product C5b, which initiates the formation of the target cell lysing MAC.

To regulate the function of C3b, multiple complement molecules, such as Factor H (FH) and Factor I (FI) interact with the newly exposed interfaces in C3b that appear after the release of C3a and the major conformational rearrangements in the CUB and TED domains (17). In a stepwise manner, fragments or domains are removed from the alpha chain to eventually inactivate all functions of C3b (1). First, FH binds C3b, after which FI interacts and removes the small fragment C3f, transforming C3b into iC3b. iC3b can no longer bind the convertase, but still acts as an opsonin. Next, FI cleaves iC3b again, releasing the larger C3c part in the fluid phase and retaining the C3dg domain on the target cell surface. Finally, C3dg is cleaved by different plasma proteases into the inactive C3d fragment.

Next to different C3(b)-regulating proteins from within the complement system, many bacterial and viral pathogens have evolved proteins to evade complement activity at the level of C3(b) (18). For example, *Staphylococcus aureus* expresses SCIN, Efb and Ecb, three different proteins that bind C3b(Bb) and inhibit convertase functioning (19, 20). *Pseudomonas aeruginosa* expresses PaE and PaAP, proteins that degrade C3 (21). Different poxvirus, including vaccina virus, variola virus, and cowpox virus express proteins (VCP, SPICE and IMP, respectively) that mimic C3b-binding regulators to prevent convertase formation (22). Next to pathogen-derived molecules, a wide variety of C3-targeting molecules, including peptides, monoclonal antibodies and nanobodies have been developed in the last decades to inhibit complement activity (23). The compstatin family, consisting of multiple cyclic peptides that inhibit C3 conversion by binding C3 and C3b, is investigated best (24). Pegcetacoplan (or Empaveli®), is a second-generation analog of compstatin, and was recently approved by the FDA as the first (and still only) C3-targeting molecule in the clinic (23, 25). It is now used for the treatment of the complement-mediated disease PNH and is under (pre-)clinical investigation for other diseases including C3G, AMD, periodontitis, transplantation, and respiratory distress syndrome in COVID-19 patients (24, 26, 27). Next to the compstatin family, multiple other C3/C3b-targeting compounds are described in literature. For example, multiple C3b binding monoclonal antibodies have been described, such as S77 (28, 29), 3E7 (30), 4C2 (31) and anti-C3-9 (32) and C3/C3b-binding nanobodies hC3Nb-1-3 (33–35). By studying

their binding site and inhibitory profiles, these molecules have proven their use in further understanding the molecular mechanisms of complement activation.

In this study we describe the development and characterization of a novel llama derived anti-C3b nanobody that inhibits complement activity. We show that our high affinity nanobody specifically binds to C3b, and not to C3. It potently inhibits the alternative, but not the classical, complement pathway. Mechanistic studies indicate that this nanobody blocks substrate cleavage by AP convertases.

RESULTS

Immunization of two llamas with human C3b

To develop C3b-specific nanobodies, two llamas were first immunized with four injections of purified human C3b (**Fig. 1B**). Subsequently, llamas were boosted with two injections containing C3b-opsonized bacteria to steer the llama's immune response towards C3b-epitopes that are available when C3b is in the surface-bound orientation. To monitor the immune response and create nanobody phage libraries, blood was drawn at day 0, 43, and 99 to collect serum and peripheral blood mononuclear cells (PBMCs). We confirmed that immunizations produced C3b-binding antibodies at day 43 and 99, that were not present at day 0, by incubating C3b-coated microtiter plates with llama sera and detecting antibody binding to C3b (**Fig. 1C**). Next, phagemid libraries were produced with nanobody genes isolated from the PBMCs collected at day 99. This yielded two phagemid libraries, each with a size of 10^9 clones.

Beads coated with high densities of C3b were used as a bait during phage display (16). Briefly, C3b was biotinylated via its thioester moiety and incubated with magnetic streptavidin beads. This way, C3b is placed on the bead surface in its natural orientation. We performed different phage display panning strategies to obtain a diverse panel of nanobodies recognizing C3b but not precursor C3. For example, phages were incubated with high-density C3b-beads, in the presence of high concentrations C3 and C3b in solution. Next, unbound phages and phages bound to C3 and C3b in solution were removed by extensive washing of the beads (negative selection). Phages bound to high density C3b-beads were subsequently eluted using a high pH buffer (positive selection). Eluted phages were rescued by infection in *E. coli* TG1. This generated bacterial output libraries for each selection strategy, in which each bacterium carried a plasmid encoding for one nanobody gene. In total, we made nine combinations of positive and negative selections, with either one or two rounds of panning (**Table 1**). Selection strategy #6,

which only consisted of one round of panning, eventually yielded the nanobody that was characterized most extensively in this study.

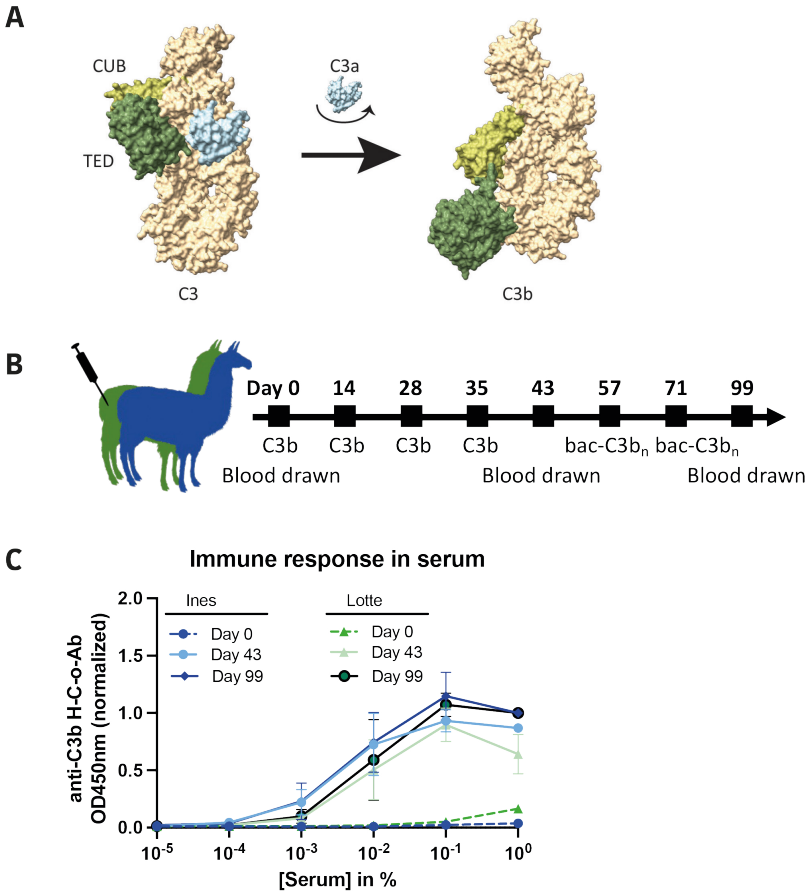

Figure 1: Immunization of two llamas with human C3b. (A) Schematic presentation of structural rearrangements upon C3 cleavage into C3a (light blue) and C3b (beige and green), using the published structures of C3b (PDB 2i07) and C3 (PDB 2a73) and depicted in a space filling representation. The CUB (light green) and TED (dark green) domains are highlighted (B) Immunization scheme of the two llamas, immunized with purified human C3b and bacteria opsonized with high densities of C3b molecules (bac-C3b$_n$). (C) Detection of anti-C3b antibodies in llama serum before immunizations (day 0), after immunizations with purified C3b in solution (day 43) and after immunizations with C3b-opsonized bacteria (day 99). C3b-binding llama antibodies were detected in an ELISA setup using polyclonal rabbit-anti-nanobody QE19 antibodies and donkey-anti-rabbit-HRP antibodies, at an OD of 450 nm. Data represents mean ± SD of 2 individual experiments.

Screening for C3b specific binders

Bacterial output libraries were cultured and plated to obtain single colonies. 92 randomly picked clones (derived from different selection strategies) and 4 negative controls were cultured in single wells. Next, 76 individual clones were successfully sequenced, revealing 29 clusters with clonally related nanobodies (>80% amino acid sequence similarity in their complementarity determining region (CDR) H3 (CDR-H3)) (**SFig. 1A**). Most of the clones originated from the IGHV3-3*01 and IGHJ4*01 germline sequences, while a small number originated from IGHV3S53*01 and IGHJ6*06 (based on IMGT database (36, 37)). Half of the clusters (14/29) contained >1 clone per cluster. The largest cluster (#22) contained 20 clones, the second largest cluster (#1) contained 9 clones, followed by a cluster (#15) with 5 clones (**SFig. 1A & B**). These numbers indicate that our phage display strategy enriched for specific CDR-H3 clusters, of which individual clones were assessed for binding to C3b.

To screen for C3b-specific nanobodies, nanobodies were expressed in the periplasm of *E. coli* BL21. Crude periplasmic extracts with unknown concentrations of the nanobodies (peri-Nbs), were obtained after a cycle of freeze-thawing. Next, peri-Nbs were used to identify C3b-binding nanobodies that do not bind to precursor C3. Briefly, C3b- and C3-coated microtiter plates were incubated with peri-Nbs and nanobody binding to both proteins was measured. Next the ratio C3b:C3 binding was calculated and the clones with the highest ratio were considered interesting to follow-up. Interestingly, >70% of our clones had a C3b:C3-binding ratio >1 (**Fig. 2A**, left panel) and 25% had a ratio >1.5 (**Fig. 2A**, right panel). Next, we compared the sequences of the top 25% and selected a panel of eight clones with diverse CDR1, CDR2 and CDR3 regions, and derived from different clusters, for follow up (**Fig. 2B & SFig. 1A & C**).

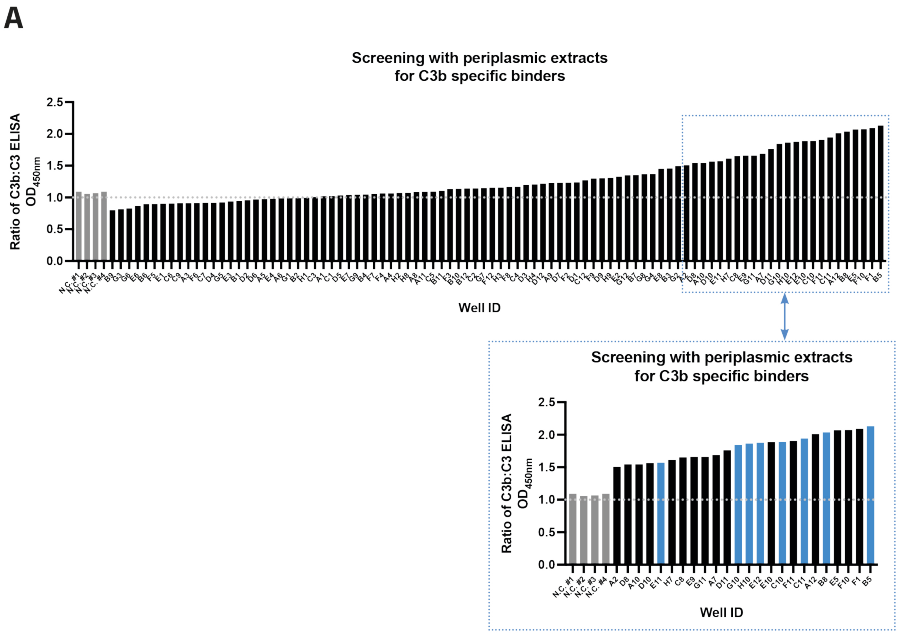

Figure 2: Screening for C3b specific binders. (A) C3b vs C3 binding pattern in ELISA of 92 unpurified periplasmic extracts containing an unknown concentration of nanobody. Negative controls were: #1 periplasmic extract of an irrelevant nanobody; #2 & #4 no bacteria present during culturing; #3 bacteria transformed with empty vector. Microtiter plates coated with C3b and C3 were incubated with periplasmic nanobody extracts (1:5 diluted in PBS), and binding of nanobodies was detected using polyclonal rabbit-anti-VHH QE19 antibodies and donkey-anti-rabbit-HRP antibodies, at an OD of 450 nm. The ratio of C3b:C3 binding was calculated and plotted on the y-axis. Fractions with ratios >1.5 were highlighted in the right panel. Blue colored bars indicate clones that were selected to purify and characterize further. Data presented are of 1 individual experiment. (B) Protein sequence alignment of the eight selected clones from (A). Amino acids annotation is according to the shapely color scheme.

Selection of UNbC3b-1 (clone B5) as specific and inhibitory anti-C3b nanobody

Next, the eight selected clones were expressed with a Myc- and 6×His-tag in *E. coli* and purified for further characterization. First, we assessed if the purified nanobodies could efficiently bind C3b in ELISA. To do so, C3b was randomly immobilized on microtiter plates and nanobodies were added in serial dilutions. Next, nanobodies were detected with polyclonal rabbit-anti-nanobody antibodies and EC50 values were calculated to determine the apparent binding affinities. Clones B5, C11, E11, E12 and G10 bound C3b with an apparent affinity in the low nanomolar range (~0.2-9.0), while clones B8, C10 and H10 bound C3b with apparent affinities of >40 nM (**Fig. 3A**). Next, we assessed if the nanobodies recognize C3b in a surface-bound orientation. To do so, nanobodies were incubated with C3b-beads as described above. Except for C10 and C11, all clones recognized surface-bound C3b, at least to some extent (**Fig. 3B**).

To confirm that the nanobodies specifically bound C3b but not precursor C3, we assessed nanobody binding to high density C3b-beads in the presence of C3 in solution. While soluble C3 decreased binding to C3b-beads of nanobodies E11, H10, and B8, the binding of clones B5, G10 and E12 was not affected by soluble C3 (**Fig. 3C**). Since this indicates that clones B5, G10 and E12 are most specific for C3b, we continued with these three clones.

To assess if clones B5, G10 and E12 inhibit complement activity we performed erythrocyte lysis assays for the AP and CP. Briefly, we incubated rabbit (AP) and antibody-opsonized-sheep (CP) erythrocytes with human serum (10% (AP) and 2.5% (CP)) and different concentrations of the nanobodies. While none of the C3b-specific nanobodies could inhibit the CP, we found that clones B5 and E12 inhibited the AP in a dose-dependent manner (**Fig. 3D & E**). Results for other clones can be found in **SFig. 2A & B**.

Taken all data together, we selected clone B5 from the panel as the most C3b-specific nanobody that also efficiently inhibits the alternative pathway of complement. From now on, we will refer to this clone (B5) as UNbC3b-1. To facilitate further characterization of UNbC3b-1 and allow direct detection and coupling of this nanobody, we cloned the UNbC3b-1 gene in a vector that replaced the Myc- 6×His-tag for an LPETG- 6×His-tag. UNbC3b-1 could now be used directly (UNbC3b-1-LH), or when labeled after sortagging with biotin (UNbC3b-1-bio) or fluorophore Alexa fluor 488 (UNbC3b-1-a488) (38). We confirmed that a change in expression system and the introduction of these tags, did not affect the ability of UNbC3b-1 to bind C3b (**SFig. 4A**) or inhibit complement activity via the AP (**SFig. 4B**).

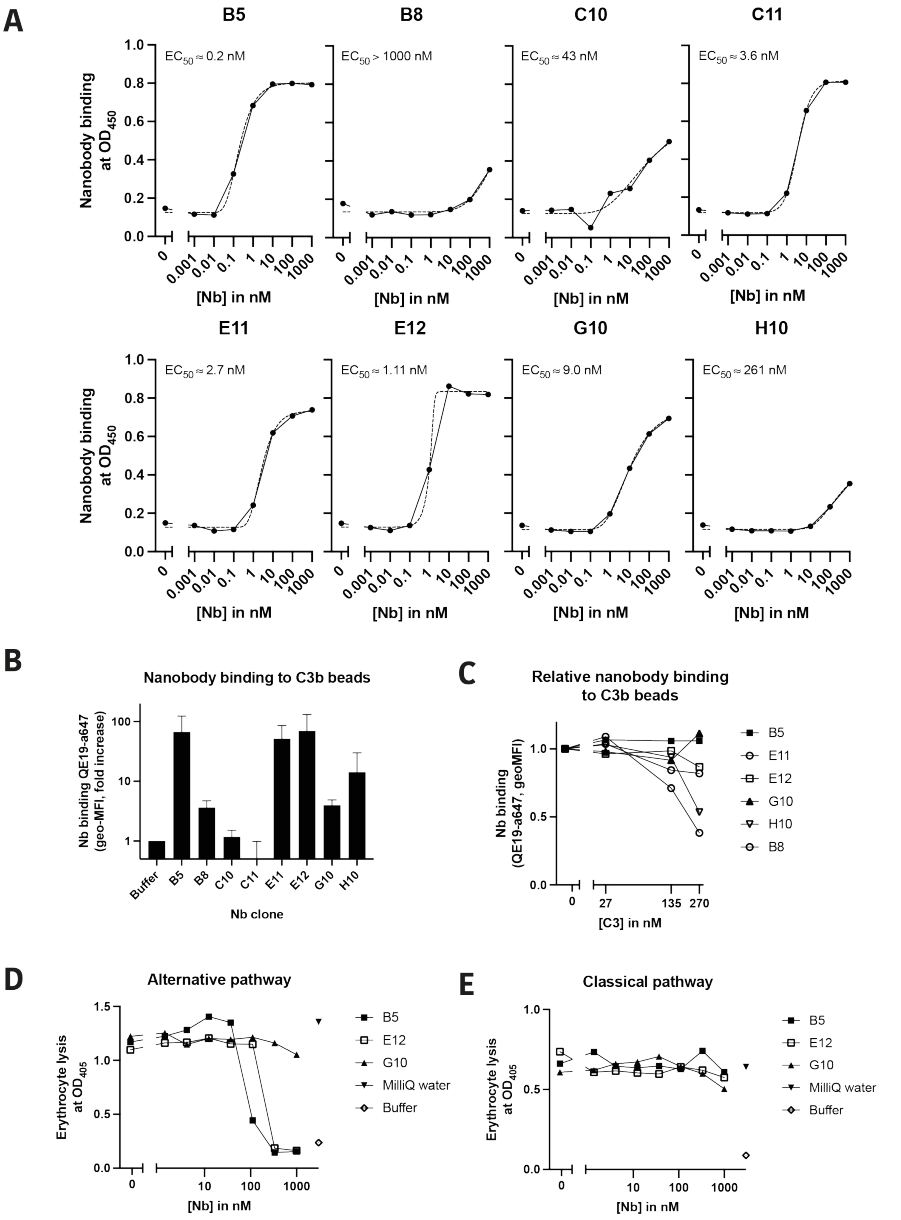

Figure 3: Selection of UNbC3b-1 (clone B5) as specific and inhibitory anti-C3b nanobody. (A) Nanobody binding to C3b in ELISA. Microtiter plates coated with C3b were incubated with a concentrations range of purified nanobody (clones B5, B8, C10, C11, E11, E12, G10 and H10). To obtain EC50 values (or apparent affinities) binding curves were fitted in GraphPad using the formula "Asymmetric Sigmoidal, 5PL, X is concentration". Data represent OD450 values of 1 individual experiment. (B) Nanobody binding to C3b molecules on a bead surface. C3b-beads were incubated

with buffer or 100 nM purified nanobody. Nanobody binding was detected using fluorescently labeled (Alexa 647) anti-VHH QE19 antibodies and measured by flow cytometry. The fold increase over the background (buffer sample) fluorescent signal was calculated and plotted on the y-axis. Data represent mean ± SD of two individual experiments. (C) Nanobody's specificity towards C3b. C3b-beads were incubated with 100 nM nanobody and increasing concentrations of C3. Nanobody binding was detected using fluorescently labeled (Alexa 647) anti-VHH QE19 antibodies and flow cytometry. Data were normalized to the condition without C3, and relative levels of nanobody binding were plotted on the y-axis. Data presented are of one individual experiment. (D) AP-mediated hemolysis of 2% rabbit erythrocytes (raE) incubated with 10% human serum and nanobodies in different concentrations (E) CP-mediated hemolysis of 2% antibody-opsonized sheep erythrocytes (shEA) incubated with 2.5% human serum and nanobodies in different concentrations. (D-E) The OD450 of the supernatant was detected as a measure of erythrocyte lysis. MilliQ and buffer were taken along as controls for 100% and 0% lysis, respectively. Data present values of one individual experiment.

UNbC3b-1 specifically binds C3b with high affinity

Next, we wanted to confirm with multiple assays that UNbC3b-1 is a C3b-specific nanobody that does not bind to C3 and other complement proteins. First, we repeated the C3b-bead competition experiment from figure 3C. Next to adding C3 in solution, we also tested the effect of soluble C3b. We observed that UNbC3b-1 binding to C3b-beads is only decreased when C3b is added in high concentrations, but not when C3 is added (**Fig. 4A**). To further assess specificity, we performed an ELISA in which microtiter plates were coated with complement proteins Bb, C4, C4b, C5, C5a, C5b6, and C6 and nanobody binding was measured. UNbC3b-1 did not cross-react with any of the other complement proteins (**SFig. 3**), except for some binding to C4 and C4b in the highest concentration tested. When we coated microtiter plates with C3b and C3, UNbC3b-1 also bound to C3 in several repeats of the experiment, albeit with lower apparent affinities than measured for C3b (**Fig. 4B**). This could indicate that UNbC3b-1, in absence of competitive pressure from C3b, binds to precursor C3. However, since C3 is easily hydrolyzed when in contact with a surface (39), we hypothesized that the observed binding here could be because the nanobody binds to the hydrolyzed form of C3 (C3(H_2O)), which is known to adopt a C3b-like conformation (40). To confirm this (and assess C3b-specificity with a different set-up) we performed size exclusion chromatography (SEC). We incubated UNbC3b-1-a488 with C3, C3b or C3 methylamine (C3-MA) in a 1:1 molar ratio. Treatment of C3 with the nucleophilic reagent methylamine allows C3 to adopt C3b-like properties (41). Samples were loaded on a Superose 6 Increase column and the OD280 and OD488 (to detect UNbC3b-1) were measured. As controls C3b, C3, C3-MA and UNbC3b-1 were applied to the column alone and the obtained chromatograms indicated that C3, C3b, and C3-MA elute in fractions between 1.5-2.0 mL, while UNbC3b-1 elutes in fractions between 2.0-2.2 mL (**SFig. 5A-D**). When UNbC3b-1 was incubated with C3b, UNbC3b-1 was eluted together with C3b in the fractions between 1.5-2.0 ml, indicating complex

formation in solution (**Fig. 4C**). When UNbC3b-1 was incubated with C3, UNbC3b-1 eluted later than C3, indicating that UNbC3b-1 does not bind C3 in solution (**Fig. 4D**). Interestingly, when UNbC3b-1 was incubated with C3-MA, the nanobody was eluted both in the fractions of C3-MA and in the fractions of the nanobody, indicating that UNbC3b-1 binds to C3-MA to some extent (**Fig. 4E**). This might explain why we measured some binding to C3 (or C3(H_2O)) in the ELISA set-up.

The kinetics of UNbC3b-1 binding to C3b was studied using surface plasmon resonance (SPR). Here, we captured UNbC3b-1-bio onto streptavidin-coupled probes and incubated those subsequently with C3b and buffer to measure association and dissociation rates. Fitting this with a 1:1 Langmuir model results in an on-rate (k_{on}) of ~4×10^{5} $M^{-1}s^{-1}$, an off-rate (k_{off}) of ~1.3×10^{-4} s^{-1}, and a calculated equilibrium binding affinity constant (K_D) of ~340 pM. However, as the obtained curves did not completely fit with 1:1 model, the affinity obtained from this experiment is merely a rough indication of its actual affinity (**Fig. 4F**). All this together confirms that UNbC3b-1 is a high affinity, C3b specific nanobody, that binds to C3b on a surface, C3b in solution and to some extent also to C3-MA, the C3(H_2O)-like molecule.

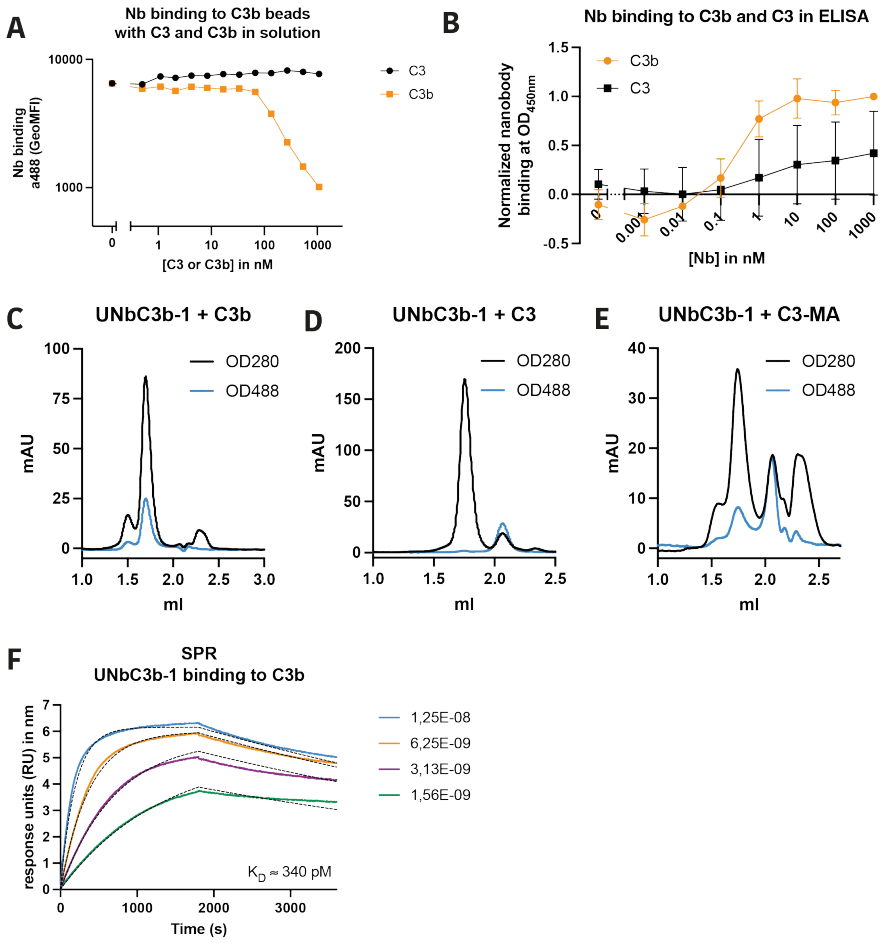

Figure 4: UNbC3b-1 specifically binds C3b with high affinity. (A) Binding of 100 nM UNbC3b-1-a488 to C3b-beads in the presence of increasing concentrations of C3b and C3 in solution, as detected by flow cytometry. Data presented are of one individual experiment. (B) ELISA to measure UNbC3b-1 binding to C3b and C3 coated on microtiter plates. Nanobody binding was detected using polyclonal rabbit-anti-VHH QE19 antibodies and donkey-anti-rabbit-HRP antibodies, at an OD of 450 nm. Data were normalized to the condition in which 1000 nM UNbC3b-1 was added to C3b. Data represent mean ± SD of 3 individual experiments. (C-E) Chromatograms obtained with SEC, using a Superose 6 Increase column and measuring absorbance at an OD of 280 nm (indicating the presence of protein, black) and of 488 nm (indicating the presence of fluorescence, blue). UNbC3b-1-a488 was incubated with C3b (C), C3 (D) or C3-MA (E). Data present values of 1 individual experiment. (F) Binding affinity curves of UNbC3b-1 obtained with a White Fox optic surface plasmon resonance (FO-SPR) sensor, using streptavidin FO-SPR probes, UNbC3b-1-biotin (330 nM) as an analyte and C3b (1.56 – 12.5 nM) as a ligand. Immobilization of UNbC3b-1-biotin was performed for 300 seconds, association was measured for 1800 seconds and dissociation for 7200 seconds, all at 26°C, while shaking at 1000 rpm. Experimental data is shown in colors and

model fit in black dotted lines. Curves were fitted with TraceDrawer, using a 1:1 model with global B_{max} (6.32), global k_{on} (4.03×10^{5} $M^{-1}s^{-1}$), global k_{off} (1.37×10^{-4} s^{-1}) and a constant BI (0.0 Signal). Data are representative for two individual experiments.

Binding of UNbC3b-1 to C3 fragments and competition with known C3/C3b inhibitors

Next, we tried to identify the binding site of UNbC3b-1 on C3b. First, we coated a microtiter plate with different C3 fragments and measured nanobody binding. UNbC3b-1 bound to iC3b and C3c, the larger C3 fragments, but not to the smaller fragments C3dg, C3d, C3a and C3a-desArg (**Fig. 5A**). This allowed us to exclude the ANA and TED domains of C3b as potential binding sites. Next, we performed a competition ELISA with different C3b-binding molecules of which the binding sites on C3b are known. We coated a microtiter plate with C3b and then added a mixture of UNbC3b-1-bio and a concentration series of other C3b-binding molecules as competitors. As a positive control for competition, we took along unbiotinylated UNbC3b-1-LH. Interestingly, of the 17 tested molecules, only one molecule (hC3Nb2) could decrease the binding of UNbC3b-1 to C3b (**Fig. 5B**). This nanobody called hC3Nb2 is identified and described by Pedersen et al. (34). Of note, the absence of competition with all other molecules tested here does not necessarily indicate that UNbC3b-1 does not bind C3b on one of these epitopes. Any absence of competition could also be a consequence of the high affinity of UNbC3b-1, making it complicated to detect competition with low(er) affinity molecules. A different competition setup, with for example pre-incubation with an excess of competitors, might provide a better insight, but was not attempted here.

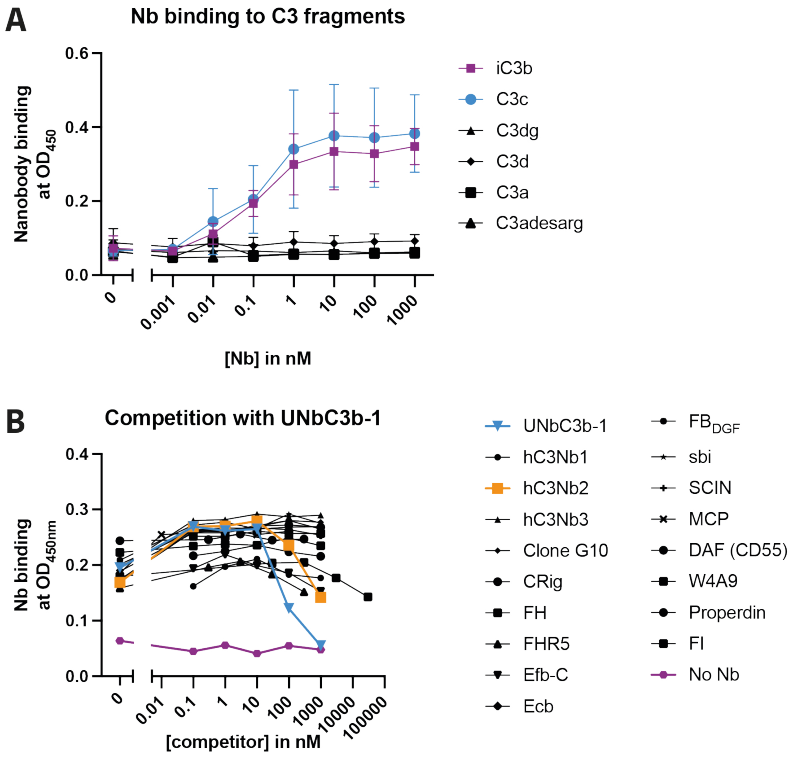

Figure 5: Binding of UNbC3b-1 to C3 fragments and competition with known C3/C3b inhibitors. (A) ELISA with UNbC3b-1-bio binding to different C3 fragments coated on microtiter plates. Nanobody binding was detected using streptavidin-HRP. Curves of iC3b (purple) and C3c (blue) are colored to highlight that UNbC3b-1 binds to these fragments. Data represent mean ± SD of 2 individual experiments. (B) Competition ELISA with C3b coated on microtiter plates that were incubated with 10 nM UNbC3b-1-biotin and different concentrations of other C3b-binding molecules. UNbC3b-1-bio binding was measured using streptavidin-HRP. Unlabeled UNbC3b-1 (blue) was taken along as a positive control for competition and a sample with no nanobody (purple) was taken along as measure of background binding. The curve of hC3Nb2 (orange) is highlighted in color since this curve indicates competition with UNbC3b-1-biotin. Data present values of one individual experiment.

UNbC3b-1 inhibits AP on the level of C3b and C5b-9 deposition

Next, we wanted to unravel the mechanism by which UNbC3b-1 blocks the AP. First, we performed complement deposition ELISAs to determine at what level the nanobody inhibits complement activity. As positive controls, we took along multiple known complement inhibitors, such as Eculizumab (C5 inhibitor, also known as Soliris®, (42)), compstatin derivative W4A9 (C3 inhibitor,(43)), SCIN (AP convertase inhibitor, (20)) and BBK32 (C1r inhibitor, (44)). As expected, UNbC3b-1 inhibited AP-mediated C5b-9

deposition (**Fig. 6A**), but here we also identified that UNbC3b-1 prevents AP-mediated C3b deposition (**Fig. 6B**). Like observed before, UNbC3b-1 does not interfere with CP-mediated C3b (**Fig. 6C**) and C5b-9 (**Fig. 6D**) deposition. Thus, UNbC3b-1 is an AP specific inhibitor that blocks C3b deposition and prevents formation of MAC pores.

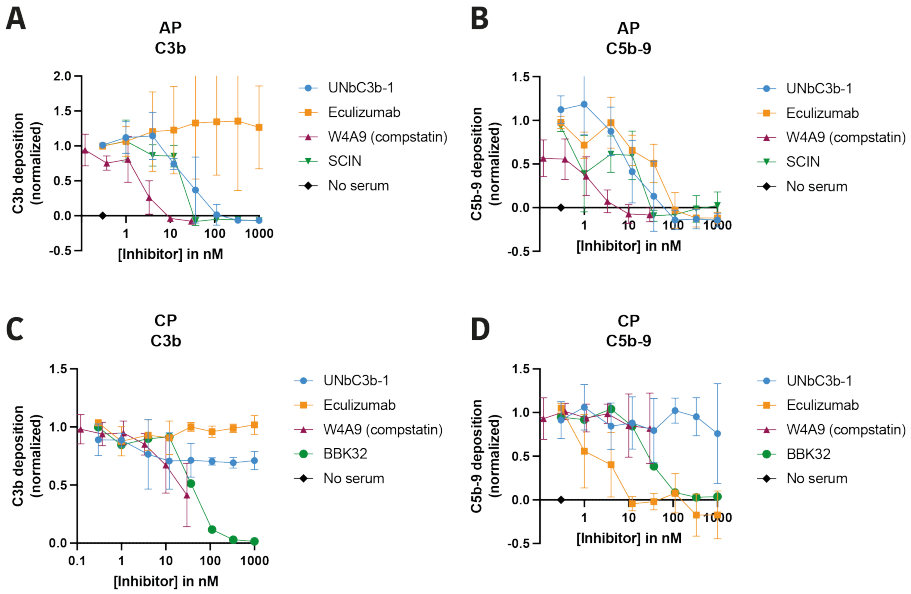

Figure 6: UNbC3b-1 inhibits the AP on the level of C3b and C5b6 deposition. (A-D) Complement deposition ELISAs with UNbC3b-1 as an inhibitor. (A-B) AP activation on an LPS-coated microtiter plate, incubated with 10% human serum and different concentrations of inhibitors. (C-D) CP activation on an IgM-coated microtiter plate, incubated with 2.5% human serum and different concentrations of inhibitors (A-D) Deposition of complement activation products C3b (A & C) and C5b-9 (B & D) on the plate was measured using specific anti-C3 and anti-C5b-9 antibodies and HRP-coupled secondary antibodies, at OD450. Data points were normalized to the condition without inhibitor and graphs represent mean ± SD of three individual experiments.

UNbC3b-1 does not block (pro)convertase formation

Since we observed that UNbC3b-1 binds to C3b and prevents C3b deposition, we hypothesized that its mechanism of action might be on the level of the C3 convertase. AP C3 convertases are formed when covalently deposited C3b molecules (from the AP, or from the CP/LP) are bound by FB and FD. This forms the initial proconvertases C3bB, and next the active C3 convertases C3bBb. This will cleave more C3 molecules and initiates an amplification loop. Here, we assessed if UNbC3b-1 inhibits complement activity by preventing C3bB and/or C3bBb formation. To study this, we used C3b-beads that allow us to functionally assess AP convertases in a purified manner (16). First, we studied whether UNbC3b-1 could prevent formation of proconvertases. To do so,

C3b-beads were incubated with UNbC3b-1 and fluorescently labeled FB_{WT} or a double gain of function mutant of FB (FB_{DGF}) that binds C3b more stably. FB binding to C3b-beads was assessed using flow cytometry. Interestingly, UNbC3b-1 did not inhibit C3bB formation since FB (WT or DGF) binding to C3b was unaffected in the presence of the nanobody (**Fig. 7A & B**). Next, we also added FD to generate active convertases (C3bBb) from proconvertases (C3bB) and again measured Bb binding to C3b-beads. Also in this setup, UNbC3b-1 did not block Bb binding to C3b-beads (**Fig. 7A & B**). Then, we tested if FD could still cleave FB in Ba and Bb in the presence of UNbC3b-1. To test this, C3b (in solution (**Fig. 7C)** or on beads (**Fig. 7D**)) was incubated with FB_{DGF}, FD and UNbC3b-1, in varying sequences/orders with 10-minute-incubation steps in between (indicated with an →). Next, supernatants were analyzed for Bb formation, using western blot. In all tested sequences in which FD was present, we observed that FB was cleaved into Bb (**Fig. 7 C & D**). The presence of UNbC3b-1 did not influence this, indicating that UNbC3b-1 does not prevent formation of an active convertase enzyme.

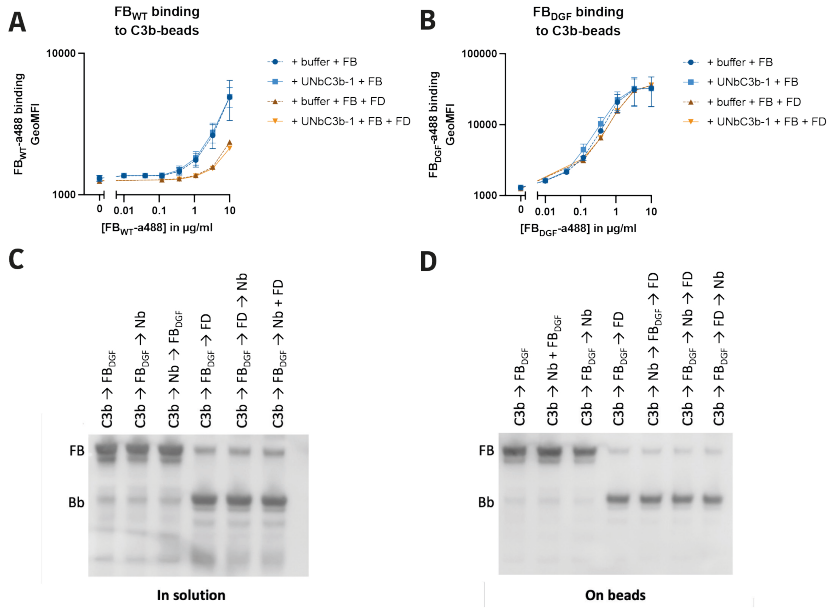

Figure 7: UNbC3b-1 does not block (pro)convertase formation. (A-B) Interaction of fluorescently labeled FB_{WT} (A) or FB_{DGF} (B) with C3b beads in the presence of UNbC3b-1 and/or FD. Binding of FB_{WT}-a488 to the beads was assessed using flow cytometry. Data represent mean ± SD of 2 individual experiments. (C-D) Cleavage of FB by FD in the presence or absence of UNbC3b-1, using C3b in solution (C) or C3b-beads (D). Proteins were added in different orders (see lanes) and Bb formation as assessed by western blot using polyclonal anti-FB-HRP labeled antibodies. Bb can be distinguished from uncleaved FB based on the height of the band (corresponding to protein size). Data presented are of one individual experiment.

UNbC3b-1 inhibits C3 and C5 cleavage by C3bBb

Here, we assessed if UNbC3b-1 inhibits substrate cleavage by the convertase. To do so, we incubated C3b-beads with UNbC3b-1, FB_{DGF}, FD and substrate C3 and added the supernatants to C3aR-cell lines, to measure presence of C3a. Indeed, we observed that UNbC3b-1 inhibits C3 cleavage by C3bBb-beads (**Fig. 8A,** purple line). Interestingly, when we introduced a washing step (indicated with @) before adding C3, UNbC3b-1 could no longer prevent C3 cleavage (**Fig. 8A,** green line). Next, we wondered if UNbC3b-1 could also inhibit C5 cleavage by the convertase. To do so we repeated the experiment, but now used C5 as a substrate instead of C3 and added the supernatants to C5aR cells to detect C5a presence. Interestingly, UNbC3b-1 did also inhibit C5 conversion (**Fig. 8B**, purple line). Next, we tested whether the inhibitory effect of UNbC3b-1 could be diminished by introducing a similar washing step as we did in the experiment with C3. Intriguingly, UNbC3b-1 could also no longer inhibit C5 cleavage in this experimental set-up (**Figure 8B**, green line).

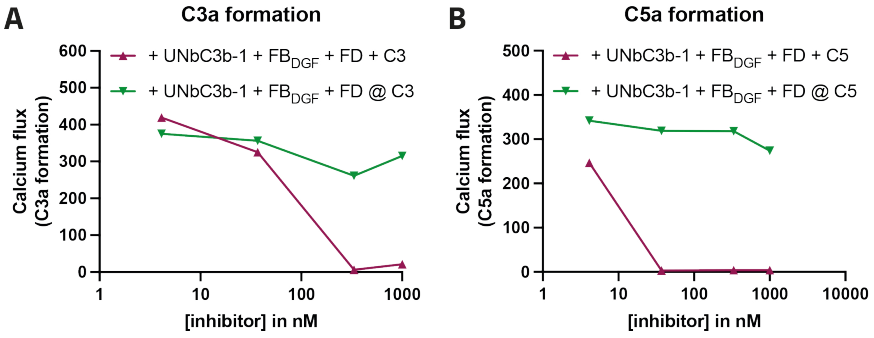

Figure 8: UNbC3b-1 inhibits C3 and C5 cleavage by C3bBb. (A & B) Calcium flux assay to measure C3a (A) and C5a (B) formation using C3b-beads and convertase components. Components were sequentially added to C3b-beads with 10-minute-incubation steps at RT in between. Washing steps are indicated with an '@'. Components were added in the following concentrations 20 µg/mL FBDGF, 5 µg/mL FD, 4.1 – 1000 nM UNbC3b-1, 20 µg/mL C3/C5. C3a and C5a levels were measured by adding the reaction supernatant to U937 C3aR and U937 C5aR cells, respectively, and cells were primed with fluo-3-AM ester, to measure calcium fluxes. Fluorescent signals were used as a measurement of ligand binding and thus C3a and C5a formation. Data are representative for two individual experiments.

AlphaFold2 prediction of UNbC3b-1 binding site on C3b

In a final attempt to clarify the exact mechanism of inhibition of UNbC3b-1, we tried to unravel the exact binding site of UNbC3b-1 on C3b. To do so, we made an *in-silico* prediction model of its potential binding site using AlphaFold2 (AF2) and superimposed this on published C3(b) and convertase structures. The software yielded 5 models that were ranked on confidence (**Fig. 9A**), with model 1 being most reliable (**Fig. 9B**). In rank 1 (orange), UNbC3b-1 is predicted to bind C3b by interacting with the MG8 and CUB domain, while facing the CUB domain (**Fig. 9B**). In rank 2 (red) and 5 (blue), UNbC3b-1 was predicted in a similar area as rank 1, but with slightly different orientations (**Fig. 9A**). In rank 4 (pink), UNbC3b-1 is predicted to bind the MG2 and CUB domains. In rank 3 (purple), UNbC3b-1 is predicted to bind to the MG7 and MG8 domains of C3b. Interestingly, in this prediction a clear clash between C3b and the nanobody can be observed (**Fig. 9A**, panel 3). Furthermore, the AF2 prediction of C3b was slightly different form the published structure of C3b (PDB 2i07). Since the rank 1 prediction was assigned the highest confidence value by AF2, we superimposed this prediction on the published structures of C3b (**Fig. 9C**, PDB 2i07), C3 (**Fig. 9D**, PDB 2a73) and C3bBb (**Fig. 9E**, PDB 2WIN) and tried to interpret if the predicted model matches our biochemical data.

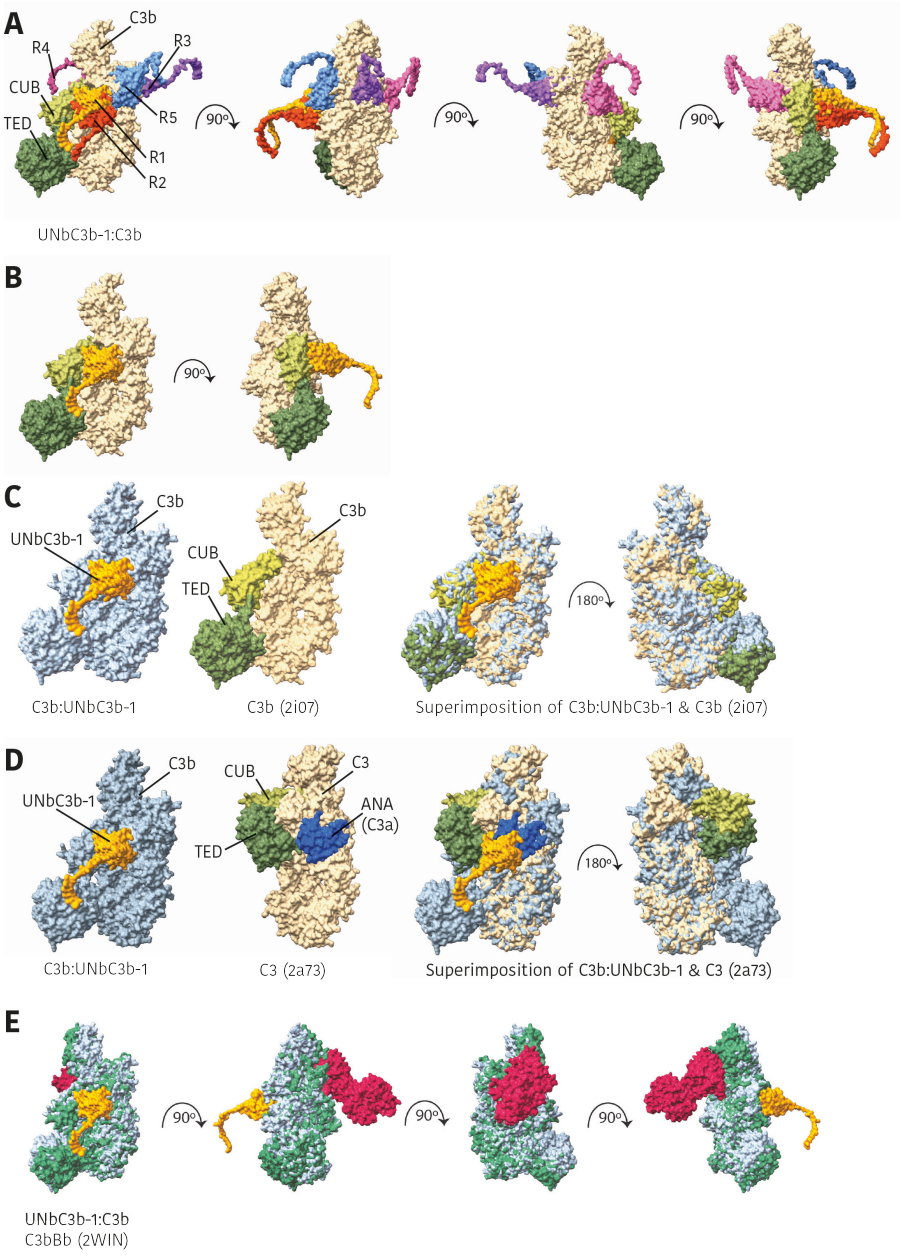

Figure 9: AlphaFold2 prediction of UNbC3b-1 binding site on C3b. (A) Docking of all five AlphaFold2 predictions (generated with ColabFold) of UNbC3b-1 binding to C3b (PDB 2i07) shown from different angles. Predictions were generated using the full length sequence of C3b and UNbC3b-1 (orange, including tag sequence) and docked into the crystal structure of C3b (beige,

CUB domain light green) using the TED domain (dark green) as a reference. C3b depicted in beige with the CUB domain in light green and the TED domain in dark green. Predictions are colored in orange (rank 1), red (rank 2), purple (rank 3), pink (rank 4) and blue (rank 5). (B) Docking of only the highest ranked AlphaFold v2.2 prediction (generated with ColabFold) of UNbC3b-1 binding to C3b (PDB 2i07). (C) In panel 1: AlphaFold2 predicted C3b (light blue) and UNbC3b-1 (orange). In panel 2: published C3b structure (beige) with the CUB (light green) and TED domains (dark green) colored (PDB 2i07).

The overlay of UNbC3b-1:C3b with C3b (PDB 2i07) shows that the AF2 predicted C3b structure resembles the published C3b structure to a very high degree (**Fig. 9C**). The overlay of UNbC3b-1:C3b and C3 lines up with the observation that UNbC3b-1 specifically binds to C3b. Based on the AF2 predicted interaction site the ANA (C3a) domain would most likely sterically clash with the nanobody (**Fig. 9D**). Furthermore, the CUB to MG8 orientation is different in C3 and C3b, which most likely prevents the nanobody from binding to C3. Next, we superimposed UNbC3b-1:C3b and C3bBb to see if this explains why UNbC3b-1 is a potent AP convertase inhibitor. The AF2 prediction lines up with the observation the UNbC3b-1 does not prevent (pro)convertase formation, since AF2 predicted it on the opposite site of C3b, far away from Bb (**Fig. 9E**). However, it does not explain with what mechanism the nanobody inhibits C3 and C5 cleavage. The predicted binding domains (CUB and MG8) are, to date, not described as sites that are involved in the convertase-substrate interactions. Therefore, we conclude that, with the current data available, the AF2 predicted binding site of UNbC3b-1 does not inform us further on its mechanism of inhibition. Moreover, it emphasizes that the proposed binding site is only a prediction and that additional experiments should be performed to confirm the exact binding site of UNbC3b-1.

To summarize, UNbC3b-1 does not inhibit formation of C3bB or C3bBb, but specifically inhibits convertase-mediated substrate cleavage. Our data show that by binding to C3b, UNbC3b-1 inhibits cleavage of both C3 and C5. However, the exact mechanism of inhibition remains to be determined.

DISCUSSION

With the identification of UNbC3b-1 as a C3b-specific nanobody, this study adds a novel complement-targeting molecule to the field of complement research. Conversion of C3 into C3b is an essential step in complement activation. Therefore, molecules that can distinguish the activated C3b product from precursor C3 are very helpful to detect and further understand the molecular mechanisms at play during complement activation. Next to UNbC3b-1, three other nanobodies that bind C3b have been described in literature, hC3Nb1 (33), hC3Nb2 (34), and hC3Nb3 (35). In our competition ELISA we identified that hC3Nb2 decreased the binding of UNbC3b-1 to C3b. This suggests that this molecule binds to C3b on a similar epitope as our nanobody UNbC3b-1. Alternatively, it could also indicate that hC3Nb2 affects the binding epitope of UNbC3b-1 on C3b (and vice versa), for example by inducing a conformational change. Interestingly, hC3Nb2 differs from UNbC3b-1 based on target and pathway specificity. hC3Nb2 recognizes C3b, C3-MA, and precursor C3 by binding to the MG3 and MG4 domains and inhibits all three activation pathways of the complement system. In contrast, nanobody UNbC3b-1 specifically inhibits the AP by selectively binding to C3b. This most likely indicates that the two molecules do not directly compete for binding to C3b, however more experimental data is required to conclude this. Similar as hC3Nb2, hC3Nb3 is not specific towards C3b since it also binds precursor C3 with high affinities. For hC3Nb1 it was initially described to bind both C3b and C3, however recent data indicate that this nanobody might be more specific for C3b (45). This nanobody inhibits the AP, but is distinct from UNbC3b-1, by binding C3b to the MG7 domain. The specific binding of UNbC3b-1 (and potentially hC3Nb1) to C3b is not unique for anti-C3b molecules. Similar as UNbC3b-1, monoclonal antibodies like S77, 3E7, H17, Anti-C3-9, and 4C2 specifically bind C3b and not C3, and inhibit the alternative pathway (29–32). Despite the overlap in target and pathway specificity, the mechanism of inhibition of UNbC3b-1 differs from the previously described monoclonal antibodies, since all these block binding of FB to C3b, while we show that UNbC3b-1 does not interfere with FB binding.

UNbC3b-1 inhibits activity of the AP and interferes with C3 and C5 convertase functioning. Although, the exact mechanism of inhibition of UNbC3b-1 remains elusive, we did show that UNbC3b-1 does not interfere with formation of the (pro)convertase, since FB binding to C3b and its cleavage by FD were unaffected. If future studies could confirm that the AF2 predicted binding site of UNbC3b-1 is correct, it would make sense that UNbC3b-1 does not interfere with FB binding to C3b, since their binding sites do not overlap. However, with the current structural models for convertase-substrate interactions, we cannot yet explain how binding to the MG8 and CUB domains would interfere with convertase activity (46, 47). At this point we can only speculate about the

potential mechanism of inhibition. Here we describe three, (yet) unverified, hypotheses: [1] UNbC3b-1 limits the flexibility of Bb, which is required to dock the C3 scissile loop near the SP domain in Bb (48). This hypothesis does not fit the current AF2 prediction, since UNbC3b-1 is predicted to bind C3b on the opposite site as Bb. [2] UNbC3b-1 inhibits the interaction between the convertases and its substrates, by binding to C3b. Current models show that C3b from the convertase interacts with C3 and C5 using the MG4, MG5 and MG7 domains (46). If UNbC3b-1 prevents the interaction of convertases with their substrate, this could suggest that the actual binding interface of UNbC3b-1 is in or near the MG3 and MG4 domains. Alternatively, it could also hint to another, yet unidentified, binding interface between convertases and their substrates. In all our purified assays we used surfaces with high densities of C3b molecules. Consequently, we generated convertases containing the 'extra' C3b molecule. Potentially, UNbC3b-1 inhibits C3 and C5 cleavage by binding to this 'extra' C3b molecule. [3] UNbC3b-1 inhibits C3 and C5 cleavage by direct interaction with C3 and C5. However, since we showed that UNbC3b-1 does not bind C3 in solution and C5 in ELISA, this is unlikely. Possibly, UNbC3b-1 interacts with a specific conformation of C3(b) (and maybe even C5) that is only present when the convertase is in direct interaction with its substrate. A study using the C5 inhibitors Eculizumab, OmCI and RaCI proposed that endogenous (C5) convertases are not pre-assembled complexes, and that C5 undergoes conformational changes upon binding to C3b and prior to its cleavage (49). This change in conformation is what they denoted as a "priming" event. Considering the high homology between C3(b) and C5, it might be that C3b in the convertase and C3 as a substrate likewise undergo such conformational changes during cleavage. Potentially, UNbC3b-1 binds C3b, C3 (or C5) in this "priming" conformation and then blocks cleavage, for example by steric hindrance. Interestingly, in our assays UNbC3b-1 only inhibited C3a and C5a formation when substrates C3 and C5 were added to the beads without a washing step in-between. This could suggest that UNbC3b-1 should be freely available in solution when C3 and C5 are interacting with the convertase. This hypothesis might match up with the AF2 predicted binding site, since UNbC3b-1 is predicted near the area where the ANA domain would be present in C3 but absent in C3b. Our observation that UNbC3b-1 binds to C3-MA might further strengthen this hypothesis, since this conformation of C3 is also described as C3b-like and might resemble this "priming" event. If this hypothesis holds true, our data suggest that the nanobody UNbC3b-1 can discriminate between these different convertase and/or substrate conformations. Despite the fact that the exact molecular mechanism of UNbC3b-1 remains elusive, the observations in this study once again demonstrates how complex the processes of C3 and C5 convertase formation and functioning are, and emphasizes the need for tools, like UNbC3b-1, to study the complement system.

Concluding, with our nanobody UNbC3b-1, this study adds a novel C3b binding molecule to the field that is distinct from previously described anti-C3b antibodies. With the increasing number of C3- and C3b-binding molecules, with different mechanisms of inhibition and pathway specificity, the incredible complex molecular mechanisms at play in C3 and C5 convertase formation and functioning become easier to unravel. Therefore, the exact determination of UNbC3b-1's binding epitope would be a crucial next step to understand the mechanism of inhibition for this nanobody. Furthermore, this nanobody could be used as tool for specific detection of complement activation product C3b. Finally, since UNbC3b-1 efficiently inhibits the AP of the complement system, this molecule might generate new insights and ideas to develop novel therapeutic complement inhibitors.

EXPERIMENTAL PROCEDURES

Proteins, serum and bacterial strains

Normal human serum from ±20 healthy donors was pooled, as previously described (50). *E. coli* strains that were used are common laboratory strains MG1655, BL21, Rosetta 2 (DE3) BL21 (Merck) and TG1 (Agilent). Complement components and inhibitors were obtained from different sources, see table II. Complement component Bb was produced by incubating C3b-PEG11-biotin with 6×His-tagged FB and 6×His-tagged FD for 1 hour at 37°C, in a molar ratio of 1:10:3. Next streptavidin-6×His was added in a 1.75:1 molar ratio compared to C3b-PEG11-biotin for 1 hour at 4°C to couple C3b-PEG11-biotin with a 6×His-tag. Next, the sample was applied to a 1 mL HisTrap FF column (GE Healthcare) and the flowthrough containing Bb was captured, dialyzed to phosphate buffered saline (PBS) and stored at -80°C.

C3b-opsonized bacteria for immunizations

E. coli bacteria strains MG1655 and BL21 were covered with human C3b molecules, similar as described before (51). To this end, C3b was site-specifically labelled with a maleimide linker (16) containing a dibenzocyclooctyne (DBCO) group at its thioester domain as described by Boero et al. (51). To prepare the bacterial strains, a single colony from *E. coli* MG1655 and BL21 was grown in Luria-Bertani (LB) medium to stationary phase after which a subculture of 1/100 was grown overnight (O/N) in LB medium containing 2 mM azide-modified keto-deoxy-octulosonate (KDO-N_3) (kind gift from Tom Wennekes), a major component of lipopolysaccharides (LPS) (52), to allow metabolic incorporation of KDO-N_3 in the LPS of these strains. Next, bacteria were washed twice with PBS to remove unincorporated KDO-N_3, resuspended in PBS containing 17% glycerol and frozen at -20°C. Frozen bacteria were treated with γ-irradiation at a dose of 10.3-10.8 kGy for ±1.5

hours (Synergy health Ede B.V. a Steris company), to ensure that bacteria incorporated with KDO-N_3 were no longer viable. To couple with C3b molecules, γ-irradiated bacteria were thawed, washed, and 2×10^9 bacteria/ml were incubated O/N, at 4°C with 2.66 μM C3b-PEG4-DBCO. The DBCO in C3b-PEG4-DBCO covalently couples with the azide (N_3) from KDO-N_3, via click-chemistry (52), resulting in the coupling of C3b molecules to the bacterial membrane (KDO-C3b). The next day, KDO-C3b bacteria were washed 3× with PBS to remove unbound C3b-PEG4-DBCO. To obtain bacteria with C3b deposition in high densities, KDO-C3b bacteria were diluted 5× in hepes buffer and three rounds of natural C3b amplification were performed. For each round we added FB (5 μg/ml), FD (0.5 μg/ml), and uncleaved C3 (100 μg/ml) and incubated the bacteria for 15 minutes at 37°C. After each round bacteria were spun down, supernatants were removed and new components were added. After the third round of amplification bacteria were washed 3× with hepes buffer and subsequently split in three equal parts. Next, bacteria were crosslinked with bis(sulfosuccinimidyl)suberate (BS3) (Thermo Scientific), paraformaldehyde (PFA) (VWR International) or not crosslinked at all, to present deposited C3b in different ways to the llamas. Crosslinking with BS3 (5 mM) was performed for 90 minutes at room temperature (RT), the reaction was quenched with 50 mM Tris, for 15 minutes at RT, after which bacteria were washed and resuspended in hepes buffer. Crosslinking with PFA (1%) was performed for 15 minutes at RT, bacteria were washed and resuspended in hepes buffer.

Immunizations

Two llamas (Lama glama), named Ines and Lotte, were immunized by administration of human C3b on day 0, 14, 28, 35, 57, and 71 by a trained veterinarian at Preclincs GmbH (Potsdam, Germany). All procedures were according to European animal welfare laws and regulations and all animals remained alive after immunization and blood collection. The first four injections each contained 12.5 μg purified C3b in solution. The last two injections contained *E. coli* bacteria opsonized with human C3b. Per injection, both llamas received $\pm1.5\times10^9$ γ-irradiated *E. coli* bacteria opsonized with a high density of C3b molecules. The llama named Ines received *E. coli* strain MG1655 and the llama named Lotte received *E. coli* strain BL21. The samples contained a mixture of the different crosslinking methods. All injections were combined with FAMA adjuvant (Gebru Biotechnic GmbH). To obtain llama serum and PBMCs, blood was drawn on day 0, day 43 and day 99.

Phage library construction

A nanobody phage display library was generated for each llama. mRNA was isolated form PBMCs (day 43 and day 99), and cDNA was created using the SuperScript™ IV First-Strand Synthesis System kit (Thermo Scientific, 18091050). We amplified the

cDNA encoding for the heavy-chain only antibodies by PCR, using primers annealing to framework 1 (FR1) and constant heavy chain 2 (CH2) domains (53). Next, DNA fragments encoding for the nanobody genes were digested and ligated into phagemid pPQ81 vector (derived from pHEN1 (54)). This fused the nanobodies to a Myc- and 6×His-tag and to pIII coat protein of M13 bacteriophage. Next, phage display libraries were transformed into competent *E. coli* TG1 bacteria (Agilent), by electroporation with a MicroPulser and corresponding electroporation cuvettes (Bio-Rad). To estimate library sizes, a serial dilution of transformed bacteria was spotted on LB agar plates and colony forming units per mL (CFU/ml) were counted.

Phage production and purification

Phages were produced according to standardized protocols (55), using the original phage display libraries obtained after immunization (day 43 and day 99) as starting material for round 1, and the bacterial libraries obtained after the first round of phage display as starting material for round 2. Briefly, *E. coli* TG1 libraries were grown in 2× concentrated yeast extract tryptone (2YT) medium, supplemented with 2% glucose and 100 µg/mL ampicillin. Next, kanamycin resistant VCSM13 helper phage (Agilent) was added and phages were purified via two rounds of polyethylene glycol precipitation.

Phage display panning

We performed two rounds of phage display, following standardized procedures (56), with in total 9 different selection strategies (**Table I**), combining different methods of antigen presentation and negative selections. Wells presenting C3b (see details below) were blocked with 200 µL/well 4% skimmed milk (Marvel) in PBS, for 1 hour at RT, while shaking. Next, wells were incubated with phages at concentrations of $\approx 10^{10}$ CFU/well (round 1) and $\approx 10^{9}$ CFU/well (round 2) in 2% Marvel in PBS, for 2 hours, while shaking. In case of negative selections with purified proteins (e.g. selection strategy #1), phages were preincubated for 30 minutes at RT on a spinning wheel with C3 (30 nM), C5 (30 nM) and/or C3b (30 nM), before being added for 2 hours to the C3b presenting wells. In case of negative selections with beads (e.g. selection strategy #7), handling was the same except that low density C3b-beads (5.0 µL/sample, at 10 mg/mL), including all phages bound by them, were removed from the sample using a magnet, prior to adding them to C3b presenting wells. Next, wells were washed 20× with 200 µl PBS + 0.05% tween-20 (PBS-T), with two 10-minute incubations (shaking) in-between washing steps. Finally, wells were washed 3 additional times using PBS. Next, phages bound to C3b were eluted using 100 µL triethanolamine solution (0.1 M, pH>10), for 15 minutes at RT, while shaking and elutions were neutralized using 50 µL Tris/HCl (1 M, pH=7.5). Phages were rescued by infecting them in *E. coli* strain TG1 bacteria at OD_{600} of 0.5, for 30 minutes, at 37°C, without shaking. Next, bacteria were grown O/N at 37°C, while

shaking, in 2YT medium, supplemented with 2% glucose and 100 µg/mL ampicillin. The next day, bacterial libraries containing the genetic material of C3b-binding nanobodies were stored in 20% glycerol at -80°C. To estimate the number of phages used as starting material (input) and the number of phages in the eluate (output), phages were serially diluted, added to *E. coli* TG1 bacteria to allow infection and spotted on LB agar plates supplemented with 2% glucose and 100 µg/mL ampicillin. After an O/N incubation at 37°C, CFU/mL were counted and estimated library sizes were calculated.

C3b presentation during phage display

When presenting C3b on plates (e.g. selection strategy #1, Table I), Nunc Maxisorp plates (VWR 735-0083, Thermo Fisher Scientific) were coated O/N, at 4°C, without shaking, with 100 µL/well C3b at a concentration of 0.1, 1.0 or 5.0 µg/mL. When presenting C3b in high densities on beads, magnetic streptavidin-coated beads (0.1, 0.2, 0.8, 2.0 or 4.0 µL/sample, at 10 mg/mL, Dynabeads M-270 Streptavidin, Invitrogen) were diluted 50× and coupled O/N at 4°C with 1 µg/mL C3b-PEG11-biotin (C3b-bio) in veronal buffered saline + 145 nM NaCl, pH 7.4 (VBS), supplemented with 2.5 mM $MgCl_2$ and 0.05% Tween-20 (VBS/$MgCl_2$/Tween). After O/N coupling, unbound C3b-bio was washed away. To obtain beads with low densities of C3b, used for counter selections, protocols were the same, except beads were diluted 3.125× instead of 50× before adding C3b-bio.

Periplasmic nanobody production for screening

Bacterial output libraries (*E. coli* TG1) were plated on LB agar plates supplemented with 2% glucose and 100 µg/mL ampicillin, incubated O/N at 37°C, to obtain single colonies. Next, single colonies were randomly picked and 92 wells containing 90 µL 2YT medium, supplemented with 2% glucose and 100 µg/mL ampicillin were inoculated with one colony/well. As negative controls, two wells were not inoculated (EM), and two wells were inoculated with a bacterium expressing a nanobody with an irrelevant target (IRR) or a bacterium containing an empty vector (PER). Bacteria were grown O/N at 37°C, without shaking. The next day, subcultures (1/100) were made in 900 µL 2YT medium with 0.1% glucose and 100 µg/mL ampicillin and grown until a clear growth difference was observed between negative controls (EM) and other wells (approximately 2.5-3 h). Then, bacterial cultures were induced by adding 1 mM isopropylthio-β-galactoside (IPTG) and grown O/N, at RT, while shaking. The next day, cultures were spun down for 10 minutes at 6000 g, and pellets were resuspended in 120 µL PBS. Next, bacterial suspensions were frozen at least O/N at -20°C or >30 minutes at -80°C, before thawing. After thawing, samples were spun down 2× for 10 minutes at 6000 g and supernatants, containing the periplasmic extracts with nanobodies in unknown concentrations, were collected and stored at -20°C, until further use.

Nanobody productions

Nanobodies containing a Myc- and 6×His-tag (further referred to as MH-clones) were produced in the periplasm of *E. coli* (57). For this, *E. coli* Rosetta 2 (DE3) BL21 cells (Merck) were transformed with pPQ81 vectors encoding the nanobody genes and C-terminal Myc- and 6×His-tags. Next, bacteria were grown O/N, at 37°C, while shaking, in 2YT medium, supplemented with 2% glucose and 100 µg/mL ampicillin. The next day, subcultures (1/20) were grown until they reached an OD_{600} of 0.6-0.9, in 2YT medium supplemented with 0.1% glucose and 100 µg/mL ampicillin. Next, nanobody expression was induced for four hours at 37°C, while shaking, by adding 1 mM IPTG. Next, cultures were spun down for 10 minutes at 6000 g, pellets were dissolved in PBS and frozen for >30 minutes at -80°C, or O/N at -20°C. Next, frozen pellets were thawed to release periplasmic extracts in the supernatant, which were collected after 15 minutes of centrifugation at 6000 g. Nanobody UNbC3b-1 (clone B5) containing an LPETG-6×His-tag (further referred to as UNbC3b-1-LH) was cloned into a pcDNA 3.4 TOPO™ vector (Thermo Fisher Scientific) and expressed in EXPI293F cells (Thermo Fisher Scientific), similar as described for complement protein C5 in Struijf et al. (57), except that here we added 1 µg/ml DNA/ml cells for transfection.

Nanobody purifications

MH-clones were isolated using immobilized metal-affinity chromatography. For this, supernatants containing the nanobodies were incubated with ROTI Garose-His/Co beads (Roth) for 30 minutes, at RT, on a spinning wheel, to bind nanobodies via their 6×His-tag. After three washing steps with PBS-T, nanobodies were eluted with 150 mM imidazole. For purification of UNbC3b-1-LH, EXPI293F supernatant was buffer exchanged to 50 mM Tris, 500 mM NaCl, pH8.0 via dialysis and 30 mM imidazole was added before application to a HiTrap Chelating column (GE Healthcare). The column was washed with 30 mM imidazole, before UNbC3b-1-LH was eluted with a 30 to 250 mM imidazole gradient, using the Äkta Pure protein chromatography system (GE Healthcare). Finally, all nanobodies were dialyzed to PBS, concentrations were measured at A_{280} using a Nanodrop One (Thermo Fisher Scientific) and nanobody size, purity and concentrations were verified using SDS-PAGE, stained with InstantBlue Safe Coomassie stain (Sigma Aldrich).

Nanobody labeling with biotin and fluorophores

We labeled UNbC3b-1-LH with biotin (further referred to as UNbC3b-1-bio) and fluorophore Alexa488 (further referred to as UNbC3b-1-a488) via sortagging (38). First, UNbC3b-1-LH was dialyzed against 50 mM Tris, 150 mM NaCl, pH8.0 (sortase buffer). Next, UNbC3b-1-LH was incubated with His-tagged Sortase A7 (His-TEVG-SrtA7, (38)) and GGG-azide (Genscript) in a 7:1:70 molar ratio, in sortase buffer supplemented with

10 mM $CaCl_2$, for 2 hours, at 4°C, while shaking. Next, 20mM imidazole was added and samples were applied to a HIS-Trap FF column (GE Healthcare), to remove UNbC3b-1-LH that did not get sortagged with GGG-azide, and flow-through, containing UNbC3b-1-GGG-azide was collected. Next, UNbC3b-1-GGG-azide was incubated for 2 hours, at RT, while shaking, with a 5× molar excess DBCO-AlexaFluor488 (a488) (JenaBioScience) or DBCO-PEG4-biotin (Santa Cruz Biotechnology) in sortase buffer. Finally, UNbC3b-1-a488 and UNbC3b-1-bio were dialyzed against PBS.

ELISA: llama antibody and nanobody binding

Nunc Maxisorp plates (VWR 735-0083) were coated O/N at 4°C, without shaking, with 50 µl antigen (C3b, C3, C3a, C4, C4b, C5, C5a, C5b6, C6, Bb, iC3b-biotin, C3c, C3dg, C3d, C3a des-Arg) at a concentration of 2 µg/mL in sterile PBS. The next day, wells were blocked for 1 hour, at RT, with either 200 µL PBS + 4% Marvel (llama immune response) or 80 µL PBS-T + 4% bovine serum albumin (BSA, Sigma) (all others). All following incubations were performed with 50µl sample/well, at RT, for 1 hour, while shaking. Samples were diluted in PBS + 1% Marvell (llama immune response or PBS-T + 1% BSA (all others) and in-between incubations wells were washed 3× with PBS-T. Unless stated here, sample concentrations are indicated on the X-axis in the corresponding figure legend. For the C3b/C3 screening ELISA, periplasmic extracts were diluted 1:5. For the competition ELISA with known C3b-binding molecules, UNbC3b-1-biotin (10 nM) was premixed with competitors in a concentration series. Compounds hC3Nb1, hC3Nb2, hC3Nb3, clone G10 (from this screen), CRIg, FH, Efb-C, Ecb, FB_{DGP}, sbi, SCIN, properdin, and FI were added in 0.1 – 1000 nM; MCP was added in 0.01 – 100 nM; FHR5 and DAF (CD55) were added in 0.3 – 300 nM; and W4A9 (compstatin derivative) was added in 0.03 – 30 µM. To detect llama antibodies and nanobodies (not via a tag), wells were incubated with 1:2000 QE19 (polyclonal rabbit-anti-nanobody antibodies, QVQ Holding BV), followed by 1:5000 polyclonal donkey-anti-rabbit-PO labeled antibodies (Jackson Immuno research). To detect biotinylated nanobodies, wells were incubated with 1:5000 tetrameric streptavidin coupled to HRP (Southern Biotech). To develop ELISAs substrates were added; 3.7 mM of O-phenylenediamine dihydrochloride + 50 mM $Na_2HPO_4 2H_2O$ + 25 mM citric acid + 0.03% H_2O_2 (llama immune response) or 100 µg/mL tetramethylbenzidine dissolved in DMSO + 100 mM NaOAc + 1.7 mM ureum peroxide (all others). All ELISAs were stopped with 0.5 M sulfuric acid and absorbance (450 nm) was measured with an iMark Microplate Reader (Biorad).

Sequencing

For sequencing, fresh O/N bacterial cultures were made using 2YT medium, supplemented with 2% glucose and 100 µg/mL ampicillin. In case of sequencing all 96 clones, 5µl of the O/N culture was added to a 96-wells plate filled with LB-agar. Plates were next

incubated for 2-3 hours at 37°C, without shaking. Plates were sealed with parafilm and send to Eurofins for Sanger sequencing. In case of sequencing 1-8 clones, bacteria were plated on LB agar plates to obtain single colonies. Next, a single colony was picked and used to inoculate a 5mL culture with 2YT medium, supplemented with 2% glucose and 100 µg/mL ampicillin, that was grown O/N at 37°C, while shaking. The next day, bacterial cultures were spun down and supernatants were removed. Next, plasmids were isolated using the NucleoSpin EasyPure kit (Macherey-Nagel), following instructors' protocols. DNA concentrations were measured using the MultiSkanGo (Thermo Scientific) and 900-1000 ng DNA was added to 5 µM forward primer, in a total volume of 10 µL milliQ water. Next, samples were sent to Eurofins for sequencing. Using the PipeBio Antibody Sequence Analysis platform resulting nucleic acid sequences were analysed and processed into nanobody amino acid sequences. The nanobody sequences were annotated for frameworks and complementarity determining regions. Sequences were aligned to IgG germlines and clustered using 80% CDR-H3 homology as a cut-off.

ELISA: complement deposition

Nunc Maxisorp plates (VWR 735-0083) were coated O/N, at 4°C, without shaking, with 3 µg/mL human IgM (Millipore) diluted in PBS (classical pathway (CP)) or with 20 µg/mL sonicated LPS from *Salmonella enteritis* (Sigma) diluted in 0.1 M sodium carbonate, pH 9.6 (alternative pathway (AP)). The next day, wells were blocked for 1 hour, at RT, while shaking, with 80 µL PBS-T supplemented with 4% BSA. Next, wells were incubated for 1 hour, RT, while shaking, with 2.5% (CP) or 10% (AP) human pooled serum, in the presence of 1.3 – 1000 nM UNbC3b-1-LH. Complement inhibitors Eculizumab, W4A9, SCIN, and BBK32 were taken along. C3b deposition was detected using 1:10.000 anti-C3 WM-1 clone digoxigenin (DIG) labeled antibodies (Sigma) and 1:8000 anti-DIG-PO antibodies (Roche). C5b-9 deposition was detected using 1:1000 monoclonal mouse anti-C5b-9 aE11 (produced in our lab, based on (58, 59)) and 1:5000 polyclonal goat-anti-mouse-PO (Southern Biotech). Complement deposition ELISAs were developed similar as described above for the nanobody binding ELISAs.

Erythrocyte lysis assays

Sheep erythrocytes (shE, Alsever Biotrading) and rabbit erythrocytes (raE, kindly provided by Utrecht University, Faculty of Veterinary medicine) were washed 3x with PBS. For the CP, shE were diluted to a 2% suspension in VBS supplemented with 0.25 mM $MgCl_2$ and 0.5 mM $CaCl_2$ (VBS++) and shE were opsonized with 1:2000 polyclonal rabbit-anti-sheep IgM antibodies (haemolytic amboceptor (60), shEA). For the AP, raE were diluted to a 2% suspension in VBS, supplemented with 5 mM $MgCl_2$ and 10 mM EGTA (VBS/Mg/EGTA). Next, raE and shEA suspensions were incubated for 10 minutes (CP) or 30 minutes (AP), at 37 °C, while shaking, with 2.5% (CP) or 10% (AP) pooled human serum,

and different concentrations of nanobodies (1.4 – 1000 nM, MH-clones). As controls, we took along a samples with erythrocytes and buffer (0% lysis), erythrocytes and milliQ water (100% lysis) and samples with serum but no nanobody. Next, samples were spun down for 7 minutes at 3500 rpm. Supernatants were diluted 1:3 with milliQ water and hemoglobin release was measured at and OD of 405 nm, in a flat-bottom plate, using an iMark Microplate Reader (Biorad).

C3b beads binding assay

Magnetic streptavidin-coupled beads (0.5 µl/sample, at a concentration of 10 mg/mL, Dynabeads M-270 Streptavidin, Invitrogen) were coupled with a high density of C3b molecules, as described above (C3b presentation during phage display). Next, nanobodies (UNbC3b-1-a488 or the eight MH-clones, all at 100 nM) were incubated with the beads and soluble C3 (27 – 270 nM or 0.5 – 1080 nM) or C3b (0.5 – 1080 nM) for 30 minutes at 4°C/RT, while shaking. To detect binding of the eight MH-clones, we next incubated beads with QE19 (QVQ Holding BV) directly labeled with fluorophore Alexa 647 (QE19-a647) for 30 minutes at 4°C, while shaking. In-between incubations, beads were washed 3× with PBS-T to remove excess nanobody, C3, C3b or QE19-a647. Next, beads were fixated for 15 minutes, at RT, by resuspending them in 100µl PBS-T supplemented with 1% PFA. Binding of nanobodies was assessed on a FACS verse flow cytometer (BD).

C3a and C5a formation assay

High density C3b beads, prepared as described above (C3b beads binding assay), were incubated with UNbC3b-1-LH (4.1 – 1000 nM), FB_{DGF} (20 µg/mL), FD (5 µg/ml), C3 (20 µg/mL) and/or C5 (20 µg/mL). Components were added subsequently, with in between a 10-minute incubation step at RT, while shaking. In case of a washing steps (indicated with an @ symbol), beads were two times collected with a magnet, supernatant was removed and beads were resuspended in VBS/$MgCl_2$/Tween buffer. The exact sequence of adding components is indicated in each figure and corresponding legends. At the final incubation step, supernatants were collected and C3a and C5a release was measured using a calcium flux assay (15, 16). For this, U937 C3aR and C5aR cells (15), at a concentration of 5×10^6 cells/ml, were incubated with 0.5 µM Fluo-3-AM ester (Invitrogen) in RPMI (Lonza) supplemented with 0.05% human serum albumin (HSA, Sanquin). Next, cells were diluted to a concentration of 1×10^6 cells/ml and divided in 200 µL/sample. Next, 20 µl supernatant, containing the C3a or C5a stimulus, was added and fluorescence was measured in time using a FACS Verse flow cytometer (BD). To calculate the amount of C3a and C5a present in the supernatants, C3a and C5a standard curves were made using purified C3a and C5a.

FB binding assay

High density C3b beads (1 µL/sample, at 10 mg/mL), prepared as described above, were incubated with 1 µM UNbC3b-1-LH, for 30 minutes at RT, while shaking. Next, beads were washed to remove unbound UNbC3b-1, and incubated with directly labeled FB_{WT}-a488 or FB_{DGF}-a488 (both 0.04 – 10 µg/ml), and FD (0.5 µg/mL), for 30 minutes, at 37°C, while shaking. Next, beads were washed and fluorescence was measured using the FACS Verse flow cytometer (BD).

FB cleavage assay and western blot

FB cleavage was assessed in solution and on beads. In solution: C3b (100 nM) was incubated with FB_{DGF} (100 nM), FD (42.5 nM) and UNbC3b-1 (1 µM). On beads: High density C3b beads (4µl beads/sample) were prepared as described above and incubated with FB_{DGF} (100 nM), FD (42.5 nM) and UNbC3b-1 (1 µM). Samples were incubated for 30 minutes, at 37°C, while shaking in VBS/$MgCl_2$ buffer. Samples were diluted 1:1 with 2× concentrated reducing SDS sample buffer (0.1 M Tris (pH 6.8), 39% glycerol, 0.6% SDS, and bromophenol blue and incubated for 5 minutes at 95°C. Samples were run on a 4-12% Bis-Tris gradient gel (Invitrogen) for 60 minutes at 200 V. Next, proteins were transferred to 0.2 µM PVDF membranes (Bio-Rat), using the Trans-Blot Turbo transfer system (BioRad). After blotting, membranes were blocked with PBS supplemented with 0.1% Tween-20 and 4% dried skim milk (ELK), for 1 hour, at 37°C, while on a roller bank. Next, blots were incubated with 1:300 diluted polyclonal goat-anti-FB (Complement Technology), washed and incubated with 1:10,000 polyclonal donkey-anti-goat-HRP (Southern Biotech), all in PBS supplemented with 0.1% Tween-20 and 1% ELK. In between all steps, membranes were washed 3× with PBS supplemented with 0.1% Tween. Blots were developed using Pierce ECL Western Blotting Substrate (Thermo Fisher Scientific), for 1 minutes at RT. Blots were imaged on a LAS4000 Imagequant (GE Healthcare).

SEC: nanobody interaction with C3, C3b, and C3-MA

UNbC3b-1-a488 (2.3 µM) was incubated with C3 (2.3 µM), C3b (2.3 µM), C3-MA (2.3 µM) or buffer (25 mM Hepes + 150 mM NaCl, pH 7.4) for 15 minutes, at RT. As controls, C3, C3b, and C3-MA samples were incubated with buffer instead of UNbC3b-1. Next, samples were filtered with a 0.22 µm Costar® SpinX tube (Corning) and 50 µL sample was loaded on a Superose 6 Increase 3.2/300 column (GE Healthcare), using the AKTA-Explorer (GE Healthcare), which measured the OD_{280} and OD_{488}.

SPR affinity determination

Binding affinity of UNbC3b-1 for C3b was assessed using a White Fox fiber optic surface plasmon resonance (FO-SPR) sensor (Fox Biosystems). UNbC3b-1-biotin (330 nM) was immobilized on streptavidin FO-SPR probes (FOx Biosystems) in PBS, pH 7.4, supplemented with 0.01% Tween-20 (PBS-$T_{0.01\%}$) for 300 seconds, at 26 °C, while shaking at 1000 rpm. Next, probes were incubated with C3b (1.56 – 12.5 nM) in PBS-$T_{0,01\%}$, at 26°C, while shaking at 1000 rpm, to allow association. After 1800 seconds, probes were incubated with PBS-$T_{0,01\%}$ for 7200 seconds, at 26°C, while shaking at 1000 rpm, to allow dissociation. FO-SPR data were collected by FOx software (FOx Biosystems) and on- and off-rates were fitted using TraceDrawer, using a 1:1 model with global B_{max}, global k_{on}, global k_{off} and a constant BI.

AlphaFold2 model prediction and evaluation

AlphaFold2 2.3.1 was used to generate *in silico* models that predict the interaction between UNbC3b-1 and C3b (61, 62).The software was run via the ColabFold v1.5.1 notebook offered via Google Collaboratory. Full length sequences of C3b and UNbC3b-1 (including the tag sequence) were submitted to ColabFold, which generated five models for each input. Prediction models were automatically ranked by confidence by the software (rank 1 = most confident). All models were initially evaluated visually using ChimeraX 1.6.1 (33) to confirm proper folding and common features. Next, a comparison of the first ranked model was made with the crystal structure of C3b (PDB 2i07) or C3 (PDB 2a73) using the Matchmaker tool in ChimeraX 1.6.1 (63). Once the predicted structure was confirmed to closely align with the crystal structure of C3b or C3, the location of the nanobody was evaluated.

Data analysis

Graphs were created with GraphPad Prism 9.3.0. Curves were fitted with GraphPad Prism 9.3.0. or with Tracedrawer 1.9.2. Models of C3, C3b and obtained via AlphaFold2 were visualized using Chimera X 1.5 (64). Nanobody sequences were analyzed and aligned using PipeBio.

SUPPORTING INFORMATION

This article contains supporting information.

FUNDING AND ADDITIONAL INFORMATION

This work was mainly funded by the Netherlands Organisation for Scientific Research (NWO) under the TTW Industrial Doctorate (grant agreement no. NWA.ID.17.036 to EMS). The project was also supported by the European Research Council (ERC) under the European Union's Horizon 2020 research and innovation programme (grant agreement No. 101001937, ERC-ACCENT to SHMR).

CONFLICT OF INTEREST

GD, ED and RH are employees of QVQ Holding BV. Other authors declare no conflict of interest.

REFERENCES

1. Merle, N. S., Church, S. E., Fremeaux-Bacchi, V., and Roumenia, L. T. (2015) Complement system part I – molecular mechanisms of activation and regulation. *Front Immunol.* **6**, 1–30
2. Merle, N. S., Noe, R., Halbwachs-Mecarelli, L., Fremeaux-Bacchi, V., and Roumenina, L. T. (2015) Complement system part II: Role in immunity. *Front Immunol.* **6**, 1–26
3. Garred, P., Tenner, A. J., and Mollnes, T. E. (2021) Therapeutic Targeting of the Complement System: From Rare Diseases to Pandemics. *Pharmacol Rev.* **73**, 792–827
4. Schröder-Braunstein, J., and Kirschfink, M. (2019) Complement deficiencies and dysregulation: Pathophysiological consequences, modern analysis, and clinical management. *Mol Immunol.* **114**, 299–311
5. Zelek, W. M., Xie, L., Morgan, B. P., and Harris, C. L. (2019) Compendium of current complement therapeutics. *Mol Immunol.* **114**, 341–352
6. Brade, V., Hall, R. E., and Colten, H. R. (1977) Biosynthesis of pro-C3, a precursor of the third component of complement. *J Exp Med.* **146**, 759–765
7. Bokisch, V. A., Dierich, M. P., and Muller-Eberhard, H. J. (1975) Third Component of Complement (C3): Structural Properties in Relation to Functions (topology of functional sites/physiologic C3 fragments/C3-membrane interaction/ immune adherence/enzyme subunit). *PNAS.* **72**, 1989–1993
8. Janssen, B. J. C., Christodoulidou, A., McCarthy, A., Lambris, J. D., and Gros, P. (2006) Structure of C3b reveals conformational changes that underlie complement activity. *Nature.* **444**, 213–216
9. Janssen, B. J. C., Huizinga, E. G., Raaijmakers, H. C. A., Roos, A., Daha, M. R., Nilsson-Ekdahl, K., Nilsson, B., and Gros, P. (2005) Structures of complement component C3 provide insights into the function and evolution of immunity. *Nature.* **437**, 505–511
10. Rooijakkers, S. H. M., Wu, J., Ruyken, M., van Domselaar, R., Planken, K. L., Tzekou, A., Ricklin, D., Lambris, J. D., Janssen, B. J. C., van Strijp, J. A. G., and Gros, P. (2009) Structural and functional implications of the complement convertase stabilized by a staphylococcal inhibitor. *Nat Immunol.* **10**, 721–727
11. Pangburn, M. K., and Muller-Eberhardt, H. J. (1986) The C3 convertase of the alternative pathway of human complement Enzymic properties of the bimolecular proteinase The association of Factor B with C3b (the major fragment of complement component C3) in the presence of Mg2+ results in the formation of. *Biochem. J.* **235**, 723–730
12. Alcorlo, M., López-Perrote, A., Delgado, S., Llorca, O., Rodríguez-Gallego, C., Yébenes, H., Rodríguez de Córdoba, S., and Subías, M. (2015) Structural insights on complement activation. *FEBS Journal.* **282**, 3883–3891
13. Rawal, N., and Pangburn, M. K. (2001) Structure/function of C5 convertases of complement. *Int Immunopharmacol.* **1**, 415–422
14. Pangburn, M. K., and Rawal, N. (2002) Structure and function of complement C5 convertase enzymes. *Biochem Soc Trans.* **30**, 1006–1010
15. Zwarthoff, S. A., Berends, E. T. M., Mol, S., Ruyken, M., Aerts, P. C., Józsi, M., de Haas, C. J. C., Rooijakkers, S. H. M., and Gorham, R. D. (2018) Functional characterization of alternative and classical pathway C3/C5 convertase activity and inhibition using purified models. *Front Immunol.* **9**, 1–13
16. Berends, E. T. M., Gorham, R. D. J., Ruyken, M., Soppe, J. A., Orhan, H., Aerts, P. C., Haas, C. J. C. De, Gros, P., and Rooijakkers, S. H. M. (2015) Molecular insights into the surface-specific arrangement of complement C5 convertase enzymes. *BMC Biol.* **13**, 1–13
17. Forneris, F., Bertram, P., Sfyroera, G., Xue, X., Ricklin, D., Wu, J., Liszewski, M. K., Gros, P., Atkinson, J. P., Lin, Z., Tzekou, A., Hauhart, R., Volokhina, E., Granneman, J. C., and Lambris, J. D. (2016) Regulators of complement activity mediate inhibitory mechanisms through a common C3b-binding mode. *EMBO J.* **35**, 1133–1149
18. Lambris, J. D., Ricklin, D., and Geisbrecht, B. V. (2008) Complement evasion by human pathogens. *Nat Rev Microbiol.* **6**, 132–142

19. Jongerius, I., Köhl, J., Pandey, M. K., Ruyken, M., Van Kessel, K. P. M., Van Strijp, J. A. G., and Rooijakkers, S. H. M. (2007) Staphylococcal complement evasion by various convertase-blocking molecules. *Journal of Experimental Medicine*. **204**, 2461–2471
20. Rooijakkers, S. H. M., Ruyken, M., Roos, A., Daha, M. R., Presanis, J. S., Sim, R. B., van Wamel, W. J. B., van Kessel, K. P. M., and van Strijp, J. A. G. (2005) Immune evasion by a staphylococcal complement inhibitor that acts on C3 convertases. *Nat Immunol*. **6**, 920–927
21. Hong, Y., and Ghebrehiwet, B. (1992) Effect of Pseudomonas aeruginosa elastase and alkaline protease on serum complement and isolated components C1q and C3. *Clin Immunol Immunopathol*. **62**, 133–138
22. Agrawal, P., Nawadkar, R., Ojha, H., Kumar, J., and Sahu, A. (2017) Complement evasion strategies of viruses: An overview. *Front Microbiol*. 10.3389/fmicb.2017.01117
23. Ricklin, D., Mastellos, D. C., Reis, E. S., Lambris, J. D., and Str, N. (2018) The renaissance of complement therapeutics. *Nat Rev Nephrol*. **14**, 26–47
24. Lamers, C., Xue, X., Smieško, M., van Son, H., Wagner, B., Berger, N., Sfyroera, G., Gros, P., Lambris, J. D., and Ricklin, D. (2022) Insight into mode-of-action and structural determinants of the compstatin family of clinical complement inhibitors. *Nat Commun*. 10.1038/s41467-022-33003-7
25. Hoy, S. M. (2021) Pegcetacoplan: First Approval. *Drugs*. **81**, 1423–1430
26. Mastellos, D. C., Yancopoulou, D., Kokkinos, P., Huber-Lang, M., Hajishengallis, G., Biglarnia, A. R., Lupu, F., Nilsson, B., Risitano, A. M., Ricklin, D., and Lambris, J. D. (2015) Compstatin: A C3-targeted complement inhibitor reaching its prime for bedside intervention. *Eur J Clin Invest*. **45**, 423–440
27. Mastellos, D. C., Ricklin, D., and Lambris, J. D. (2019) Clinical promise of next-generation complement therapeutics. *Nat Rev Drug Discov*. **18**, 707–729
28. Lachmann, P. J., Lay, E., and Seilly, D. J. (2018) Experimental confirmation of the C3 tickover hypothesis by studies with an Ab (S77) that inhibits tickover in whole serum. *FASEB Journal*. **32**, 123–129
29. Katschke, K. J., Stawicki, S., Steffek, M., Yin, J., Xi, H., Sturgeon, L., Hass, P. E., Loyet, K. M., DeForge, L., Wu, Y., van Lookeren Campagne, M., and Wiesmann, C. (2009) Structural and functional analysis of a C3b-specific antibody that selectively inhibits the alternative pathway of complement. *Journal of Biological Chemistry*. **284**, 10473–10479
30. DiLillo, D. J., Pawluczkowycz, A. W., Peng, W., Kennedy, A. D., Beum, P. V., Lindorfer, M. A., and Taylor, R. P. (2006) Selective and efficient inhibition of the alternative pathway of complement by a mAb that recognizes C3b/iC3b. *Mol Immunol*. **43**, 1010–1019
31. Koistinen, V., Wessberg, S., and Leikola, J. (1989) Common Binding Region of Complement Factors B, H and CR1 on C3b Revealed by Monoclonal Anti-C3d. *Complement Inflamm*. **6**, 270–280
32. Becherer, J. D., Alsenz, J., Esparza, I., Hack, E., and Lambris, J. D. (1992) Segment Spanning Residues 727-768 of the Complement C3 Sequence Contains a Neoantigenic Site and Accommodates the Binding of CR1, Factor H, and Factor B1. *Biochemistry*. **31**, 1787–1794
33. Jensen, R. K., Pihl, R., Gadeberg, T. A. F. F., Jensen, J. K., Andersen, K. R., Thiel, S., Laursen, N. S., and Andersen, G. R. (2018) A potent complement factor C3–specific nanobody inhibiting multiple functions in the alternative pathway of human and murine complement. *Journal of Biological Chemistry*. **293**, 6269–6281
34. Pedersen, H., Jensen, R. K., Hansen, A. G., Gadeberg, T. A. F., Thiel, S., Laursen, N. S., and Andersen, G. R. (2020) A C3 specific nanobody that blocks all three activation pathways in the human and murine complement system. *Journal of Biological Chemistry*. 10.1074/jbc.RA119.012339
35. Pedersen, H., Jensen, R. K., Jensen, J. M. B., Fox, R., Pedersen, D. V., Olesen, H. G., Hansen, A. G., Christiansen, D., Mazarakis, S. M. M., Lojek, N., Hansen, P., Gadeberg, T. A. F., Zarantonello, A., Laursen, N. S., Mollnes, T. E., Johnson, M. B., Stevens, B., Thiel, S., and Andersen, G. R. (2020) A Complement C3–Specific Nanobody for Modulation of the Alternative Cascade Identifies the C-Terminal Domain of C3b as Functional in C5 Convertase Activity. *The Journal of Immunology*. **205**, 2287–2300

36. Lefranc, M. P., Giudicelli, V., Duroux, P., Jabado-Michaloud, J., Folch, G., Aouinti, S., Carillon, E., Duvergey, H., Houles, A., Paysan-Lafosse, T., Hadi-Saljoqi, S., Sasorith, S., Lefranc, G., and Kossida, S. (2015) IMGT R, the international ImMunoGeneTics information system R 25 years on. *Nucleic Acids Res.* **43**, D413–D422
37. Ehrenmann, F., Duroux, P., and Ginestoux, C. (2020) IMGT Repertoire (IG and TR) Collier de Perles: alpaca (Vicugna pacos) IGHV. *https://www.imgt.org/IMGTrepertoire/2D-3Dstruct/Colliers_dyn.php?english=alpaca&latin=Vicugna%20pacos&group=IGHV&gene=IGHV3-3&domain=VH&numacc=AM773729*
38. Jeong, H. J., Abhiraman, G. C., Story, C. M., Ingram, J. R., and Dougan, S. K. (2017) Generation of Ca2+-independent sortase A mutants with enhanced activity for protein and cell surface labeling. *PLoS One.* **12**, 1–15
39. Nilsson, B., and Nilsson Ekdahl, K. (2012) The tick-over theory revisited: Is C3 a contact-activated protein? *Immunobiology.* **217**, 1106–1110
40. Chen, Z. A., Pellarin, R., Fischer, L., Sali, A., Nilges, M., Barlow, P. N., and Rappsilber, J. (2016) Structure of complement C3(H2O) revealed by quantitative cross-linking/mass spectrometry and modeling. *Molecular and Cellular Proteomics.* **15**, 2730–2743
41. Pangburn, M. K., Schreiber, R. D., and Muller-eberhard, H. J. (1981) Formation of the initial C3 convertase of the alternative complement pathway. Acquisition of C3b-like Activities by Spontaneous Hydrolysis of the Putative Thioester in Native C3'. *Journal of Experimental Medicine.* **154**, 856–867
42. Schatz-Jakobsen, J. A., Zhang, Y., Johnson, K., Neill, A., Sheridan, D., and Andersen, G. R. (2016) Structural Basis for Eculizumab-Mediated Inhibition of the Complement Terminal Pathway. *The Journal of Immunology.* **197**, 337–344
43. Gorham, R. D., Forest, D. L., Khoury, G. A., Smadbeck, J., Beecher, C. N., Healy, E. D., Tamamis, P., Archontis, G., Larive, C. K., Floudas, C. A., Radeke, M. J., Johnson, L. V., and Morikis, D. (2015) New compstatin peptides containing n-terminal extensions and non-natural amino acids exhibit potent complement inhibition and improved solubility characteristics. *J Med Chem.* **58**, 814–826
44. Garcia, B. L., Zhi, H., Wager, B., Höök, M., and Skare, J. T. (2016) Borrelia burgdorferi BBK32 Inhibits the Classical Pathway by Blocking Activation of the C1 Complement Complex. *PLoS Pathog.* 10.1371/journal.ppat.1005404
45. Jensen, R. K., Pihl, R., Gadeberg, T. A. F., Jensen, J. K., Andersen, K. R., Thiel, S., Laursen, N. S., and Andersen, G. R. (2023) Correction: A potent complement factor C3–specific nanobody inhibiting multiple functions in the alternative pathway of human and murine complement. *Journal of Biological Chemistry.* 10.1074/jbc.RA117.001179
46. de Jorge, E. G., Yebenes, H., Serna, M., Tortajada, A., Llorca, O., and de Córdoba, S. R. (2018) How novel structures inform understanding of complement function. *Semin Immunopathol.* **40**, 3–14
47. Fredslund, F., Laursen, N. S., Roversi, P., Jenner, L., Oliveira, C. L. P., Pedersen, J. S., Nunn, M. A., Lea, S. M., Discipio, R., Sottrup-Jensen, L., and Andersen, G. R. (2008) Structure of and influence of a tick complement inhibitor on human complement component 5. *Nat Immunol.* **9**, 753–760
48. Torreira, E., Tortajada, A., Montes, T., Rodríguez de Córdoba, S., and Llorca, O. (2009) 3D structure of the C3bB complex provides insights into the activation and regulation of the complement alternative pathway convertase. *Proc Natl Acad Sci U S A.* **106**, 882–887
49. Jore, M. M., Johnson, S., Sheppard, D., Barber, N. M., Li, Y. I., Nunn, M. A., Elmlund, H., and Lea, S. M. (2016) Structural basis for therapeutic inhibition of complement C5. *Nat Struct Mol Biol.* **23**, 378–386
50. Berends, E. T. M., Dekkers, J. F., Nijland, R., Kuipers, A., Soppe, J. A., van Strijp, J. A. G., and Rooijakkers, S. H. M. (2013) Distinct localization of the complement C5b-9 complex on Gram-positive bacteria. *Cell Microbiol.* **15**, 1955–1968
51. Boero, E., Gorham, R. D., Francis, E. A., Brand, J., Teng, L. H., Doorduijn, D. J., Ruyken, M., Muts, R. M., Lehmann, C., Verschoor, A., van Kessel, K. P. M., Heinrich, V., and Rooijakkers, S. H. M. (2023) Purified complement C3b triggers phagocytosis and activation of human neutrophils via complement receptor 1. *Sci Rep.* 10.1038/s41598-022-27279-4

52. Gautam, S., Gniadek, T. J., Kim, T., and Spiegel, D. A. (2013) Exterior design: Strategies for redecorating the bacterial surface with small molecules. *Trends Biotechnol*. **31**, 258–267
53. De Haard, H. J. W., Bezemer, S., Ledeboer, A. M., Müller, W. H., Boender, P. J., Moineau, S., Coppelmans, M. C., Verkleij, A. J., Frenken, L. G. J., and Verrips, C. T. (2005) Llama antibodies against a lactococcal protein located at the tip of the phage tail prevent phage infection. *J Bacteriol*. **187**, 4531–4541
54. Hoogenboom, H. R., Griffiths, A. D., Johnson, K. S., Chiswell, D. J., Hudson, P., and Winter, G. (1991) Multi-subunit proteins on the surface of filamentous phage: Methodologies for displaying antibody (Fab) heavy and light chains. *Nucleic Acids Res*. **19**, 4133–4137
55. Marks, J. D., Hoogenboom, H. R., Bonnert, T. P., Mccafferty, J., Griffiths, A. D., and Winter, G. (1991) By-passing Immunization Human Antibodies from V-gene Libraries Displayed on Phage. *J. Mol. Biol*. **222**, 581–597
56. Gangaiah, D., Ryan, V., Van Hoesel, D., Mane, S. P., Mckinley, E. T., Lakshmanan, N., Reddy, N. D., Dolk, E., and Kumar, A. (2022) Recombinant Limosilactobacillus (Lactobacillus) delivering nanobodies against Clostridium perfringens NetB and alpha toxin confers potential protection from necrotic enteritis. *Microbiology Open*. 10.1002/mbo3.1270
57. Struijf, E. M., De la O Becerra, K. I., Ruyken, M., de Haas, C. J. C., van Oosterom, F., Siere, D. Y., van Keulen, J. E., Heesterbeek, D. A. C., Dolk, E., Heukers, R., Bardoel, B. W., Gros, P., and Rooijakkers, S. H. M. (2023) Inhibition of cleavage of human complement component C5 and the R885H C5 variant by two distinct high affinity anti-C5 nanobodies. *Journal of Biological Chemistry*. 10.1016/j.jbc.2023.104956
58. Mollnes, T. E., Harboe, M., and Tschopp, J. (1985) Monoclonal Antibodies Recognizing a Neoantigen of Poly(C9) Detect the Human Terminal Complement Complex in Tissue and Plasma. *Scand J Immunol*. **22**, 183–195
59. Bayly-Jones, C., Ho, B. H. T., Lau, C., Leung, E. W. W., D'Andrea, L., Lupton, C. J., Ekkel, S. M., Venugopal, H., Whisstock, J. C., Mollnes, T. E., Spicer, B. A., and Dunstone, M. A. (2023) The neoepitope of the complement C5b-9 Membrane Attack Complex is formed by proximity of adjacent ancillary regions of C9. *Commun Biol*. 10.1038/s42003-023-04431-y
60. Klerx, J. P. A. M., Beukelrnan, C. J., Dijk, H. Van, and Willers, J. M. N. (1983) Microassay for Colorimetric Estimation of Complement Activity in Guinea Pig, Human and Mouse Serum. *J Immunol Methods*. **63**, 215–220
61. Jumper, J., Evans, R., Pritzel, A., Green, T., Figurnov, M., Ronneberger, O., Tunyasuvunakool, K., Bates, R., Žídek, A., Potapenko, A., Bridgland, A., Meyer, C., Kohl, S. A. A., Ballard, A. J., Cowie, A., Romera-Paredes, B., Nikolov, S., Jain, R., Adler, J., Back, T., Petersen, S., Reiman, D., Clancy, E., Zielinski, M., Steinegger, M., Pacholska, M., Berghammer, T., Bodenstein, S., Silver, D., Vinyals, O., Senior, A. W., Kavukcuoglu, K., Kohli, P., and Hassabis, D. (2021) Highly accurate protein structure prediction with AlphaFold. *Nature*. **596**, 583–589
62. Mirdita, M., Schütze, K., Moriwaki, Y., Heo, L., Ovchinnikov, S., and Steinegger, M. (2022) ColabFold: making protein folding accessible to all. *Nat Methods*. **19**, 679–682
63. Pettersen, E. F., Goddard, T. D., Huang, C. C., Couch, G. S., Greenblatt, D. M., Meng, E. C., and Ferrin, T. E. (2004) UCSF Chimera - A visualization system for exploratory research and analysis. *J Comput Chem*. **25**, 1605–1612
64. Pettersen, E. F., Goddard, T. D., Huang, C. C., Meng, E. C., Couch, G. S., Croll, T. I., Morris, J. H., and Ferrin, T. E. (2021) UCSF ChimeraX: Structure visualization for researchers, educators, and developers. *Protein Science*. **30**, 70–82
65. Sarrias, M. R., Franchini, S., Canziani, G., Argyropoulos, E., Moore, W. T., Sahu, A., and Lambris, J. D. (2001) Kinetic Analysis of the Interactions of Complement Receptor 2 (CR2, CD21) with Its Ligands C3d, iC3b, and the EBV Glycoprotein gp350/220. *The Journal of Immunology*. **167**, 1490–1499
66. Forneris, F., Ricklin, D., Wu, J., Tzekou, A., Wallace, R. S., Lambris, J. D., and Gros, P. (2010) Structures of C3b in complex with factors B and D give insight into complement convertase formation. *Science (1979)*. **330**, 1816–1820

67. Doorduijn, D. J., Bardoel, B. W., Heesterbeek, D. A. C., Ruyken, M., Benn, G., Parsons, E. S., Hoogenboom, B. W., and Suzan, S. H. (2020) Bacterial killing by complement requires direct anchoring of membrane attack complex precursor C5b-7. *PLoS Pathog.* 10.1371/journal.ppat.1008606
68. Hammel, M., Sfyroera, G., Ricklin, D., Magotti, P., Lambris, J. D., and Geisbrecht, B. V. (2007) A structural basis for complement inhibition by Staphylococcus aureus. *Nat Immunol.* **8**, 430–437
69. Geisbrecht, B. V., Bouyain, S., and Pop, M. (2006) An optimized system for expression and purification of secreted bacterial proteins. *Protein Expr Purif.* **46**, 23–32
70. Hammel, M., Sfyroera, G., Pyrpassopoulos, S., Ricklin, D., Ramyar, K. X., Pop, M., Jin, Z., Lambris, J. D., and Geisbrecht, B. V. (2007) Characterization of Ehp, a secreted complement inhibitory protein from Staphylococcus aureus. *Journal of Biological Chemistry.* **282**, 30051–30061

ABBREVIATIONS

2YT, 2 times concentrated yeast extract tryptone medium; AF2, AlphaFold2; AMD, age-related macular degeneration; ANA , anaphylatoxin domain; AP, alternative pathway; bac-C3b$_n$, bacteria opsonized with high densities of C3b molecules; BS3, bis(sulfosuccinimidyl)suberate; BSA, bovine serum albumin; C3-MA, C3 methylamine; C3(H_2O), hydrolyzed form of C3; C345c/CTC, C-terminal domain; C3b-bio, C3b-PEG11-biotin; C3G, C3 glomerulopathy; CDR, complementarity determining region; CFU/ml, colony forming units per mL; CP, classical pathway; CUB, C1r/C1s, Uegf, Bmp1 domain; DBCO, dibenzocyclooctyne; DIG, digoxigenin; EM, wells that were not inoculated with bacteria; ERC, European research council; FB, factor B; FB_{DGF}, FB double gain of function mutant; FB_{WT}, FB wildtype; FD, factor D; FH, factor H; FI, factor I; FO-SPR, fiber optic surface plasmon resonance; HSA, human serum albumin; IPTG, isopropylthio-β-galactoside; IRR, nanobody with irrelevant target; KDO-N_3, azide-modified keto-deoxy-octulosonate; LB, Luria-Bertani; LD, low density; LNK, linker domain; LP, lectin pathway; LPS, lipopolysaccharides; MAC, membrane attack complex; MG, macroglobulin; MH-clones, nanobodies containing a Myc- 6×His-tag; NOW, Netherlands Organisation for Scientific Research; O/N, overnight; PBMC, peripheral blood mononuclear cells; PBS, phosphate buffered saline; PBS-T, PBS supplemented with 0.05% Tween-20; PBS-$T_{0.01\%}$, PBS supplemented with 0.01% Tween-20; PER, bacterium containing an empty vector; peri-Nbs, nanobodies in the crude periplasmic extracts; PFA, paraformaldehyde; PNH, paroxysmal nocturnal hemogobinuria; QE19, polyclonal rabbit-anti-nanobody antibodies; QE19-a647, QE19 antibodies coupled with fluorophore Alexa 647; raE, rabbit erythrocytes; RT, room temperature; SEC, size exclusion chromatography; shE, sheep erythrocytes; shEA, sheep erythrocytes opsonized with antibodies (amboceptor); SP, serine protease; SPR, surface plasmon resonance; TED, thioester-containing domain; UNbC3b-1-a488, nanobody UNbC3b-1 labeled with fluorophore Alexa 488; UNbC3b-1-bio, nanobody UNbC3b-1 biotinylated; UNbC3b-1-LH, nanobody UNbC3b-1 with an LPETG-6×His tag; VBS, veronal buffered saline supplemented with 145 nM NaCl, at pH 7.4; VBS/Mg/EGTA, VBS supplemented with 5 mM $MgCl_2$ and 10 mM EGTA; VBS/$MgCl_2$/Tween, VBS supplemented with 2.5 mM $MgCl_2$ and 0.05% Tween-20.

TABLES

Table I: Selection strategies for phage display

#	Library		Round 1			Round 2		
	Day	Llama	surface	[C3b]*	Negative selection	surface	[C3b]	Negative selection
1	43	1 & 2	Plate	5.0	none	Plate	0.1	C3 C5
2							1.0	none
3						Beads	0.2	C3 C5
4							2.0	C3 C5
5	99	1 & 2	Beads	4.0	none	-	-	-
6					LD beads** C3 C3b	-	-	-
7						Beads	0.1	LD beads C3 C3b
8							0.2	LD beads C3 C3b
9							0.8	LD beads C3 C3b

* Plate: amount of coated C3b in µg/ml. Beads: volume of C3b-coated beads in µl
** Low density (LD) beads: density of C3b molecules is approximately 16x lower than on regular C3b beads.

Table II: sources of complement proteins and inhibitors

#	Component	Source	Company/in-house	references
1	C3	Human plasma	In-house	(16)
2	C3b	Human plasma	In-house	(65)
3	C3b-PEG11-biotin	Human plasma	In-house	(15)
4	C3b-PEG4-DBCO	Human plasma	In-house	(51)
5	C3-MA	Human plasma	In-house	(15)
6	C3a		Complement Technology	
7	C3a desArg		Calbiochem	
8	iC3b-PEG11-biotin	Human plasma	In-house	unpublished
9	C3c		Complement Technology	
10	C3dg	Recombinant	In-house	unpublished
11	C3d		Complement Technology	
12	FB_{WT}	Recombinant	In-house	(15)
13	FB_{WT}-a488	Recombinant	In-house	unpublished
14	FB_{DGF}		In-house, plasmid kind gift from Piet Gros	(66)
15	FB_{DGF}-a488	Recombinant	In-house	unpublished
16	FD	Recombinant	In-house	(15)
17	Bb	Recombinant	In-house	See methods
18	C4		Complement Technology	
19	C4b		Complement Technology	
20	C5	Recombinant	In-house	(57)
21	C5a		Bachem, Zwitzerland	
22	C5b6		Complement Technology	
23	C6	Recombinant	In-house	(67)
24	hC3Nb1	Recombinant	In-house, based on	(33)
25	hC3Nb2	Recombinant	In-house, based on	(34)
26	hC3Nb3	Recombinant	In-house, based on	(35)
27	CRig		Kindly provided by Genentech (south San Fransico, CA, USA)	(15)
28	FH		Complement technology	
29	Efb-C	Recombinant	In-house	(68, 69)
30	Ecb	Recombinant	In-house	(70)

31	Sbi		In-house	unpublished
32	SCIN	Recombinant	In-house	(20)
33	properdin		Complement Technology	
34	FI		Complement Technology	
35	MCP		Pepro Tech	
36	FHR5		R&D systems	
37	DAF (CD55)		R&D systems	
38	W4A9		Genscript, based on	(43)
39	Eculizumab	Recombinant	In-house	(57)
40	BBK32		Kind gift from Brandon Garcia	(44)

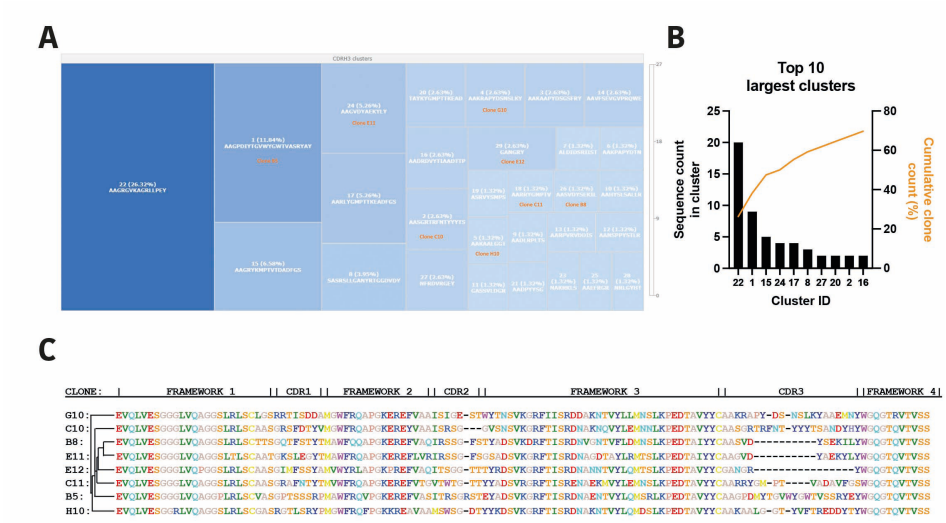

Supporting Figure 1: Sequence analysis of all screened clones. (A) Schematic representation of different clusters containing >80% sequence similarity in the CDR-H3 region. CDR-H3 amino acid sequences are depicted, and cluster sizes are indicated in percentages and color (the darker the higher the percentage). The cluster origin of the eight selected nanobodies is annotated in orange text. (B) The cluster size of the top 10 largest clusters are depicted in a bar-graph with the cumulative cluster count depicted in orange. (C) Amino acid sequence alignment of the 8 selected clones, with the different framework and CDR regions indicated. Phylogenetic tree indicates cluster relatedness and colors depict types of amino acid, using the shapely color scheme.

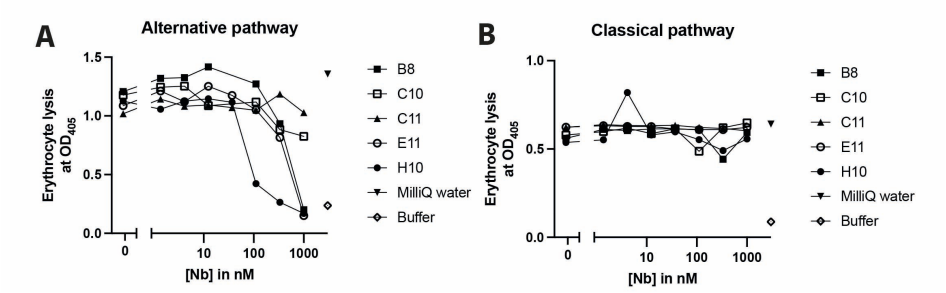

Supporting Figure 2: Inhibition of complement by nanobody clones that were not selected. (A) AP-mediated hemolysis of 2% rabbit erythrocytes (raE) incubated with 10% human serum and nanobodies in different concentrations (B) CP-mediated hemolysis of 2% antibody-opsonized sheep erythrocytes (shEA) incubated with 2.5% human serum and nanobodies in different concentrations. (A-B) The OD450 of the supernatant was detected as a measure of erythrocyte lysis. MilliQ and buffer were taken along as controls for 100% and 0% lysis, respectively. Data present values of one individual experiment.

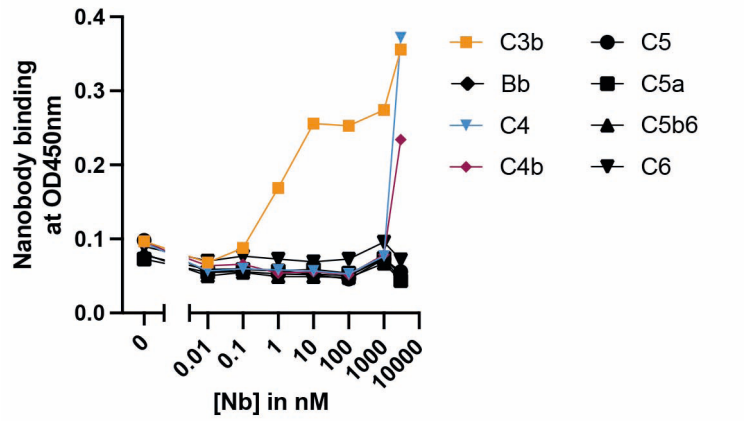

Supporting figure 3: UNbC3b-1 specifically binds to C3b, not to other complement components. Cross reactivity of UNbC3b-1 with other complement components. Bb, C4, C4b, C5, C5a, C5b6, and C6 were coated on microtiter plates, different concentrations of UNbC3b-1 were added, and binding was assessed using polyclonal rabbit-anti-VHH QE19 antibodies and donkey-anti-rabbit-HRP antibodies, at an OD of 450 nm.

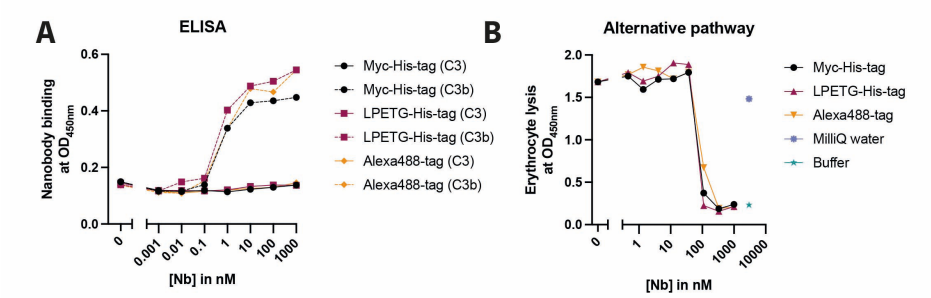

Supporting figure 4: **LPETG-His tag and fluorophores do not influence UNbC3b-1 binding and inhibition.** (A) ELISA with C3 and C3b coated on microtiter plates which were incubated with different batches of nanobody, in different concentrations. Nanobody binding was assessed using polyclonal rabbit-anti-VHH QE19 antibodies and donkey-anti-rabbit-HRP antibodies, at an OD of 450 nm. (B) AP-mediated hemolysis of 2% rabbit erythrocytes (raE) incubated with 10% human serum and different batches of nanobody in different concentrations. MilliQ and buffer were taken along as controls for 100% and 0% lysis, respectively. (A-B) Data presented are of one individual experiment.

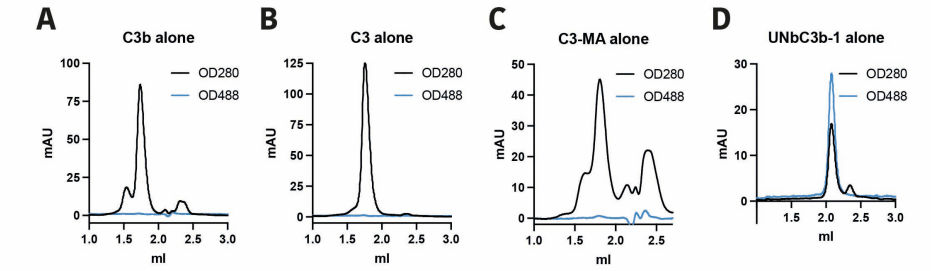

Supporting figure 5: SEC runs of C3b, C3, and UNbC3b-1. (A-C) Size exclusion chromatography controls with C3b (A), C3 (B), and UNbC3b-1-a488 (C) run individually on a Superose 6 Increase column. The OD was measured at 280 nm and 480 nm. Data presented are of one individual experiment.

3

Inhibition of cleavage of human complement component C5 and the R885H C5 variant by two distinct high affinity anti-C5 nanobodies

Eva M. Struijf[1]*, Karla I De la O Becerra[2]*, Maartje Ruyken[1], Carla J.C. de Haas[1], Fleur van Oosterom[1], Danique Y. Siere[1], Joanne E. van Keulen[1], Dani A. C. Heesterbeek[1], Edward Dolk[3], Raimond Heukers[3], Bart W. Bardoel[1], Piet Gros[2], Suzan H.M. Rooijakkers[1]#

[1]*Medical Microbiology, University Medical Center Utrecht, Utrecht University, Utrecht, the Netherlands.*
[2]*Structural Biochemistry, Bijvoet Centre for Biomolecular Research, Department of Chemistry, Faculty of Science, Utrecht University, Utrecht, the Netherlands.*
[3]*QVQ Holding BV, Utrecht, The Netherlands*
**Equal contribution*
#Corresponding author: s.h.m.rooijakkers@umcutrecht.nl

Published in Journal of Biological Chemistry, August 2023, volume 299, Issue 8, 104956

Abstract

The human complement system plays a crucial role in immune defense. However, its erroneous activation contributes to many serious inflammatory diseases. Since most unwanted complement effector functions result from C5 cleavage into C5a and C5b, development of C5 inhibitors, such as clinically approved monoclonal antibody eculizumab, are of great interest. Here, we developed and characterized two anti-C5 nanobodies, UNbC5-1 and UNbC5-2. Using surface plasmon resonance, we determined a binding affinity of 119.9 pM for UNbC5-1 and 7.7 pM for UNbC5-2. Competition experiments determined that the two nanobodies recognize distinct epitopes on C5. Both nanobodies efficiently interfered with C5 cleavage in a human serum environment, as they prevented red blood cell lysis via membrane attack complexes (C5b-9) and the formation of chemoattractant C5a. The cryo-EM structure of UNbC5-1 and UNbC5-2 in complex with C5 (3.6 Å resolution) revealed that the binding interfaces of UNbC5-1 and UNbC5-2 overlap with known complement inhibitors eculizumab and RaCI3, respectively. UNbC5-1 binds to the MG7 domain of C5, facilitated by a hydrophobic core and polar interactions, and UNbC5-2 interacts with the C5d domain mostly by salt bridges and hydrogen bonds. Interestingly, UNbC5-1 potently binds and inhibits C5 R885H, a genetic variant of C5, that is not recognized by eculizumab. Altogether, we identified and characterized two different, high affinity nanobodies against human C5. Both nanobodies could serve as diagnostic and/or research tools to detect C5 or inhibit C5 cleavage. Furthermore, the residues targeted by UNbC5-1 hold important information for therapeutic inhibition of different polymorphic variants of C5.

Introduction

The complement system is an important part of the human innate immune system that is involved in many different biological processes. During embryonal tissue development, it plays a crucial role in cell differentiation and proliferation (1–3). Later in life, complement is best known for its role in clearing pathogens during infection, but also remains involved in maintaining homeostasis, by removing apoptotic cells and immune complexes (4). Although the complement system is tightly regulated, unwanted complement activation is the root cause of a variety of diseases, including paroxysmal nocturnal hemoglobinuria (PNH), atypical hemolytic uremic syndrome (aHUS), and age-related macular degeneration (AMD). Furthermore, erroneous complement activity contributes in more prevalent complex multifactorial diseases like systemic lupus erythematosus (SLE), Alzheimer's disease, and COVID-19 (5).

The complement system can be activated via three distinct pathways: the classical pathway (CP), the lectin pathway (LP), and the alternative pathway (AP). Together, these pathways result in three major effector functions: [1] opsonization, [2] chemo-attraction of immune cells, and [3] direct target cell lysis (6). A central complement component is C5, which circulates in blood at a concentration of ±75 µg/ml (7). C5 is a 190 kDa protein, consisting of two disulfide linked chains (α: 115 kDa, amino acids 678-1676 and β: 75 kDa, amino acids 19-673) (8) and the protein contains a core of eight macroglobulin (MG) domains, and four other domains ('complement C1r/C1s, Uegf, Bmp1' (CUB), C345c, C5d and C5a) (8, 9). During complement activation, C5 convertases (C4b2bC3b and C3bBbC3b) are formed on the target surface, which cleave native C5 molecules in C5a (8 kDa) and C5b (181 kDa). While C5a is released in the fluid phase, where it functions as a chemoattractant, C5b interacts with complement proteins C6, C7, C8, and multiple copies of C9, forming the membrane attack complex (MAC) (6).

Since multiple (unwanted) complement effector functions result from the cleavage of C5, many complement inhibitors have been identified and developed to target this particular molecule. Human pathogens have evolved immune evasion proteins to specifically block the cleavage of C5. For example, *Staphylococcus aureus* expresses staphylococcal superantigen-like protein 7 (SSL7), a protein that potently binds and inhibits cleavage of human C5 (10). Furthermore, ticks (*Ornithodoros moubata*, *Rhipicephalus pulchellus*, and *Rhipicephalus appendiculatus*) contain C5 inhibiting proteins OmCI (11), CirpT (12), and RaCI1, 2, 3 (13), respectively, in their saliva. Furthermore, different snake species have evolved a C5-targeting molecule, called cobra venom factor (CVF) (14). This protein structurally resembles complement component C3b and, when bound by Bb, can interact with and cleave human C5 molecules.

In addition to pathogen-derived C5 inhibitors, a wide variety of C5-targeting molecules, including monoclonal antibodies have been developed (15, 16). Of these, the best known is the monoclonal antibody eculizumab, that is FDA approved, and which binds to C5 and prevents its cleavage by blocking the interaction of C5 with the C5 convertases (17). After the introduction of eculizumab into the clinic, a genetic polymorphism in the C5 α-chain was identified in a group of poor responders, where a histidine is located in position 885 instead of an arginine (C5 R885H) (18). The structural model of eculizumab and C5 revealed that Arg885 in C5 and Phe101 in eculizumab form a crucial interaction for binding and inhibiting C5 (19–21).

In this study, we identify and characterize two llama-derived nanobodies that specifically bind and inhibit human complement C5. They bind to C5 with picomolar affinities on two distinct epitopes. Interestingly, one of these nanobodies has an overlapping epitope with eculizumab and is still able to inhibit C5 R885H.

Results

Identification of two C5-targeting nanobodies that interfere with complement

To develop nanobodies targeting C5, llamas were successfully immunized with recombinant human C5 and nanobody phage libraries were generated (**SFig. 1A & B**)**.** After two rounds of phage display panning, ~200 clones were produced in the periplasm of *Escherichia coli* and unpurified periplasmic fractions were used to screen for clones that bind C5 in ELISA or inhibit complement activity in a CP hemolysis assay. Based on the nanobody sequences and a CP hemolysis assay, used to screen for potent inhibitors (examples shown in **SFig. 1C**) two clones were selected to further characterize, denoted UNbC5-1 and UNbC5-2. UNbC5-1 (13.5 kDa) and UNbC5-2 (12.9 kDa) are significantly distinct, with only 30% amino acid sequence similarity in their complementarity determining regions (CDR) (**Fig. 1A**). Next, UNbC5-1 and UNbC5-2 were purified to assess their ability to block complement activity in human serum. Using a CP hemolysis assay (22), we confirmed that UNbC5-1 and UNbC5-2 were potent complement inhibitors (**Fig. 1B**). Both nanobodies blocked complement-mediated lysis in a dose-dependent manner. As controls we took along in-house produced C5 inhibitors RaCI3 and a monoclonal IgG antibody with the same primary sequence as clinically approved eculizumab (Ecu-mab). The IC_{50} values of UNbC5-1 and UNbC5-2 are in the same range as that of RaCI3 (**Table I**). On a molar basis, Ecu-mab was roughly 3-15 times more potent in blocking C5 cleavage than UNbC5-1 and UNbC5-2. This might partially be explained by the fact that Ecu-mab has two antigen-binding domains per molecule and the nanobodies have only one.

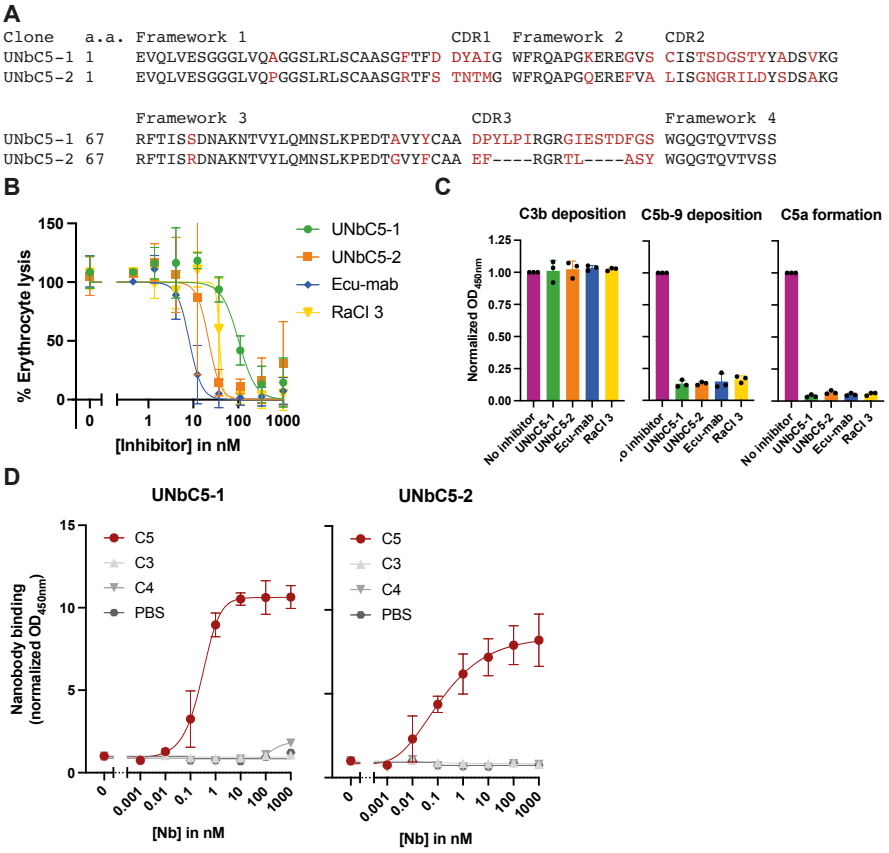

Figure 1: Identification of two C5-targeting nanobodies that interfere with complement. (A) Protein sequence alignment of UNbC5-1 and UNbC5-2. Frameworks 1-4 and CDRs 1-3 are indicated. Conserved amino acids are indicated in black and unique amino acids are indicated in red. (B) CP mediated hemolysis of antibody-coated sheep erythrocytes incubated with 2.5% normal human serum and a titration of our nanobodies UNbC5-1 and UNbC5-2 and known complement inhibitors RaCI3 and Ecu-mab. The OD405 values of the supernatants were measured, the % erythrocyte lysis was calculated using the 0% lysis (buffer) and 100% lysis (milliQ water) control samples. (C) CP complement activation on an IgM-coated microtiter plate, incubated with 4% human serum in the presence of buffer (no inhibitor) or 1000 nM inhibitor. Deposition of complement activation products C3b and C5b-9 on the plate was measured using specific anti-C3 and anti-C5b-9 antibodies and HRP-coupled secondary antibodies, at OD450. C5a formation was measured by adding the supernatant of the reaction to a microtiter plate coated with C5a capture antibodies and C5a was detected with a specific C5a detection antibody and HRP-coupled secondary antibodies, at OD450. Data points were normalized to the maximum levels of C3b and C5b-9 deposition and to the maximum levels of C5a formation when no inhibitor was added. (D) Nanobody binding to complement protein C5 and not homologs C3 and C4. Microtiter plates were coated with complement proteins and incubated with increasing concentrations of UNbC5-1 and

UNbC5-2. Nanobody binding was measured using polyclonal rabbit-anti-VHH QE19 antibodies and donkey-anti-rabbit-HRP antibodies, at an OD of 450 nm. Coating with PBS was taken along as a negative control. Data information: (A) sequences were aligned using T-coffee (44). (B-D) Data represent mean ± SD of 3 individual experiments (B & D) curves were fitted and IC_{50} and EC_{50} values were obtain.

To confirm that UNbC5-1 and UNbC5-2 block complement at the level of C5, we assessed their capacity to block different steps of the complement reaction. Using an ELISA-based complement activity assay (23), we observed that neither UNbC5-1 nor UNbC5-2 affect the initial steps of complement activation since there is no inhibition of C3b deposition on IgM-coated microtiter plates that were incubated with serum (**Fig. 1C**). However, UNbC5-1 and UNbC5-2 can prevent the formation of deposited C5b-9 complexes and the release of C5a into the supernatant. Thus, we show that UNbC5-1 and UNbC5-2 block complement activity at the level of C5 cleavage. Consistent with this finding, UNbC5-1 and UNbC5-2 could also prevent complement-mediated hemolysis by the alternative pathway (**SFig. 1D**).

To assess whether UNbC5-1 and UNbC5-2 are indeed specific for C5, we studied the binding to complement proteins C3 and C4, which share sequence and structural homology with C5 (24). In ELISA, UNbC5-1 and UNbC5-2 showed a dose-dependent binding to C5, while no cross-reactivity with C3 or C4 was observed (**Fig. 1D**). UNbC5-1 and UNbC5-2 bind C5 with EC_{50} values of 0.38 ± 0.2 and 0.12 ± 0.01 nM, respectively (**Table I**). Altogether these data show that UNbC5-1 and UNbC5-2 are C5-specific nanobodies that can interfere with complement activity.

Table I. IC_{50} and EC_{50} values for UNbC5-1, UNbC5-2, Ecu-mab and RaCI3 for inhibiting complement activity and binding complement C5

Inhibitor	IC_{50} (nM) CP	EC_{50} (nM) C5 WT	EC_{50} (nM) C5 R885H
UNbC5-1	137 ± 83	0.38 ± 0.20	1.5 ± 0.4
UNbC5-2	24 ± 15	0.12 ± 0.01	22.4 ± 17.0
Ecu-mab	9 ± 4	0.05 ± 0.01	ND
RaCI3	42 ± 8	-	-

Binding and inhibition curves were fitted using the GraphPad Prism 9.3.0 function "[inhibitor] vs. normalized response – variable slope" & "Asymmetrical Sigmoidal, 5PL, X is concentration". IC_{50} and EC_{50} values were calculated for 3 individual experiments, using the fitted curves and SD were determined.

UNbC5-1 and UNbC5-2 bind C5 with picomolar affinity and recognize distinct epitopes

Next, we used surface plasmon resonance (SPR) to determine the affinities of UNbC5-1 and UNbC5-2 for C5. Briefly, biotinylated nanobodies were coupled to streptavidin coated biosensors and a kinetic titration with C5 was performed to determine k_{on} rates (**Table II**). Next, a dissociation step was performed to measure k_{off} rates and K_D values were calculated. UNbC5-1 binds C5 with a K_D of 119.9 pM (**Fig. 2A**) and UNbC5-2 binds C5 with a kD of 7.7 pM (**Fig. 2B**). As a reference, we took along Ecu-mab and measured a C5 binding affinity of 104 pM, which is in the same range as the published affinity of eculizumab (17.6-120 pM) (**SFig. 2)** (19, 25, 26). To assess whether the two nanobodies bind overlapping epitopes, we performed competition experiments by ELISA. C5-coated microtiter plates were incubated with Myc-labeled UNbC5-1 (UNbC5-1-Myc) in the presence or absence of unlabeled UNbC5-2. After washing, binding of UNbC5-1-Myc to C5 was quantified. We observed that the presence of UNbC5-2 did not affect binding of UNbC5-1-Myc to C5 (**Fig. 2C**). As a control, we showed that UNbC5-1 was able to compete with UNbC5-1-Myc. These data indicate that UNbC5-1 and UNbC5-2 can bind C5 simultaneously and not compete for the same epitope.

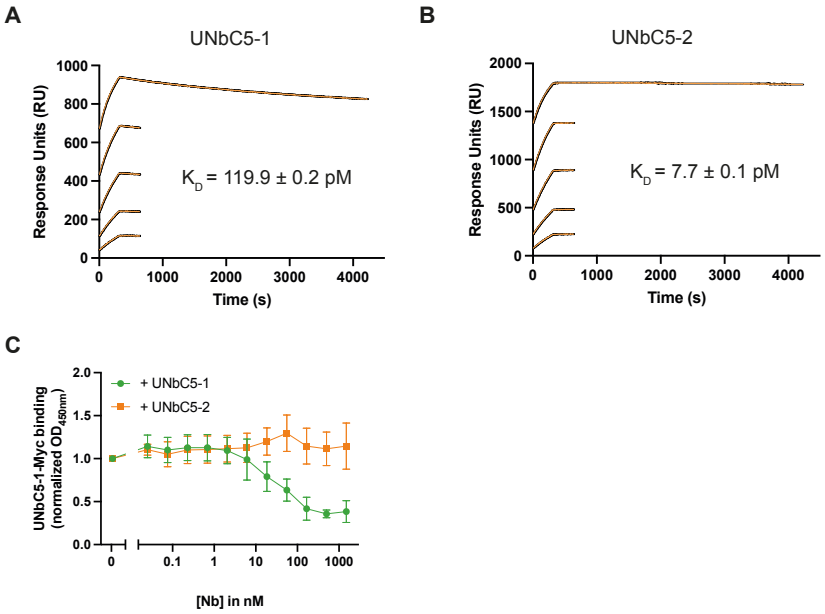

Figure 2: UNbC5-1 and UNbC5-2 bind C5 with picomolar affinity and recognize distinct epitopes. (A-B) SPR curves with UNbC5-1-biotin (biotinylation method [2]) (A) and UNbC5-2-biotin (biotinylation method [1]) (B) as a ligand and C5 as an analyte at concentrations of 12.5, 6.25, 3.13, 1.56, and 0.78 nM, evaluated over 4000 seconds. Experimental data is shown in black, and model fit in orange. (C) Competition ELISA with C5-coated microtiter plates incubated with 5 nM NbC5-1-Myc and a titration of untagged UNbC5-1 or UNbC5-2. Binding of UNbC5-1-Myc to C5 was measured using anti-Myc antibodies and an HRP-coupled secondary antibody, at OD450. Data was normalized on maximum binding of UNbC5-1-Myc, measured when no untagged nanobody was added. Data information: (A-B) Experiments were carried out in duplicate as individual experiments at 25˚C. (C) Data represent mean ± SD of 3 individual experiments.

Table II. Binding affinities of UNbC5-1, UNbC5-2 and Ecu-mab for complement C5

Nanobody	k_{on} ($M^{-1}s^{-1}$)x 10^5	k_{off} (s^{-1})x 10^{-6}	K_D (pM)
UNbC5-1	2.713 ± 0.002	3.254 ± 0.06	119.9 ± 0.2
UNbC5-2	2.937 ± 0.008	0.227 ± 0.03	7.7 ± 0.1
Ecu-mab	3.661 ± 0.003	3.810 ± 0.10	104.0 ± 0.4

Nanobody and Ecu-mab affinities were determined by SPR using C5 as analyte and nanobodies and Ecu-mab as a ligand. All measurements were performed in duplicate. Kinetics were determined using Scrubber 2.0 (BioLogic Software).

Cryo-EM structures of UNbC5-1 and UNbC5-2 in complex with C5

To obtain structural insights into the nanobody binding sites and inhibitory mechanisms, we determined the structure of both non-overlapping nanobodies in complex with C5, using single-particle cryo-EM. The micrographs collected showed well-distributed particles in vitreous ice (**SFig. 3A**). Image processing was performed in CryoSPARC v3.3/3, where the 2D classification already showed secondary structural features of C5 in complex with both nanobodies (**SFig. 3B**). 3D classification and refinement of the cryo-EM density map led to an overall map resolution of 3.6 Å, which allowed the subsequent model building of the C5:UNbC5-1:UNbC5-2 structure (**SFig. 3C**). The structure was built using the previously described C5 crystal structure (3CU7) and AlphaFold generated nanobody models (9, 27). The final refinement of the structure in Phenix 1.20.1 showed acceptable model statistics and stereochemistry (**Table III**). **SFig. 4A & B** show the maps and the resulting models for both C5:nanobody interfaces. Due to a lack of density, the C-terminal C345c domain could not be modeled. A similar flexibility of this C-terminal domain was observed in other C5 cryo-EM structures (9, 12), and the different arrangement of C345c in different crystal structures (9, 10, 13, 19, 28).

Overall, analysis of the C5 molecule in the C5:UNbC5-1:UNbC5-2 structure revealed interesting differences compared to the C5 crystal structure with pdb 3CU7 (**Fig. 3B, left panel**). Most apparent was the different arrangement of the C5a containing the C5 cleavage site, Arg751 – Leu752. While residues Asp746 – Met754 are disordered in native C5 (pdb 3CU7), they adopt a helical conformation in the C5:UNbC5-1:UNbC5-2 structure, internalizing the cleavage site, Arg751 (**Fig. 3B, right panel**). Moreover, our C5 structure also slightly deviates from the structure of C5 bound to CVF (pdb 3PVM) (**SFig. 5A**) (13, 19, 28, 29), with the most apparent differences found in C5a, similar as described above for native C5 (**SFig. 5B**). Interestingly, the conformation of C5 in complex with our nanobodies is similar to those observed for C5 in complex with eculizumab-Fab (pdb 5I5K) and OmCI-RaCI3 (pdb 5HCC) (**SFig. 5C**). In all these structures the scissile loop in the C5a domain adopts a similar helical conformation (**SFig. D)**. In conclusion, the differences between the structure of C5:UNbC5-1:UNbC5-2 and native C5 are similar to the previously described C5 structures in complex with known inhibitors.

Binding Interfaces

UNbC5-1 and UNbC5-2 bind to the C5 α-chain on opposite domains and with a different epitope-paratope architecture (**Fig. 3A**). C5:UNbC5-1 displays a binding interface consisting of a hydrophobic core surrounded by polar interactions, whereas the C5:UNbC5-2 interface is mostly formed by salt bridges and hydrogen bonds.

The interface between C5 and nanobody UNbC5-1 buried a total area of 1,535 Å^2(30). UNbC5-1 binds to domain MG7 in C5. This domain is considered a known target for inhibitory molecules for C5 and its homologous complement proteins C4b and C3/C3b. Reported inhibitors that target this domain in C5 are antibody eculizumab (and its derivatives) (19), while nanobodies NbE3 and hC4Nb8 (22, 31) target domain MG7 in C4b, and nanobody hC3Nb1 (32), targets domain MG7 in C3/C3b. In addition, proposed convertase models (SCIN-convertase (pdb 2WIN), and CVF-C5 (pdb 3PVM)) suggest the involvement of this domain in the convertase-substrate interaction (29, 33). Nanobody UNbC5-1 binds to the connecting loops of the four-stranded antiparallel β-sheet in the MG7 domain in C5 (**Fig. 3C & D**). Most of the interface in UNbC5-1 is formed by the extended CDR3, with limited contribution of CDR1 and 2. Residues Tyr101 – Ile104, of the CDR3 loop, form a hydrophobic core that interacts with three of C5-MG7 loops with residues Met853, Val888, Trp917, and Phe918. Furthermore, nanobody residues, Arg105 forms a cation-π interaction with residue Trp917 in C5 (**Fig. 3C**). The paratope architecture is also maintained by residues Tyr32 of CDR1 and Tyr101 of CDR3 that sandwich Phe100 of CDR3, where Tyr101 interacts with C5-MG7 residue Lys887 (**Fig. 3D**). Additionally, CDR3 residues Arg107 and Asp113 form salt bridges with Glu915 and Arg885 of C5-MG7, respectively (**Fig. 3C**). Finally, CDR1 helps to stabilize the interface with interactions between CDR1 Asp31 and MG7 Thr850. CDR2 may also contribute to the interface due to its backbone proximity to C5-MG7, nevertheless sidechain interactions cannot be assigned unambiguously.

The C5:UNbC5-2 buried a surface area of 1,084 Å^2 (30). The C5 binding epitope of UNbC5-2 comprises residues of several α-helices and loops of the C5d domain (**Fig. 3E**). Similar as the MG7 domain, the C5d domain is targeted by multiple complement inhibitors, including OmCI and RaCI3 (13). The C5 interface is formed by the three CDRs of the nanobody, with a major contribution of CDR3. Residue Ile57 of CDR2 interacts with a hydrophobic patch formed by residues Pro1160 – Val1162 in C5d. Additionally, some electrostatic interactions are formed between C5d residue Lys1091 and residue Glu99 of CDR3, and C5d residue Asp1165 with Arg103 from CDR3. Moreover, hydrogen bond interactions are formed between Arg101 from CDR3 and C5d-residue Leu1197, and between C5d residue Asp1157 and the backbones of Pro100 and Arg101 of CDR3. Additionally, the backbone of Asp1157 also interacts with residue Thr33 of CDR1. Other observed interactions are C5d residue Gln1097 and residue Asn54 of CDR2 and stacking of residue Arg103 with Phe1156 of C5d.

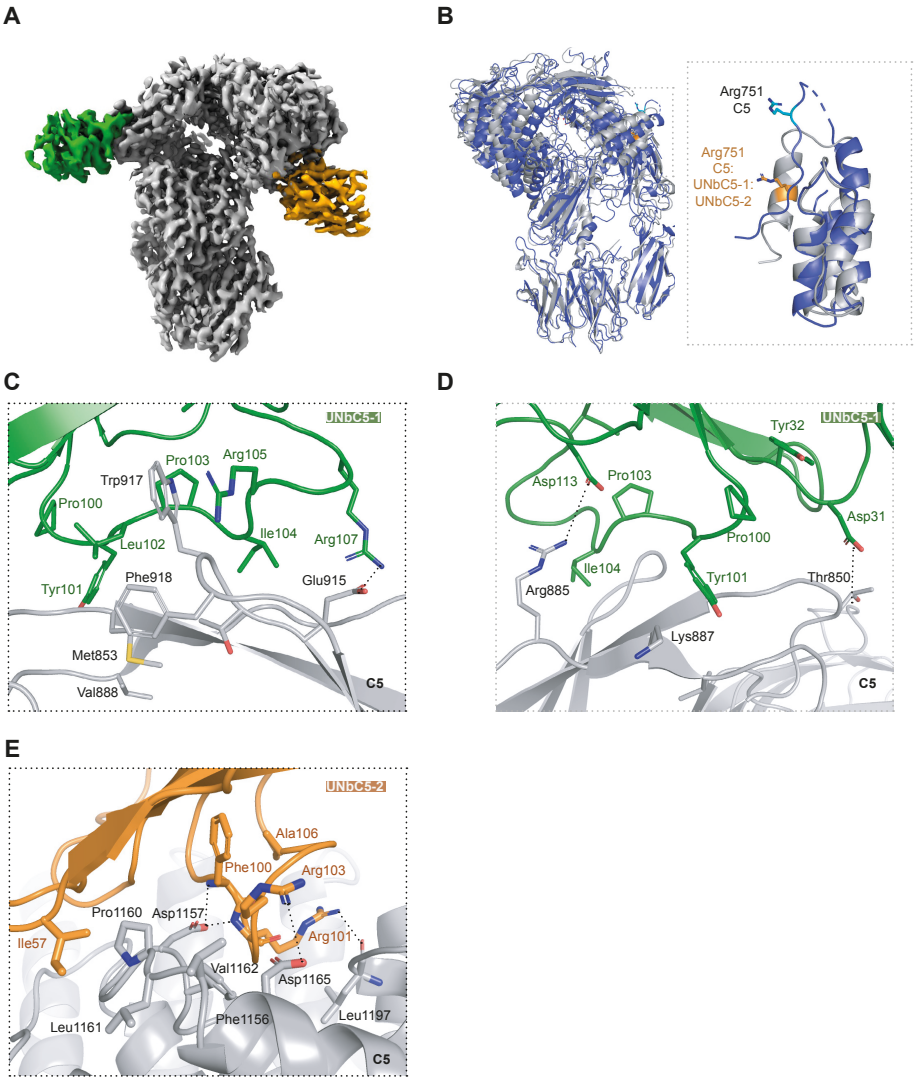

Figure 3: Cryo-EM structures of UNbC5-1 and UNbC5-2 in complex with C5. (A) Cryo-EM density map of the C5:UNbC5-1:UNbC5-2 complex at 3.6 Å resolution, with C5 colored in gray, UNbC5-1 in green, and UNbC5-2 in orange. (B) Comparison of the C5 structure excluding the C345c domain (3CU7, blue) to the C5 of the C5:UNbC5-1:UNbC5-2 structure (grey). Left panel shows both structures in cartoon representation, superimposed and aligned by the C5 MG-ring. Domains C5a, C5d, and CUB of the C5:UNbC5-1:UNbC5-2 structure shows a displacement when compared to the C5 structure. Right panel shows a zoom in of the domain C5a reoriented and aligned, both structures with residue R751 showed as sticks in orange for the C5:UNbC5-1:UNbC5-2 structure and in cyan for C5 (3CU7). (C-E) Zoom in on the C5 interface with nanobodies UNbC5-1 (C, D),

and UNbC5-2 (E), in the same colors introduced in panel A. Amino acids that likely contribute to the interface are shown as sticks representation and annotated. Data information: (A) Cryo-EM density map visualized in ChimeraX and (B-F) figures produced in PyMOL from refined structure.

The C5-binding interface of UNbC5-2 partly overlaps with RaCI3

The UNbC5-2 interface in C5 is close to that of RaCI3, therefore we next compared the structure of C5:UNbC5-1:UNbC5-2 with C5-OmCI-RaCI3 (pdb 5HCC) (**Fig. 4A**). RaCI3 binds to the cleft formed by domain MG1, MG2 and C5d, interacting with all 3 domains of C5 (13). A detailed comparison revealed six overlapping residues between the UNbC5-2 and RaCI3 interfaces on C5d (**Fig. 4B**) (13). In contrast to the C5-RaCI3 interactions, which are mostly driven by extensive van der Waals interactions and hydrogen bonds, the C5:UNbC5-2 interface include hydrophobic interactions with residues Pro1160 – Val1162, a hydrogen bond with Gln1097 and a salt bridge with residue Asp1165 of C5d. To investigate whether UNbC5-2 and RaCI3 can bind C5 simultaneously, we performed an SPR assay. Here we used a Fab domain with the same primary sequence as the Fab domain of eculizumab (Ecu-Fab) as a bait to capture C5 and sequentially injected RaCI3 and UNbC5-2. As expected, we measured association of C5 and RaCI3 (**Fig. 4C**). Interestingly, there was no increase in signal when UNbC5-2 was added. This indicates that UNbC5-2 and RaCI3 cannot bind C5 together. To conclude, the structural model and SPR assay indicate that the binding epitopes of UNbC5-2 and RaCI3 on C5 partially overlap and that both inhibitors cannot bind C5 simultaneously.

UNbC5-1 competes with eculizumab on binding the MG7 domain of C5

A comparative analysis of C5-eculizumab-Fab and C5:UNbC5-1:UNbC5-2, showed an extensive overlap of both the eculizumab-Fab and UNbC5-1 epitope (**Fig. 5A**), with 6 overlapping residues (**Fig. 5B**). The eculizumab-Fab epitope extends through the antiparallel β-strands of the C5-MG7 domain, while the UNbC5-1 epitope is shifted downwards and binds part of the β-strands and their connecting loops (19). eculizumab binds the critical C5 residue Arg885 through a hydrophobic core formed by eculizumab residues Trp33, Phe101 and Trp107 (21). Instead, UNbC5-1 forms a salt bridge with C5-Arg885, at the edge of the epitope interface (**Fig. 3D**). Both, UNbC5-1 in our structural data and biochemical data with eculizumab (21), show interactions with C5-residues Trp917, Arg885 and Lys887, indicating a binding overlap for both inhibitors (19, 21). To confirm with an *in vitro* experiment that UNbC5-1 competes with eculizumab for C5 binding, we performed a competition ELISA. Briefly, we coated C5 and measured binding of UNbC5-1 in the presence of a titration of Ecu-mab. As a negative control we added RaCI3 instead of Ecu-mab. Consistent with the structural data, we observed a decrease in UNbC5-1 binding in the presence of Ecu-mab, but not with RaCI3 (**Fig. 5C**).

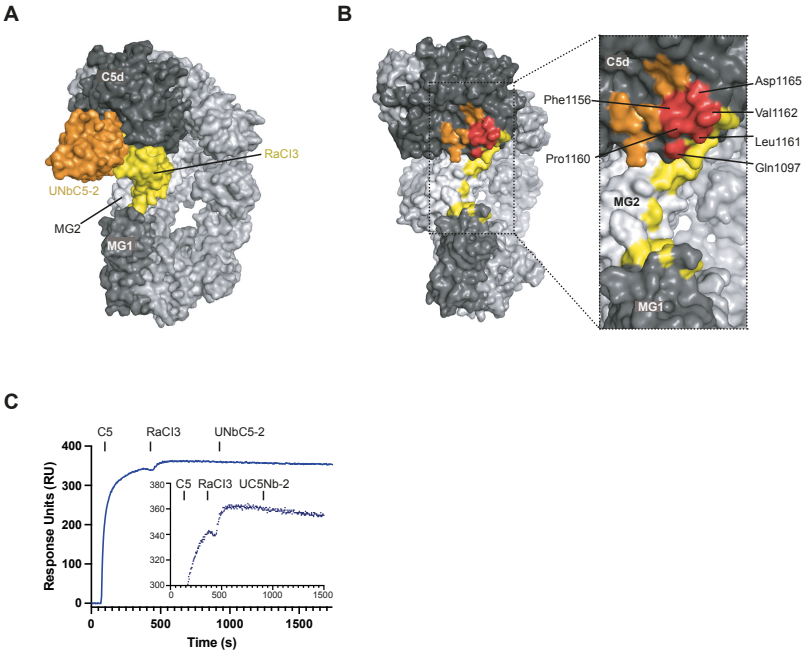

Figure 4: The C5-binding interface of UNbC5-2 partially overlaps with RaCI3. (A) Superposition of the C5:UNbC5-1:UNbC5-2 and the C5-RaCI3 complex in surface representation with UNbC5-2 in orange, RaCI3 in yellow, most of the C5 domains in light gray, MG1 in medium gray and C5d in dark gray. (B) Left panel shows a 45˚ rotation view of panel A, where footprint of epitopes of UNbC5-2, RaCI3 and their overlapping residues (red) are colored according to panel A. Right panel shows a zoom in of UNbC5-2 and RaCI3 epitopes where overlapping residues are annotated. (C) Competition SPR between UNbC5-2 and RaCI3. Ecu-Fab was used as a bait, followed up by injections of 100nM C5, RaCI3 and UNbC5-2, at time points 60, 360, and 900 seconds, respectively. Injection of RaCI3 shows binding to C5 bound to Ecu-Fab. Additionally, sequential injection of UNbC5-2 at 900 seconds showed no signal increase, denoting competition. Figure also shows a zoom-in of RaCI3 and UNbC5-2 injections from time 0 to 1500 seconds where RU 300-380 are shown. Data information: (A, B) Figures produced in PyMOL.(C) Experiments performed in duplicate.

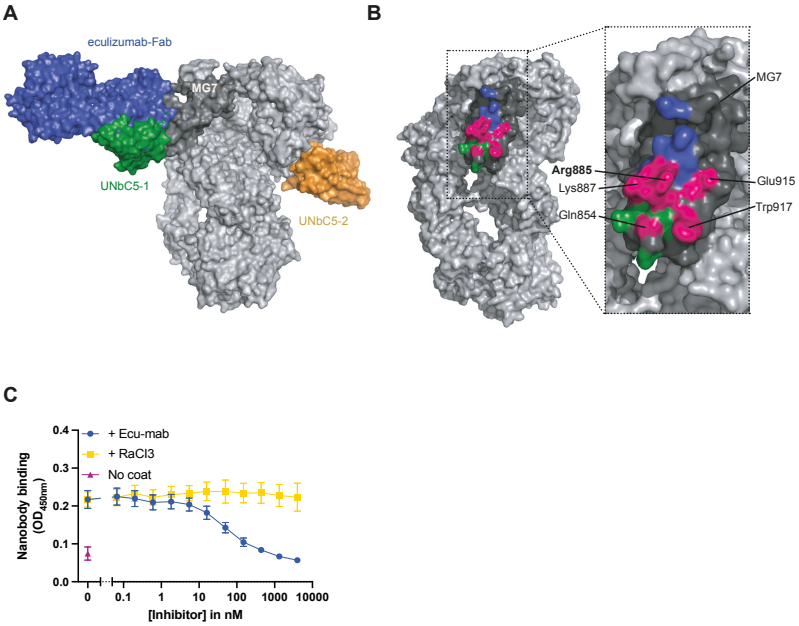

Figure 5: UNbC5-1 competes with eculizumab in binding to the MG7 domain of C5. (A) Superposition of the C5:UNbC5-1:UNbC5-2 and the C5-eculizumab-Fab complex structure. Surface representation shows epitope overlap between UNbC5-1 and eculizumab-Fab. UNbC5-1 is shown in green, UNbC5-2 in orange, eculizumab-Fab in blue, most domains of C5 in light gray and domain MG7 in dark gray. (B) Left panel shows a 45˚ rotation of panel A. Right panel shows a zoom in of the epitope of UNbC5-1 (green) and eculizumab-Fab (blue) on the MG7 domain (dark grey) with an extensive overlap (pink) of the epitope between the interface of both molecules in C5. The overlapping amino acids for both interfaces are indicated, with residue R885 in bold. (C) Competition ELISA with C5-coated microtiter plates incubated with 300 nM UNbC5-1 and a titration of Ecu-mab or RaCl3 (5.49-4000 nM, 3-fold). Binding of UNbC5-1 to C5 was measured using polyclonal rabbit-anti-VHH QE19 antibodies and donkey-anti-rabbit-HRP antibodies, at OD 450 nm. Data information: (A, B) Figures produced in PyMOL, (C) Data represent mean ± SD of 4 individual experiments.

UNbC5-1 and UNbC5-2 bind and inhibit the human C5 variant R885H and are not cross-reactive with murine C5

Next, we wondered if UNbC5-1 could recognize the genetic variant C5 R885H (18), that is not targeted by eculizumab. First, we coated microtiter plates with C5 WT and C5 R885H, added UNbC5-1 or Ecu-mab and measured their binding. As described for eculizumab (18, 20), we observed in ELISA and SPR that Ecu-mab binds C5 R885H poorly (**Fig. 6A & SFig. 6A**). Interestingly, UNbC5-1 binds C5 R885H efficiently (**Fig. 6B & Table I**), with a binding affinity of 15.5 nM (**SFig. 6B)**. This affinity is roughly 100× lower compared to the affinity for C5 WT, which confirms that residue 885 is involved in the binding interface of UNbC5-1 and C5, but is not crucial for its interaction, like it is for eculizumab. Next, we assessed whether UNbC5-1 was also able to prevent complement-mediated erythrocyte lysis with C5 R885H. To assess this, we incubated antibody-coated sheep erythrocytes with C5 depleted serum, repleted with physiological concentrations of C5 WT or C5 R885H. Consistent with the binding data, we observed that Ecu-mab failed to inhibit complement activity via C5 R885H (**Fig. 6C**). On the contrary, UNbC5-1 inhibits complement activity with C5 R885H and C5 WT to a similar extent (**Fig. 6D**). Furthermore, for UNbC5-2, which binds C5 to an epitope unrelated to amino acid 885, we also observed similar binding efficiencies in ELISA (**SFig. 6C)**. Next, we show that UNbC5-2 inhibits complement mediated lysis with comparable potencies using C5 R885H and C5 WT (**SFig. 6D**). Finally, we assessed if UNbC5-1 and UNbC5-2 are cross-reactive with murine C5. Therefore, we performed an AP erythrocyte lysis assay with rabbit erythrocytes and mouse serum. Next to control C5-inhibitors Ecu-mab and RaCI3, we included SSL7, a C5 inhibitor that is described to be cross-reactive with murine C5 (34). UNbC5-1 and UNbC5-2 did not prevent erythrocyte lysis with murine serum (**SFig. 6E**). As expected SSL7 potently inhibited erythrocyte lysis with murine serum, while RaCI3 only inhibited in the two highest concentrations tested and Ecu-mab did not inhibit at all. A sequence alignment of human and murine C5 confirmed that cross-reactivity would be unlikely, since multiple amino acids involved in the C5:nanobody interfaces are different in C5 from mouse compared to C5 from human (**SFig. 6F).** Altogether, these data show that UNbC5-1 and UNbC5-2 bind and inhibit human C5 WT and the genetic variant C5 R885H, but are not cross-reactive with murine C5.

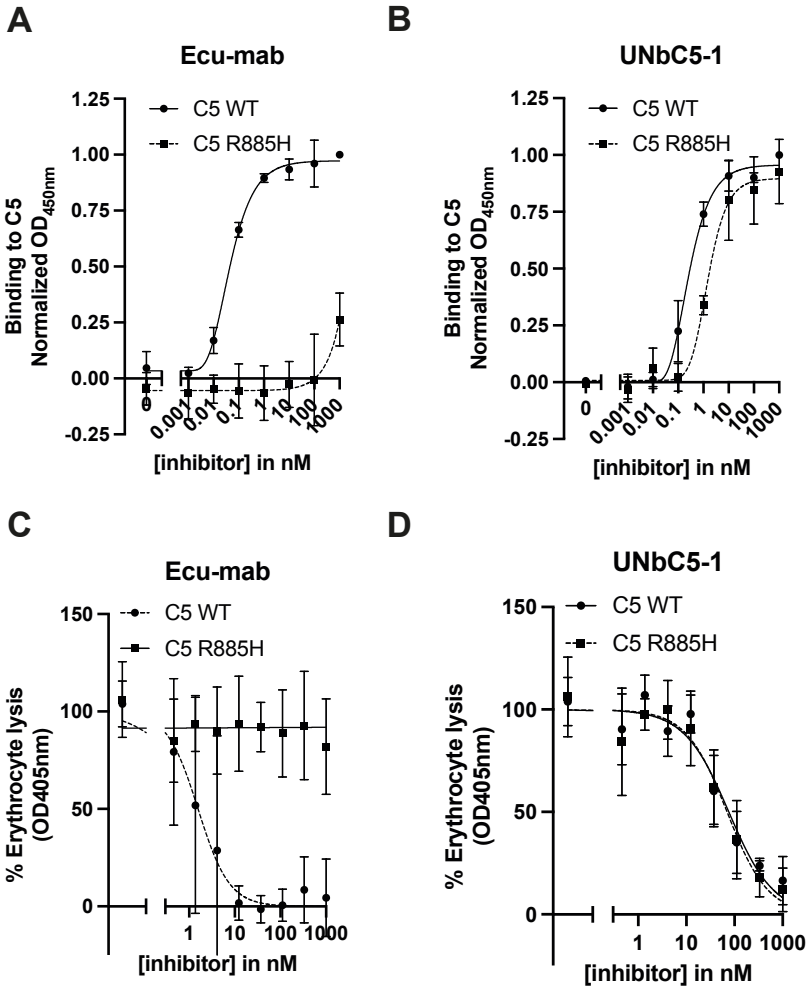

Figure 6: UNbC5-1 binds and inhibits C5 variant R885H. (A-B) Binding of Ecu-mab (A) and UNbC5-1 (B) to C5 WT and C5 R885H, using C5 WT- or C5 R885H-coated microtiter plates, incubated with increasing concentrations of Ecu-mab or UNbC5-1. Binding was assessed with a monoclonal anti-human-kappa antibody (A) or polyclonal rabbit-anti-VHH QE19 antibodies (B) and donkey-anti-rabbit-HRP secondary antibodies (A, B), at OD450. (C-D) CP mediated hemolysis of antibody-coated sheep erythrocytes incubated with 2.5% C5 depleted human serum, repleted with physiological concentrations of C5 WT or C5 R885H and a titration of Ecu-mab (C) or UNbC5-1 (D). The OD450 values of the supernatants were measured, and the % erythrocyte lysis was calculated using a 0% (buffer) and 100% (milliQ water) control sample. Data information: (A-D) Data represent mean ± SD of 3 individual experiments and curves were fitted.

Discussion

With the identification of UNbC5-1 and UNbC5-2 as specific, high affinity C5 targeting nanobodies, this study adds two new C5 inhibitors to the field. We determined the structure of C5 in complex with both nanobodies UNbC5-1 and UNbC5-2 simultaneously to identify their binding interfaces and potentially get insight into the modes of action. This approach was chosen for experimental efficiency and was performed similarly for C5 in complex with inhibitors CirpT, OmCI, and RaCI1, 2, 3 (12, 13).

For UNbC5-1, the mode of action is likely similar to that of eculizumab, since both the cryo-EM structure and competitive binding experiment, reveal overlapping C5-binding sites. For eculizumab it was suggested that binding to the MG7 domain sterically hinders the interaction between C5 and the C5 convertase, preventing C5 cleavage (19).

For UNbC5-2, the inhibitory mechanism is less evident. Because the binding interface of UNbC5-2 partially overlaps with RaCI3 (13), the inhibitory mechanism could be similar to RaCI. For the RaCI family it is suggested that binding to C5d (together with OmCI), induces a conformational change in C5 in which the disordered and exposed scissile loop (residues Asp746 – Met754) is altered into an ordered α-helix with the cleavage site (Arg751 – Leu752) unavailable for C5 cleavage (13, 19, 28, 35). As observed for eculizumab-Fab (derived from mice (19)), OmCI-RaCI3 (derived from ticks (13)) and knob K92 (derived from cows (28)), our llama-derived nanobodies similarly induce a conformational change that leads to the formation of an ordered scissile loop in C5a. The formation of an α-helix is comparable to the conformational change described for small molecule inhibitor (compound 7), which directly interacts with the scissile loop in C5a (36). Since we generated a combined structure with both nanobodies, it is impossible with our data to attribute this proposed mechanism of inhibition to either UNbC5-1 or UNbC5-2, or both. Nevertheless, this structural change in C5 has been suggested to be part of the inhibitory mechanism for the RaCI family, and more recently also for knob K92 (28). This, together with our data, suggests that this partial molecular movement of the α-chain and helical rearrangement of the scissile loop is a common inhibitory mechanism that can be triggered by various C5-inhibitors from different sources and targeting different epitopes across the molecule (12, 19, 28).

Although eculizumab is proven to be an effective therapy in controlling diseases like aHUS, a drawback is therapy resistance in a small proportion of patients with C5 polymorphism (18). This was explained by the fact that the interaction of eculizumab with the Arg885 residue is essential for binding (21). Interestingly, we observed that UNbC5-1 can bind and can inhibit the R885H variant of C5. Even though UNbC5-1 does

interact with Arg885, the structure suggests that mutation of Arg885 into a histidine has less impact on the C5:UNbC5-1 interface, because Arg885 interacts mostly with a polar patch (formed by residues Glu915 of MG7, and Arg107 and Asp113 of CDR3 at the edge of the interface) and a His-885 variant could probably still establish a polar interaction. In contrast, Arg885 extends into a hydrophobic pocket in the eculizumab interface surrounded by bulky sidechain amino acids such as Trp33, Phe101, and Trp107 where a histidine sidechain might be too small to extend inward and interact, therefore disrupting the core interaction of the interface (19, 21). We propose that the detailed binding interface of UNbC5-1 and C5 is a good starting point to further optimize reactivity of UNbC5-1 towards the genetic variant of C5 R885H and obtain more insight in the requirements for efficient C5 inhibition in general.

In the last decades, diverse C5 targeting molecules have been identified and developed, including monoclonal antibodies, single domain antibodies, small molecules, nucleic acid-based therapies, pathogen derived proteins and peptides, but no nanobodies (16). In contrast, nanobodies against other complement components (C1q (37), C3 (32, 38, 39), C4 (22, 31), properdin (40, 41)) and a complement receptor (CRIg (42, 43)) were previously identified. The use of nanobodies as therapeutic molecules has gained increasing interest in many different fields, especially since the successful introduction of the first nanobody in the clinic, Caplacizumab (targeting plasma protein von Willebrand factor) (44). Compared to conventional antibodies, nanobodies lack an Fc-tail to activate the immune system, which is favorable when complement inhibition is the goal. At the same time, the lack of an Fc-tail shortens the half-life of nanobodies in circulation, while improving tissue penetration. In addition to their therapeutic potential, nanobodies are increasingly used as tools in research and diagnostics because they are easy to produce and label with for example fluorophores (45, 46) or to conjugate to solid matrixes for chromatography (47). Also, the presented C5-specific nanobodies could be developed for specific detection of C5 in complex biological specimens or for affinity purification of C5 from human plasma. Furthermore, their inhibitory action makes them suited as tools to inhibit the complement system at level of C5 cleavage, thereby studying the role of complement in diseases.

To conclude, in this study we developed and characterized two anti-C5 nanobodies that bind C5 with picomolar affinities and efficiently inhibit complement at the level of C5 cleavage. Both nanobodies can be used to detect C5 and inhibit C5 cleavage for diagnostic and/or research purposes. Finally, both nanobodies have the potential to be further developed for therapeutic purposes and detailed binding interfaces obtained here could help to further develop high affinity C5 inhibitors that are reactive to different genetic variants of C5.

Experimental procedures

Serum, proteins and complement inhibitors

Normal human serum was obtained from a pool of healthy donors as previously described (48). C5 depleted serum was obtained from Complement Technology. Complement protein C3 was isolated and purified from freshly obtained human plasma, as described before (49). Complement protein C4 was obtained from Complement Technology. Complement proteins C5 WT (unless stated differently) and C5 R885H and complement inhibitor RaCI3 were recombinantly produced and purified in our lab, using EXPI293F cells.

C5 WT and C5 R885H

For C5 expression, we used the pcDNA 3.4 TOPO™ vector (ThermoFisher Scientific). This vector was made circular by inserting a multiple cloning site (pcDNA34-MCS) using the pcDNA 3.4 TOPO™ TA cloning kit (ThermoFisher Scientific). The XbaI and AgeI restriction sites, adjacent to the original pcDNA34-TOPO site, were used to clone the Cystatin(S) signal peptide (coding for MARPLCTLLLLMATLAGALA) with an upstream KOZAK (ACCACC) sequence and a downstream NheI and NotI cloning site, followed by a C-terminal sequence coding for a linker (GGGGS), an LPETGG site and a 6x Histidine tag (pcDNA34-Cystatin(S)-Linker-LPETG-HIS vector). The 13 and 15 bp sequences, adjacent to the XbaI and AgeI site and the original pcDNA34-TOPO site, were left intact. Subsequently, the C5 gene (a kind gift from U-Protein Express, Utrecht) without start and stop codon was cloned into this vector, using the NheI and NotI sites (**Table IV**). For cloning the C5-R885H mutant, we used overlap extension PCR to introduce the R885H mutation using the pcDNA34-Cystatin(S)-C5-Linker-LPETG-HIS vector as a template. Primers used: 5-XbaI: 5'GACCGATCCAGCCTCCGG ACTCTAGAGGATCGAAC & 3-R885H: 5' GAGCCCTCTACTTTCTGG**T**GCACACAT TTGGAGGACTTTG combined with 5-R885H: CTCCAAATGTGTGC**A**CCAGAAAG TAGAGGGCTCCTC & 3-AgeI: 5' GATATCAAACTCATTACTAACCGGTAGGGATC GAAC, with R885H mutations depicted in bold. The final C5-R885H PCR product was cloned into the XbaI and AgeI site of the pcDNA34-MCS vector using Gibson assembly (New England Biolabs). After verification of the correct sequences, the C5 and C5-R885H plasmids were used to transfect EXPI293F cells (ThermoFisher Scientific). EXPI293F cells were grown in EXPI293 medium (Life Technologies) in culture filter cap Erlenmeyer bottles (Corning) on a rotation platform (125 rotations/min) at 37°C, 8% CO_2. One day before transfection, cells were diluted to $2x10^6$ cells/ml. The next day, cells were diluted to $2x10^6$ cells/ml using SFM4Transfx-293 medium, containing UltraGlutamine I (VWR International) prior to transfection using PEI (Polyethylenimine HCl MAX; Polysciences). Therefore, 0.5 µg DNA/ml cells, containing 50% empty pcDNA34-MCS "dummy" vector, was added to Opti-MEM (1:10 of total volume;

Gibco) and gently mixed. After adding PEI (1 µg/ml) in a PEI/DNA (w/w) ratio of 5:1, the mixture was incubated at room temperature for 20 min and then added dropwise to the cells while manually rotating the Erlenmeyer culture bottle. After 3 to 5 h, 1 mM valproic acid was added to the transfected cells. After 5 days of expression, the cell supernatant was collected by centrifugation and filtration (0.45 µM). C5 and C5-R885H supernatants were concentrated and buffer exchanged to 25 mM Hepes, 500 mM NaCl, 5 mM benzamidine, pH8.2 using the QuixStand benchtop system (Ge Healthcare) and 25 mM imidazole was added before application to a HiTrap Chelating column (GE Healthcare). The column was washed with 50 mM imidazole, before C5 and C5-R885H were eluted using 175 mM imidazole using the Äkta Pure protein chromatography system (GE Healthcare). C5 and C5-R885H were dialyzed to PBS and stored at -80°C.

RaCI 3

For RaCI 3 expression, a RaCI 3 gBlock was cloned into the NheI/NotI site of our pcDNA34-Cystatin(S)-LPETG-HIS vector (**Table IV**). This vector was cloned as described for C5 WT, with the exception that this pcDNA34 construct lacks the GGGGS linker. After verification of the correct sequence, the plasmid was used to transfect EXPI293F cells, as described for the expression of C5 WT and C5 R885H. A total of 1 µg DNA/ml of cells was used. RaCI 3 was isolated using a HISTrap FF column (Cytiva, GE Healthcare) in the Äkta Pure protein chromatography system (GE Healthcare), according the manufacturer's description. Before application to the column, the supernatant was dialyzed against 50 mM Tris, 500 mM NaCL, pH8.0 and 30 mM imidazole was added to reduce aspecific binding. RaCI 3 protein was eluted from the column via a 30 to 250 mM imidazole gradient. Fractions containing protein were collected and dialysed against 50 mM Tris/300 mM NaCl, pH8.0.

Ecu-mab and Ecu-Fab

A human IgG2/4 monoclonal antibody with the same primary sequence as clinically approved eculizumab, denoted as Ecu-mab, was produced and purified in our lab. Briefly, the heavy and light chain variable plus constant region amino acid sequences of eculizumab (17) were from patent (WO2017044811A1). gBlocks containing codon optimized sequences of the VH + constant & VL + constant region with an upstream KOZAK and HAVT20 signal peptide were cloned into the XbaI/AgeI site of the pcDNA34-MCS vector, using Gibson assembly (New England Biolabs) (**Table IV**). After verification of the correct sequence, plasmids were used to transfect EXPI293F cells (Thermo Fisher Scientific), as described for the expression of C5 WT and C5 R885H, with the only exception that 1 µg DNA/ml of cells was used with a ratio of light chain:heavy chain of 3:2. Ecu-mab was purified using a HiTrap Protein A column (GE Healthcare) and the ÄKTA Pure (GE Healthcare), according to the manufacturer's description. Ecu-mab fractions were pooled and dialyzed against PBS. The Ecu-mab preparation was analyzed by gel filtration on a

Superdex 200 10/300 GL column (GE Healthcare) and stored at -20°C when >95% of Ecu-mab appeared as monomeric antibody. For Ecu-Fab (a Fab domain with the same primary sequence as the Fab domain of eculizumab), the light chain vector was similar as used for Ecu-mab IgG. The heavy chain constant region of Ecu-Fab ends with the amino acid sequence EPKSC, followed by a flexible linker (GGGGS), LPETG site and a 6x histidine tag. The gBlock containing the codon optimized sequence of the VH + constant Fab region with an upstream KOZAK and HAVT20 signal peptide was cloned into the XbaI/AgeI site of the pcDNA34-MCS vector, using Gibson assembly (New England Biolabs) (**Table IV**). The expression of Ecu-Fab in EXPI293 cells was similar as described for Ecu-mab IgG. The expression supernatant was dialyzed against 50 mM Tris, 500 mM NaCl, pH8.0 and 30 mM imidazole was added before application to a HISTrap column (GE Healthcare). Elution of Ecu-Fab was performed by a gradient of 30 to 250 mM imidazole. Isolated Ecu-Fab was dialyzed against PBS and stored at 4°C and -80°C.

Llama immunization, phage library, phage display & periplasmic fractions

Two llamas (lama glama) were immunized with recombinant human C5 (WT). Phage display libraries were produced according to standard protocols (50). Briefly, cDNA was generated from RNA isolated from llama peripheral blood mononuclear cells (PBMCs). Nanobody-encoding genes were cloned into a phagemid pPQ81 vector (a derivative of pHEN1 (51)), and two phage display libraries with estimated sizes of 10^8 clones/library were generated. To select C5 binding nanobodies, we produced phages and performed two rounds of phage display, according to standard procedures (52, 53), with the antigen immobilized on Nunc Maxisorp plates (VWR 735-0083, Thermo Fisher Scientific) in different concentrations (round 1: 0.5 and 5.0 µg/ml, round 2: 0.1 and 1.0 µg/ml) to have diversity in stringency. Phages (~10^{10} CFU/well round 1 and ~10^9 CFU/well round 2) were added for 2 h, at room temperature (RT) and after incubation wells were washed extensively, to remove unbound phages. Phages were eluted with triethanolamine solution (pH >10), for 15 minutes, at RT, while shaking, and rescued by infection in *E. coli* TG1 bacteria. Next, bacteria were plated and ~200 single colonies were picked to obtain bacterial cultures with one clone/culture. Nanobody expression in the periplasm of E. coli was induced using isopropylthio-β-galactoside (IPTG) for 4 h. Periplasmic fractions were collected via a cycle of freeze and thawing.

Nanobody production and purification

Nanobodies with Myc- and His-tags

For nanobody productions, pPQ81 vectors (derived from pHEN1 (51)) encoding the nanobody genes were transformed into *E. coli* Rosetta 2 (DE3) BL21 cells (Merck). pPQ81 vectors provided nanobodies with C-terminal Myc- and His-tags (AAASGSLEQKLISEEDLNGAAHHHHHHGAA). Transformed bacteria were inoculated in

2× Yeast Extract Tryptone (2YT) medium supplemented with 2% glucose and 100 µg/ml ampicillin and grown shaking, at 37°C, overnight (O/N). The next day cultures were diluted 1:20 in 2YT medium supplemented with 0.1% glucose and 100 µg/ml ampicillin and grown at 37°C, shaking, until an OD_{600} of 0.6-0.9 was obtained. Then, nanobody production was induced with 1 mM IPTG and expression was continued for 4 hours at 37°C or O/N at RT, shaking. Next, cultures were spun down for 10 minutes at 6000 g. Pellets were dissolved in PBS and frozen for >30 minutes at -80°C or O/N at -20°C and thawed, to release periplasmic fractions in the supernatant. Thawed pellets were centrifuged for 15 minutes at 6000 g. Next, immobilized metal-affinity chromatography (IMAC) was used with ROTI Garose-His/Co beads (Roth) to purify nanobodies via their His-tag. After binding to the beads, nanobodies were eluted with 150 mM imidazole. Subsequently, nanobodies were dialyzed to PBS and concentrations were determined at A_{280} using the Nanodrop One (Thermo Fisher Scientific). For both nanobodies production yields were ±5 mg/L bacterial culture. Finally, nanobody size, purity and concentration were verified using SDS-PAGE (**SFig. 7**), stained with InstantBlue Safe Coomassie stain (Sigma Aldrich).

Nanobodies without a Myc-tag

To produce nanobodies without a Myc-tag, nanobody genes were recloned in the pYQ11 vector (previously published as pYQVQ11 (54)), which encodes for a C-terminal C-Direct tag (derived from a FLAG-EPEA tag) containing a free thiol (cysteine) and an EPEA (Glu, Pro, Glu, Ala) purification tag (C-tag, Thermo Fisher Scientific). Vectors were transformed into yeast cells (Saccharomyces cerevisiae strain VWK18 (55)). For expression cells were inoculated in Yeast Peptone (YP) medium supplemented with 2% glucose and grown for 24 hours, at 30°C, shaking. Next, cultures were diluted 1:20 in Yeast Nitrogen Base (YNB) medium supplemented with 2% glucose and grown at 30°C, shaking. After 24 hours, cultures were diluted 1:10 by adding YP medium, supplemented with 2% glucose and 1% galactose. Nanobody production was continued for >64 hours, at 30°C, shaking, until an OD_{600} of >20 was reached. Next, cells were spun down for 20 minutes at 6000 g and supernatants were collected, filter sterilized (0.45 µm) and stored at 4°C until purification. Produced nanobodies were purified from yeast supernatants using a CaptureSelect C-tag column (Thermo Fisher Scientific) and an Äkta Start (Cytiva). For this, the supernatants were adjusted to neutral pH by adding 10× PBS. Bound nanobodies were washed with at least 5 column volumes of PBS and eluted off with 20 mM citrate buffer supplemented with 150 mM NaCl, pH 3.0. Next, samples were neutralized with 100 mM Tris, pH 7.5 and dialyzed to PBS. Protein concentration was determined at A_{280} using a MultiScan (Thermo Fisher Scientific). Finally, nanobody size, purity and concentration were confirmed using SDS-PAGE, followed by Instant Blue Safe Coomassie staining.

Biotinylated nanobodies, Ecu-mab and Ecu-Fab

Nanobodies and eculizumab(-Fab) were biotinylated using two methods. [1] Nanobody sequences were modified to contain a C-terminal LPETG-His motif and were subsequent produced and purified in *E. coli* BL21 Rosetta, like described above. After purification 50 µM LPETG-His nanobody was incubated with 25 µM His-tagged Sortase A7 (His-Tevg-SrtA7) (56) and 1 mM GGGK-Biotin (provided by Louris Feitsma, Medicinal Chemistry, Utrecht University), in 50 mM Tris, supplemented with 300 mM NaCl, for 2 hours, at 4°C. His-Tevg-SrtA7 was modified, expressed in *E. coli* and purified using its His-tag, in our lab. Next, samples were equilibrated with 20 mM imidazole and run over an HisTrap FF column to remove all His-tagged compounds from the reaction. Subsequently, a 30 kDa Amicon Tube (Merck Millipore) was used to concentrate the biotinylated nanobodies. To remove excess GGGK-biotin, samples were run over a Zeba™ Spin Desalting column (Thermo Fisher Scientific). [2] Myc-His-tagged nanobodies produced in *E. coli* and Ecu-mab and Ecu-Fab, were randomly biotinylated via N-hydrocysucciminimidyl (NHS)-labeling. Briefly, nanobodies at a concentration of 50-70 µM were incubated for 2 hours, at 4°C, with 20× molar excess of EZ link™ NHS-PEG4-Biotin (Thermo Fisher Scientific, 210901BID), in PBS, pH 7.4. Unreacted linker was separated with Bio-Spin 6 columns (BioRad), that were previously equilibrated in PBS. The nanobody concentrations were determined using a Nanodrop One.

Erythrocyte lysis assays

Sheep (Alsever Biotrading) and rabbit blood (kindly provided by Utrecht University, Faculty of Veterinary Medicine) was washed 3× with PBS and diluted to a 2% erythrocyte suspension in VBS (Veronal buffered saline + 145 nM NaCl, pH7.4). For the CP, sheep erythrocytes, pre-opsonized with 1:2000 polyclonal rabbit-anti-sheep IgM (haemolytic amboceptor (57)), were used and VBS was supplemented with 0.25 mM $MgCl_2$ and 0.5 mM $CaCl_2$ (VBS++). For the AP, rabbit erythrocytes were used and VBS was supplemented with 5 mM $MgCl_2$ and 10 mM EGTA (VBS/MgEGTA). Periplasmic fractions (1:5 diluted with PBS) or purified nanobodies (0.45-1000 nM, 3-fold) were incubated for 10 minutes at RT with normal human serum (CP: 2.5%, AP: 10%) or 2.5% C5 depleted serum, repleted with physiological concentrations of C5 WT or C5 R885H. Next nanobody-serum mixes were added to 2% erythrocyte suspensions and samples were incubated at 37°C, shaking, (CP: 10 minutes, AP: 30 minutes). Afterwards plates were spun down for 7 minutes at 3500 rpm. Supernatants were diluted 1:3 with milliQ water and haemoglobin release was measured in a flat-bottom plate, using an iMark Microplate Reader (Biorad) at 405 nm.

ELISA: Coating, incubation times & development

Unless stated differently, Nunc Maxisorp plates (VWR 735-0083, Thermo Fisher Scientific) were coated with 2 µg/ml purified protein, diluted in PBS, in a volume of 50 µl. Plates

were incubated O/N, at 4°C, non-shaking. Next, plates were blocked with 80 µl 4% BSA in PBS + 0.05% Tween-20 (PBS-T). All following incubation steps were performed in 50 µl 1% BSA PBS-T, shaking, at RT, for 1 hour. In-between all steps, plates were washed 3× with PBS-T. To develop the ELISAs, tetramethylbenzidine (TMB) substrate solution of 6 mg/ml, dissolved in DMSO, was used to activate the enzyme labeled antibodies, unless stated differently. When a color change was observed, the reaction was stopped with 0.5 M sulfuric acid and absorbance was measured at 450 nm using an iMark Microplate Reader.

Immune response ELISA

Wells coated with C5 were incubated with llama serum to measure the presence of C5 binding llama antibodies. Llama serum was diluted in PBS, supplemented with 1% skimmed milk (Marvel). Llama antibodies were detected using 1:2000 primary polyclonal rabbit-anti-VHH antibody QE19 (QVQ Holding BV) and 1:5000 secondary polyclonal donkey-anti-rabbit-HRP antibodies (Jackson Immuno Research). ELISA was developed using 3.7 mM O-phenylenediamine dihydrochloride + 50 mM $Na_2HPO_4 2H_2O$ + 25 mM citric acid + 0.03% H_2O_2 and the reaction was stopped with 0,5 M sulfuric acid.

Binding ELISA

Wells coated with purified complement components C3, C4, C5 WT or C5 R885H were used to assess the binding of our nanobodies and Ecu-mab to different complement proteins. Nanobodies and Ecu-mab were added in a 10-fold titration (0.001-1000 nM). Next, wells containing nanobodies were incubated with 1:2000 primary polyclonal rabbit-anti-VHH antibody QE19 (QVQ Holding BV) and 1:5000 secondary polyclonal donkey-anti-rabbit-HRP antibodies (Jackson Immuno Research). To detect Ecu-mab binding, wells were incubated with anti-human-kappa-HRP (Southern Biotech) detection antibodies.

Competition ELISA

Plates coated with purified complement component C5, were used to assess if our nanobodies compete. 5 nM UNbC5-1-Myc was incubated with a titration of untagged UNbC5-2 (0.025-1500 nM, 3-fold) for 10 minutes, at RT and subsequently added to the C5 coated wells. Next, wells were incubated with 1:2000 primary monoclonal mouse-anti-Myc-tag clone 9B11 #2274 (Cell Signaling Technologies), followed by 1:5000 secondary monoclonal goat-anti-mouse-PO (Southern Biotech). To assess competition between our nanobodies and Ecu-mab/RaCI3, 300 nM of UNbC5-1 or UNbC5-2 was incubated with a titration of Ecu-mab or RaCI3 (5.49-4000 nM, 3-fold) for 10 minutes at RT, prior to adding it to the C5 coated wells. Next, nanobody binding was detected using primary polyclonal rabbit-anti-VHH antibody QE19 and 1:5000 secondary polyclonal donkey-anti-rabbit-HRP antibodies.

Classical Pathway Complement ELISA

Plates were coated with 3 µg/ml human IgM (Millipore) in 0.1 M sodiumcarbonate, pH 9.6. 1000 nM inhibitor (UNbC5-1, UNbC5-2, Ecu-mab or RaCI3) was incubated with 4% normal human serum, added to the IgM coated wells, and incubated for 1 hour, at 37°C, shaking. To measure C5a formation, 25 µl of the supernatant was diluted with 25 µl 1% BSA PBS-T and added to a Nunc Maxisorp plate coated with 1 µg/ml anti-C5a capture antibody (C5a DuoSet ELISA kit, R&D systems). Next, we detected C5a with 2 µg/ml anti-C5a detection antibody (C5a DuoSet ELISA kit, R&D systems), followed by an incubation of 1:5000 streptavidin-HRP (Southern Biotech). To measure deposition of C3b on the IgM coated plates, 1:10,000 primary anti-C3 WM-1 clone digoxigenin (DIG) labeled antibodies (Sigma), and 1:8000 secondary anti-DIG-PO antibodies (Roche) were added. To measure deposition of C5b-9 on the IgM coated plates, 1:1000 primary monoclonal mouse-anti-C5b-9 aE11 (produced in our lab, based on (58, 59)) and 1:5000 secondary polyclonal goat-anti-mouse-PO were used.

Surface plasmon resonance (SPR)

Planar streptavidin coated chips (P-strep, Sens BV) were spotted with biotinylated UNbC5-1 (method [2]), UNbC5-2 (method [1]), and Ecu-mab (method [1]) (25 and 50 nM, in duplicate) under a continuous flow for 1 hour using a microspotter (Wasatch). Subsequent SPR experiments were carried out in the IBIS-MX96 (IBIS Technologies) with SPR buffer (20 mM HEPES pH 7.4, 150 mM NaCl, 0.005% Tween-20). Initial testing showed limited regeneration with different high ionic strength (20 mM HEPES, 2 M NaCl, pH 7.4); ion containing (20 mM HEPES, 150 mM NaCl, 1 M $MgCl_2$, pH 7.4); or low pH regeneration buffers (10 mM Glycine, pH 3.0). Therefore, the method of kinetic titration was selected to perform accurate affinity determination. C5 was injected in a series of 14 steps 2-fold dilutions, at concentrations of 0.78, 1.56, 3.13, 6.25, and 12.50 nM, without regeneration on nanobodies or Ecu-mab coated surfaces. Determination of affinities for C5 R885H were performed with the same protocol, using concentrations of 25, 50, 100, 200, and 400 nM. The last step of dissociation ran for 60 and 35 minutes, respectively, for reliable determination of the K_{off}. Kinetics were determined using Scrubber 2.0 (BioLogic Software), where simple bimolecular models were used to fit the data. Due to unsuccessful coating on the chip surface and the instability of RaCI3 and C5, we used Ecu-Fab-biotin (method [2]) as a ligand in the competition assay. C5, RaCI3 and UNbC5-2 were injected sequentially at concentrations of 100 nM, with 5 minutes association and 4 minutes dissociation for RaCI3 and UNbC5-2.

Cryo-electron microscopy

Sample Preparation and Data Collection

C5, purchased from Complement Technologies, was diluted to a final concentration of 1 µM and gently mixed with a 1.5× molar excess of UNbC5-1 and UNbC5-2. The sample was diluted in PBS and incubated on ice for 20 minutes before freezing on glow discharged R1.2/1.3 200 mesh Au holey carbon grids (Quantifoil). The grids were then plunge frozen in ethane using a Vitrobot Mark IV (Thermo Fisher Scientific), at 4°C. Cryo-EM data was collected on a 200 kV Talos Arctica microscope (Thermo Fisher Scientific) equipped with a K2 summit detector (Gatan) and a post column 20 eV energy filter. Movies were collected in EPU (Thermo Fisher Scientific) at a magnification of 130,000× with a pixel size of 1.04 Å/pix. Two datasets were collected in two collection sessions with similar settings of 40 frames with a total exposure of 54 and 57 e-/Å^2, and a defocus range of -0.8-2.6 µm.

Data Processing

The datasets of the C5:UNbC5-1:UNbC5-2 complex contained 1461 and 2349 movies (**SFig. 3A**). Both data sets were processed independently in CryoSPARC v3.2/3 with the same workflow until 2D classification. Overall, the workflow for each dataset started with patch-based motion correction and patch-based contrast function estimation (CTF) in CryoSPARC, followed by exposure curation that led to a total of 1253 and 1840 exposures, respectively. Then 100 movies of each data set were selected to perform a round of blob picking. Particles were extracted three times binned to 3.14 Å/pix and several rounds of 2D classification were performed to clean and select adequate templates for the CryoSPARC template picker. After template selection, the particles were picked and extracted unbinned with a 320-pixel box, particles of both datasets were merged, and an initial cleanup was performed through 2D classification. 1,483,794 particles from 2D selection were then submitted to generate four initial models (**SFig. 3B**), that resulted in one good model that was further submitted to two initial model rounds (**SFig. 3C**). The resulted model with 193,009 particles was further selected for refinement. One round of non-uniform refinement led to a density map with a 3.73 Å resolution, which was further improved to 3.60 Å after local and global CTF refinement followed by a final non-uniform refinement. Global resolution was calculated according to the gold standard FSC = 0.143 criterion (**SFig. 3D**). Postprocessing such as sharpening and local resolution was also performed in CryoSPARC (**SFig. 3C & E**).

Model building, refinement and structure figures

To build the model of the C5:UNbC5-1:UNbC5-2 complex, models for the two nanobodies were generated through AlphaFold (27) based on nanobody sequences. The C5 molecule comprising chains α and β of pdb 3CU7 (9), was also used in combination with the nanobody models to rigid-body fit them into the cryo-EM maps using UCSF ChimeraX (60, 61). The model was then iteratively refined using Coot and Phenix real-space refine (62, 63) with geometric restraints. The C345c domain of C5 was not included in the final structures because of the weak density in the map. Figures with protein structures were prepared using PyMOL, as well as the calculation for interface area between C5 and nanobodies (retrieved from: http://www.pymol.org/pymol) (30). Figures with cryo-EM densities were created using UCSF ChimeraX (60, 61) The statistics of the structure come from the refinement in Phenix.

Data analysis & statistical testing

Nanobody sequences were aligned using T-coffee (64). Bar and line graphs were created using GraphPad Prism 9.3.0. Binding and inhibition curves were fitted in GraphPad Prism 9.3.0 using the functions "[inhibitor] vs. normalized response -- Variable slope" & "Asymmetric Sigmoidal, 5PL, X is concentration". Fitted curves of 3 individual experiments were used to calculate IC_{50} and EC_{50} values with SD in GraphPad Prism 9.3.0. SPR data was analyzed in Scrubber 2.0 and plotted in GraphPad Prism 9.3.0.

Data availability

The model coordinates and cryo-EM density maps of the C5 structure in complex with nanobodies UNbC5-1 and UNbC5-2 have been deposited under the following accession numbers 8CML and EMD-16730.

Supporting information

This article contains supporting information.

Acknowledgments

We thank Wouter Beugelink, Dr. Ramon van den Bos and Dr. Itziar Serna Martin for their valuable input and scientific advice.

Funding and additional information

This work was mainly supported by the Netherlands Organisation for Scientific Research (NWO) under the TTW Industrial Doctorate (grant agreement no. NWA.ID.17.036 to EMS) and the Consejo Nacional de Ciencia y Tecnología in Mexico (grant agreement No. CVU 604718 to KdB). The project also received funding from the European Research Council (ERC) under the European Union's Horizon 2020 research and innovation programme (grant agreement No. 101001937, ERC-ACCENT to SHMR and No. 787241, ERC-C-CLEAR to PG).

Conflict of interest statement

ED and RH are employees of QVQ Holding BV. Other authors declare no conflict of interest.

References

1. Reichhardt, M. P., Lundin, K., Lokki, A. I., Recher, G., Vuoristo, S., Katayama, S., Tapanainen, J. S., Kere, J., Meri, S., and Tuuri, T. (2019) Complement in Human Pre-implantation Embryos: Attack and Defense. *Front Immunol.* **10**, 1–12
2. Chen, L., Fukuda, N., Shimizu, S., Kobayashi, H., Tanaka, S., Nakamura, Y., Matsumoto, T., and Abe, M. (2020) Role of complement 3 in renin generation during the differentiation of mesenchymal stem cells to smooth muscle cells. *Am J Physiol Cell Physiol.* **318**, C981–C990
3. Lee, J. D., Coulthard, L. G., and Woodruff, T. M. (2019) Complement dysregulation in the central nervous system during development and disease. *Semin Immunol.* 10.1016/j.smim.2019.101340
4. Merle, N. S., Noe, R., Halbwachs-Mecarelli, L., Fremeaux-Bacchi, V., and Roumenina, L. T. (2015) Complement system part II: Role in immunity. *Front Immunol.* **6**, 1–26
5. Garred, P., Tenner, A. J., and Mollnes, T. E. (2021) Therapeutic Targeting of the Complement System: From Rare Diseases to Pandemics. *Pharmacol Rev.* **73**, 792–827
6. Merle, N. S., Church, S. E., Fremeaux-Bacchi, V., and Roumenia, L. T. (2015) Complement system part I – molecular mechanisms of activation and regulation. *Front Immunol.* **6**, 1–30
7. Schreiber, R. D., and Müller-Eberhard, H. J. (1978) Assembly of the cytolytic alternative pathway of complement from 11 isolated plasma proteins*. *Journal of Experimental Medicine.* **148**, 1722–1727
8. Laursen, N. S., Magnani, F., Gottfredsen, R. H., Petersen, S. V., and Andersen, G. R. (2012) Structure, Function and Control of Complement C5 and its Proteolytic Fragments. *Curr Mol Med.* **12**, 1083–1097
9. Fredslund, F., Laursen, N. S., Roversi, P., Jenner, L., Oliveira, C. L. P., Pedersen, J. S., Nunn, M. A., Lea, S. M., Discipio, R., Sottrup-Jensen, L., and Andersen, G. R. (2008) Structure of and influence of a tick complement inhibitor on human complement component 5. *Nat Immunol.* **9**, 753–760
10. Laursen, N. S., Gordon, N., Hermans, S., Lorenz, N., Jackson, N., Wines, B., Spillner, E., Christensen, J. B., Jensen, M., Fredslund, F., Bjerre, M., Sottrup-Jensen, L., Fraser, J. D., and Andersen, G. R. (2010) Structural basis for inhibition of complement C5 by the SSL7 protein from Staphylococcus aureus. *Proc Natl Acad Sci U S A.* **107**, 3681–3686
11. Nunn, M. A., Sharma, A., Paesen, G. C., Adamson, S., Lissina, O., Willis, A. C., and Nuttall, P. A. (2005) Complement Inhibitor of C5 Activation from the Soft Tick Ornithodoros moubata. *The Journal of Immunology.* **174**, 2084–2091
12. Reichhardt, M. P., Johnson, S., Tang, T., Morgan, T., Tebeka, N., Popitsch, N., Deme, J. C., Jore, M. M., and Lea, S. M. (2020) An inhibitor of complement C5 provides structural insights into activation. *Proc Natl Acad Sci U S A.* **117**, 362–370
13. Jore, M. M., Johnson, S., Sheppard, D., Barber, N. M., Li, Y. I., Nunn, M. A., Elmlund, H., and Lea, S. M. (2016) Structural basis for therapeutic inhibition of complement C5. *Nat Struct Mol Biol.* **23**, 378–386
14. Vogel, C. W., and Fritzinger, D. C. (2010) Cobra venom factor: Structure, function, and humanization for therapeutic complement depletion. *Toxicon.* **56**, 1198–1222
15. Harris, C. L., Pouw, R. B., Kavanagh, D., Sun, R., and Ricklin, D. (2018) Developments in anti-complement therapy; from disease to clinical trial. *Mol Immunol.* **102**, 89–119
16. Harris, C. L. (2018) Expanding horizons in complement drug discovery: challenges and emerging strategies. *Semin Immunopathol.* **40**, 125–140
17. Rother, R. P., Rollins, S. A., Mojcik, C. F., Brodsky, R. A., and Bell, L. (2007) Discovery and development of the complement inhibitor eculizumab for the treatment of paroxysmal nocturnal hemoglobinuria. *Nat Biotechnol.* **25**, 1256–1264
18. Nishimura, J., Yamamoto, M., Hayashi, S., Ohyashiki, K., Ando, K., Brodsky, A. L., Noji, H., Kitamura, K., Eto, T., Takahashi, T., Masuko, M., Matsumoto, T., Wano, Y., Shichishima, T., Shibayama, H., Hase, M., Li, L., Johnson, K., Lazarowski, A., Tamburini, P., Inazawa, J., Kinoshita, T., and Kanakura, Y. (2014) Genetic Variants in C5 and Poor Response to eculizumab. *New England Journal of Medicine.* **370**, 632–639

19. Schatz-Jakobsen, J. A., Zhang, Y., Johnson, K., Neill, A., Sheridan, D., and Andersen, G. R. (2016) Structural Basis for eculizumab-Mediated Inhibition of the Complement Terminal Pathway. *The Journal of Immunology*. **197**, 337–344
20. Brachet, G., Bourquard, T., Gallay, N., Reiter, E., Gouilleux-Gruart, V., Poupon, A., and Watier, H. (2016) eculizumab epitope on complement C5: Progress towards a better understanding of the mechanism of action. *Mol Immunol*. **77**, 126–131
21. Volk, A. L., Hu, F. J., Berglund, M. M., Nordling, E., Strömberg, P., Uhlen, M., and Rockberg, J. (2016) Stratification of responders towards eculizumab using a structural epitope mapping strategy. *Sci Rep*. 10.1038/srep31365
22. de la O Becerra, K. I., Oosterheert, W., van den Bos, R. M., Xenaki, K. T., Lorent, J. H., Ruyken, M., Schouten, A., Rooijakkers, S. H. M., van Bergen en Henegouwen, P. M. P., and Gros, P. (2022) Multifaceted Activities of Seven Nanobodies against Complement C4b. *The Journal of Immunology*. **208**, 2207–2219
23. Roos, A., Bouwman, L. H., Munoz, J., Zuiverloon, T., Faber-Krol, M. C., Fallaux-van den Houten, F. C., Klar-Mohamad, N., Hack, C. E., Tilanus, M. G., and Daha, M. R. (2003) Functional characterization of the lectin pathway of complement in human serum. *Mol Immunol*. **39**, 655–668
24. Muller-Eberhard, H. J. (1986) the Membrane Attack Complex of Complement. *Ann. Rev. Immunol*. **4**, 503–28
25. Rother, R. P., Rollins, S. A., Mojcik, C. F., Brodsky, R. A., and Bell, L. (2007) Discovery and development of the complement inhibitor eculizumab for the treatment of paroxysmal nocturnal hemoglobinuria. *Nat Biotechnol*. **25**, 1256–1264
26. Parker, C. (2009) eculizumab for paroxysmal nocturnal haemoglobinuria. *The Lancet*. **373**, 759–767
27. Jumper, J., Evans, R., Pritzel, A., Green, T., Figurnov, M., Ronneberger, O., Tunyasuvunakool, K., Bates, R., Žídek, A., Potapenko, A., Bridgland, A., Meyer, C., Kohl, S. A. A., Ballard, A. J., Cowie, A., Romera-Paredes, B., Nikolov, S., Jain, R., Adler, J., Back, T., Petersen, S., Reiman, D., Clancy, E., Zielinski, M., Steinegger, M., Pacholska, M., Berghammer, T., Bodenstein, S., Silver, D., Vinyals, O., Senior, A. W., Kavukcuoglu, K., Kohli, P., and Hassabis, D. (2021) Highly accurate protein structure prediction with AlphaFold. *Nature*. **596**, 583–589
28. Macpherson, A., Laabei, M., Ahdash, Z., Graewert, M., James, R., Schulze, M. S. E. D. D., Crennell, S., Robinson, S. A., Holmes, B., Oleinikovas, V., Nilsson, P. H., Snowden, J., Ellis, V., Eirik, T., Deane, C. M., Svergun, D., Lawson, A. D. G. G., Den, J. Van, Birtley, J. R., Schulze, M. S. E. D. D., Crennell, S., Robinson, S. A., Holmes, B., Oleinikovas, V., Nilsson, P. H., Snowden, J., Ellis, V., Mollnes, T. E., Deane, C. M., Svergun, D., Lawson, A. D. G. G., and van den Elsen, J. (2021) The allosteric modulation of complement C5 by knob domain peptides. *Elife*. **10**, 1–49
29. Laursen, N. S., Andersen, K. R., Braren, I., Spillner, E., Sottrup-Jensen, L., and Andersen, G. R. (2011) Substrate recognition by complement convertases revealed in the C5-cobra venom factor complex. *EMBO Journal*. **30**, 606–616
30. Schrödinger, L., and DeLano, W. (2020) PyMOL. *PyMOL*
31. Zarantonello, A., Presumey, J., Simoni, L., Yalcin, E., Fox, R., Hansen, A., Olesen, H. G., Thiel, S., Johnson, M. B., Stevens, B., Laursen, N. S., Carroll, M. C., and Andersen, G. R. (2020) An Ultrahigh-Affinity Complement C4b-Specific Nanobody Inhibits In Vivo Assembly of the Classical Pathway Proconvertase. *The Journal of Immunology*. **205**, 1678–1694
32. Jensen, R. K., Pihl, R., Gadeberg, T. A. F. F., Jensen, J. K., Andersen, K. R., Thiel, S., Laursen, N. S., and Andersen, G. R. (2018) A potent complement factor C3–specific nanobody inhibiting multiple functions in the alternative pathway of human and murine complement. *Journal of Biological Chemistry*. **293**, 6269–6281
33. Rooijakkers, S. H. M., Wu, J., Ruyken, M., van Domselaar, R., Planken, K. L., Tzekou, A., Ricklin, D., Lambris, J. D., Janssen, B. J. C., van Strijp, J. A. G., and Gros, P. (2009) Structural and functional implications of the complement convertase stabilized by a staphylococcal inhibitor. *Nat Immunol*. **10**, 721–727
34. Bestebroer, J., Aerts, P. C., Rooijakkers, S. H. M., Pandey, M. K., Köhl, J., van Strijp, J. A. G., and Haas, C. J. C. De (2010) Functional basis for complement evasion by staphylococcal superantigen-like 7. *Cell Microbiol*. **12**, 1506–1516

35. Schatz-Jakobsen, J. A., Pedersen, D. V., and Andersen, G. R. (2016) Structural insight into proteolytic activation and regulation of the complement system. *Immunol Rev*. **274**, 59–73
36. Nilsson, P. H., Johnson, C., Quach, Q. H., Macpherson, A., Durrant, O., Pischke, S. E., Fure, H., Landsem, A., Bergseth, G., Schjalm, C., Haugaard-Kedström, L. M., Huber-Lang, M., van den Elsen, J., Brekke, O.-L., and Mollnes, T. E. (2021) A Conformational Change of Complement C5 Is Required for Thrombin-Mediated Cleavage, Revealed by a Novel Ex Vivo Human Whole Blood Model Preserving Full Thrombin Activity. *The Journal of Immunology*. **207**, 1641–1651
37. Laursen, N. S., Pedersen, D. V, Gytz, H., Zarantonello, A., Magnus, J., Jensen, B., Hansen, A. G., Thiel, S., and Andersen, G. R. (2020) Functional and Structural Characterization of a Potent C1q Inhibitor Targeting the Classical Pathway of the Complement System. *Front Immunol*. **11**, 1–15
38. Pedersen, H., Jensen, R. K., Hansen, A. G., Gadeberg, T. A. F., Thiel, S., Laursen, N. S., and Andersen, G. R. (2020) A C3 specific nanobody that blocks all three activation pathways in the human and murine complement system. *Journal of Biological Chemistry*. **295**, 8746–8758
39. Pedersen, H., Jensen, R. K., Jensen, J. M. B., Fox, R., Pedersen, D. V., Olesen, H. G., Hansen, A. G., Christiansen, D., Mazarakis, S. M. M., Lojek, N., Hansen, P., Gadeberg, T. A. F., Zarantonello, A., Laursen, N. S., Mollnes, T. E., Johnson, M. B., Stevens, B., Thiel, S., and Andersen, G. R. (2020) A Complement C3–Specific Nanobody for Modulation of the Alternative Cascade Identifies the C-Terminal Domain of C3b as Functional in C5 Convertase Activity. *The Journal of Immunology*. **205**, 2287–2300
40. Pedersen, D. V., Rösner, T., Hansen, A. G., Andersen, K. R., Thiel, S., Andersen, G. R., Valerius, T., and Laursen, N. S. (2020) Recruitment of properdin by bi-specific nanobodies activates the alternative pathway of complement. *Mol Immunol*. **124**, 200–210
41. Pedersen, D. V., Gadeberg, T. A. F., Thomas, C., Wang, Y., Joram, N., Jensen, R. K., Mazarakis, S. M. M., Revel, M., El Sissy, C., Petersen, S. V., Lindorff-Larsen, K., Thiel, S., Laursen, N. S., Fremeaux-Bacchi, V., and Andersen, G. R. (2019) Structural basis for properdin oligomerization and convertase stimulation in the human complement system. *Front Immunol*. **10**, 1–19
42. Zheng, F., Put, S., Bouwens, L., Lahoutte, T., Matthys, P., Muyldermans, S., De Baetselier, P., Devoogdt, N., Raes, G., and Schoonooghe, S. (2014) Molecular imaging with macrophage crig-targeting nanobodies for early and preclinical diagnosis in a mouse model of rheumatoid arthritis. *Journal of Nuclear Medicine*. **55**, 824–829
43. Wen, Y., Ouyang, Z., Schoonooghe, S., Luo, S., De Baetselier, P., Lu, W., Muyldermans, S., Raes, G., and Zheng, F. (2017) Structural evaluation of a nanobody targeting complement receptor Vsig4 and its cross reactivity. *Immunobiology*. **222**, 807–813
44. Duggan, S. (2018) Caplacizumab: First Global Approval. *Drugs*. **78**, 1639–1642
45. van Ineveld, R. L., Kleinnijenhuis, M., Alieva, M., de Blank, S., Barrera Roman, M., van Vliet, E. J., Martínez Mir, C., Johnson, H. R., Bos, F. L., Heukers, R., Chuva de Sousa Lopes, S. M., Drost, J., Dekkers, J. F., Wehrens, E. J., and Rios, A. C. (2021) Revealing the spatio-phenotypic patterning of cells in healthy and tumor tissues with mLSR-3D and STAPL-3D. *Nat Biotechnol*. **39**, 1239–1245
46. Rashidian, M., Keliher, E. J., Bilate, A. M., Duarte, J. N., Wojtkiewicz, G. R., Jacobsen, J. T., Cragnolini, J., Swee, L. K., Victora, G. D., Weissleder, R., and Ploegh, H. L. (2015) Noninvasive imaging of immune responses. *Proc Natl Acad Sci U S A*. **112**, 6146–6151
47. Pabst, T. M., Wendeler, M., Wang, X., Bezemer, S., Hermans, P., and Hunter, A. K. (2017) Camelid VHH affinity ligands enable separation of closely related biopharmaceuticals. *Biotechnol J*. 10.1002/biot.201600357
48. Berends, E. T. M., Dekkers, J. F., Nijland, R., Kuipers, A., Soppe, J. A., van Strijp, J. A. G., and Rooijakkers, S. H. M. (2013) Distinct localization of the complement C5b-9 complex on Gram-positive bacteria. *Cell Microbiol*. **15**, 1955–1968
49. Berends, E. T. M., Gorham Jr, R. D., Ruyken, M., Soppe, J. A., Orhan, H., Aerts, P. C., Haas, C. J. C. De, Gros, P., and Rooijakkers, S. H. M. (2015) Molecular insights into the surface-specific arrangement of complement C5 convertase enzymes. *BMC Biol*. **13**, 1–13

50. De Haard, H. J. W., Bezemer, S., Ledeboer, A. M., Müller, W. H., Boender, P. J., Moineau, S., Coppelmans, M. C., Verkleij, A. J., Frenken, L. G. J., and Verrips, C. T. (2005) Llama antibodies against a lactococcal protein located at the tip of the phage tail prevent phage infection. *J Bacteriol*. **187**, 4531–4541
51. Hoogenboom, H. R., Griffiths, A. D., Johnson, K. S., Chiswell, D. J., Hudson, P., and Winter, G. (1991) Multi-subunit proteins on the surface of filamentous phage: Methodologies for displaying antibody (Fab) heavy and light chains. *Nucleic Acids Res*. **19**, 4133–4137
52. Marks, J. D., Hoogenboom, H. R., Bonnert, T. P., Mccafferty, J., Griffiths, A. D., and Winter, G. (1991) By-passing Immunization Human Antibodies from V-gene Libraries Displayed on Phage. *J. Mol. Biol*. **222**, 581–597
53. Gangaiah, D., Ryan, V., Van Hoesel, D., Mane, S. P., Mckinley, E. T., Lakshmanan, N., Reddy, N. D., Dolk, E., and Kumar, A. (2022) Recombinant Limosilactobacillus (Lactobacillus) delivering nanobodies against Clostridium perfringens NetB and alpha toxin confers potential protection from necrotic enteritis. *Microbiologyopen*. 10.1002/mbo3.1270
54. Heukers, R., Mashayekhi, V., Ramirez-Escudero, M., De Haard, H., Verrips, T. C., Van Bergen En Henegouwen, P. M. P., and Oliveira, S. (2019) Vhh-photosensitizer conjugates for targeted photodynamic therapy of met-overexpressing tumor cells. *Antibodies*. **8**, 1–13
55. Gorlani, A., Lutje Hulsik, D., Adams, H., Vriend, G., Hermans, P., and Verrips, T. (2012) Antibody engineering reveals the important role of J segments in the production efficiency of llama single-domain antibodies in Saccharomyces cerevisiae. *Protein Engineering, Design and Selection*. **25**, 39–46
56. Jeong, H. J., Abhiraman, G. C., Story, C. M., Ingram, J. R., and Dougan, S. K. (2017) Generation of Ca2+-independent sortase A mutants with enhanced activity for protein and cell surface labeling. *PLoS One*. **12**, 1–15
57. Klerx, J. P. A. M., Beukelrnan, C. J., Dijk, H. Van, and Willers, J. M. N. (1983) *Microassay for Colorimetric Estimation of Complement Activity in Guinea Pig, Human and Mouse Serum*
58. Mollnes, T. E., Harboe, M., and Tschopp, J. (1985) Monoclonal Antibodies Recognizing a Neoantigen of Poly(C9) Detect the Human Terminal Complement Complex in Tissue and Plasma. *Scand J Immunol*. **22**, 183–195
59. Bayly-Jones, C., Ho, B. H. T., Lau, C., Leung, E. W. W., D'Andrea, L., Lupton, C. J., Ekkel, S. M., Venugopal, H., Whisstock, J. C., Mollnes, T. E., Spicer, B. A., and Dunstone, M. A. (2023) The neoepitope of the complement C5b-9 Membrane Attack Complex is formed by proximity of adjacent ancillary regions of C9. *Commun Biol*. 10.1038/s42003-023-04431-y
60. Pettersen, E. F., Goddard, T. D., Huang, C. C., Meng, E. C., Couch, G. S., Croll, T. I., Morris, J. H., and Ferrin, T. E. (2021) UCSF ChimeraX: Structure visualization for researchers, educators, and developers. *Protein Science*. **30**, 70–82
61. Goddard, T. D., Huang, C. C., Meng, E. C., Pettersen, E. F., Couch, G. S., Morris, J. H., and Ferrin, T. E. (2018) UCSF ChimeraX: Meeting modern challenges in visualization and analysis. *Protein Science*. **27**, 14–25
62. Emsley, P., and Cowtan, K. (2004) Coot: Model-building tools for molecular graphics. *Acta Crystallogr D Biol Crystallogr*. **60**, 2126–2132
63. Afonine, P. V., Poon, B. K., Read, R. J., Sobolev, O. V., Terwilliger, T. C., Urzhumtsev, A., and Adams, P. D. (2018) Real-space refinement in PHENIX for cryo-EM and crystallography. *Acta Crystallogr D Struct Biol*. **74**, 531–544
64. Di Tommaso, P., Moretti, S., Xenarios, I., Orobitg, M., Montanyola, A., Chang, J. M., Taly, J. F., and Notredame, C. (2011) T-Coffee: A web server for the multiple sequence alignment of protein and RNA sequences using structural information and homology extension. *Nucleic Acids Res*. **39**, 13–17

Abbreviations

The abbreviations used here are: sdAb, single-domain antibody; SPR, surface plasmon resonance; C5b-9 & MAC, membrane attack complex; PNH, paroxysmal nocturnal hemoglobinuria; aHUS, atypical hemolytic uremic syndrome; AMD, age-related macular degeneration; SLE, systemic lupus erythematosus; CP, classical pathway; LP, lectin pathway; AP, alternative pathway; MG, macroglobulin; CUB, complement C1r/C1s Uegf Bmp1; SSL7, staphylococcal superantigen-like protein 7; CVF, cobra venom factor; CDR, complementarity determining regions; Ecu-mab, a monoclonal IgG antibody with the same primary sequence as eculizumab; Ecu-Fab, a Fab domain with the same parental sequence as the Fab domain of eculizumab; 2YT, 2× yeast extract tryptone; O/N, overnight; PBMCs, peripheral blood mononuclear cells; RT, room temperature; IPTG, isopropylthio-β-galactoside; IMAC, immobilized metal-affinity chromatography; YP, yeast peptone; YNB, yeast nitrogen base; NHS, N-hydrocysucciminidyl; VBS, veronal buffered saline; PBS-T, phosphate buffered saline supplemented with Tween; TMB, tetramethylbenzidine; DIG; digoxigenin; ERC, European Research Council.

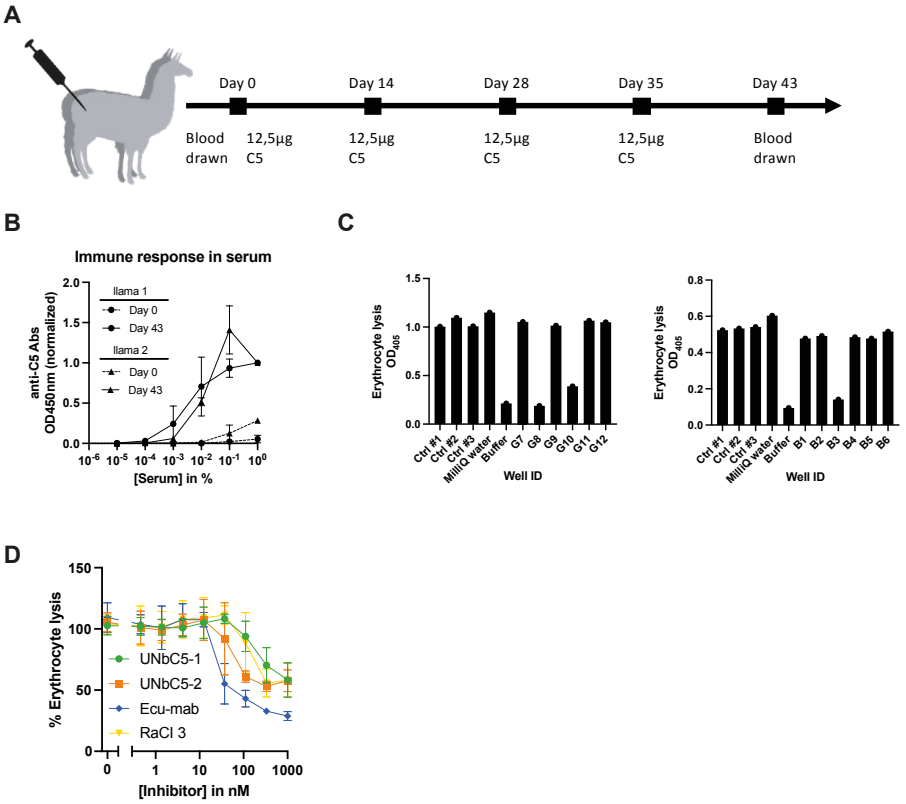

Supporting figure 1: Identification of UNbC5-1 and UNbC5-2. (A) Schematic representation of immunization scheme for two llamas. (B) Immune response against C5 measured in llama serum at day 0 and day 43 using an ELISA. Purified human C5 was coated on microtiter plates. Next, llama serum was added and binding of llama-antibodies was measured using polyclonal rabbit-anti-VHH QE19 antibodies and donkey-anti-rabbit-HRP antibodies, at an OD of 450 nm. Data was normalized against the highest concentration of serum, for both llamas individually. (C) CP hemolysis assay to screen for complement inhibiting nanobodies, in which clones UNbC5-1 (G8) and UNbC5-2 (B3) were identified as potent inhibitors. As controls we included periplasmic fractions of a bacteria expressing an irrelevant nanobody (ctrl #1), expressing an empty vector (ctrl #2), or no bacterial culture (ctrl #3). MilliQ water and buffer were taken along to measure maximum and minimum levels of erythrocyte lysis. (D) AP mediated hemolysis of rabbit erythrocytes incubated with 10% normal human serum and a titration of our nanobodies UNbC5-1 and UNbC5-2 and known complement inhibitors RaCI3 and Ecu-mab. The OD405 values of the supernatants were measured and the % erythrocyte lysis was calculated using a 0% (buffer) and 100% (MilliQ) control sample. Data information: (B-D) Data represent mean ± SD of 1 (C) 2 (B) or 3 (D) individual experiments.

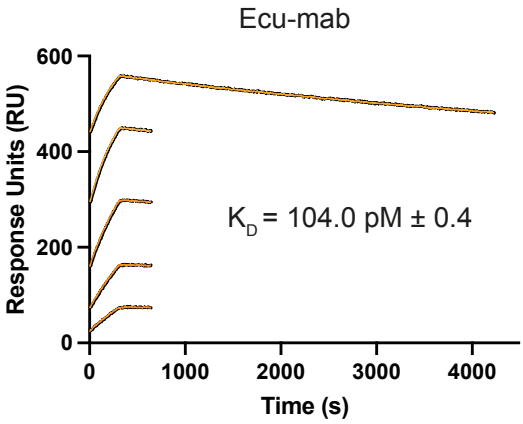

Supporting figure 2: Determination of the affinity of Ecu-mab for C5. SPR curves of Ecu-mab as a ligand and C5 as an analyte at concentrations of 12.5, 6.25, 3.13, 1.56, and 0.78 nM evaluated over 4000 seconds.

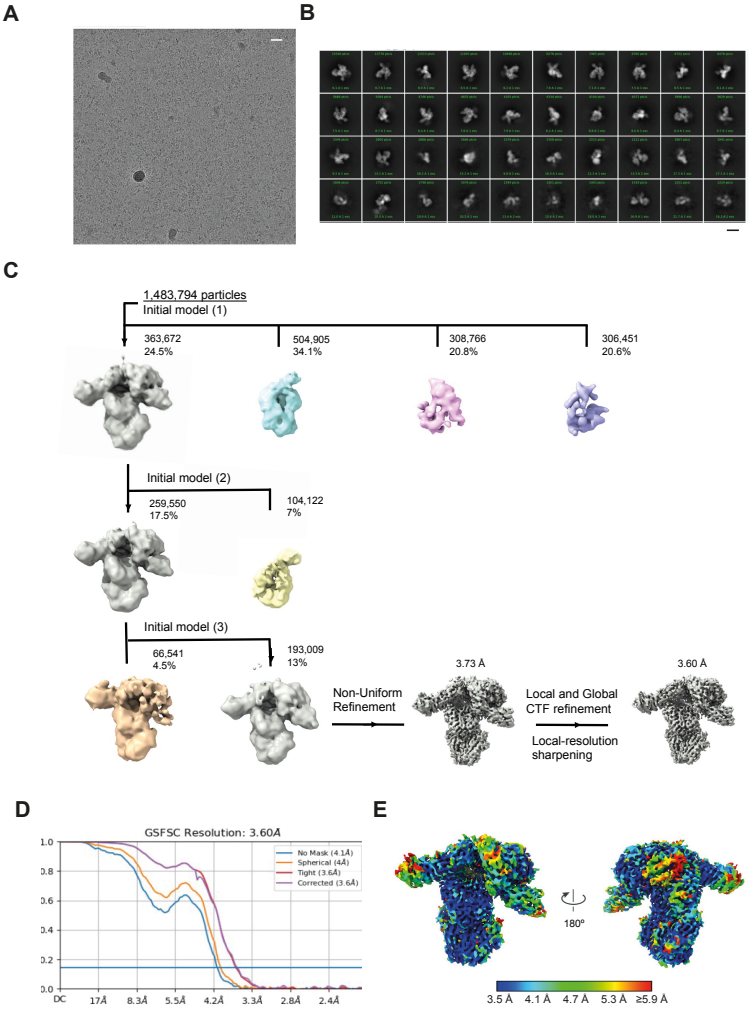

Supporting figure 3: Cryo-EM image processing of C5 in complex with UNbC5-1 and UNbC5-2 datasets. (A) Micrograph of C5:UNbC5-1:UNbC5-2 particles in vitreous ice. The scale bar length is 200 Å. (B) Selected 2D-class averages of the complex generated in CryoSPARC. The scale bar length is 100 Å. (C) Three rounds of 3D Initial model classification and subsequent refinement strategy for the C5:UNbC5-1:UNbC5-2 reconstruction. (D) Fourier-shell correlation plots for the gold-standard refined C5:UNbC5-1:UNbC5-2 reconstruction, computed from unmasked (blue), with a spherical mask (orange), tight mask (red), and corrected (purple). (E) C5:UNbC5-1:UNbC5-2 complex density map colored by local resolution (blue = high, red = low), computed in CryoSPARC.

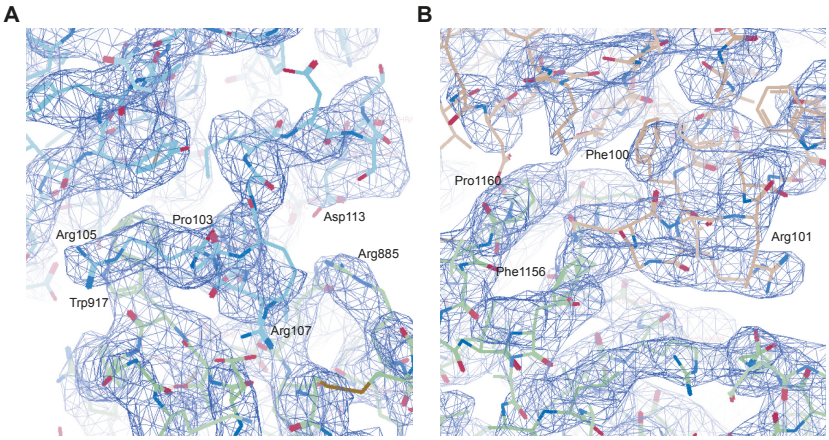

Supporting figure 4: Interfaces of C5 and UNbC5-1 or UNbC5-2. (A-B) Cryo-EM density maps depicting the interface of C5 (green) and UNbC5-1 (cyan) (A) or C5 (green) and UNbC5-2 (orange) (B) in detail. Densities are depicted delineated in dark blue and important residues of the interfaces are indicated. Figures were made in Coot (61).

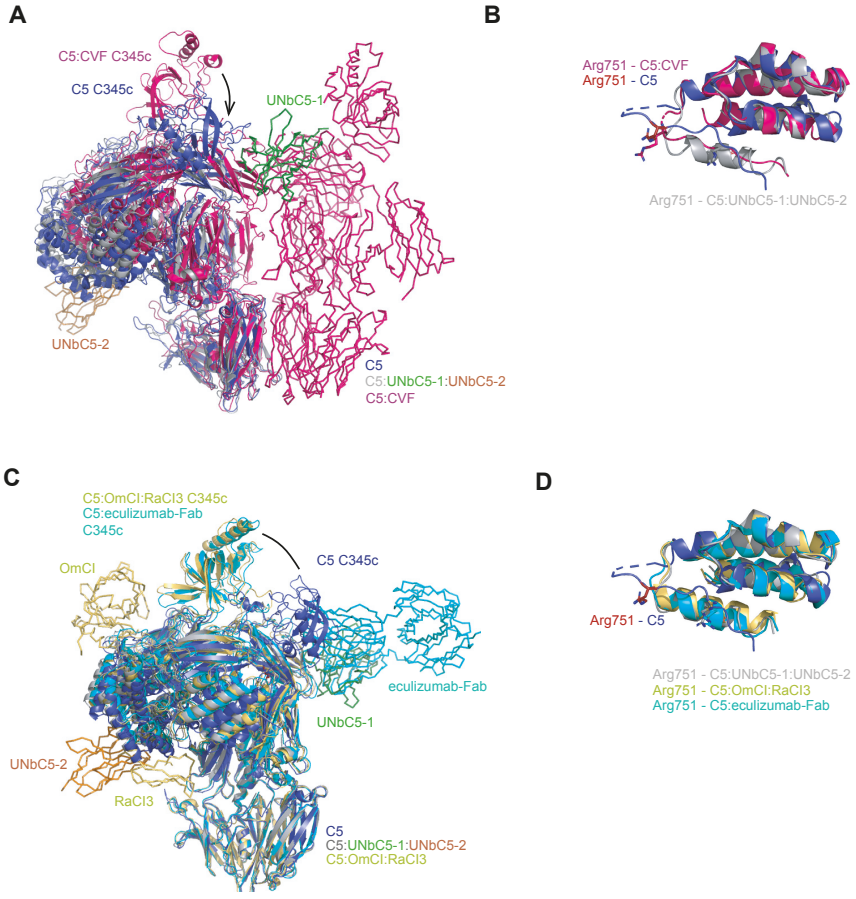

Supporting figure 5: Structural comparison of C5:UNbC5-1:UNbC5-2 with C5 and C5 inhibitors eculizumab-Fab, OmCI-RaCI3, CVF and CVF with a small inhibitory molecule. (A) Micrograph of C5:UNbC5-1:UNbC5-2 particles in vitreous ice. The scale bar length is 200 Å. (B) Selected 2D-class averages of the complex generated in CryoSPARC. The scale bar length is 100 Å. (C) Three rounds of 3D Initial model classification and subsequent refinement strategy for the C5:UNbC5-1:UNbC5-2 reconstruction. (D) Fourier-shell correlation plots for the gold-standard refined C5:UNbC5-1:UNbC5-2 reconstruction, computed from unmasked (blue), with a spherical mask (orange), tight mask (red), and corrected (purple). (E) C5:UNbC5-1:UNbC5-2 complex density map colored by local resolution (blue = high, red = low), computed in CryoSPARC.

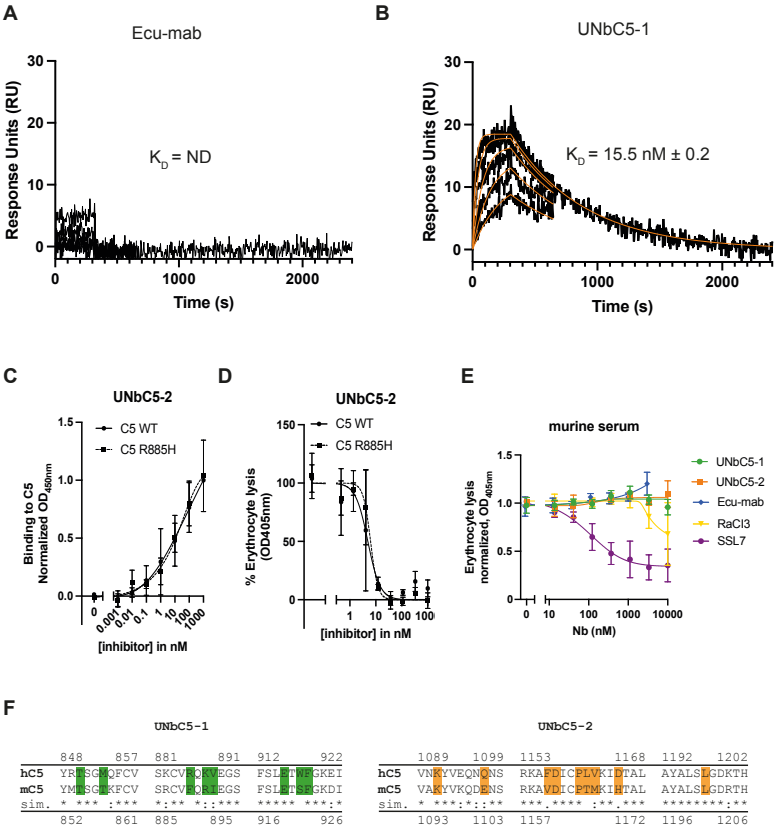

Supporting figure 6: UNbC5-2 binding to and inhibition of C5 R885H. (A-B) SPR curves with Ecu-mab (A) and UNbC5- 1 (B) as a ligand and C5 R885H as an analyte at concentrations of 400, 200, 100, 50, and 25 nM evaluated over 2400 seconds. (C) Binding of UNbC5-2 to C5 WT and C5 R885H, using C5 WT or C5 R885H coated microtiter plates, incubated with increasing concentrations of UNbC5-2. Binding was assessed with a monoclonal anti-human-kappa antibody and an HRP-labeled secondary antibodies, at OD450. (D) CP mediated hemolysis of antibody-coated sheep erythrocytes incubated with 2.5% C5 depleted human serum, repleted with physiological concentrations of C5 WT or C5 R885H and a titration of UNbC5-2. The OD405 values of the supernatants were measured, and the % erythrocyte lysis was calculated using a 0% (buffer) and 100% (MilliQ) control sample. (E) AP mediated hemolysis of rabbit erythrocytes incubated with 10% murine serum and different concentrations of C5 inhibitors. The OD405 values of the supernatants were measured and data were normalized to the condition without inhibitor. (F) sequence alignment of human and murine C5 to compare nanobody binding interfaces in both C5 molecules. Colored amino acids (green for UNbC5-1 and orange for UNbC5-2) indicate amino acids from C5 involved in the binding interfaces. Annotation (sim.): conserved amino acid (*), amino acid with strong similar properties (:), amino acid with weakly similar properties (.). Data represent mean ± SD of 2 (A-B) and 3 (C-E) individual experiments. (C-E) Curves were fitted.

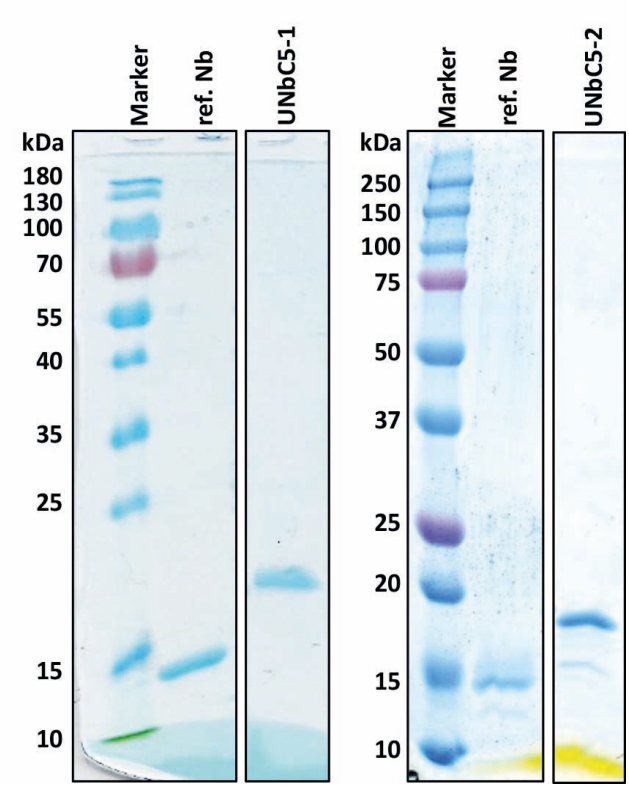

Supporting figure 7: UNbC5-1 and UNbC5-2 on SDS-PAGE. SDS-PAGE to check for purity, size and concentration, UNbC5-1 and UNbC5-2. For both nanobodies and the reference nanobody (ref. Nb) 1 µg was loaded.

4

Identification and characterization of a non-inhibitory nanobody that specifically targets complement C5b6 complex

Eva M. Struijf[1], Jamie S. Depelteau[2], Fleur van Oosterom[1], Maartje Ruyken[1], Robbin Hutten[3], Danique Y. Siere[1], Piet Gros[2], Dani A.C. Heesterbeek[1], Gillian Dekkers[3], Edward Dolk[3], Raimond Heukers[3], Bart W. Bardoel[1], Suzan H.M. Rooijakkers[1#]

[1]Medical Microbiology, University Medical Center Utrecht, Utrecht University, Utrecht, the Netherlands
[2]Structural Biochemistry, Bijvoet Centre for Biomolecular Research, Department of Chemistry, Faculty of Science, Utrecht University, Utrecht, the Netherlands
[3]QVQ Holding BV, Utrecht, the Netherlands
 # Corresponding author: s.h.m.rooijakkers@umcutrecht.nl

Complement system, innate immunity, nanobody, C5, C6, C5b6, membrane attack complex (MAC)

Abstract

The human complement system eliminates invading microbes by insertion of ring-structured membrane attack complex pores (MAC, or C5b-9) into target cell membranes. MAC assembly is a stepwise process, initiated by C5b6, a bimolecular complex of C5 cleavage product C5b, and C6. During C5b6 formation, both C5 and C6 undergo major structural rearrangements, revealing various neo-epitopes. In this study, we develop and characterize a C5b6-specific nanobody. Llamas were immunized with purified C5b6 to generate VHH phage libraries. Using phage display, we identify three nanobodies that bound C5b6, but not C5 and C6. The three nanobodies had >90% amino acid sequence similarity and competed for the same epitope on C5b6. Using size exclusion chromatography, we confirmed that one of these three nanobodies (termed UNbC5b6-1) forms a stable complex with C5b6 in solution, but not with precursors C5 and C6. Using surface plasmon resonance, we determined that UNbC5b6-1 binds C5b6 with an affinity of 49.5 pM. UNbC5b6-1 does not interfere with MAC assembly in erythrocyte lysis assays with human serum or purified complement components. In conclusion, we have identified and characterized a non-inhibitory nanobody that specifically binds C5b6 with high affinity. UNbC5b6-1 could be used to detect C5b6 formation and study molecular mechanisms of MAC assembly.

Introduction

The complement system is a protein network in human plasma and body fluids that is part of the innate immune system. Its activation induces multiple effector functions that all lead to the clearance of foreign or altered host cells, such as invading microbes, tumor cells and apoptotic cells (1, 2). First, complement activation results in recruitment and activation of immune cells. Second, complement labels target cells with opsonins to mark them for phagocytosis. Third, complement directly eliminates target cells by the formation of ring-structured membrane attack complex (MAC) pores. All complement effectors result from a rapid protein cascade that is driven by protein cleavage steps, conformational changes, and formation of large protein complexes (3, 4). Also, the assembly of the multiprotein MAC pore is a stepwise unidirectional process, which starts with the formation of protein complex C5b6 (5). The C5b6 complex first interacts with complement protein C7 (C5b-7), followed by C8 (C5b-8) and MAC pore assembly is finalized upon interaction and polymerization of ±18 copies of C9 (C5b-9) (6–10).

Molecules that distinguish complement activation products from precursor proteins have proven their value in fundamental and diagnostic complement research. Best known is monoclonal antibody (mAb) ae11 that reacts with polymeric C9 within MAC pores (11, 12). In this study, we aim to develop a molecule for specific detection of the complement activation product C5b6. C5b6 (282 kDa) is a bimolecular stable complex that consists of complement proteins C5b (185 kDa) and C6 (103 kDa) (**Fig. 1A**) (5, 8, 13). It is formed when surface-bound C5 convertases cleave native C5 molecules in the presence of C6 (14). C5 is a large protein (190 kDa) that belongs to the C3/C4/C5 protein family (15–18). The protein is composed of two chains (alpha and beta) and consists of a core of eight macroglobulin (MG) domains (MG1-MG8) and four other domains (C1r/C1s UEGF BMP1 (CUB), C345c (also known as netrin module (NTR)), C5a, and C5d) (**Fig. 1B**). The C6 protein belongs to the MAC-perforin/cholesterol-dependent cytolysin (MACPF/CDC) superfamily and consists of a central MACPF domain with multiple thrombospondin-like (TS), factor I-MAC (FIM) and complement control protein (CCP) domains (5, 13, 14, 19, 20) (**Fig. 1C**). The cleavage of C5 releases C5a (8 kDa) and induces large conformational rearrangements, in which the C5d domain moves down and away from the MG-ring (13), forming the metastable activation product C5b (181 kDa). Due to these conformational rearrangements, C6 binds to (neo-)epitopes in C5b with an extensive interface (14). This binding induces major conformational rearrangements in C6 converting it from a rather tall and flat protein into a hairpin-shaped fold that stabilizes C5b (13). C5b is intrinsically labile and in absence of C6, it aggregates and rapidly loses its activity (half-life of ±2.5') (14). The C5b6 complex has high structural

homology with both precursors C5 and C6, but also contains many neo-epitopes that are required for C5b-7 formation (**Fig. 1A**) (21, 22).

Llama-derived nanobodies have proven to be good at specific recognition of conformational epitopes. Due to their relatively small size (±15 kDa) and convex-shaped paratope, they can more easily reach protein clefts and enzymatic crypts and thus bind neo-epitopes (23–26). Therefore, this study sets out to develop and characterize a llama-derived nanobody that specifically binds to the complement activation product C5b6 and not to its precursor proteins C5 and C6.

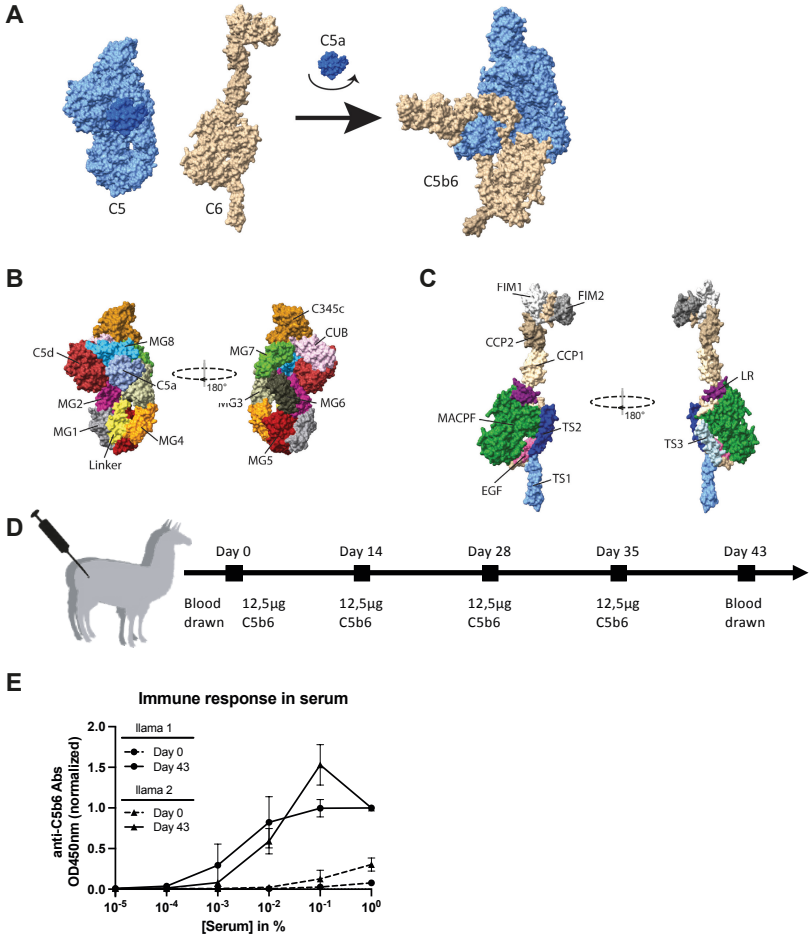

Figure 1: Successful immunization of two llamas with human C5b6. (A) Formation of C5b6 complex from precursor proteins C5 and C6, using the published structures (C5b6 PDB: 4A5W, C5 PDB: 3CU7, C6 PDB: 3T5O) and depicting it in a space filling representation. Major structural rearrangements in several domains of C5 and C6 occur upon C5 cleavage and C5b:C6 interaction, revealing neo-epitopes. (B-C) Space filling representations of C5 (B) and C6 (C) structures, highlighting the domains with different colors. (D) Schematic representation of immunization scheme of two llamas. (E) Detection of anti-C5b6 antibodies in llama serum before and after immunizations. Microtiter plates were coated with purified C5b6 and incubated with llama serum. Bound Llama antibodies were detected using polyclonal rabbit-anti-VHH QE19 antibodies and donkey-anti-rabbit- HRP antibodies, at an OD of 450 nm. Data represents mean ± SD of 2 individual experiments.

Results

Immunization and identification of C5b6 specific nanobodies

To generate nanobodies targeting human C5b6, two llamas were immunized intramuscularly with purified C5b6 complex, followed by three boost injections (**Fig. 1D**). At day 0 and 43, llama blood was drawn and serum was used to assess the presence of a C5b6-specific immune response. C5b6-coated microtiter plates were incubated with serial dilutions of serum and for both llamas substantially more C5b6-binding antibodies were detected on day 43 compared to day 0, indicating that immunizations were successful (**Fig. 1E**). Next, two phage display libraries were generated by ligating the variable heavy chain of heavy chain only antibodies (VHH) genes from isolated peripheral blood mononuclear cells (PBMCs) from both llamas into a phagemid vector (**Supporting Fig. 1**), resulting in estimated library sizes of approximately 10^8 transformants. C5b6 binding nanobodies were then selected by two rounds of biopanning. In the first round, we performed a positive selection for phages binding randomly immobilized C5b6. To increase the chance of finding C5b6 neo-epitope binders, we added a negative selection with native C5 and C6 in the second panning round. After both rounds, phages were eluted from C5b6 and rescued by infection into *Escherichia coli* (*E. coli*). Sequencing of individual clones revealed 63 clusters of nanobody clones with >80% amino acid sequence homology in their complementarity-determining region (CDR) H3 (CDR-H3) region. Despite the diversity in the framework regions and CDR sequences, almost all nanobodies originated from IGHV3-3*01 and IGHJ4*01 germline sequences (based on IMGT database (27, 28)). Of these CDR-H3 clusters, 16 contained more than one clone per cluster, indicating enrichment of binding clones in the two rounds of panning.

Identification of eight C5b6-specific nanobodies

Next, crude periplasmic extracts were used to screen for nanobodies binding to C5b6 by ELISA. Out of all clones tested, eight clones showed stronger binding to C5b6 than to C5 or C6 (**Fig. 2A**). Sequence alignment of these eight candidates revealed a high amino acid diversity in all CDR regions (**Fig. 2B**). However, of these eight candidates, three clones (A12, B7 and E7) showed >90% amino acid sequence similarity in the CDR regions. The remaining five clones all derived from different CDR-H3 families.

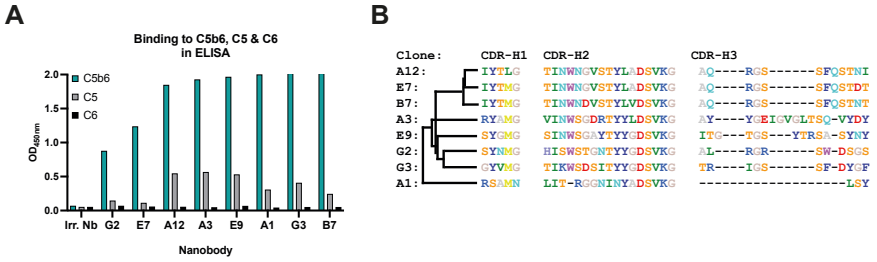

Figure 2: Identification of C5b6-specific nanobodies. (A) Binding pattern of eight nanobodies (Nb) in crude periplasmic extracts from screen for C5b6 specific binders. Microtiter plates coated with C5b6, C5 or C6 extracts were incubated with crude periplasmic extracts. Binding of nanobodies was detected using polyclonal rabbit-anti-VHH QE19 antibodies and donkey-anti-rabbit-HRP antibodies, at an OD of 450 nm, n=1. (B) Protein sequence alignment of eight nanobodies. CDR-H1, CDR-H2 and CDR-H3 are depicted. Amino acids are colored according to the shapely color scheme.

Selection of UNbC5b6-1 as a C5b6-specific nanobody from a panel of eight clones

Since the above binding data is based on crude periplasmic extracts (with unknown nanobody concentrations), we next expressed and purified the eight selected nanobodies. After purification, only the three clones with a high sequence similarity (A12, B7 and E7) turned out to be efficient and specific C5b6 binders. These clones bound C5b6 in ELISA with an apparent affinity of approximately 1 nM and showed very little to no binding to precursor proteins C5 and C6 (**Fig. 3A)**. Other nanobodies (A1 and G2) bound C5b6 with a lower apparent affinity (approximately 50 and 25 nM, respectively) or also bound to C5 (A3, E9, and G3). Next, we biotinylated the three C5b6-specific clones (A12, B7 and E7) at the C-terminus via site-specific sortagging (29) and performed a competition ELISA to assess if these clones compete for the same binding epitope on C5b6. Briefly, C5b6-coated microtiter plates were incubated with biotinylated nanobody (A12-bio, B7-bio and E7-bio) and a concentration range of unlabeled nanobodies. Binding of A12-bio, B7-bio and E7-bio to C5b6 was measured using peroxidase-labeled streptavidin. As a positive control, we combined the biotinylated and unlabeled nanobody of the same clone (e.g. A12-bio + A12) and as a negative control we used an irrelevant nanobody (Irr Nb) that does not bind to C5b6. As expected, unlabeled nanobodies B7 and E7, like control A12, reduced the binding of A12-bio to C5b6 in a concentration dependent manner (**Fig 3B**) and vice versa (**Fig. 3C & D**). Since these data show that nanobodies A12, B7 and E7 compete for the same epitope on C5b6, we selected one nanobody (clone B7) for further characterization. From now on, we will refer to nanobody B7 as UNbC5b6-1.

This nanobody has a molecular weight of 13.0 kDa and its full sequence is shown in **supporting figure 2.** Thus, we selected UNbC5b6-1 as a C5b6-specific nanobody from a panel of eight purified nanobodies.

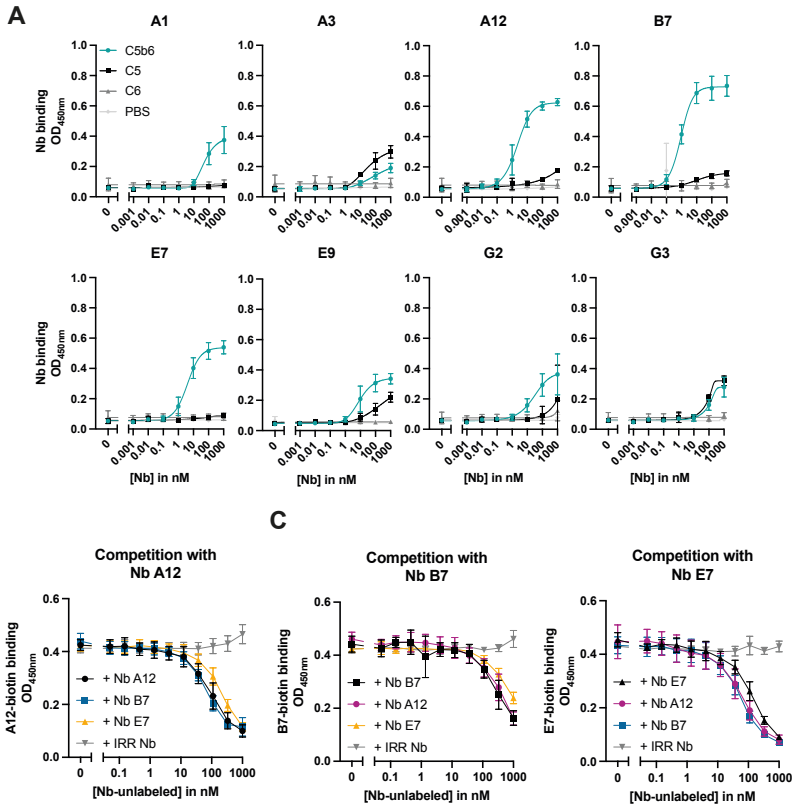

Figure 3: Selection of UNbC5b6-1, a C5b6-specific nanobody. (A) Binding patterns of eight purified nanobodies (Nb). Each panel represents the binding of one nanobody to C5b6, C5 and C6. Microtiter plates were coated with 2 µg/ml C5b6, C5 or C6, incubated with purified nanobody and nanobody binding was assessed using polyclonal rabbit-anti-VHH QE19 antibodies and donkey-anti-rabbit-HRP antibodies, at an OD of 450 nm. (B-D) Nanobodies A12, B7 and E7 compete for binding to C5b6. Biotinylated nanobody (30 nM) was preincubated with unlabeled nanobody (0.05 – 1000 nM) and added to microtiter plates coated with 2 µg/ml C5b6. Binding of biotinylated nanobodies to C5b6 was detected using streptavidin coupled to peroxidase, at an OD of 450 nm. An irrelevant (IRR) nanobody that does not compete with A12, B7 and E7 was taken along as negative control. (B) Binding of A12-biotin. (C) Binding of B7-biotin (D) Binding of E7-biotin. (A-D) data represents mean ± SD of 3 individual experiments. (A) Binding curves were fitted in GraphPad Prism 9.3.0 using the function "Asymmetric Sigmoidal, 5PL, X is concentration". Apparent affinity values were obtained from the non linear fit results from GraphPad Prism (EC50 value).

UNbC5b6-1 forms a stable complex with C5b6 in solution

To confirm specific binding between UNbC5b6-1 and C5b6 complexes, we performed size exclusion chromatography (SEC). Briefly, purified C5b6, C5 and C6 were incubated with UNbC5b6-1, loaded on a Superose 6 Increase column and fractions were captured. When UNbC5b6-1 was incubated with C5b6, C5 and C6, the chromatograms show a peak between 1.4-1.9 mL retention volume, where C5b6, C5 and C6 are expected to elute (complement peaks) (**Fig. 4A**). UNbC5b6-1 alone (purple) is eluted in the fractions between 1.9-2.1 mL (nanobody peak). When UNbC5b6-1 is incubated with C5b6 (blue), the height of the nanobody peak substantially decreases, but not when UNbC5b6-1 is incubated with C5 (black) or C6 (grey). ELISA analyses confirmed that UNbC5b6-1 is only present in the complement peaks when incubated with C5b6 (blue), and not when incubated with C5 (grey) or C6 (black) (**Fig. 4B**). Concluding, UNbC5b6-1 forms a stable complex in solution with C5b6, but not with C5 and C6.

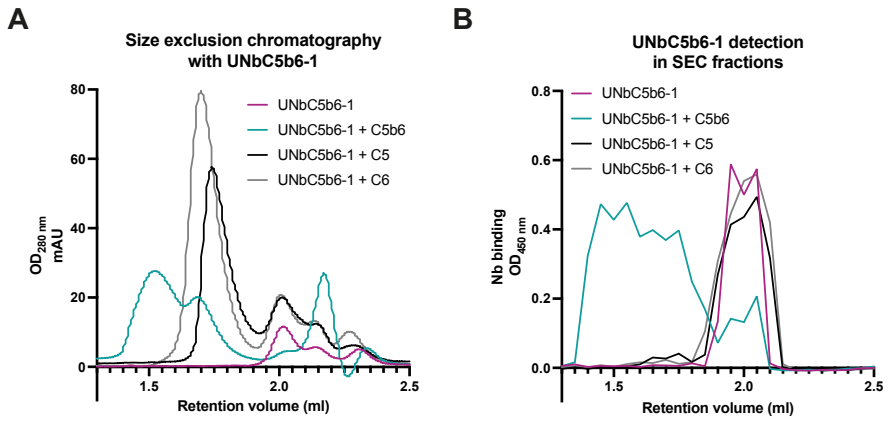

Figure 4: UNbC5b6-1 forms a stable complex with C5b6 in solution. (A) UNbC5b6-1 specifically binds C5b6 in solution. Overlay of chromatograms obtained with SEC, using a Superose 6 Increase column, and measuring absorbance at an OD of 280 nm. Chromatograms from runs with UNbC5b6-1 alone (purple), UNbC5b6-1 incubated in a 1:1 molar ratio with C5b6 (blue), with C5 (black), and with C6 (grey) and eluted fractions were collected, n=1. Complement proteins elute between 1.4-1.9 ml (complement peaks) and UNbC5b6-1 elutes between 1.9-2.1 ml (nanobody peak) (B) Eluted fractions from panel A were coated on microtiter plates and the presence of nanobodies in these fractions was detected using polyclonal rabbit-anti-VHH QE19 antibodies and donkey-anti-rabbit-HRP antibodies, at an OD of 450 nm, n=1.

UNbC5b6-1 binds C5b6 with an affinity of ≈50 pM

Next, we characterized the binding kinetics of UNbC5b6-1 to C5b6, by performing surface plasmon resonance (SPR). Briefly, streptavidin probes were coupled with biotinylated UNbC5b6-1 (UNbC5b6-1-bio) and incubated with different concentrations of C5b6 (1.56 – 25 nM) to assess the association kinetics. Next, the probes were incubated with buffer to assess dissociation. Association and dissociation curves were fitted to determine on rates (k_{on}), off rates (k_{off}) and binding affinity (K_D) (**Table 1**). In this setup, UNbC5b6-1 was able to bind C5b6 with a measured k_{on} of 1.45×10^{5} Ms^{-1} and a k_{off} of 7.15×10^{-6} s^{-1}, resulting in a K_D value of 49.5 ± 0.2 pM (**Fig. 5**).

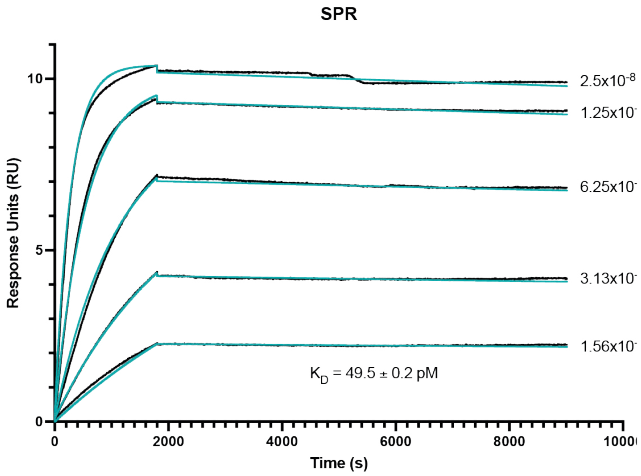

Figure 5: UNbC5b6-1 binds C5b6 with a picomolar affinity. Binding affinity curves of UNbC5b6-1 obtained with a White Fox optic surface plasmon resonance (FO-SPR) sensor, using streptavidin FO-SPR probes, UNbC5b6-1-biotin (330 nM) as an analyte and C5b6 (1.56 – 25 nM) as a ligand. Immobilization of UNbC5b6-1-biotin was performed for 300", association was measured for 1800" and dissociation for 7200", all at 26°C. Experimental data is shown in black and model fit in blue. Curves were fitted using TraceDrawer with a local B_{max}, global k_{on}, global k_{off} and a constant BI. Data represent a graph that is representative of three individually performed experiments.

UNbC5b6-1 does not interfere with complement activity

Next, we investigated if UNbC5b6-1 interferes with complement activation. To do so, we performed two complement-mediated erythrocyte lysis experiments with sheep erythrocytes that were sensitized with antibodies (ShEA). First, we incubated ShEA with UNbC5b6-1, added human serum as a source of complement and measured ShEA lysis by the release of hemoglobin in the supernatant. Eculizumab, a known C5 inhibitor (30), was added as a positive control for inhibition. Interestingly, UNbC5b6-1 did not inhibit complement-mediated erythrocyte lysis in >1% serum (**Fig. 6A**). Only in the lower serum concentrations (0.15-0.6%) a small inhibitory effect could be measured, which was far less pronounced as compared to the inhibitory effect of Eculizumab. In the second assay, we replaced human serum for purified preformed C5b6 and purified C7, C8 and C9. This allowed us to study MAC assembly with C5b6 complexes bound to UNbC5b6-1, prior to the addition of C7, C8, C9, and ShEA. Also in this set-up, UNbC5b6-1 did not inhibit MAC-mediated lysis, neither did Eculizumab (**Fig. 6B**). In conclusion, UNbC5b6-1 does not affect MAC assembly and complement mediated erythrocyte lysis.

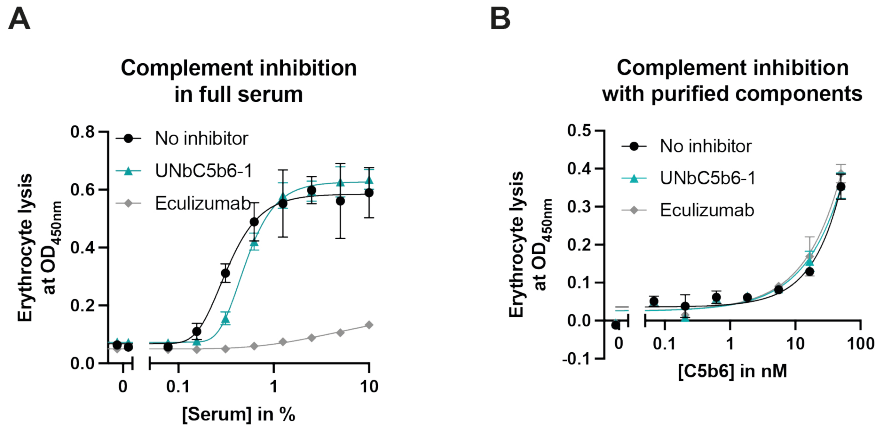

Figure 6: UNbC5b6-1 does not interfere with complement activity. (A) Complement-mediated hemolysis of antibody-coated sheep erythrocytes (shEA, 2% suspension) incubated with human serum (0 – 10%) and 300 nM inhibitor. (B) Complement-mediated hemolysis of shEA (2% suspension) incubated with purified complement components. Purified C5b6 (0 – 50 nM) was incubated with 300 nM inhibitor prior to addition of 2% shEA and purified C7 (100 nM), C8 (100 nM), and C9 (500 nM). (A-B) The OD at 405 nm of the supernatant was detected as a measure of erythrocyte lysis. Data represent mean ± SD of 3 individual experiments and curves were fitted in Graph Pad Prism 9.3.0 using the function “Asymmetric Sigmoidal ,5PL, X is concentration”.

Discussion

This study describes the identification and characterization of UNbC5b6-1, a C5b6 specific llama-derived nanobody. We show that the nanobody binds C5b6 with picomolar affinity and that it does not bind to the C5b6 precursors C5 and C6. Furthermore, UNbC5b6-1 does not interfere with MAC assembly in human serum and when using purified complement proteins.

The identification of UNbC5b6-1 as specific C5b6 binder confirms the idea that nanobodies are suitable for detecting complement activation products and complexes. Previously, others have identified nanobodies recognizing conformation specific epitopes in complement components C4b (31, 32) and C3/C3b (33–35). Such nanobodies are now used in complement research and will contribute to the molecular and functional understanding of complement activation. Although mAbs against MAC precursors C5, C6, and C7 are commercially available, specific detection tools for intermediate activation products of the MAC are still limited. The best known and described is mAb ae11 that binds to polymerized C9 and is frequently used to detect (soluble) MAC pores (11, 12). For C5b6 detection, only one study, by Stach *et al.*, described the identification of eight mAbs specifically binding C5b6 (36). These mAbs were derived from a naïve mouse library. To obtain high affinity mAbs, *in vitro* affinity maturation by diversification of the CDR-H1 and CDR-H2 regions was performed. Despite their efforts, they obtained mAbs with affinities of approximately 550 nM that did not inhibit MAC assembly in a serum environment. Next to the mAbs described by Stach *et al.*, multiple mAbs were described to bind to C5b6 and inhibit MAC assembly, including mAbs 1C9, 7D4, 4G2, 10B6 (37, 38). Although most of these antibodies were of high affinity, they all lacked specificity to discriminate between the activated C5b6 complex and precursor proteins C5 and C6, like UNbC5b6-1 does.

In complement-mediated erythrocyte lysis assays with human serum and with purified complement components, UNbC5b6-1 does not interfere with MAC assembly. During the first steps of MAC assembly, when newly formed C5b6 complexes interact with complement component C7, the MACPF domain in C6 structurally rearranges and aligns with the structural homologous MACPF domain in C7 (22). This interaction further extends the MACPF domains in C5b6 and C7 and exposes hydrophobic domains in the transmembrane segments of C5b, C6 and C7, making the C5b-7 complex lipophilic and anchoring the MAC-precursor complex to the target membrane and allowing further MAC assembly in the target membrane (22, 39, 40). The absence of inhibition by UNbC5b6-1 allows us to hypothesize on the binding site of UNbC5b6-1 on C5b6. It could simply indicate that the binding epitopes of UNbC5b6-1 and C7 are not overlapping and that

the binding epitope of UNbC5b6-1 is not involved in MAC assembly. Alternatively, it could be that UNbC5b6-1 and C7 bind to C5b6 with an (partially) overlapping epitope, without the nanobody exerting an inhibitory effect on MAC assembly. Both UNbC5b6-1 and C7 bind C5b6 with affinities in the picomolar range (41, 42). This could mean that binding of UNbC5b6-1 can be lost upon C5b-7 formation, for example due to steric hindrance. Alternatively, it could mean that C7 binding to C5b6 is not affected by the presence of UNbC5b6-1, despite (partially) overlapping epitopes. Unfortunately, due to technical difficulties, we were not able to unravel the effect of C5b-7 formation on UNbC5b6-1 binding to C5b6. Furthermore, we endeavored multiple attempts of negative stain electron microscopy (EM) and *in silico* modeling using AlphaFold2 (AF2) to identify the exact binding interface of UNbC5b6-1 and C5b6. Unfortunately, in negative stain EM, C6 turned out to be too flexible to resolve the C5b6 structure in complex with our nanobody. When using AF2, we did obtain multiple models of C5b6 binding sites, but we have so far failed to confirm the proposed binding sites via biochemical data. Due to limited computational resources, we were forced split the C5b6 molecule into three subunits (C5b alpha, C5b beta and C6) and model UNbC5b6-1 binding sites to these subunits separately. Therefore, we missed many potential binding sites on the C5b:C6 interface. Especially because UNbC5b6-1 is specific for C5b6, the C5b:C6 interface-epitopes would be of high interest to model with AF2. Furthermore, the proposed binding sites on C5b (alpha and beta) and on C6 that we did obtain with AF2, could not be validated experimentally due to the inability to purify C5b without C6, and to obtain C6 in the "C5b6 conformation", without C5b present. All in all, further studies are required to identify and experimentally confirm the UNbC5b6-1 binding site on C5b6.

With the identification and characterization of UNbC5b6-1, a C5b6-specific, high affinity, non-inhibitory nanobody, this study adds a valuable anti-C5b6 molecule to the field of complement research. The nanobody identified in this study could be used as a detection tool and help to further understand the molecular steps involved in MAC assembly.

Experimental procedures

Serum and proteins

Human serum from ±20 healthy donors was collected and pooled, as previously described (43). Purified complement proteins C5b6 and C8 are obtained from Complement Technology. For the preparation of purified C5b6 Complement Technology cleaves C5 molecules, present in normal human serum by natural alternative pathway C3/C5 convertases in the absence of C7 (44). Complement components C6 and C7 were expressed in HEK293E cells at U-Protein Express, as described previously (45). Complement components C5, and C9 and complement inhibitor Eculizumab were expressed in EXPI293F cells and purified as described previously (45, 46).

Immunizations and construction of phage libraries

Two llamas (Lama glama) were immunized at Preclinics GmbH by a trained veterinarian with 4 shots, containing 12.5 µg human C5b6 each in combination with FAMA adjuvant (Gerbu Biotechnic GmbH), on day 0, 14, 28 and 35. On day 0 and day 43 blood was drawn, to obtain serum and PBMCs. To create phage display libraries, mRNA was isolated from PBMCs (day 43), and cDNA was made using the SuperScript™ IV First-Strand Synthesis System kit (Thermo, 18091050). Next, the cDNA encoding heavy-chain only antibodies was amplified by PCR using primers annealing to framework 1 (FR1) and constant heavy chain 2 (CH2) domains, as previously described (47). Next, DNA fragments were digested and ligated into phagemid pPQ81, fusing the nanobodies to a Myc- and 6×His-tag and to pIII coat protein. Next, the libraries were transformed into competent *E. coli* TG1 cells (Agilent) by electroporation using a MicroPulser and corresponding electroporation cuvettes (Bio-Rad). Library sizes were estimated by spotting a serial dilution of transformed *E. coli* TG1 on Luria-Bertani (LB) agar plates and counting colony forming units per mL (CFU/mL).

Phage display

Phages were produced and purified using 2× yeast extract tryptone (2YT) medium, supplemented with 2% glucose and 100 µg/mL ampicillin, kanamycin resistant VCSM13 helper phage (Agilent), and two rounds of polyethylene glycol precipitation, as previously described (48). Phage display was performed according to standard procedures (49), with the following specific conditions. For the first panning round, Nunc Maxisorp plates (VWR 735-0083, Thermo Fisher Scientific) were coated overnight (O/N) with 100 µL/well of 0.5 and 5.0 µg/mL C5b6, at 4°C, without shaking. For the second panning round, the concentration of immobilized C5b6 was lowered to 0.1 and 1.0 µg/mL. In addition, wells were incubated with phosphate buffered saline (PBS) alone as negative control. The next day, plates were blocked with 200 µL/well 4% skimmed milk (Marvel) in PBS,

for 1 h at room temperature (RT), while shaking. Next, the wells were incubated with phages (≈10^{10} CFU/well for the first round and ≈10^{9} CFU/well for the second round) in 2% Marvel in PBS, for 2 h, while shaking. In the second round of panning, phages were pre-incubated for 30' at RT on a spinning wheel with 35.7 nM of C5 and C6 (10× molar excess compared to coated C5b6 concentration), before being added for 2h to the C5b6 coated wells. Next, the wells were washed extensively (subsequently: 10× wash with 200 µL PBS + 0.05% Tween-20 (PBS-T); 10' incubation with PBS-T at RT, while shaking; 10× wash with 200 µL PBS-T; 10' incubation with PBS-T at RT; 3× wash with 200 µL PBS). Bound phages were eluted from the wells with 100 µL of 0.1 M triethanolamine solution (pH>10) for 15' at RT, while shaking. Elutions were neutralized by the addition of 50 µL of 1 M Tris/HCl (pH=7.5) and phages were rescued by infection in *E. coli* TG1 bacteria (at OD_{600} of 0.5) for 30' at 37°C, without shaking. Next, 2YT medium, supplemented with 2% glucose and 100 µg/mL ampicillin was added to the infected bacteria and incubated O/N at 37°C, while shaking. The next day, bacterial cultures of the rescued phages were stored in 20% glycerol at -80°C. The number of phages/mL used at the start of the selection (input) and in the eluate were estimated by serial dilution of phages in PBS, followed by infection with *E. coli* TG1. Bacteria were spotted on LB agar plates, supplemented with 2% glucose and 100 µg/mL ampicillin, incubated O/N at 37°C and CFU/mL were calculated.

Nanobody production, purification, and labeling

Nanobodies expressing a Myc- and 6×His tag were produced and purified similar as described before (46). Briefly, nanobody genes were fused with a C-terminal Myc- and 6×His-tags, expressed in the periplasm of *E. coli* BL21 Rosetta II cells and purified via their 6×His-tag by immobilized metal affinity chromatography. To obtain nanobodies labeled with biotin, nanobody sequences were cloned into a pRSET vector with the NdeI/NotI multiple cloning sites and subsequently transformed into *E. coli* BL21 (DE3). For nanobody production, *E. coli* BL21 (DE3) was cultured in LB medium supplemented with 20 mM glucose and when bacteria reached an exponential growth phase (OD_{600} 0.5-0.7) nanobody expression was induced for 4 h with 1 mM isopropylthio-β-galactoside. Next, bacteria were pelleted and nanobodies were isolated denatured using 6 M guanidine in the presence of 10 mM imidazole. Supernatants were loaded on a HisTrap FF column, using an ÄKTA Explorer, according to manufacturer's protocol. Nanobodies were eluted from the column with a gradient of imidazole (10 – 200 mM). Next, nanobodies were renatured by dialysis against PBS. Next, nanobodies with a C-terminal LPETG-his motif were biotinylated by sortagging (29), similar as described before (46). Finally, nanobody sizes and purities were confirmed with SDS-PAGE, concentrations were measured at OD_{280} and nanobodies were stored at -20°C or at 4°C, until further use.

ELISA: Coating, incubation time & development

Unless stated differently, Nunc Maxisorp plates were coated O/N at 4°C with 50 µL of either purified protein (C5b6, C5, C6) at 2 µg/mL, or SEC fractions, diluted 1:1 in PBS. The next day, wells were blocked at RT, without shaking, for 1 h. Blocking was done with 200 µL PBS + 4% Marvel (immune response & crude periplasmic binding) or 80 µL PBS-T + 4% bovine serum albumin (BSA) (others). All following incubations were performed in 50 µL/well, while shaking, for 1 h at RT. Samples were diluted in either PBS + 1% Marvel or PBS-T + 1% BSA (respectively to blocking buffers). In between all incubations, wells were washed 3x with PBS-T. To detect llama antibodies and unlabeled nanobodies, wells were incubated with polyclonal rabbit-anti-nanobody antibodies QE19 (1:2000, QVQ Holding BV) followed by polyclonal donkey-anti-rabbit-HRP detection antibodies (1:5000, Jackson Immuno Research). To detect biotinylated nanobodies, wells were incubated with streptavidin-HRP (1:5000, Southern Biotech). For the immune response and crude periplasmic binding ELISA 3.7 mM of O-phenylenediamine dihydrochloride + 50 mM Na_2HPO_4 $2H_2O$ + 25 mM citric acid + 0.03% H_2O_2 was used as a substrate. For all others 100 µg/mL tetramethylbenzidine dissolved in DMSO + 100 mM NaOAc + 1.7 mM ureum peroxide was used as a substrate. In all cases, 0.5 M sulfuric acid was used to stop the reaction. Absorbance (450 nm) was measured with an iMark Microplate Reader (Biorad).

Erythrocyte lysis assays

Veronal buffered saline + 145 nM NaCl, pH 7.4 supplemented with 0.25 mM $MgCl_2$ and 0.5 mM $CaCl_2$ was used as buffer. Sheep erythrocytes were washed 3x with PBS and pre-opsonized with 1:2000 polyclonal rabbit-anti-sheep IgM antibodies (produced in our lab). Sheep erythrocytes opsonized with antibodies are further referred to as shEA. For screening with periplasmic extracts, crude extracts (1:5 diluted in PBS) were incubated with 2.5% human serum and a 2% shEA suspension, for 15', at 37°C, shaking. For complement inhibition in human serum, 300 nM purified nanobodies or Eculizumab was incubated with human serum (0-10%) and 2% shEA, for 45', at 37°C, shaking. For complement inhibition with purified components different concentrations of C5b6 (0-50 nM) was pre-incubated with 300 nM nanobody or Eculizumab, for 10', at RT. Next, samples were incubated with 100 nM C7, 100 nM C8, 500 nM C9, and 2% shEA suspension, for 45', at 37°C, shaking. In all assays, shEA were incubated with 50 µL milliQ water (100% lysis) and 50 µL buffer (0% lysis) as controls to calculate percentages of hemolysis. After final incubations, plates were spun down for 7', 3500 rpm and supernatants were 1:3 diluted with milliQ water. Hemoglobin release was measured at an OD_{405}, using an iMark Microplate Reader (Biorad).

SEC: nanobody interaction with C5, C6 and C5b6

UNbC5b6-1 (2.1 µM) was incubated with C5b6 (1.4 µM), C5 (2.1 µM), C6 (2.1 µM) or buffer (25 mM Hepes + 150 mM NaCl, pH 7.4) for 15', at RT. Next, samples were filtered with a 0.22 µm Costar® SpinX tube (Corning) and 50 µL sample was loaded on a Superose 6 Increase 3.2/300 column (GE Healthcare), using the AKTA-Explorer (GE Healthcare). OD_{280} was measured and fractions of 50 µL were collected to detect presence of UNbC5b6-1 by ELISA.

SPR affinity determination

Kinetics of UNbC5b6-1 binding to C5b6 was assessed on a White Fox fiber optic surface plasmon resonance (FO-SPR) sensor (FOx Biosystems) using streptavidin FO-SPR probes (FOx Biosystems). Biotinylated UNbC5b6-1 (330 nM) was immobilized on streptavidin probes in PBS, pH 7.4, supplemented with 0.01% Tween-20 (PBS-$T_{0.01\%}$), at 1000 rpm, 26°C for 300" after which probes were incubated with (1.56 - 25 nM) C5b6 in PBS-$T_{0,01\%}$. Association was measured for 1800" and dissociation was measured for 7200", in PBS-$T_{0,01\%}$, both while shaking at 1000 rpm, 26°C. FO-SPR data were collected by FOx software (FOx Biosystems) and on- and off-rates were fitted using TraceDrawer, using a Local B_{max}, global k_{on}, global k_{off} and a constant BI.

Data analysis & statistical testing

Illustrations were created with BioRender. Graphs were created with GraphPad Prism 9.3.0. Curves were fitted with GraphPad Prism 9.3.0. or with Tracedrawer. Nanobody sequences were aligned using T-coffee (50).

Supporting information

This article contains supporting information.

Funding and additional information

This work was mainly funded by the Netherlands Organisation for Scientific Research (NWO) under the TTW Industrial Doctorate (grant agreement no. NWA.ID.17.036 to EMS). The project was also supported by the European Research Council (ERC) under the European Union's Horizon 2020 research and innovation programme (grant agreement No. 101001937, ERC-ACCENT to SHMR and No. 787241, ERC-C-CLEAR to PG).

Conflict of interest

RoH, GD, ED and RaH are employees of QVQ Holding BV. Other authors declare no conflict of interest.

Abbreviations

The abbreviations used here are: MAC, Membrane Attack Complex; C5b-9, Membrane Attack Complex; C5b-7, Membrane attack complex precursor consisting of C5b, C6, and C7; C5b-8, Membrane attack complex precursor consisting of C5b, C6, C7, and C8; VHH, Variable heavy chain of heavy chain only antibodies, nanobody; MACPF/CDC, MAC-perforin/cholesterol-dependent cytolysin; mAb, monoclonal antibody; MG, macroglobulin; CUB, C1r/C1s UEGF BMP1; NTR, netrin module; TS, thrombospondin-like; FIM, factor I-MAC; CCP, complement control protein; VHH, variable heavy chain of heavy chain only antibodies; PBMC, peripheral blood mononuclear cells; *E. coli*, *Escherichia coli*; CDR, complementarity determining region; CDRH1-3, CDR Heavy chain domain 1, 2, or 3; Irr Nb, irrelevant nanobody; X-bio, biotinylated nanobody (clone X); SEC, size exclusion chromatography; SPR, surface plasmon resonance; k_{on}, association rate; k_{off}, dissociation rate; K_D, binding affinity; ShEA, sheep erythrocytes sensitized with antibodies; EM, electron microscopy; AF2, AlphaFold 2; FR1, framework 1; CH2, constant heavy chain 2; LB, Luria-Bertani; CFU, colony forming units; 2YT, 2× yeast extract tryptone; O/N, overnight; PBS, phosphate buffered saline; Marvel, skimmed milk; RT, room temperature; PBS-T, PBS supplemented with 0.05% Tween-20; PBS-$T_{0.01\%}$, PBS supplemented with 0.01% Tween-20; BSA, bovine serum albumin; FO-SPR, Fox fiber optic surface plasmon resonance; Nb, nanobody.

References

1. Merle, N. S., Noe, R., Halbwachs-Mecarelli, L., Fremeaux-Bacchi, V., and Roumenina, L. T. (2015) Complement system part II: Role in immunity. *Front Immunol.* **6**, 1–26
2. Gasque, P. (2004) Complement: A unique innate immune sensor for danger signals. *Mol Immunol.* **41**, 1089–1098
3. Merle, N. S., Church, S. E., Fremeaux-Bacchi, V., and Roumenia, L. T. (2015) Complement system part I – molecular mechanisms of activation and regulation. *Front Immunol.* **6**, 1–30
4. de Jorge, E. G., Yebenes, H., Serna, M., Tortajada, A., Llorca, O., and de Córdoba, S. R. (2018) How novel structures inform understanding of complement function. *Semin Immunopathol.* **40**, 3–14
5. Aleshin, A. E., Schraufstatter, I. U., Stec, B., Bankston, L. A., Liddington, R. C., and DiScipio, R. G. (2012) Structure of complement C6 suggests a mechanism for initiation and unidirectional, sequential assembly of Membrane Attack Complex (MAC). *Journal of Biological Chemistry.* **287**, 10210–10222
6. Muller-Eberhard, H. J. (1986) the Membrane Attack Complex of Complement. *Ann. Rev. Immunol.* **4**, 503–28
7. Serna, M., Giles, J. L., Morgan, B. P., and Bubeck, D. (2016) Structural basis of complement membrane attack complex formation. *Nat Commun.* **7**, 1–7
8. Hadders, M. A., Bubeck, D., Roversi, P., Hakobyan, S., Forneris, F., Morgan, B. P., Pangburn, M. K., Llorca, O., Lea, S. M., and Gros, P. (2012) Assembly and Regulation of the Membrane Attack Complex Based on Structures of C5b6 and sC5b9. *Cell Rep.* **1**, 200–207
9. Morgan, B. P., Walters, D., Serna, M., and Budeck, D. (2016) Terminal complexes of the complement system : new structural insights and their relevance to function. *Immunol Rev.* **274**, 141–151
10. Bayly-Jones, C., Bubeck, D., and Dunstone, M. A. (2017) The mystery behind membrane insertion: A review of the complement membrane attack complex. *Philosophical Transactions of the Royal Society B: Biological Sciences*. 10.1098/rstb.2016.0221
11. Mollnes, T. E., Harboe, M., and Tschopp, J. (1985) Monoclonal Antibodies Recognizing a Neoantigen of Poly(C9) Detect the Human Terminal Complement Complex in Tissue and Plasma. *Scand J Immunol.* **22**, 183–195
12. Bayly-Jones, C., Ho, B. H. T., Lau, C., Leung, E. W. W., D'Andrea, L., Lupton, C. J., Ekkel, S. M., Venugopal, H., Whisstock, J. C., Mollnes, T. E., Spicer, B. A., and Dunstone, M. A. (2023) The neoepitope of the complement C5b-9 Membrane Attack Complex is formed by proximity of adjacent ancillary regions of C9. *Commun Biol*. 10.1038/s42003-023-04431-y
13. Aleshin, A. E., DiScipio, R. G., Stec, B., and Liddington, R. C. (2012) Crystal structure of C5b-6 suggests structural basis for priming assembly of the membrane attack complex. *Journal of Biological Chemistry.* **287**, 19642–19652
14. DiScipio, R. G., Linton, S. M., and Rushmere, N. K. (1999) Function of the factor I modules (FIMS) of human complement component C6. *Journal of Biological Chemistry.* **274**, 31811–31818
15. Schreiber, R. D., and Müller-Eberhard, H. J. (1978) Assembly of the cytolytic alternative pathway of complement from 11 isolated plasma proteins*. *Journal of Experimental Medicine.* **148**, 1722–1727
16. Muller-Eberhard, H. J. (1988) Molecular organization and function of the complement system. *Annual review Biochemistry.* **57**, 321–347
17. Bramham, J., Thai, C. T., Soares, D. C., Uhrín, D., Ogata, R. T., and Barlow, P. N. (2005) Functional insights from the structure of the multifunctional C345C domain of C5 of complement. *Journal of Biological Chemistry.* **280**, 10636–10645
18. Laursen, N. S., Magnani, F., Gottfredsen, R. H., Petersen, S. V., and Andersen, G. R. (2012) Structure, Function and Control of Complement C5 and its Proteolytic Fragments. *Curr Mol Med.* **12**, 1083–1097
19. Chakravarti, D. N., Chakravarti, B., Parra, C. A., and Muller-Eberhard, H. J. (1989) Structural homology of complement protein C6 with other channel-forming proteins of complement. *Proc Natl Acad Sci U S A.* **86**, 2799–803

20. Lukassen, M. V, Franc, V., Hevler, J. F., and Heck, A. J. R. (2021) Similarities and differences in the structures and proteoform profiles of the complement proteins C6 and C7. *Proteomics*. 10.1002/pmic.202000310.This
21. DiScipio, R. G. (1992) Formation and structure of the C5b-7 complex of the lytic pathway of complement. *Journal of Biological Chemistry*. **267**, 17087–17094
22. Preissner, K. T., Podack, E. R., and Muller-Eberhard, H. J. (1985) The membrane attack complex of complement: relation of C7 to the metastable membrane binding site of the intermediate complex C5b-7. *The Journal of Immunology*. **135**, 445–451
23. Uchański, T., Pardon, E., and Steyaert, J. (2020) Nanobodies to study protein conformational states. *Curr Opin Struct Biol*. **60**, 117–123
24. De Genst, E., Silence, K., Decanniere, K., Conrath, K., Loris, R., Rg Kinne, J., Muyldermans, S., and Wyns, L. (2006) Molecular basis for the preferential cleft recognition by dromedary heavy-chain antibodies. *PNAS*. **103**, 4586–4591
25. Lauwereys, M., Arbabi Ghahroudi, M., Desmyter, A., Kinne, J., Hölzer, W., De Genst, E., Wyns, L., and Muyldermans, S. (1998) Potent enzyme inhibitors derived from dromedary heavy-chain antibodies. *EMBO J*. **17**, 3512–3520
26. Laeremans, T., Sands, Z. A., Claes, P., De Blieck, A., De Cesco, S., Triest, S., Busch, A., Felix, D., Kumar, A., Jaakola, V. P., and Menet, C. (2022) Accelerating GPCR Drug Discovery With Conformation-Stabilizing VHHs. *Front Mol Biosci*. 10.3389/fmolb.2022.863099
27. Lefranc, M. P., Giudicelli, V., Duroux, P., Jabado-Michaloud, J., Folch, G., Aouinti, S., Carillon, E., Duvergey, H., Houles, A., Paysan-Lafosse, T., Hadi-Saljoqi, S., Sasorith, S., Lefranc, G., and Kossida, S. (2015) IMGT R, the international ImMunoGeneTics information system R 25 years on. *Nucleic Acids Res*. **43**, D413–D422
28. Ehrenmann, F., Duroux, P., and Ginestoux, C. (2020) IMGT Repertoire (IG and TR) Collier de Perles: alpaca (Vicugna pacos) IGHV. *https://www.imgt.org/IMGTrepertoire/2D-3Dstruct/Colliers_dyn.php?english=alpaca&latin=Vicugna%20pacos&group=IGHV&gene=IGHV3-3&domain=VH&numacc=AM773729*
29. Jeong, H. J., Abhiraman, G. C., Story, C. M., Ingram, J. R., and Dougan, S. K. (2017) Generation of Ca2+-independent sortase A mutants with enhanced activity for protein and cell surface labeling. *PLoS One*. **12**, 1–15
30. Rother, R. P., Rollins, S. A., Mojcik, C. F., Brodsky, R. A., and Bell, L. (2007) Discovery and development of the complement inhibitor eculizumab for the treatment of paroxysmal nocturnal hemoglobinuria. *Nat Biotechnol*. **25**, 1256–1264
31. De la O Becerra, K. I., Oosterheert, W., van den Bos, R. M., Xenaki, K. T., Lorent, J. H., Ruyken, M., Schouten, A., Rooijakkers, S. H. M., van Bergen en Henegouwen, P. M. P., and Gros, P. (2022) Multifaceted Activities of Seven Nanobodies against Complement C4b. *The Journal of Immunology*. **208**, 2207–2219
32. Zarantonello, A., Presumey, J., Simoni, L., Yalcin, E., Fox, R., Hansen, A., Olesen, H. G., Thiel, S., Johnson, M. B., Stevens, B., Laursen, N. S., Carroll, M. C., and Andersen, G. R. (2020) An Ultrahigh-Affinity Complement C4b-Specific Nanobody Inhibits In Vivo Assembly of the Classical Pathway Proconvertase. *The Journal of Immunology*. **205**, 1678–1694
33. Jensen, R. K., Pihl, R., Gadeberg, T. A. F. F., Jensen, J. K., Andersen, K. R., Thiel, S., Laursen, N. S., and Andersen, G. R. (2018) A potent complement factor C3–specific nanobody inhibiting multiple functions in the alternative pathway of human and murine complement. *Journal of Biological Chemistry*. **293**, 6269–6281
34. Pedersen, H., Jensen, R. K., Hansen, A. G., Gadeberg, T. A. F., Thiel, S., Laursen, N. S., and Andersen, G. R. (2020) A C3 specific nanobody that blocks all three activation pathways in the human and murine complement system. *Journal of Biological Chemistry*. 10.1074/jbc.RA119.012339
35. Pedersen, H., Jensen, R. K., Jensen, J. M. B., Fox, R., Pedersen, D. V., Olesen, H. G., Hansen, A. G., Christiansen, D., Mazarakis, S. M. M., Lojek, N., Hansen, P., Gadeberg, T. A. F., Zarantonello, A., Laursen, N. S., Mollnes, T. E., Johnson, M. B., Stevens, B., Thiel, S., and Andersen, G. R. (2020) A Complement C3–Specific Nanobody for Modulation of the Alternative Cascade Identifies the C-Terminal Domain of C3b as Functional in C5 Convertase Activity. *The Journal of Immunology*. **205**, 2287–2300

36. Stach, L., Dinley, E. K. H., Tournier, N., Bingham, R. P., Gormley, D. A., Bramhall, J. L., Taylor, A., Clarkson, J. E., Welbeck, K. A., Harris, C. L., Feeney, M., Hughes, J. P., Sepp, A., Batuwangala, T. D., Kitchen, S. J., and Nichols, E. M. (2021) Novel selection approaches to identify antibodies targeting neoepitopes on the c5b6 intermediate complex to inhibit membrane attack complex formation. *Antibodies*. 10.3390/antib10040039
37. Lin, K., Zhang, L., Kong, M., Yang, M., Chen, Y., Poptic, E., Hoffner, M., Xu, J., Tam, C., and Lin, F. (2020) Development of an anti-human complement C6 monoclonal antibody that inhibits the assembly of membrane attack complexes. *Blood Adv.* **4**, 2049–2057
38. Zelek, W. M., Taylor, P. R., and Morgan, B. P. (2019) Development and characterization of novel anti-C5 monoclonal antibodies capable of inhibiting complement in multiple species. *Immunology*. **157**, 283–295
39. Hammer, C. H., Nicholson, A., and Mayer, M. M. (1975) On the mechanism of cytolysis by complement: evidence on insertion of C5b and C7 subunits of the C5b,6,7 complex into phospholipid bilayers of erythrocyte membranes. *Proc Natl Acad Sci U S A*. **72**, 5076–5080
40. Marshall, P., Hasegawa, A., Davidson, E. A., Nussenzweig, V., and Whitlow, M. (1996) Interaction between Complement Proteins C5b-7 and Erythrocyte Membrane Sialic Acid. *J Exp Med*. **184**, 1225–1232
41. Podack, E. R., Biesecker, G., Kolb, W. P., and Müller-Eberhard, H. J. (1978) The C5b-6 Complex: Reaction with C7, C8, C9. *The Journal of Immunology*. **121**, 484–490
42. Thai, C.-T., and Ogata, R. T. (2005) Recombinant C345C and Factor I Modules of Complement Components C5 and C7 Inhibit C7 Incorporation into the Complement Membrane Attack Complex 1. *The Journal of Immunology*. **174**, 6227–6232
43. Berends, E. T. M., Dekkers, J. F., Nijland, R., Kuipers, A., Soppe, J. A., van Strijp, J. A. G., and Rooijakkers, S. H. M. (2013) Distinct localization of the complement C5b-9 complex on Gram-positive bacteria. *Cell Microbiol*. **15**, 1955–1968
44. Complement Technology C5b,6 Complex Product Description Complement Technology. [online] https://www.complementtech.com/uploads/catalog/61c1f0a5d8cd7 (Accessed April 26, 2023)
45. Doorduijn, D. J., Heesterbeek, D. A. C., Ruyken, M., De Haas, C. J. C., Stapels, D. A. C., Aerts, P. C., Rooijakkers, S. H. M., and Bardoel, B. W. (2021) Polymerization of C9 enhances bacterial cell envelope damage and killing by membrane attack complex pores. *PLoS Pathog*. **17**, 1–23
46. Struijf, E. M., De La O Becerra, K. I., Ruyken, M., Van Oosterom, F., Siere, D. Y., Heesterbeek, D. A. C., Dolk, E., Heukers, R., Bardoel, B. W., Gros, P., and Rooijakkers, S. H. M. (2023) Inhibition of cleavage of human complement component C5 and the R885H C5 variant by two distinct high affinity anti-C5 nanobodies. *BioRXIV*. 10.1101/2023.02.22.529391
47. De Haard, H. J. W., Bezemer, S., Ledeboer, A. M., Müller, W. H., Boender, P. J., Moineau, S., Coppelmans, M. C., Verkleij, A. J., Frenken, L. G. J., and Verrips, C. T. (2005) Llama antibodies against a lactococcal protein located at the tip of the phage tail prevent phage infection. *J Bacteriol*. **187**, 4531–4541
48. Marks, J. D., Hoogenboom, H. R., Bonnert, T. P., Mccafferty, J., Griffiths, A. D., and Winter, G. (1991) By-passing Immunization Human Antibodies from V-gene Libraries Displayed on Phage. *J. Mol. Biol*. **222**, 581–597
49. Gangaiah, D., Ryan, V., Van Hoesel, D., Mane, S. P., Mckinley, E. T., Lakshmanan, N., Reddy, N. D., Dolk, E., and Kumar, A. (2022) Recombinant Limosilactobacillus (Lactobacillus) delivering nanobodies against Clostridium perfringens NetB and alpha toxin confers potential protection from necrotic enteritis. *Microbiology Open*. 10.1002/mbo3.1270
50. di Tommaso, P., Moretti, S., Xenarios, I., Orobitg, M., Montanyola, A., Chang, J. M., Taly, J. F., and Notredame, C. (2011) T-Coffee: A web server for the multiple sequence alignment of protein and RNA sequences using structural information and homology extension. *Nucleic Acids Res*. **39**, 13–17

Table 1. Association rates, dissociation rates and binding affinity of UNbC5b6-1 for C5b6

Analyte	Ligand	Conc. Ligand in M	B_{max}	Est. error	k_{on} (1/(M*s))	Est. error	k_{off} (1/s)	Est. error	K_D	Est. error	BI (Signal)	Chi^2 (signal^2)	U-value: k_{on}/k_{off} (%)
UNbC5b6-1	C5b6	2.5×10^{-8}	10.25	$\pm6.82\times10^{-5}$	1.45×10^{5}	*±1,25*	7.15×10^{-6}	*±3.37*$\times10^{-8}$	4.95×10^{-11}	*±2.34*$\times10^{-13}$	0.2	0.01	0.6
		1.25×10^{-8}	9.79	$\pm5.19\times10^{-5}$	1.45×10^{5}	*±1,25*	7.15×10^{-6}	*±3.37*$\times10^{-8}$	4.95×10^{-11}	*±2.34*$\times10^{-13}$	0.2	0.01	0.6
		6.25×10^{-9}	8.84	$\pm1.88\times10^{-4}$	1.45×10^{5}	*±1,25*	7.15×10^{-6}	*±3.37*$\times10^{-8}$	4.95×10^{-11}	*±2.34*$\times10^{-13}$	0.1	0.01	0.6
		3.13×10^{-9}	7.73	$\pm1.74\times10^{-4}$	1.45×10^{5}	*±1,25*	7.15×10^{-6}	*±3.37*$\times10^{-8}$	4.95×10^{-11}	*±2.34*$\times10^{-13}$	0.1	0.01	0.6
		1.56×10^{-9}	6.91	$\pm2.17\times10^{-3}$	1.45×10^{5}	*±1,25*	7.15×10^{-6}	*±3.37*$\times10^{-8}$	4.95×10^{-11}	*±2.34*$\times10^{-13}$	0	0.01	0.6

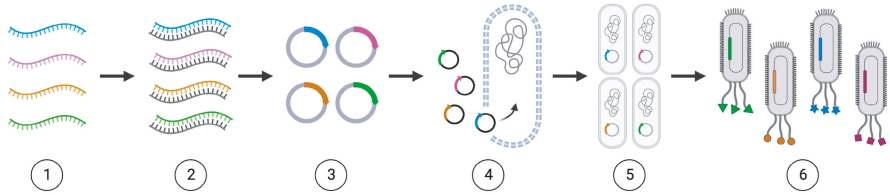

Supporting figure 1: Phage display library generation and selection strategy. Schematic and stepwise representation of phage display library construction and phage display selection strategy. (1) Isolated mRNA, obtained from llama peripheral blood mononuclear cells. (2) cDNA production and specific amplification of VHH genes. (3) Digestion and ligation of VHH genes in phagemid vectors. (4) Transformation into E. coli TG1. (5) E. coli TG1 library formation. (6) phage production and purification. Figure created with BioRender. co


```
Ruler:      0          10         20         30         40         50         60
                      FR-H1                 CDR-H1     FR-H2           CDR-H2
UNbC5b6-1: EVQQVESGGGLVQAGGSLRLSCAASGGTFS IYTMG WFRQAPGKEREIVA TINWNDVSTYLVDSVKG

Ruler:          70         80         90         100        110        120
                           FR-H3                 CDR-H3        FR-H4
UNbC5b6-1: RFIISRDNAKNTVYLQMNSLKPEDTAVYYCAA AQRGSSFQSTNT YGQGTQVTVSS
```

Supporting figure 2: Full sequence of UNbC5b6-1. Protein sequence of UNbC5b6-1. Nanobody frameworks (FR-H1, FR-H2, FR-H3, FR-H4) and variable regions (CDR-H1, CDR-H2, CDR-H3) are depicted. Amino acids are colored according to the shapely color scheme.

5

General discussion

In this thesis, we developed and characterized four novel llama-derived nanobodies against human complement proteins: UNbC3b-1 against C3b (chapter 2); UNbC5-1 and UNbC5-2 against C5 (chapter 3); and UNbC5b6-1 against C5b6 (chapter 4). To do so, we immunized two llamas, created nanobody phage display libraries, and performed multiple rounds of phage display panning. For all complement proteins used during immunizations, we successfully identified multiple nanobodies. In the end, we prioritized four nanobodies for further characterization because of their potent binding and inhibitory activity or their unique capacity to discriminate activated complement products from their precursors.

Nanobodies targeting complement

Over the recent years, other research groups also successfully developed llama-derived nanobodies against different complement proteins, regulators, and receptors. **Figure 1** provides a summarizing overview of all complement-targeting nanobodies described to date (1–9). Most nanobodies are specific and bind their target with high affinity. Also, for many nanobodies, structural studies were performed to pinpoint their exact binding epitope. These recent data and the work described in this thesis thus indicate that development of llama-derived nanobodies is a successful and efficient approach to discover novel complement targeting molecules. In fact, the amount of nanobodies identified during my PhD, was much larger than the four described in this thesis. For all complement targets used during immunizations, we were able to mount a specific immune response in the llamas and subsequently select large panels of specific nanobodies. While the identification of nanobodies in general was efficient, it was sometimes challenging to select which nanobodies were most interesting to follow up for further biochemical and functional characterization. The latter is a time-consuming process and forced us to only characterize four nanobodies in greater detail. Consequently, we have obtained large sets of other unique nanobodies that bind (and inhibit) the targets described in this thesis (C3b, C5 and C5b6) and other complement targets (FB/Bb, C3, and C6). Therefore, I am optimistic that this thesis can serve as a valuable starting point to further explore and characterize the nanobodies that were generated during my PhD.

The benefits of nanobodies

One of the most important reasons to develop llama-derived nanobodies during this thesis, instead of for example monoclonal antibodies, was the high preference of nanobodies to recognize conformational epitopes (10–13). This fitted well with our goal to discriminate between complement activation products and precursor proteins, which often only differ from each other in their conformational state(14). So, the question is now whether similar results could have been obtained with conventional antibodies. For the anti-C5 nanobody UNbC5-1 the answer is simply yes since we identified that this nanobody has an overlapping epitope with the monoclonal antibody Eculizumab (15, 16). For UNbC5-2 the answer is a bit less certain, but we think that it would be possible to target this epitope with a monoclonal antibody. The specific binding interface is not hidden in a cryptic cleft and the involved amino are all in close proximity and appear like a linear epitope. For the other two nanobodies, UNbC3b-1 and UNbC5b6-1 it is unfortunately more difficult to answer this question since we did not unravel their exact binding sites. Nevertheless, both nanobodies could discriminate between activated and precursor proteins, which was our goal.

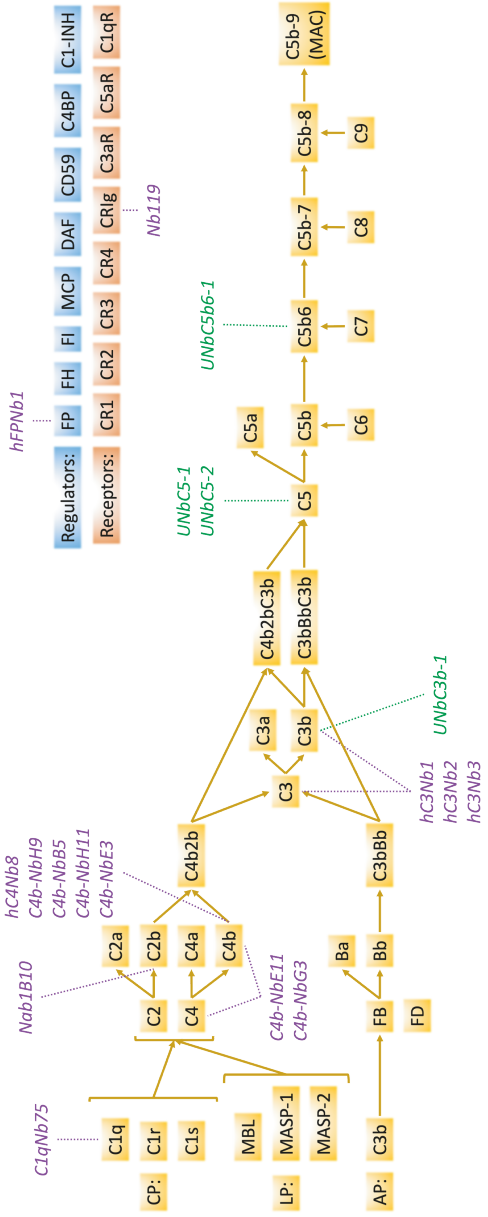

Figure 1: Schematic overview of the current collection of anti-complement nanobodies. In green the nanobodies described in this thesis and in purple the nanobodies previously described by others.

Next to their specificity, nanobodies are also known for their high affinities (17). Also the nanobodies identified in this thesis bound their targets in the picomolar range. A study by Stach et al. developed monoclonal antibodies specifically targeting C5b6, using a naïve antibody library and *in vitro* affinity maturation(18). Although they identified multiple specific clones, they failed to identify clones of high affinity. Using our llama immunization strategies, which always included a series of immunizations and for example in the case of C3b presented the antigen in different formats, we facilitated *in vivo* affinity maturation. Furthermore, by performing phage display panning with the nanobody libraries and a wide variety of selection strategies, including negative selections with different levels of stringency, we might have steered our selection to nanobodies with high affinities and specificities for activation products.

The anti-complement nanobody collection

With at least 14 complement targeting nanobodies previously identified and the four nanobodies that were characterized in this thesis (**Figure 1**), the collection of nanobodies targeting complement has rapidly expanded in the last years. I hope this encourages others to develop novel nanobodies targeting complement proteins following similar procedures. Simplest would be to develop nanobodies targeting precursor proteins that circulate in serum, such as C2, FD, and C9. However, the complement field would really benefit from more nanobodies that discriminate activated complement products from precursor proteins. For example, nanobodies that can distinguish MAC precursors (C5b-7, C5b-8) from native proteins (C5, C6, C7, etc.) and full MAC complexes would allow to study the process of MAC assembly in greater detail. This could help to unravel the molecular mechanisms required for a MAC pore to be cytolytic in host and pathogenic cells (19, 20). With our nanobody UNbC5b6-1, the first step of MAC assembly can now be detected, but this is not sufficient to follow and detect each step of MAC assembly individually.

Next to the nanobody targeting MAC precursor C5b6, we also made various attempts to identify nanobodies that could discriminate between C3 and C5 convertases, since these would be valuable tools to further understand the molecular requirements of C5 convertase formation and functioning. Although it is currently not known if the proteins forming the convertase (C3b and Bb) are structurally different in a C3 convertase and a C5 convertase, we still tried to obtain C5 convertase specific nanobody (21). To do so, we immunized llamas with soluble, stabilized AP convertases and C3b-opsonized bacteria in the presence or absence of C5. With these immunizations we attempted to boost the llamas' immune responses towards (neo-)epitopes (if at all) specifically present in these complexes. Like we did for C3b, C5 and C5b6, we could detect AP convertase-binding antibodies in the serum of llamas. However, despite multiple attempts with different

phage display panning strategies and many screenings assays, we did not identify nanobodies that were specifically binding to C5 convertases, and not to C3 convertases and precursor proteins. Even though we did not succeed to identify C5 convertase specific nanobodies during my PhD, I am still hopeful that nanobodies are promising molecules to achieve this goal in the future. Their paratope shape, long CDR-H3 loop and their preference for conformational epitopes makes them good candidates to bind cryptic clefts located in (C5) convertases (10). Furthermore, the nanobodies described in this thesis might also help to further unravel the exact molecular requirements for C3 convertases to become C5 convertases. One suggestion would be to develop multivalent nanobodies, such as bispecifics or trispecifics that target C3b, Bb, and C5, simultaneously. Although future studies should explore the exact requirements for such multivalent molecules, I would suggest that at least that the linker lengths should be adjusted to the specific distances between individual epitopes and that the individual nanobodies should be of rather low affinity. Mediated by avidity, the latter could enable specific binding to convertase complexes, without efficient binding to the individual nanobody targets (22).

Although most nanobodies identified by other groups have different targets than the here-described nanobodies, three nanobodies identified by the group of Prof. Andersen (hC3Nb1 (6), hC3Nb2 (7), and hC3Nb3 (8)) appear similar to our UNbC3b-1 nanobody. However, biochemical and functional studies show that UNbC3b-1 differs from the hC3Nbs. While UNbC3b-1 specifically recognizes C3b, hC3Nb2 and hC3Nb3 bind to both C3 and C3b. For hC3Nb1 it was reported that it could recognize both C3b and C3. However, in a recent publisher correction, the authors suggest that this nanobody may also bind better to C3b than to C3 (23). Nevertheless, UNbC3b-1 and hC3Nb1 show different mechanisms of action. While hC3Nb1 inhibits the AP by preventing proconvertase formation and blocking the C3 convertase-substrate interaction, we found that UNbC3b-1 blocks AP convertase activity without blocking the formation of (pro)convertases. Finally, although we were not successful in determining the exact binding epitope of UNbC3b-1, its binding and inhibition profile is distinct from the hC3Nbs, suggesting that it binds C3b on a different epitope than the previously described anti-C3(b) nanobodies.

Future directions for the nanobodies identified in this thesis

The nanobodies described in this thesis could directly be used in complement research as they are presented here. However, further characterization is still valuable, especially if these nanobodies would be used as diagnostic or therapeutic agents. The identification of the exact binding sites of UNbC3b-1 and UNbC5b6-1 is an important next step. Artificial intelligence (AI) might help in identifying the binding sites of nanobodies. For example, the development of DeepMind's neural network model

AlphaFold2 (AF2) has given an enormous boost to the structural prediction of proteins based on their amino acid sequence. While effective for many proteins (24), employing AF2 for complement-nanobody predictions taught us that it is still rather difficult to obtain reliable predictions. This is likely due to the size of complement proteins and complexes, which requires more computational resources than were available to us. Consequently, AF2 either predicted hypothetical binding interfaces on different sites of the molecule (for example in the case of C3b and UNbC3b-1) or forced us to 'break up' the sequence in two smaller pieces (for example in the case of C5b6 and UNbC5b6-1), which prevented AF2 to model the C5b:C6 interfaces properly. Fortunately, since the field of AI is moving forward with a high pace, programs such as AF2 might be able to reliably predict interaction sites in the near future. Furthermore, AI might be used to predict specific modifications that improve nanobody affinities, specificities and cross-reactivities.

Therapeutic anti-complement nanobodies

Although the work in this thesis was mainly aimed to develop novel tools to study the complement system, the identification of novel complement inhibitors might contribute to the development of novel complement-mediating therapies. Unwanted complement activation is the root cause in multiple blood-related diseases and in many other diseases complement activation contributes to disease severity (25, 26). The introduction of Eculizumab into the clinic has evidenced how beneficial complement inhibition can be. More than 15 years later, a couple of complement-mediating medicine are used in the clinic for a wider variety of diseases (25–28). Nevertheless, the treatment options for complement-mediated diseases are still rather limited, and for Eculizumab treatment limitations have also been identified. For example, in patients treated with Eculizumab residual complement activity by incomplete inhibition can sometimes be detected and is often problematic in these patients. Studies using Eculizumab and OmCI (also known as Coversin) showed that by targeting the C5 molecule on two distinct sites, residual activity could be abolished (29, 30). Since we identified that UNbC5-1 and UNbC5-2 target C5 on two distinct sites, our nanobodies might be explored for synergistic effects and could be used to study the potential of dual treatment to overcome residual complement activity. Another limitation of Eculizumab and Ravulizumab is that these molecules are not effective in patients bearing a fully functional genetic variant of C5 (called C5 R885H), since it can no longer bind this C5 (31). This genetic variant was found in 1-3.5% of the healthy Japanese and Han Chinese population and a similar mutation (R885S) was identified in a Dutch patient, with no Asian ancestry (31, 32). In chapter 4 we show that nanobody UNbC5-1 has an overlapping epitope with Eculizumab and that it can bind C5 R885H and inhibits its cleavage. With the detailed information on the binding interface of UNbC5-1 and C5, this nanobody might be further developed as

a potent complement inhibitor, and this information could serve as a starting point to improve existing and develop novel C5 inhibitors.

If the nanobodies presented in this thesis would be further developed as complement inhibiting medicine, pharmacodynamics should be considered. The short half-life of nanobodies is acknowledged as a major disadvantage, especially when used for the long-term treatment of chronic diseases (33, 34). Fortunately, multiple methods, including PEGylation, Fc-tail fusion, fusion to serum albumin and multimerization, could be applied to increase their half-lives (35–37). On the other hand, the intrinsic short half-life of nanobodies might also be beneficial when therapeutic intervention is only required for a short period of time, for example in the case of acute sepsis and patients undergoing transplantations. Next to a short half-life, immunogenicity should be taken into consideration if nanobodies would be applied therapeutically. Despite the fact that llama-derived nanobodies have >80% homology with human VH domains, there still is a low risk of an anti-nanobody immune response (38, 39) . To overcome this, multiple studies have invested in the development of human heavy-chain only antibodies, using transgenic mice (40, 41) and rats (42). With the FDA approval of the first nanobody-based therapy Cablivi (or caplacizumab, targeting von Willebrand factor) in 2019, the long road ahead for nanobodies as complement-mediating medicine is at least paved (43, 44).

REFERENCES

1. Laursen, N. S., Pedersen, D. V, Gytz, H., Zarantonello, A., Magnus, J., Jensen, B., Hansen, A. G., Thiel, S., and Andersen, G. R. (2020) Functional and Structural Characterization of a Potent C1q Inhibitor Targeting the Classical Pathway of the Complement System. *Front Immunol*. **11**, 1–15
2. Chen, J. Y., Zhang, L., Luo, L., Yang, M., Chen, Y., and Lin, F. (2023) A nanobody-based complement inhibitor targeting complement component 2 reduces hemolysis in a complement humanized mouse model of autoimmune hemolytic anemia. *Clinical Immunology*. 10.1016/j.clim.2023.109678
3. Zarantonello, A., Presumey, J., Simoni, L., Yalcin, E., Fox, R., Hansen, A., Olesen, H. G., Thiel, S., Johnson, M. B., Stevens, B., Laursen, N. S., Carroll, M. C., and Andersen, G. R. (2020) An Ultrahigh-Affinity Complement C4b-Specific Nanobody Inhibits In Vivo Assembly of the Classical Pathway Proconvertase. *The Journal of Immunology*. **205**, 1678–1694
4. De la O Becerra, K. I., Oosterheert, W., van den Bos, R. M., Xenaki, K. T., Lorent, J. H., Ruyken, M., Schouten, A., Rooijakkers, S. H. M., van Bergen en Henegouwen, P. M. P., and Gros, P. (2022) Multifaceted Activities of Seven Nanobodies against Complement C4b. *The Journal of Immunology*. **208**, 2207–2219
5. Struijf, E. M., De la O Becerra, K. I., Ruyken, M., de Haas, C. J. C., van Oosterom, F., Siere, D. Y., van Keulen, J. E., Heesterbeek, D. A. C., Dolk, E., Heukers, R., Bardoel, B. W., Gros, P., and Rooijakkers, S. H. M. (2023) Inhibition of cleavage of human complement component C5 and the R885H C5 variant by two distinct high affinity anti-C5 nanobodies. *Journal of Biological Chemistry*. 10.1016/j.jbc.2023.104956
6. Jensen, R. K., Pihl, R., Gadeberg, T. A. F. F., Jensen, J. K., Andersen, K. R., Thiel, S., Laursen, N. S., and Andersen, G. R. (2018) A potent complement factor C3–specific nanobody inhibiting multiple functions in the alternative pathway of human and murine complement. *Journal of Biological Chemistry*. **293**, 6269–6281
7. Pedersen, H., Jensen, R. K., Hansen, A. G., Gadeberg, T. A. F., Thiel, S., Laursen, N. S., and Andersen, G. R. (2020) A C3 specific nanobody that blocks all three activation pathways in the human and murine complement system. *Journal of Biological Chemistry*. **295**, 8746–8758
8. Pedersen, H., Jensen, R. K., Jensen, J. M. B., Fox, R., Pedersen, D. V., Olesen, H. G., Hansen, A. G., Christiansen, D., Mazarakis, S. M. M., Lojek, N., Hansen, P., Gadeberg, T. A. F., Zarantonello, A., Laursen, N. S., Mollnes, T. E., Johnson, M. B., Stevens, B., Thiel, S., and Andersen, G. R. (2020) A Complement C3–Specific Nanobody for Modulation of the Alternative Cascade Identifies the C-Terminal Domain of C3b as Functional in C5 Convertase Activity. *The Journal of Immunology*. **205**, 2287–2300
9. Pedersen, D. V., Gadeberg, T. A. F., Thomas, C., Wang, Y., Joram, N., Jensen, R. K., Mazarakis, S. M. M., Revel, M., El Sissy, C., Petersen, S. V., Lindorff-Larsen, K., Thiel, S., Laursen, N. S., Fremeaux-Bacchi, V., and Andersen, G. R. (2019) Structural basis for properdin oligomerization and convertase stimulation in the human complement system. *Front Immunol*. **10**, 1–19
10. De Genst, E., Silence, K., Decanniere, K., Conrath, K., Loris, R., Rg Kinne, J., Muyldermans, S., and Wyns, L. (2006) Molecular basis for the preferential cleft recognition by dromedary heavy-chain antibodies. *PNAS*. **103**, 4586–4591
11. Lauwereys, M., Arbabi Ghahroudi, M., Desmyter, A., Kinne, J., Hölzer, W., De Genst, E., Wyns, L., and Muyldermans, S. (1998) Potent enzyme inhibitors derived from dromedary heavy-chain antibodies. *EMBO J*. **17**, 3512–3520
12. Lee, H. T., Park, U. B., Jeong, T. J., Gu, N., Lee, S. H., Kim, Y., and Heo, Y. S. (2021) High-resolution structure of the vWF A1 domain in complex with caplacizumab, the first nanobody-based medicine for treating acquired TTP. *Biochem Biophys Res Commun*. **567**, 49–55
13. De Groof, T. W. M., Bobkov, V., Heukers, R., and Smit, M. J. (2019) Nanobodies: New avenues for imaging, stabilizing and modulating GPCRs. *Mol Cell Endocrinol*. **484**, 15–24
14. Gros, P., Milder, F. J., and Janssen, B. J. C. (2008) Complement driven by conformational changes. *Nat Rev Immunol*. **8**, 48–58

15. Rother, R. P., Rollins, S. A., Mojcik, C. F., Brodsky, R. A., and Bell, L. (2007) Discovery and development of the complement inhibitor eculizumab for the treatment of paroxysmal nocturnal hemoglobinuria. *Nat Biotechnol*. **25**, 1256–1264
16. Brachet, G., Bourquard, T., Gallay, N., Reiter, E., Gouilleux-Gruart, V., Poupon, A., and Watier, H. (2016) Eculizumab epitope on complement C5: Progress towards a better understanding of the mechanism of action. *Mol Immunol*. **77**, 126–131
17. Muyldermans, S. (2013) Nanobodies: Natural Single-Domain Antibodies. *Annu Rev Biochem*. **82**, 775–797
18. Stach, L., Dinley, E. K. H., Tournier, N., Bingham, R. P., Gormley, D. A., Bramhall, J. L., Taylor, A., Clarkson, J. E., Welbeck, K. A., Harris, C. L., Feeney, M., Hughes, J. P., Sepp, A., Batuwangala, T. D., Kitchen, S. J., and Nichols, E. M. (2021) Novel selection approaches to identify antibodies targeting neoepitopes on the c5b6 intermediate complex to inhibit membrane attack complex formation. *Antibodies*. 10.3390/antib10040039
19. Doorduijn, D. J., Rooijakkers, S. H. M., and Heesterbeek, D. A. C. (2019) How the Membrane Attack Complex Damages the Bacterial Cell Envelope and Kills Gram-Negative Bacteria. *BioEssays*. **1900074**, 1–9
20. Xie, C. B., Jane-Wit, D., and Pober, J. S. (2020) Complement Membrane Attack Complex: New Roles, Mechanisms of Action, and Therapeutic Targets. *American Journal of Pathology*. **190**, 1138–1150
21. de Jorge, E. G., Yebenes, H., Serna, M., Tortajada, A., Llorca, O., and de Córdoba, S. R. (2018) How novel structures inform understanding of complement function. *Semin Immunopathol*. **40**, 3–14
22. Wang, J., Kang, G., Yuan, H., Cao, X., Huang, H., and de Marco, A. (2022) Research Progress and Applications of Multivalent, Multispecific and Modified Nanobodies for Disease Treatment. *Front Immunol*. **12**, 1–19
23. Jensen, R. K., Pihl, R., Gadeberg, T. A. F., Jensen, J. K., Andersen, K. R., Thiel, S., Laursen, N. S., and Andersen, G. R. (2023) Correction: A potent complement factor C3–specific nanobody inhibiting multiple functions in the alternative pathway of human and murine complement. *Journal of Biological Chemistry*. 10.1074/jbc.RA117.001179
24. Jumper, J., Evans, R., Pritzel, A., Green, T., Figurnov, M., Ronneberger, O., Tunyasuvunakool, K., Bates, R., Žídek, A., Potapenko, A., Bridgland, A., Meyer, C., Kohl, S. A. A., Ballard, A. J., Cowie, A., Romera-Paredes, B., Nikolov, S., Jain, R., Adler, J., Back, T., Petersen, S., Reiman, D., Clancy, E., Zielinski, M., Steinegger, M., Pacholska, M., Berghammer, T., Bodenstein, S., Silver, D., Vinyals, O., Senior, A. W., Kavukcuoglu, K., Kohli, P., and Hassabis, D. (2021) Highly accurate protein structure prediction with AlphaFold. *Nature*. **596**, 583–589
25. Zelek, W. M., Xie, L., Morgan, B. P., and Harris, C. L. (2019) Compendium of current complement therapeutics. *Mol Immunol*. **114**, 341–352
26. Harris, C. L. (2018) Expanding horizons in complement drug discovery: challenges and emerging strategies. *Semin Immunopathol*. **40**, 125–140
27. Bortolotti, M., Barcellini, W., and Fattizzo, B. (2023) Molecular pharmacology in complement-mediated hemolytic disorders. *Eur J Haematol*. 10.1111/ejh.14026
28. Hoy, S. M. (2021) Pegcetacoplan: First Approval. *Drugs*. **81**, 1423–1430
29. Harder, M. J., Höchsmann, B., Dopler, A., Anliker, M., Weinstock, C., Skerra, A., Simmet, T., Schrezenmeier, H., and Schmidt, C. Q. (2019) Different Levels of Incomplete Terminal Pathway Inhibition by Eculizumab and the Clinical Response of PNH Patients. *Front Immunol*. **10**, 1–7
30. Harder, M. J., Kuhn, N., Schrezenmeier, H., von Zabern, I., Weinstock, C., Simmet, T., Ricklin, D., Lambris, J. D., Skerra, A., Anliker, M., and Schmidt, C. Q. (2017) Incomplete inhibition by eculizumab: mechanistic evidence for residual C5 activity during strong complement activation. *Blood*. **129**, 970–980
31. Nishimura, J., Yamamoto, M., Hayashi, S., Ohyashiki, K., Ando, K., Brodsky, A. L., Noji, H., Kitamura, K., Eto, T., Takahashi, T., Masuko, M., Matsumoto, T., Wano, Y., Shichishima, T., Shibayama, H., Hase, M., Li, L., Johnson, K., Lazarowski, A., Tamburini, P., Inazawa, J., Kinoshita, T., and Kanakura, Y. (2014) Genetic Variants in C5 and Poor Response to Eculizumab. *New England Journal of Medicine*. **370**, 632–639

32. Langemeijer, S., Nishimura, J.-I., Weston-Davies, W., Nunn, M. A., Kanakura, Y., Mackie, I. J., and Muus, P. (2015) C5 Polymorphism in a Dutch Patient with Paroxysmal Nocturnal Hemoglobinuria (PNH) and No Asian Ancestry, Resistant to Eculizumab, but in Vitro Sensitive to Coversin. *Blood*. **126**, 1209–1209
33. Harmsen, M. M., and De Haard, H. J. (2007) Properties, production, and applications of camelid single-domain antibody fragments. *Appl Microbiol Biotechnol*. **77**, 13–22
34. Hoey, R. J., Eom, H., and Horn, J. R. (2019) Minireview Structure and development of single domain antibodies as modules for therapeutics and diagnostics. 10.1177/1535370219881129
35. Faassen, H. Van, Ryan, S., Henry, K. A., Raphael, S., Yang, Q., Rossotti, M. A., Brunette, E., Jiang, S., Haqqani, A. S., Sulea, T., Mackenzie, C. R., Tanha, J., and Hussack, G. (2020) Serum albumin-binding VHHs with variable pH sensitivities enable tailored half-life extension of biologics. *The FASEB Journal*. **00**, 1–17
36. Chanier, T., and Chames, P. (2019) Nanobody Engineering: Toward Next Generation Immunotherapies and Immunoimaging of Cancer. *Antibodies*. **8**, 13
37. Dennis, M. S., Zhang, M., Gloria Meng, Y., Kadkhodayan, M., Kirchhofer, D., Combs, D., and Damico, L. A. (2002) Albumin binding as a general strategy for improving the pharmacokinetics of proteins. *Journal of Biological Chemistry*. **277**, 35035–35043
38. Ackaert, C., Smiejkowska, N., Xavier, C., Sterckx, Y. G. J., Denies, S., Stijlemans, B., Elkrim, Y., Devoogdt, N., Caveliers, V., Lahoutte, T., Muyldermans, S., Breckpot, K., and Keyaerts, M. (2021) Immunogenicity Risk Profile of Nanobodies. *Front Immunol*. 10.3389/fimmu.2021.632687
39. Klarenbeek, A., El Mazouari, K., Desmyter, A., Blanchetot, C., Hultberg, A., de Jonge, N., Roovers, R. C., Cambillau, C., Spinelli, S., Del-Favero, J., Verrips, T., de Haard, H. J., and Achour, I. (2015) Camelid Ig V genes reveal significant human homology not seen in therapeutic target genes, providing for a powerful therapeutic antibody platform. *MAbs*. **7**, 693–706
40. Drabek, D., Janssens, R., Boer, E. de, Rademaker, R., Kloess, J., Skehel, J., and Grosveld, F. (2016) Expression cloning and production of human heavy-chain-only antibodies from murine transgenic plasma cells. *Front Immunol*. 10.3389/fimmu.2016.00619
41. Drabek, D., Janssens, R., van Haperen, R., and Grosveld, F. (2022) A Transgenic Heavy Chain IgG Mouse Platform as a Source of High Affinity Fully Human Single-Domain Antibodies for Therapeutic Applications. in *Single-Domain Antibodies. Methods in Molecular Biology*
42. Clarke, S. C., Ma, B., Trinklein, N. D., Schellenberger, U., Osborn, M. J., Ouisse, L. H., Boudreau, A., Davison, L. M., Harris, K. E., Ugamraj, H. S., Balasubramani, A., Dang, K. H., Jorgensen, B., Ogana, H. A. N., Pham, D. T., Pratap, P. P., Sankaran, P., Anegon, I., van Schooten, W. C., Brüggemann, M., Buelow, R., and Aldred, S. F. (2019) Multispecific antibody development platform based on human heavy chain antibodies. *Front Immunol*. 10.3389/fimmu.2018.03037
43. Duggan, S. (2018) Caplacizumab: First Global Approval. *Drugs*. **78**, 1639–1642
44. Morrison, C. (2019) Nanobody approval gives domain antibodies a boost. *Nat Rev Drug Discov*. **18**, 485–487

6

Nederlandse samenvatting (Dutch summary)

Short English summary

Dankwoord (Acknowledgements)

About the author

List of publications

PhD Training certificate – Graduate School of Life Sciences

Nederlandse samenvatting (Dutch summary)

Introductie

Het complement systeem

Het complement systeem is een belangrijk onderdeel van het menselijk immuunsysteem die ons beschermt tegen binnendringers. Het bestaat uit een collectie van ongeveer 30 eiwitten die circuleren in het bloed en andere lichaamsvloeistoffen. Middels een complexe kettingreactie waarin eiwitten worden geknipt kan het complement systeem onder andere ziekteverwekkers, dode cellen en tumorcellen opruimen. Het complement systeem doet dit via drie belangrijke mechanismen: 1) het zichtbaar maken van de binnendringer voor andere delen van het immuunsysteem (opsonisatie); 2) immuun cellen aantrekken naar de plek van activatie (chemoattractie); 3) het vormen van een eiwit porie ("membrane attack complex"(MAC)) die binnendringers direct doodt door gaten te maken in hun celwand. In de afwezigheid van bijvoorbeeld een ziekteverwekker circuleren de complement eiwitten in hun niet-geactiveerde vorm (oftewel voorloper eiwitten) door het lichaam. Echter, als een binnendringer gedetecteerd wordt (bijvoorbeeld door antilichamen), activeren de eiwitten elkaar één voor één door middel van enzymatische knipstappen en/of veranderingen van de vorm (conformationele veranderingen). In **Figuur 1** is een gedetailleerd schematisch overzicht weergegeven van alle stappen van complement activatie.

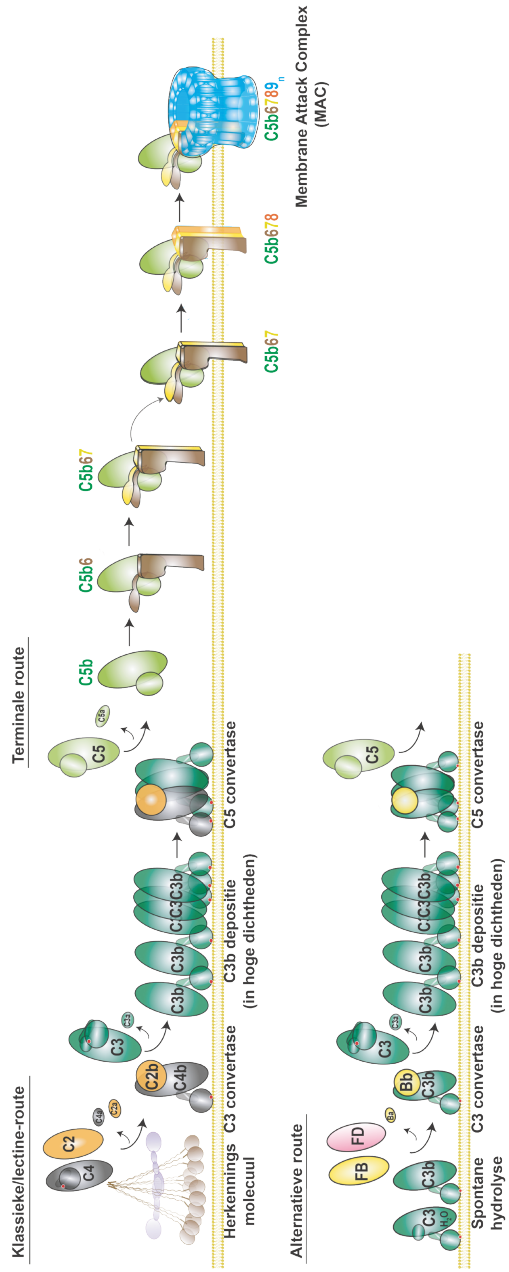

Figuur 1: Schematische weergave van complement activatie aan het oppervlak van een binnendringer. Complement activatie gaat via 3 routes en werkt op een stapsgewijze manier waarin de complement eiwitten verschillende knipstappen en conformationele veranderingen ondergaan.

C3 en C5 zijn centrale complement eiwitten

Tijdens de activatie van het complement systeem worden er enzymatische eiwitcomplexen gevormd die we C3 en C5 convertases noemen (**Figuur 1**). De C3 convertases knippen C3 in C3a en C3b, en de C5 convertases knippen C5 in C5a en C5b. Deze twee knipstappen zijn cruciaal voor het uitvoeren van de drie belangrijkste effector functies van het complement systeem (**Figuur 2**). Ten eerste, C3a en C5a zijn twee kleine moleculen die na de knip worden losgelaten en werken als potente chemo-attractieve moleculen die sterk bijdragen aan de ontstekingsreactie. Ten tweede, C3b is een groot molecuul dat een conformatie verandering ondergaat en vervolgens bindt aan het celoppervlak. Vanuit daar kan het binden aan verschillende cellen van het immuunsysteem door in interactie te vormen met complement receptoren. Deze cellen kunnen de met C3b-geopsoniseerde cel vervolgens opeten (fagocyteren). Bovendien amplificeert C3b de activatie van het complement systeem door het vormen van nieuwe convertases. Ten derde, initieert C5b de formatie van MAC poriën. Wanneer C5 geknipt wordt, ondergaat C5b grote conformationele veranderingen. Hierdoor kan C6 binden aan C5b, en wordt het C5b6 complex gevormd. Vervolgens binden complement eiwitten C7, C8 en meerdere kopieën van C9 aan het C5b6 complex. Dit leidt tot de vorming van de MAC porie in de celwand van de binnendringer en zorgt voor directe celdood.

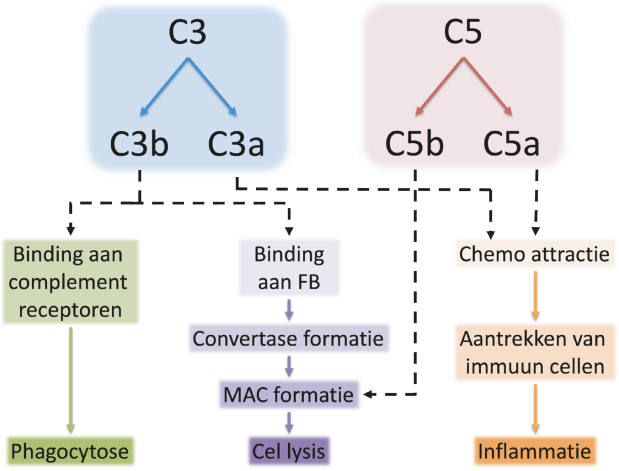

Figuur 2: Schematische weergave van de verschillende effector functies van het complement systeem die plaatsvinden na het knippen van C3 en C5.

Complement onder- en over activatie is geassocieerd met ziektes

Omdat het complement systeem bij veel processen betrokken is, is het belangrijk dat het systeem goed gereguleerd wordt. In het geval van te weinig activatie krijgen ziekteverwekkers vrij baan wat leidt tot infecties. In het geval van te veel complement

activatie kan het systeem de gezonde lichaamseigen cellen aanvallen, en spreken we van een auto-immuun ziekte. Voorbeelden hiervan zijn de ziektes paroxysmale nachtelijke hemoglobinurie (PNH), atypisch hemolytisch-uremisch syndroom (aHUS), en leeftijdsgerelateerde maculadegeneratie (LMD).

Kleine antilichamen afkomstig uit lama's

Antilichamen zijn belangrijke eiwitten van het immuunsysteem die heel gericht aan een lichaamsvreemd deeltje kunnen binden. Deze moleculen zijn Y-vormig en herkennen hun unieke lichaamsvreemde deeltje met de combinatie van twee domeinen (VH + VL) (**Figuur** 3, weergegeven in groen). Bijna alle gewervelde organismen maken deze antilichamen om zich te beschermen tegen binnendringers. In 1993 werd een speciaal type antilichamen ontdekt in het bloed van lama's en andere kameelachtigen. Deze antilichamen lijken heel erg op "gewone" (conventionele) antilichamen, maar ze missen een aantal domeinen (**Figuur 3**). Als gevolg hiervan zijn ze kleiner dan conventionele antilichamen en herkennen ze hun antigen met slechts één enkel domein. Dit domein, ook wel het VHH-domein genoemd, kan als los molecuul verkregen worden en staat ook wel bekend als Nanobody® of "single-domain antibody" (sdAb). Nanobodies zijn ongeveer 10x keer kleiner dan conventionele antilichamen en door hun unieke vorm kunnen ze beter onderscheid maken tussen de verschillende conformaties van eiwitten. Zoals hierboven al beschreven wordt complement activatie gedreven door een kettingreactie van knipstappen en conformationele veranderingen van onder andere complement eiwitten C3 en C5. Daarom zijn nanobodies uitermate geschikt om onderscheid te maken tussen bijvoorbeeld voorloper eiwitten C3, C5 en C6 en de geactiveerde eiwitten C3b en C5b6.

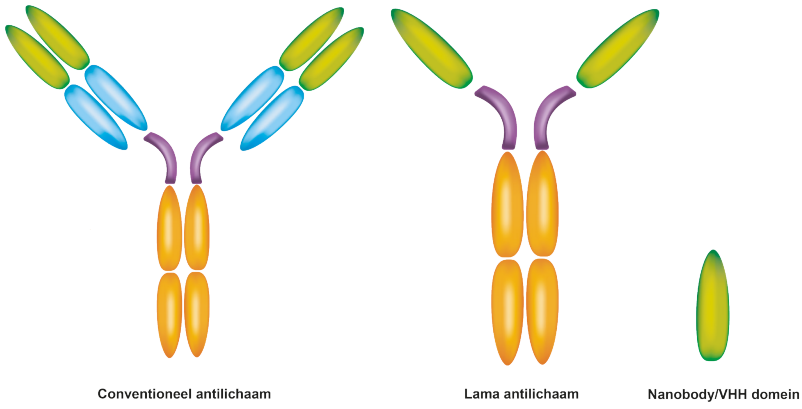

Figuur 3: Schematische weergave van de verschillende domeinen aanwezig in een conventioneel antilichaam, een lama antilichaam en een nanobody (of VHH domein).

Doelstellingen van dit proefschrift

De rol van het complement systeem in gezondheid en ziekte wordt al jarenlang onderzocht. Desondanks zijn er nog steeds grote fundamentele en klinische vragen die onbeantwoord zijn. Het ontwikkelen van nieuwe hulpmiddelen en medicijnen die complement activatie kunnen remmen en/of detecteren zijn daarom nog steeds nodig. In dit onderzoek is het ons doel om nanobodies te ontwikkelen tegen verschillende complement eiwitten. We focussen op centraal complement eiwit C5 en de activatie producten C3b en C5b6.

Bevindingen

In dit proefschrift hebben we de identificatie en karakterisatie beschreven van vier verschillende nanobodies gericht tegen eiwitten uit het complement systeem. Om deze nanobodies te verkrijgen hebben we twee lama's geïmmuniseerd met gezuiverde complement eiwitten, eiwitcomplexen en bacteriën geopsoinseerd met complement eiwitten. Na de immunisaties hebben we bloed afgenomen bij de lama's. Hieruit konden we antilichaam producerende cellen isoleren en vervolgens de genen die coderen voor de nanobody domeinen isoleren en kloneren in bacteriën die geschikt zijn om "faagdisplay" mee te doen. Faagdisplay is een techniek om uit miljoenen verschillende nanobodies alleen de nanobodies te selecteren die aan de eiwitten van onze interesse binden. Na het selecteren van de bindende nanobodies hebben we gescreend voor nanobodies met verschillende eigenschappen, zoals specificiteit, affiniteit en remming. Vervolgens hebben we een viertal nanobodies geselecteerd om uitgebreid te karakteriseren.

In **hoodstuk 1** geven we een uitgebreide introductie over het complement systeem en nanobodies. We focussen ons voornamelijk op complement eiwitten C3 en C5 en beschrijven hoe deze eiwitten geactiveerd worden door C3 en C5 convertases. We beschrijven hoe deze eiwitten conformationeel veranderen en hoe hun activatieproducten vervolgens een rol spelen in verdere activatie van het complement systeem. Bovendien beschrijven we wat nanobodies zijn, hoe deze verschillen van conventionele antilichamen en leggen we uit waarom er in dit proefschrift gekozen is om nanobodies te ontwikkelen.

In **hoofdstuk 2** beschrijven we de identificatie van nanobody UNbC3b-1, die aan complement activatie product C3b bindt. Met technieken als "flow cytometrie" en "size exclusion chromatography" laten we zien dat dit nanobody specifiek aan C3b bindt en niet aan voorloper eiwit C3. Bovendien heeft UNbC3b-1 een hoge affiniteit voor

C3b. Door middel van functionele experimenten laten we zien dat UNbC3b-1 activatie van een deel van het complement systeem remt. Het nanobody remt namelijk wel de alternatieve route, maar niet de klassieke route (zie **Figuur 1** voor een overzicht van de verschillende activatie routes). We hebben laten zien dat UNbC3b-1 voorkomt dat C3 en C5 convertases hun substraten C3 en C5 kunnen knippen. Ondanks dat we het exacte mechanisme hiervan niet hebben kunnen ontrafelen, laten we wel zien dat UNbC3b-1 niet de vorming van deze convertases blokkeert.

In **hoofdstuk 3** beschrijven we de identificatie en karakterisatie van twee anti-C5 nanobodies (UNbC5-1 en UNbC5-2) die op twee verschillende plaatsen aan C5 binden. Beide nanobodies blokkeren de knip van C5 op een efficiënte manier. In deze studie hebben we de exacte bindingsplaats van UNbC5-1 en UNbC5-2 bepaald door middel van de techniek “cryo-elektronenmicroscopie”. Hieruit bleek dat UNbC5-2 op dezelfde plek aan C5 bindt als een eerder beschreven molecuul, genaamd RaCI3. Nanobody UNbC5b-1 bindt aan C5 op dezelfde plek als eculizumab. Dit is een conventioneel antilichaam tegen C5 die in de kliniek wordt gebruikt om complement-gemedieerde ziektes te behandelen. Ondanks de successen van eculizumab, zijn er een aantal patiënten waarbij het medicijn niet goed werkt. Dit komt omdat deze patiënten een genetische variant van het complement eiwit C5 hebben, genaamd C5 R885H, en eculizumab hier niet aan kan binden. In onze studie laten we zien dat het nanobody UNbC5-1 wel aan C5 R885H kan binden en dat het, in tegenstelling tot eculizumab, de knip van C5 R885H wel kan remmen.

In **hoofdstuk 4** beschrijven we de identificatie van een specifiek anti-C5b6 nanobody, genaamd UNbC5b6-1. Met verschillende technieken, zoals “ELISA” en “surface-plasmon resonance”, laten we zien dat dit nanobody met hoge affiniteit aan C5b6 bindt. Met behulp van de technieken “ELISA” en “size exclusion chromtography” laten we zien dat dit nanobody niet kan binden aan de voorloper eiwitten C5 en C6, en daarmee dus specifiek is voor C5b6. Bovendien laten we zien dat dit nanobody geen effect heeft op complement activatie.

In **hoofdstuk 5** vatten we onze bevindingen samen en plaatsen we deze in het grotere geheel van het nanobody- en complement veld. Allereerst geven we een overzicht van alle anti-complement nanobodies die momenteel zijn beschreven in de literatuur en laten we zien welke nanobodies wij met deze onderzoeken toevoegen (**Figuur 4**). We vergelijken de nanobodies in deze thesis met een aantal anti-complement nanobodies die veel overeenkomsten hebben. Bovendien beschrijven we waar de uitdagingen tijdens ons onderzoek lagen en welke nanobodies waardevol zijn om te gaan ontwikkelen in de

toekomst. Als laatste beschrijven we hoe de nanobodies uit deze thesis zouden kunnen bijdragen in het veld van complement onderzoek en therapie.

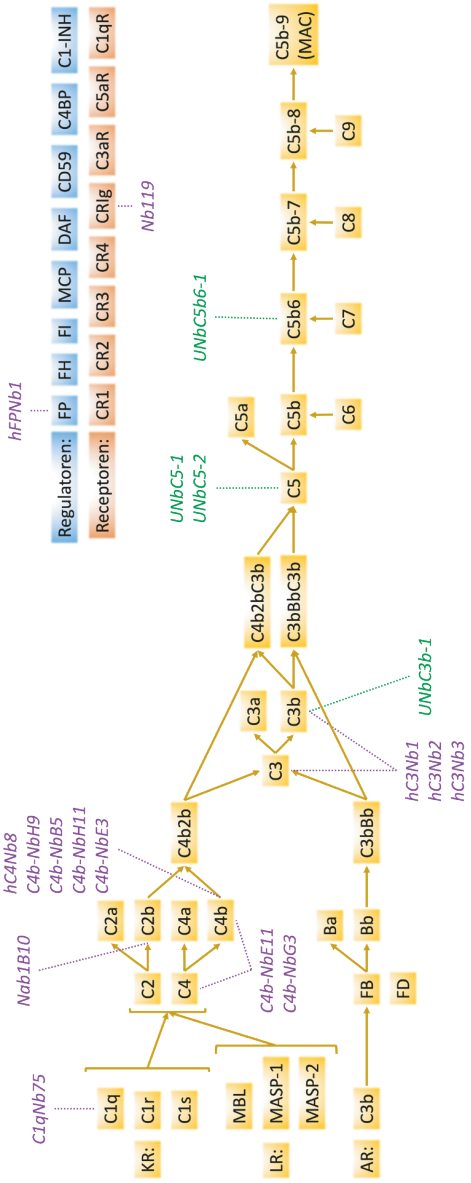

Figuur 4: Schematisch overzicht van alle anti-complement nanobodies die momenteel zijn beschreven in de literatuur. In groen aangegeven zijn de nanobodies beschreven in dit proefschrift en in paars aangegeven zijn de nanobodies die in de literatuur zijn beschreven door anderen. KR staat voor klassieke route, LR voor lectine-route, AR voor alternatieve route.

Ter conclusie

In dit proefschrift beschrijven we de ontwikkeling, identificatie en karakterisatie van vier nieuwe anti-complement nanobodies. Hiermee laten we zien dat het ontwikkelen van nanobodies tegen complement eiwitten een goede aanpak is om dit soort nieuwe moleculen en hulpmiddelen te ontwikkelen. De nanobodies beschreven in deze thesis kunnen nu en in de toekomst gebruikt worden om belangrijke fundamentele en klinische vraagstukken met betrekking tot het complement systeem verder te ontrafelen. Bovendien zouden sommige van deze nanobodies gebruikt kunnen worden om nieuwe medicijnen te ontwikkelen die overactiviteit van het complement systeem kunnen remmen.

Short English summary

The complement system is an important part of the human immune system that fights invading pathogens and removes apoptotic host cells, tumor cells and immune complexes. It consists of roughly 30 proteins that circulate in the blood and other body fluids and its activity is driven by proteolytic cascades and conformational changes. The role of the complement system in health and disease is extensively being studied. Although huge progress is made in the last decades, there are still major fundamental and clinical questions that yet remained unanswered. Novel tools and therapeutics that can inhibit, and/or discriminate complement precursor proteins from activation proteins are therefore still needed. We aimed to develop llama-derived nanobodies directed towards different complement components. In this thesis, we focused on central complement component C5 and activation products C3b and C5b6. To obtain complement targeting nanobodies, we immunized two llamas, created nanobody phage display libraries, and performed multiple rounds of phage display panning. For all complement proteins used during immunizations, we successfully identified multiple nanobodies. In the end, we prioritized four nanobodies for further characterization because of their potent binding and inhibitory activity or their unique capacity to discriminate activated complement products from their precursors. Briefly, UNbC3b-1 targeting C3b (chapter 2) specifically binds complement activation product C3b and not precursor C3 and efficiently inhibits alternative pathway convertase functioning. UNbC5-1 and UNbC5-2 (chapter 3) are two potent C5 inhibiting nanobodies that bind C5 on distinct sites. Using cryo-EM we identified the exact binding sites of UNbC5-1 and UNbC5-2 and showed that they overlap with the binding sites of known complement inhibitors eculizumab and RaCI3, respectively. Furthermore, we show that UNbC5-1 can also bind and inhibit a genetic variant of C5, called C5 R885H, which cannot be bound and inhibited by eculizumab. UNbC5b6-1 (chapter 4) is a nanobody that specifically binds to the complement activation complex C5b6, but not to precursor proteins C5 and C6. This nanobody does not interfere with complement activity. All in all, the here identified nanobodies can serve as tools to gain a better understanding of the molecular mechanisms of complement activation and hold promise for further development as diagnostic tools and therapeutics.

Dankwoord (acknowledgements)

Nou, het is zo ver. Ik mag mijn dankwoord gaan opschrijven. Iets waar ik al vanaf het begin van mijn PhD naar uit kijk. Want zeg nou zelf, dit is toch verreweg het leukste hoofdstuk om te lezen ;-D. Maar nu het dan eindelijk zo ver is, en mijn proefschrift dus echt af is, schuif ik het toch steeds een beetje voor me uit. Blijkt het na ruim 4,5 jaar toch lastiger dan ik dacht om letterlijk en figuurlijk het laatste hoofdstuk van mijn PhD af te sluiten. Maar ik ga het toch doen, **het is eindelijk tijd om alle mensen te bedanken die zo'n ongelooflijke bijdrage hebben gehad aan dit boekje, maar vooral ook aan mijn leven binnen en buiten mijn PhD.**

Allereerst, **Suzan**, bedankt voor zoveel dingen! Onwijs bedankt voor al het vertrouwen dat je me al zo snel hebt gegeven. Ik vond het heel gaaf en leerzaam om samen met jou een beurs aan te schrijven. Ik bewonder jouw analytisch denkvermogen, je ijzersterke geheugen en je drive om alles echt tot op de bodem, en zelfs een beetje eronder, uit te willen zoeken. Ik waardeer je interesse en onze eerlijke en open gesprekken, ook over de moeilijkere dingen. Je hebt me geleerd om wat meer vertrouwen te hebben in mijn kunnen als wetenschapper en om vaker de controle los te laten. Ik vond het heel leuk dat je nog speciaal naar Uitgeest kwam voor een privé housewarming en voel me vereerd dat ik als eerste OIO ooit voor je heb mogen koken.

Aaah **Dani**, wat was jij niet voor mij, van stagebegeleider tot copromotor, en alles wat ertussenin zat. Ik kan bij jou echt met alles terecht en vaak had jij al net iets eerder dan ik door wat ik nodig had. Ik vind jou een ongelooflijk goede wetenschapper, een grandioze begeleider, en vooral een superfijn persoon. Ik kijk met een grote glimlach terug op alle feestjes, alle goede grapjes, de leuke foto's en de ontelbare gezellige koffiemomentjes. Bedankt voor al jouw bijdragen! Zeker het laatste jaar had niet gelukt zonder jouw hulp.

Bart, bedankt voor al jouw goede vragen. Zowel wetenschappelijk ben je erg goed in het stellen van de essentiële vragen, maar ook over de manier waarop we onderzoek doen. Je wist met jouw vragen vaak de gevoelige snaar te raken, waardoor ik ging nadenken over waarom we iets nou eigenlijk deden, en of ik dat zelf ook écht interessant vond om te onderzoeken. Ik denk dat je meer dan dat je je beseft hebt bijgedragen aan mijn ontwikkeling en aan dit boekje.

Jos, bedankt voor al je gevraagde en soms ook ongevraagde adviezen. Ze waren allemaal even waardevol. Zowel wetenschappelijk als carrière-technisch. Jouw deur staat altijd open en dat heb ik enorm gewaardeerd. Ik zie bij jou een enorme passie

voor wetenschap, maar misschien nog wel een grotere passie in het bijstaan van al die jonge, soms ietwat naïeve, PhD studenten. Je hebt in ieder geval mij heel erg geholpen met al je vragen, antwoorden en adviezen.

Ik wil ook graag **prof. dr. Nicole van de Kar, prof. dr. Raymond Schiffelers**, **dr. Balthasar Heesters**, **prof. dr. Femke van Wijk** en **prof. dr. Piet Gros** bedanken voor het kritisch doorlezen en beoordelen van mijn proefschrift. Bovendien wil ik **Femke** extra bedanken voor het plaatsnemen in mijn begeleidingscommissie. Gelukkig hebben we elkaar niet vaak hoeven spreken in deze rol, maar ik vond het fijn dat dit kon wanneer het nodig zou zijn. Daarnaast wil ik **Piet** extra bedanken voor de waardevolle samenwerking met jou en jouw team. Ik vond het fascinerend om te zien hoe jij nadenkt over de wetenschap en hoe je met net verkregen informatie à la minute een nieuw model kunt maken van de C5 convertase. I want to thank the many members of your team with whom I have been collaborating throughout my PhD, **Ramon van de Bos**, **Itziar Serna Martin, Karla de la O' Becerra** and **Jamie Depelteau**. You all taught me a lot about structural biology and I enjoyed it a lot to join our forces and collaborate in many projects.

Graag wil ik ook iedereen bij QVQ bedanken. **Edward** en **Raimond**, bedankt voor het vertrouwen in dit project en alle support die jullie me de gehele tijd hebben gegeven. Bedankt voor alle leuke overleggen en jullie waardevolle input, later ook met **Gillian** en **Robbin**. Ik vond het onwijs leerzaam en leuk om bij en met jullie in het lab te mogen werken. **Daphne** en **Marjolein**, bedankt dat ik jullie ontelbaar veel vragen mocht stellen, ook al was het soms 3 keer dezelfde! Ik heb de teamspirit bij QVQ altijd heel erg gewaardeerd, en dat komt echt door **Lianne, Floor, Mark, Stephie, Joyce, Sander**, en alle andere QVQ'ers! Bedankt voor deze toptijd!

En na iedereen bij QVQ bedankt te hebben, moet ik natuurlijk de twee hoofdrolspelers uit mijn boekje in het zonnetje zetten: **Lotte** en **Ines**. Zonder jullie geen boekje, zonder jullie geen gelach tijdens presentaties en dankzij jullie hebben heel veel mensen onthouden wat ik (ongeveer) voor werk doe. Dus dank daarvoor! Jullie worden gewaardeerd en ik gun jullie nog een heel lang, gelukkig, gezond, en grazend lama pensioen!

Y luego, las paranimfas más maravillosas, entusiastas y siempre felices que puedo imaginar, **Julia** y **Leire**. Was this correct Spanish? If not, blame google translate. Thank you for teaching me mucho palabras de hoy, and very important phrases that are just applicable to almost every situation (que racista & que pija, hihihi). Dear **Leirooo**, just thank you for being you! Your happiness always made me smile, your sincere interest in every detail of my personal life was wonderful. I enjoyed the many parties & dance

moves, but especially our short career as fake guitar players with cono de trafico as our hats. I was so happy to hear that you came back to the MMB for a second time, and I am so happy that you were there for me throughout my PhD! Sweet sweet **Julia**! The moment you joined the MMB, I knew this girl I want to become friends with! You are an amazing person, a great listener, super funny, and of course a super scientist, although sometimes your stories are a bit faag to me (hahaha). Thank you for being the best roommate, your hugs in the hallway, and always the question how I was doing. You are the best! Oh and once again, thank you for taking care of my phone when I didn't forget it at your party!

Dan de personen zonder wie dit boekje er echt niet had kunnen zijn: **Carla, Kok, Lisette, Maartje,** en **Piet**. Dankzij jullie is het écht een feestje om te werken bij de MMB. Het is zo onwijs fijn om te weten dat je altijd bij jullie terecht kunt met vragen en jullie verzetten zo ongelooflijk veel werk voor (en gelukkig ook met) ons! En dan is het ook nog eens supergezellig met jullie! **Carla**, bedankt voor de lessen in cloneren, je oprechte interesse en ik heb echt met je genoten (tijdens de karaoke) in Girona! **Kok**, quick-question-Kok, die bijnaam doet je eer aan! Ik heb je gemist toen je met je welverdiende pensioen bent gegaan, maar ik vind het stiekem wel heel leuk dat je weer een klein beetje terug gaat komen naar de MMB! **Lisette**, ik kan altijd erg lachen om je droge humor! Jij laat je niet zomaar gek maken, daar houd ik van! En ondertussen knalde je er ook nog eens megagrote proeven met mijn nanobodies uit! **Maartje**, bedankt voor alle gezellige gesprekken op het lab, waar kon ik met jou niet over praten. Ik was (en ben) altijd blij als ik jou even tegenkom op de gang of bij de koffie of in het lab. En, uiteraard bedankt voor de ongelooflijke hoeveelheid experimenten die je voor me gedaan hebt! Mega-Maartje!! **Piet,** bedankt voor jouw positiviteit, je grapjes om even het ijs te breken en vooral je oprechte vragen als het even iets minder goed ging. Ik moet vaak aan je tips denken tijdens het hardlopen en dat motiveert me altijd!

Ook heel veel dank aan de drie fantastische meiden **Joanne**, **Fleur** en **Danique** die hun stages bij mij kwamen doen. Ik heb ervan genoten om jullie te begeleiden, ik heb veel van jullie geleerd (ik hoop jullie toch ook wat van mij ;-D). Bedankt voor al jullie bijdragen aan dit boekje, het waren er een hoop!

En dan al mijn leuke, lieve, slimme grappige (oud) collega's bij de MMB. Ik heb genoten van alle lunches, koffiepauzes, feestjes, keten-op-het-lab momentjes en kerstschoonmaken samen. **Sjors** en **Priscilla**, dat wij alle drie op dezelfde dag startte gaf meteen een speciale band. Ik ben blij hoe we al deze tijd met elkaar konden sparren, advies vragen, hard lachen of soms ook gewoon even lekker klagen. **Lisanne** en **Remy**, ik vond het een feestje om bij jullie op kantoor te zitten, vooral als jullie er tegelijkertijd

waren! Thanks voor alle gezellige momenten en fijne gesprekken over eigenlijk alles. **Dennis** en **Seline**, jullie mis ik echt wel heel erg op het lab. Als ik aan de MMB denk, denk ik toch wel echt aan jullie, maar gelukkig spreken we elkaar toch nog af en toe buiten de MMB! Dank jullie wel voor jullie waardevolle adviezen over mijn vervolg carrière! **Astrid**, bedankt voor al je vrolijkheid en gezelligheid en natuurlijk dank dat ik jouw paranimf mocht zijn, wat een eer! Je bent een fantastische wetenschapper, echt een voorbeeld! **Kulsum** and **Marije** (of eigenlijk Marieje) super nice that you both came back to the MMB. We worked together a lot shorter than I hoped for, but I am certain that we will see each other many times! You are both awesome and will rock this PhD! **Yvonne,** dankjewel voor al je harde werk, vaak achter de schermen. Je stond altijd voor me klaar en ik vond het fijn samenwerken. Ik wens je ook al het geluk in je nieuwe uitdaging met je B&B (klinkt toch nog een beetje hetzelfde als MMB gelukkig ;-D). Also, a big thanks to **Andras, Pieter-Jan, Erik, Magda, Leonardo, Frerich, Coco, Elena, Rita, Anneroos, Adinda, Tristan, Barath** and **Ruben** for your valuable questions, insights, and 'gezelligheid' in and outside the lab(meetings). And of course, a big thanks to all (former) colleagues **Janneke, Manon, Marieke, Ninée, Coco, Matteo, Roos, Shu, Axel, Stephanie, Gosia, Paul, Hendrik, Patrique, Lidewij, Julian, Angelino** and **Jelle** for the many memorable coffee breaks, ICEA activities, Buitendagen, MMB-café's, and many other events that made my PhD a wonderful time.

Dan wil ik ook **Martijn** van HSK heel erg bedanken. Je hebt een belangrijke rol gespeeld in het laatste jaar van mijn PhD en me geholpen om me weer goed te voelen, mezelf beter te leren kennen en om persoonlijke uitdagingen aan te gaan. Ik heb een heleboel goede tips van je gehad, en kan iedereen een beetje Martijn in zijn/haar leven aanraden! Bedankt!

Naast alle collega's hebben mijn lieve vrienden een onmisbare rol gespeeld tijdens mijn PhD. Van jullie kreeg ik de onvoorwaardelijke steun en de nodige afleiding. Iedereen van **de Badeendjes,** de **CHAOS meiden**, en **alle vrienden die ik via Koen** ken (dat zijn er nog een hoop, dus ik doe het even zo) DANK voor alle leuke weekendjes weg, kermis-feestjes, verjaardagen, kerstdiners, dagjes weg, Rock & Roll weekenden, familiefeestjes, en wat nog meer! Met jullie kan ik altijd lachen, is het altijd gezellig en is die nodige ontspanning altijd zo gevonden! **Richard** and **Cathy**, thanks for showing us all these wonderful places in Utrecht. We had great nights together full of fun, joy, whiskey, karaoke, cocktails, good food and relaxation, and I look forward to the new chapters laying ahead of us in our super-grown-up houses. Dankjewel **Emmy** voor het introduceren van het PhD-leven. Ik vond het heel fijn dat ik met al mijn vragen in het begin alleen maar de gang van de Warande hoefde over te steken, en ze aan jou kon vragen. Ook bedankt voor alles wat we samen hebben gedeeld. Bedankt dat we er

voor elkaar waren in de af en toe moeilijke tijden! Lieve **Naomi**, dank voor je eerlijke nuchterheid, je humor, je interesse en gewoon voor jou. Je bent een super dierbare vriendin en ik kan bij jou altijd alles kwijt. Ik hoop dat we nog heel vaak jarig zijn (een keer of 4 per jaar zou leuk zijn), zodat we lekker vaak op verjaardag lunch kunnen gaan. Lieve **Lara**, thanks voor alles wat we samen kunnen delen. Dat we vaak een beetje anders naar het leven kijken waardeer ik echt enorm en vooral omdat we daar zo goed over kunnen praten met elkaar. Ik leer een hoop van je, en hoop dat nog heeeeeel lang te blijven doen! Je bent een lief en mooi mens en je mag trots zijn op je prachtige gezin! Kat, kat, kat, lekker nat! Wat kan ik met jullie lachen lieve **Katinka** en **Kelly**! Jullie zijn echt de ideale uitlaatklep. Gelukkig is er altijd wel één van ons lekker op een piek! En als we een beetje mazzel hebben, zijn we het alle drie tegelijk. Ik vind het van onschatbare waarde hoe goed we met elkaar kunnen praten, lachen, huilen, huilen van het lachen, en dit zo allemaal een keer of 4 per avond! Jullie zijn top, goud, awesome, en nog zo veel meer!

En naast al die lieve vrienden heb ik natuurlijk ook nog mijn super dierbare familie! Ik wil iedereen van de familie **Struijf**, **Verduin**, **Spaansen** en **Vessies** bedanken voor jullie eindeloze interesse! Met in het bijzonder alle **oma's**, ik vind het een cadeautje om dit nog met jullie te kunnen delen. Helaas heeft **opa** dit boekje niet meer gezien, maar het was enorm leuk om te zien hoe trots hij erop was dat ik een onderzoek deed met mijn eigen beurs.

Lieve **Sjaak** en **Arnoldine**, bedankt voor al jullie betrokkenheid, de vele belletjes en appjes om te horen hoe het gaat en natuurlijk de logeerpartijtjes. Ik heb heel lekker bij jullie zitten schrijven en ik weet dat de deur altijd open staat!

Lieve **Jack** en **Jet**, bedankt dat ik me bij jullie thuis voel. Dat ik onderdeel ben van de familie en dat jullie altijd betrokken zijn en me steunen. Ik ben ongelooflijk blij dat we nu weer lekker bij elkaar in de buurt wonen en we in ieder geval één keer in de week samen eten. Ik vind onze band heel bijzonder en ik hoop dat we samen nog heel veel mooie nieuwe herinneringen gaan maken! Lieve **Gré**, bedankt voor al je interesse! Al je appjes om me succes te wensen met een presentatie of een groot experiment. Je onthield het soms nog beter dan ikzelf dat er iets belangrijks op de planning stond die dag. Bedankt voor alle kopjes thee om de dag lekker mee door te nemen. Bedankt voor het grootbrengen van de allerleukste en liefste jongen die ik ken (en jij natuurlijk ook bedankt hiervoor he Jack!). Je wordt ongelooflijk gemist, en ook zeker weer nu.

Lieve **Renée, Patrick, Hugo** en **Adam**, of hoe ik jullie eigenlijk liever noem: Lieve **Runnie**, **Patty-boy**, **Bügel** en **Adam** (shit… ik heb nog geen goede bijnaam voor Adam, en shit, ik mag natuurlijk geen shit zeggen, want anders gaan die jongens ons nazeggen, oeps, hahaha). **Runnie**, met jou heb ik aan een half woord genoeg, en soms is zelfs die niet nodig, om helemaal de slappe lach te krijgen. Ik vind het altijd heerlijk dat niemand ons begrijpt, behalve wijzelf. Die momenten van lachen zijn wel echt een goed voorbeeld van ultiem geluk. Het is ook niet zo gek dat ik regelmatig vanuit het UMC met je belde, gewoon om weer even blijer te worden! **Patty-boy**, hahaha ik deed het gewoon nog een keer, dankjewel voor je aandacht, je knuffels, je oprechte interesse, en dat ik me altijd meer dan welkom voel bij jullie. Lieve **Hugo** en **Adam**, wat ben ik trots op jullie en blij dat ik jullie van zo dicht bij groot mag zien worden. Jullie hebben mij zo veel geluksmomentjes bezorgd in de afgelopen jaren. Als ik even moe was van werk, of even niet wist hoe ik dingen aan moest pakken, dan appte ik Renée en dan kreeg ik de leukste foto's van jullie doorgestuurd om me weer helemaal erbovenop te krijgen. Nu kunnen we zelfs samen videobellen, en het is ongelooflijk hoe veel plezier ik daar uit haal. Ik hoop dat jullie je leven lang zo kunnen blijven lachen als jullie nu al kunnen, dan komt alles goed!

Lieve **Martijn** en **Denise**, oftewel **de sniefs**! Dank jullie wel dat jullie er altijd voor mij zijn. Al onze padel avondjes hebben me geholpen om te ontspannen, en als dat niet echt lukte, om even wat frustratie eruit te gooien. Bedankt voor jullie geduld en support daarin! Ik vond het heerlijk om vlak bij elkaar te wonen en elkaar zo regelmatig te zien. Ik mis dat nu ook best wel, maar gelukkig kunnen we er nu weer makkelijker logeerpartijtjes van maken. Ook bedankt voor jullie eerlijkheid, luisterend oor en goede gesprekken.

Marty en **Runnie**, ik ben trots dat jullie mijn broer en zus zijn! <3 Zullen we hem even samen inzetten: "wonderteam, wonderteam, hulp in nood…"

Lieve **Lenie**, of naja **Leen**, of eigenlijk voelt **mam** hier ook wel op z'n plaats! Bedankt! Voor wie je bent, voor wat je doet, voor hoe je dat doet en voor al je liefde die je ons geeft. Ik ben ongelooflijk trots op jou, op hoe je in het leven staan en hoe je weer geniet van alle mooie dingen! Al besef je het je misschien niet elke dag, je bent elke dag weer een voorbeeld voor me om met opgeheven hoofd, liefdevol en tegelijkertijd krachtig door te zetten. Ik hou van je mam! Bedankt voor al je support de afgelopen jaren, dat je zo trots op me bent en bedankt dat ik altijd bij je terecht kan! Lieve **Geer**, ik mis je nog elke dag en ik baal er zo van dat je al zo veel hoogtepunten niet hebt mogen meemaken. Ik ben je dankbaar voor wat je me allemaal hebt geleerd. Allemaal dingen die ik mooi kon gebruiken tijdens m'n PhD, maar zeker ook daarbuiten. Bijvoorbeeld om

nieuwsgierig te zijn, vragen te stellen, en niet altijd de voor de hand liggende, om ook wel kritisch te zijn, om door te zetten, om kansen te zien, en om veel plezier te maken met de mensen waar je van houdt. Je motiveert me elke dag in mijn gedachte. En ik weet dat je ongelooflijk trots op me zou zijn, omdat je dat eigenlijk altijd was. Dankjewel dat ik daar geen seconde aan hoef te twijfelen. Ik mis je enorm en ik hoop dat je hier toch een beetje van hebt kunnen mee genieten.

En dan **Koen** (ik zal je sparen, en niet al mijn bijnamen die ik voor je heb hier noemen, al jeuken m'n handen om dat wel te doen), hoe moet ik jou nou bedanken? Hoe doe je dat, iemand bedanken die echt ALLES voor je is en er ALTIJD voor je is. Ik ben dit stukje denk ik al 50 keer opnieuw begonnen te schrijven, en elke keer voelt het alsof ik je zo niet genoeg kan bedanken. Dus ik denk dat dat de waarheid is, ik kan je met een stukje tekst simpelweg niet genoeg bedanken (en n=50 is aardig betrouwbaar ;-D). Toch laat ik 1 van die 50 pogingen hier staan, in de hoop dat het toch een beetje in de buurt komt van wat ik allemaal tegen je wil zeggen. Lieve lieve **Koen**, jij hebt mij de afgelopen jaren door dik en dun gesteund. Je stond altijd, maar dan ook echt altijd, voor me klaar. Bij alle dagen dat ik balend thuiskwam, nam jij de tijd om naar me te luisteren. Bij alle dagen dat ik juichend thuiskwam, omdat er iets juist goed gelukt was jij daar om het samen te vieren. Je hebt me enorm geholpen om dicht bij mezelf te blijven, om de balans te vinden als ik die even kwijt was en om geluk ten alle tijden voorop te zetten, en die PhD met een lach op mijn gezicht af te maken. Je bent voor mij echt de ideale, nuchtere, eerlijke, lieve, grappige, loyale en stabiele basis waar ik altijd op terug kan vallen. Ik ben je hier ongelooflijk dankbaar voor en doe er alles aan om dat ook voor jou te zijn. Ik hoop dat wij voor altijd samen kunnen blijven lachen om de allersimpelste dingen. Onze grapjes vervelen mij nooit en ik wil je dan ook vooral bedanken voor al het plezier wat je toevoegt aan mijn leven en alle liefde die je me geeft! Ik hou van jou! p.s. dat je me vanaf nu Dr. Eva moet noemen is geen grapje hè, dat is bloedserieus!

About the author

Eva Struijf was born on February 24th, 1995 in Akersloot, The Netherlands. In 2013, she graduated from secondary school (VWO) at the Jac. P. Thijsse College in Castricum. That same year she started her Bachelor's study Gezondheid en Leven at the Vrije Universiteit Amsterdam. There she followed the Honours Programme, joined the board of the faculty student council and performed a research internship for three months at the department of molecular cell biology & structural biology in the groups of Dr. Rob van Spanning and Dr. Dirk Bald. In 2016, Eva completed her Bachelor cum laude and with Honours. In September 2016, Eva started with the Master's programme Infection and Immunity at Utrecht University, which she finished cum laude in 2018. During her Master, Eva did a research internship for nine months in the department of medical microbiology (MMB), in the group of Prof. Dr. Suzan Rooijakkers, under the supervision of Dr. Dani Heesterbeek. Next, she did a research internship for six months in the department of Laboratory of translational immunology (LTI, currently known as CTI), in the group of Prof. Dr. Femke van Wijk, under the supervision of Dr. Judith Wienke. During this period, Eva wrote a grant proposal together with Prof. Dr. Suzan Rooijakkers and the company QVQ for a newly developed grant by the NWO, which was called "TTW Industrial Doctorate". This grant was awarded to Eva (NAW.ID.17.036) and funded a four-years PhD research project. In November 2018, she started with her PhD research project in the lab of Prof. Dr. Suzan Rooijakkers, in the department of medical microbiology (MMB). For these studies she closely collaborated with QVQ and together they have developed multiple llama-derived nanobodies targeted to different proteins from the human complement system. The main findings of this work have been described in this thesis, have been published in a peer-reviewed journal and have been presented at multiple (inter)national scientific conferences.

List of publications

Related to this thesis

Struijf EM, De la O Becerra KI, Ruyken M, de Haas CJC, van Oosterom F, Siere DY, van Keulen JE, Heesterbeek DAC, Dolk E, Heukers R, Bardoel BW, Gros P, Rooijakkers SHM. Inhibition of cleavage of human complement component C5 and the R885H C5 variant by two distinct high affinity anti-C5 nanobodies. Journal of Biological Chemistry. 2023 Aug;299(8):104956. Doi: 10.1016/j.jbc.2023.104956. Epub 2023 Jun 23. PMID: 37356719

Struijf EM, Depelteau JS, van Keulen JE, Ruyken M, Dekkers G, Siere DY, Dolk E, Bardoel BW, Heukers R, Heesterbeek DAC, Rooijakkers SHM. Identification of a C3b-specific nanobody that blocks alternative pathway convertases. Manuscript in preparation.

Struijf EM, Depelteau JS, van Oosterom F, Ruyken M, Hutten R, Siere DY, Gros P, Heesterbeek DAC, Dekkers G, Dolk E, Heukers R, Bardoel BW, Rooijakkers SHM. Identification and characterization of a non-inhibitory nanobody that specifically targets complement C5b6 complex. Manuscript in preparation.

Other publications

Wienke J, Veldkamp SR, **Struijf EM**, Yousef Yengej FA, van der Wal MM, van Royen-Kerkhof A, van Wijk F. T cell interaction with activated endothelial cells primes for tissue-residency. Frontiers in Immunology. 2022 Sep 12;13:827786. Doi: 10.3389/fimmu.2022.827786. eCollection 2022. PMID: 36172363

PhD Training certificate – Graduate School of Life Sciences

Discipline-specific educational activities	# ECTS
Aria II/III cell sorter operator training (2018)	**1.0**
Introduction in Techniques and Facilities (2018)	**0.3**
I&I PhD retreat (2018, 2019, 2021, 2022)	**1.5**
IUIS Webinars (2020)	**0.9**
General educational activities	
GSLS PhD Day (2019, 2020, 2021)	**0.9**
The Art of Presenting Science (2020)	**1.0**
Adobe InDesign Essentials (2019)	**0.6**
Scientific Artwork with Photoshop and Illustrator (2019)	**0.6**
BioBusiness Summer School (2019)	**1.5**
Psychological flexibility (2020)	**1.0**
Writing a Scientific Paper (2019)	**1.5**
Achieving your Goals and Performing more Successfully in your PhD (2021)	**1.0**
Statistics for in the lab: in vivo et in vitro (2019)	**1.5**
PhACE workshop (2023)	**0.6**
PROUT Motivation and Negotiation workshop (2021)	**0.6**
Symposia/conferences (oral/poster presentation) and other activities	
NVVI Spring Symposium (2023)	**0.6**
Nanobody Symposium Brussel (2021)	**1.2**
Science for Life (2018, 2019)	**1.2**
Koepel conference (2019, 2022, 2023)	**1.8**
Hycult Complement congress (2022)	**0.6**
EMBO Meeting Antibodies and Complement (2023)	**1.2**
KNVM Spring meeting (2020)	**0.6**
Total number of ECTS	**21.7**